CHARACTERIZATION, MODELLING AND OPTIMIZATION OF GELCASTED Si_3N_4 BASED CERAMIC COMPOSITES

Submitted in partial fulfillment of the requirements

for the award of the degree of

Doctor of Philosophy

by

T. NAGAVENI

Roll No: 701237

Department of Mechanical Engineering
NATIONAL INSTITUTE OF TECHNOLOGY
WARANGAL – 506004
Telangana State, INDIA.

June – 2017

CHARACTERIZATION, MODELLING AND OPTIMIZATION OF GELCASTED Si_3N_4 BASED CERAMIC COMPOSITES

Submitted in partial fulfilment of the requirements

for the award of the degree of

Doctor of Philosophy

by

T. NAGAVENI

Roll No: 701237

Supervisor:

Dr. C.S.P. Rao

Professor

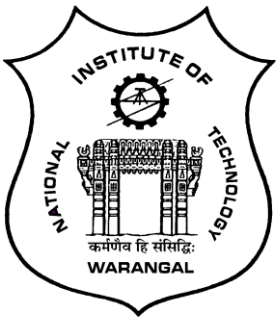

Department of Mechanical Engineering

NATIONAL INSTITUTE OF TECHNOLOGY

WARANGAL – 506004

Telangana State, INDIA.

June – 2017

THESIS APPROVAL FOR Ph.D.

This thesis entitled **"Characterization, Modelling and Optimization of Gelcasted Si_3N_4 based Ceramic Composites"** by **Mrs. T. Nagaveni** is approved for the degree of Doctor of Philosophy.

Examiners

_____

_____

_____

Supervisor

Dr. C. S. P. Rao

Professor, Mechanical Engineering Department, NIT Warangal

Chairman

Prof. P.Bangaru babu

Head, Mechanical Engineering Department, NIT Warangal

NATIONAL INSTITUTE OF TECHNOLOGY

WARANGAL – 506 004, Telangana State, INDIA

CERTIFICATE

This is to certify the thesis entitled **"Characterization, Modelling and Optimization of Gelcasted Si_3N_4 based Ceramic Composites"** submitted by **Mrs. T. Nagaveni** for, Roll No. 701237, to **National Institute of Technology, Warangal** in partial fulfilment of the requirements for the award of the degree of **Doctor of Philosophy in Mechanical Engineering** is a record of bonafide research work carried out by him under my supervision and guidance. This work has not been submitted elsewhere for the award of any degree.

Place: Warangal.
Date: 25-06-17

Dr. C.S.P. Rao
(Supervisor)
Professor,
Department of Mechanical Engineering,
National Institute of Technology,
Warangal, Telangana State.

NATIONAL INSTITUTE OF TECHNOLOGY

WARANGAL – 506 004, Telangana State, INDIA

DECLARATION

This is to certify that the work presented in the thesis entitled "**Characterization, Modelling and Optimization of Gelcasted Si_3N_4 based Ceramic Composites**", is a bonafide work done by me under the supervision of **Dr. C.S.P. Rao**, Professor, Department of Mechanical Engineering, NIT Warangal, India and has not been submitted for the award of any degree to any other University or Institute.

I declare that this written submission represents my ideas in my own words and where ever others ideas or words are included have been adequately cited and referenced with the original sources. I also declare that I have adhered to all principles of academic honesty and integrity and have not misrepresented or fabricated or falsified any idea/data/fact/source in my submission. I understand that any violation of the above will cause for disciplinary action by the institute and can also evoke penal action from the sources which have thus not been properly cited or from whom proper permission has not been taken when needed.

Place: Warangal.
Date: 25-06-17

T. NAGAVENI
Roll No. 701237

Dedicated to

my Parents

ACKNOWLEDGEMENTS

I would like to express my sincere gratitude and profound indebtedness to **Dr. C.S.P. Rao**, Professor of Mechanical Engineering, National Institute of Technology, Warangal for giving me an opportunity to carry out doctoral work under his esteemed supervision. This work is a reflection of his thoughts, ideas and concepts. Prof. C.S.P. Rao looks at things in the right perspective, and it has truly been a learning experience working with him. I owe a lot to him for making me a part of the continuity of the profession.

I extend my sincere gratitude to **Prof. G.R.C. Reddy** I/c Director, National Institute of Technology Warangal and also to **Prof. T. Srinivasa Rao**, former Director, National Institute of Technology, Warangal, India for providing the necessary facilities and encouragement throughout my work.

I am thankful to **Prof. P. Bangaru Babu**, Head, Department of Mechanical Engineering, NIT Warangal and other faculty members for their encouragement and support extended during this period.

It's my great opportunity to express my deepest gratitude to the Departmental Scrutiny Committee members, **Dr. N. Selvaraj**, Professor, **Dr. R. Narasimha Rao**, Associate Professor and **Dr. P. Subhash Chandra Bose**, Assistant Professor, Department of Mechanical Engineering, and **Dr. N. Narasaiah**, Associate Professor, Department of Metallurgical and Materials Engineering for their adeptness and many discussions during the research period.

I am grateful to **Vice-chancellor** and **Registrar** of Osmania University for deputing me to pursue my PhD work under Quality Improvement Program (Q.I.P) at Department of Mechanical Engineering, National Institute of Technology, Warangal. I wish to express my sincere gratitude to all my colleagues of Department of Mechanical Engineering, University College of Engineering, Osmania University, Hyderabad for their constant support and motivation to carry out my research work.

I express my sincere thanks to my co-scholars **Kishore Kumar Kandi, Vishnu Murthy, Neelima Devi Chinta, P Madhukar , Siva Prasad Nandhyala** and **Sandeep**, NIT Warangal for their support and help in completion of this thesis. I thank my friend **Mr.Balaji Padya**, Scientist-C, ARCI for helping me to carry out some part of characterization in his lab.

I would like to extend my heartfelt thanks to **Dr. Shirish Sonawane**, Associate Professor, Dept. of Chemical Engineering and **Dr. Sathish Babu**, Asst. Professor, Dept. of Biotechnology, NIT Warangal for their constant help and encouragement. Special thanks to my friend **Mrs.K.Sheshma** and family for hospitality.

I thank my husband **Dr. S. Srinu Naik**, Associate Professor, Department of Chemical Engineering, University College of Technology, Osmania University, Hyderabad, T.S. India for his patience, personal sacrifices and moral support throughout research period. I express my love to my son **Snithik Chauhan** and my daughter **Sciensika** for giving me wonderful smile and the joyful moments. A special debt of deep gratitude to my parents and family members for their unceasing sacrifices, endeavors and encouragement.

Finally, I would also like to acknowledge the help given by all the persons who have directly or indirectly supported the work.

T. NAGAVENI

PUBLICATIONS

International Journals

1. **T.Nagaveni** et al., "*Gel Casting of Si_3N_4-SiO_2 Ceramic Composites and Evaluation of their Characteristics*", Mechanical Engineering for Sustainable Development- State-of-the-Art Research", Apple Academic press, 2017.
2. **T. Nagaveni** et al., "*Preparation and characterization of Si_3N_4-BN ceramic composites by Gelcasting*", Material Science Research India, 13 (1) 28-33 (2016).
3. **T. Nagaveni** et al., "*Development of Silicon Nitride-Based Ceramic Radomes — A Review*", International Journal of applied ceramics technology, 12(5): 909–920 (2015). DOI: 10.1111/ijac.12305.
4. **T. Nagaveni** et al., "*A multi-gene genetic programming modelling and multi objective optimization of gelcasting of porous silicon nitride ceramics*", International Journal of Advanced Manufacturing Technology, (Minor revisions Submitted)
5. **T. Nagaveni** et al., "*A multi-gene genetic programming modelling and multi objective optimization of gelcasting of Si_3N_4-SiO_2-BN ceramics*" (under preparation)

International Conference proceedings:

1. **T. Nagaveni** et al., "*Gel Casting of Si_3N_4-SiO_2 Ceramic Composites and Evaluation of their Characteristics*", 1st International and 18th ISME Conference, NIT Warangal, February 23 – 25, 2017.
2. **T. Nagaveni** et al., "*Study on stability of Si_3N_4- BN aqueous suspension using polyethylenimine as dispersant*", 8th International Conference on Chemical, Ecology and Environmental Sciences (ICCEES'2016) , Dubai (UAE), Jan. 12-13, 2016.
3. **T. Nagaveni** et al., "*Effect of monomer content and ratio of monomer content on porosity of Gelcasting composites*", International conference on recent innovations in Mechanical Engineering-(ICRIME-2015), Chennai, May 15-16th, 2015.
4. **T. Nagaveni** et al., "*Some Chemo-Rheological studies of aqueous Silicon Nitride suspensions in gelcasting process*", All India Manufacturing Technology Design and Research (AIMTDR) conference, IIT Guwahati, December 12-14th, 2014.
5. **T. Nagaveni** et al., "*Rheological studies of aqueous Silicon Nitride slurries in gelcasting process*", International conference on Chemical and Bioprocess Engineering, NIT Warangal, November 16-17th, 2013.

ABSTRACT

Silicon nitride based ceramics has interesting mechanical, thermal and chemical properties, which suggests great potential for structural applications, even at high temperatures. The usage of silicon nitride in such applications largely depends on the ability to reliably and economically mass produce complex shaped components. This is a challenge for the ceramic industry using traditional processing techniques. Furthermore, forming complex shaped parts by machining and grinding of final sinter parts is seldom viable as it is very expensive. Advanced ceramic processing methods such as colloidal direct casting offer a way to produce complex shapes. This study builds upon the gelcasting near net shape casting technique by successfully developing a new slurry formulation and processing technique. Among the fabrication techniques for ceramic composites, gelcasting has recently attracted much attention as being a versatile, low cost and environmental friendly process.

A radome is a weatherproof, structural enclosure that protects a microwave or radar antenna and is made of a material that receives the electromagnetic signal from the antenna. The main function of a radome is to protect an antenna from environment destructions, like wind, snow, ice and freezing temperatures to rain, sun and even lightning. The Radome materials are compelled to work in severe environments with lightweight, low dielectric constant, low tangent loss, high flexural strength to withstand handling, aerodynamic and thermal stresses, high thermal shock resistance.

Based on the thorough Literature survey, gap is identified and formulates the problem on processing and characterization of Si_3N_4 based composites using gelcasting method by varying precursor amounts, solid loadings, monomers and its contents and to identify the best suitable material for wave transparent materials. Silicon dioxide (SiO_2) and Boron nitride (BN) powders were added to silicon nitride to improve the dielectric properties. Effect of various process parameters of gelcasting on mechanical and dielectric properties are to be studied on these Si_3N_4 based ceramic composites. The author proposes a new composite of Si_3N_4, SiO_2 and BN for radomes which has got excellent properties. In this study, Si_3N_4, Si_3N_4-SiO_2, Si_3N_4-BN and Si_3N_4-SiO_2-BN were developed as model materials to study the preparation technique of gelcasting. Basic factors such as solid loading, monomer content,

ratio of monomers and amount of initiator and catalyst that would affect the final morphologies and the effect of additives have been studied.

The effect of SiO_2 on the microstructure and dielectric properties of Si_3N_4-SiO_2 ceramic were investigated. After sintering for 2h at 1500^0C, Si_3N_4-SiO_2 ceramic composites having a bending strength of 60.24~179.56 MPa and a dielectric constant of 3.2~6.8 at 1~30 MHz frequency were obtained. The mechanical properties of Si_3N_4 based ceramics are found to decrease with the increase of SiO_2 content, while the dielectric properties are improved. The low dielectric properties of porous Si_3N_4- SiO_2 ceramic composites made them one of the most candidate materials for wave transparent applications.

Polyethylenimine (PEI) was selected as the dispersant for the aqueous dispersion of Si_3N_4–10v%BN powder mixture. The effects of the dispersant concentrations and pH values on zeta potentials of Si_3N_4–BN powders were investigated in detail. Zeta potential values for both powders obtained as negative whenever the pH increases from 2 to 12 or with the addition of 1wt% PEI. Well- dispersed Si_3N_4 suspension and BN suspension were obtained by the addition of 1 wt% of PEI at pH 10. The rheological behaviour of Si_3N_4 and BN aqueous suspensions was also studied and discussed. Finally, a high solid loading (42 vol%), low viscosity (380 mPa s at 100 s^{-1}) Si_3N_4–BN aqueous suspension was successfully prepared. It was observed that the suspensions exhibited shear thinning behaviour with relatively low viscosity which could satisfy the gelcasting process

It was concluded that, Si_3N_4-SiO_2 ceramic composite fabricated using 50 vol% solid loading, 10 wt% MAM content , ratio of monomer (MAM:MBAM) 1:10 and 5vol% SiO_2 sintered at 1550°C has bulk density of 1.93 g/cm^3, porosity of 42.3 %, flexural strength of 117.83±5.91 MPa and dielectric constant of 5.72. On the other hand, Si_3N_4-BN fabricated using 40 vol% solid loading, 10 wt% MAM content, ratio of monomer (MAM:MBAM) 1:10 and with 5 vol% BN sintered at 1680°C has bulk density of 1.85g/cm^3, porosity of 32.34 %, flexural strength of 142.93±3.34 MPa and dielectric constant of 5.2. Si_3N_4-SiO_2-BN ceramic composite exhibited flexural strength and dielectric constant up to 123 MPa and 4.4 for 33% porosity and 55 MPa and 3.2 for 42% porosity, respectively, making them suitable to be considered for wave transparent applications.

In this work, experiments on gelcasting of silicon nitride porous ceramics were performed with respect to solid loading, the monomer content and the ratio of the monomers. It is also evident from the number of experimental works that the gelcasting parameters have complex relations with the flexural strength and porosity. A new method, the multi gene genetic programming (MGGP) technology to predict the flexural strength and the porosity of the sintered silicon nitride ceramic was used. The study showed that the expected results of the flexural strength and porosity of the arrangement formed by experimental data are favorable and also generalize the testing data. Subsequently, a multi-objective problem is formulated for an optimal combination of settings to maximize the flexural strength and porosity to obtain multiple sets of optimal solutions to allow a ceramic engineer to choose a specific optimal set of input variables based on the particular requirements.

CONTENTS

LIST OF FIGURES

LIST OF TABLES

ABBREVIATIONS

APS	Ammonium persulfate
TEMED	Tetramethylethylenediamine
DE	Dielectric constant
FS	Flexural strength
HAS	Hydrolysis Assisted Solidification
MAM	Methacrylamide
MBAM	*N*,*N'*-Methylenebisacrylamide
MC	Monomers content
Por.	Porosity
PEG	Polyethylene glycol
SL	Solid loading
RM	Ratio of monomers
SEM	Scanning electron microscopy
TEMED	*N*,*N*,*N'*,*N'*- Tetramethylethylenediamine
XRD	X-Ray Diffractometer

NOMENCLATURE

η	Viscosity
τ	Shear stress
γ	Shear rate
P	Fracture load
L	Length of support span
b	Width of the sample
h	Height
BD	Bulk Density
AP	Apparent porosity
W_1	Dry Weight
W_3	Soaked Weight
W_2	Suspended weight
ρ	Density
ε	Dielectric constant
c	Capacitance
d	Thickness of the specimen
A	Area of the cross-sectional surface
L_0	Length of the sample after sintering
L	Length of the sample after sintering
R^2	Coefficient of determination

CHAPTER 1

INTRODUCTION

1.1. Introduction

Ceramics have been known to mankind since the earliest civilization and have performed a significant role in evolution and improvement in human civilization. Ceramic materials are inorganic compounds at high temperature and are classified as traditional or conventional ceramics made of clay-based materials and advanced ceramics, made of synthetic raw have specific structural and functional properties[1]. These ceramics are oxides (Al_2O_3, TiO_2, ZrO_2, SiO_2), nitrides (Si_3N_4, AlN, BN), carbides (SiC, B_4C) and borides [2]. Most of the advanced ceramic materials have a significant fraction of covalent bonding which ensures improved high-temperature properties like high melting point, strength at high temperature etc. The improved high-temperature mechanical properties, coupled with high wear, oxidation, and chemical resistance makes it suitable for many advanced and strategic applications such as ceramic bearings and grinding media, automobile parts, turbine plates, radomes, space shuttle tiles, bioceramics, piezoelectric ceramics, ceramic armors etc [3].

The ceramic matrix composite coalesces to provide the ceramic reinforcement phase along with ceramic matrix with superior properties for ceramic materials. The major objective of reinforcement is to enhance properties such as toughness, hardness, thermal conductivity, electrical conductivity, thermal shock resistance and thermal expansion coefficient of the composites[4]. The blend of these features makes them attractive to industrial application materials. The ceramic properties are determined by the properties of the individual phases in the ceramic sample. There are many factors that determine the phase distribution and their functionality in the ceramic based systems. The manufacturing processes also play a key role in sintered ceramics properties. Secondary phases of ceramics have numerous advantages like such phases are able to produce considerable structural changes and alter all properties of monolithic materials. For example, the phases that could form a strong boundary with the matrix could significantly decrease the creep rate at elevated temperatures.

Silicon nitride based ceramics have interesting mechanical, thermal and chemical properties, which suggests great potential for structural applications, even at high temperatures. In addition, it has one of its main characteristics of the phenomenon of in-situ reinforcement, which is evident by the anisotropic grain growth during sintering, making elongated grains[5]. These elongated grains act as a convincing effect on the mechanical strength of the material to achieve a high fracture toughness of 10 MPa.$m^{½}$. For most ceramics, this value does not exceed more than 4 MPa. This phenomenon of in-situ reinforcement which has been carefully studied in order to produce Si_3N_4-based ceramics has been explored in recent years in order to obtain a high mechanical performance in ceramics.

1.2. Electromagnetic Theory

After the development of electromagnetic theory in the nineteenth century, the technical equipment using electromagnetic waves (EM) is widely used in the art Applications. Electromagnetic waves emitted by energy sources Wavelength, as a wireless data transfer is used for various purposes, Broadcasting, medical applications, images, detection of foreign bodies, etc. Interaction with atmospheric air inspection, electromagnetic transferring information between remote devices such as satellites, space etc. The electromagnetic spectrum illustrates all the wavelengths of light. To understand the relationship between the wavelength and the corresponding frequency can detect the electromagnetic spectrum, as shown in Figure 1.1. The whole range of electromagnetic wave frequencies from the lowest to the highest is radio, infrared, visible light, ultraviolet, X-ray, and gamma ray waves. Visible light rays are at the shorter end of the wavelengths ranging from 400 to 700nm[6].

The wavelength of the electromagnetic wave is an important parameter. The physical interaction between objects and electromagnetic waves of comparable size are mainly used in engineering. The detection of objects at the nano scale on the macro scale is carried out by electromagnetic method. Electromagnetic waves composed of electric and magnetic energy field waves. Thus, Electromagnetic wave propagation needs energy. Electromagnetic waves can move all the way through space, where information about wireless systems and the transmission of energy between the terminals that use them. The distance travelled by the electromagnetic wave depends on power transmitter frequency (or wavelength), the

characteristics of the transmitter etc. Under climatic conditions, internal constituents of atmospheric air can interact with travelling electromagnetic wave.

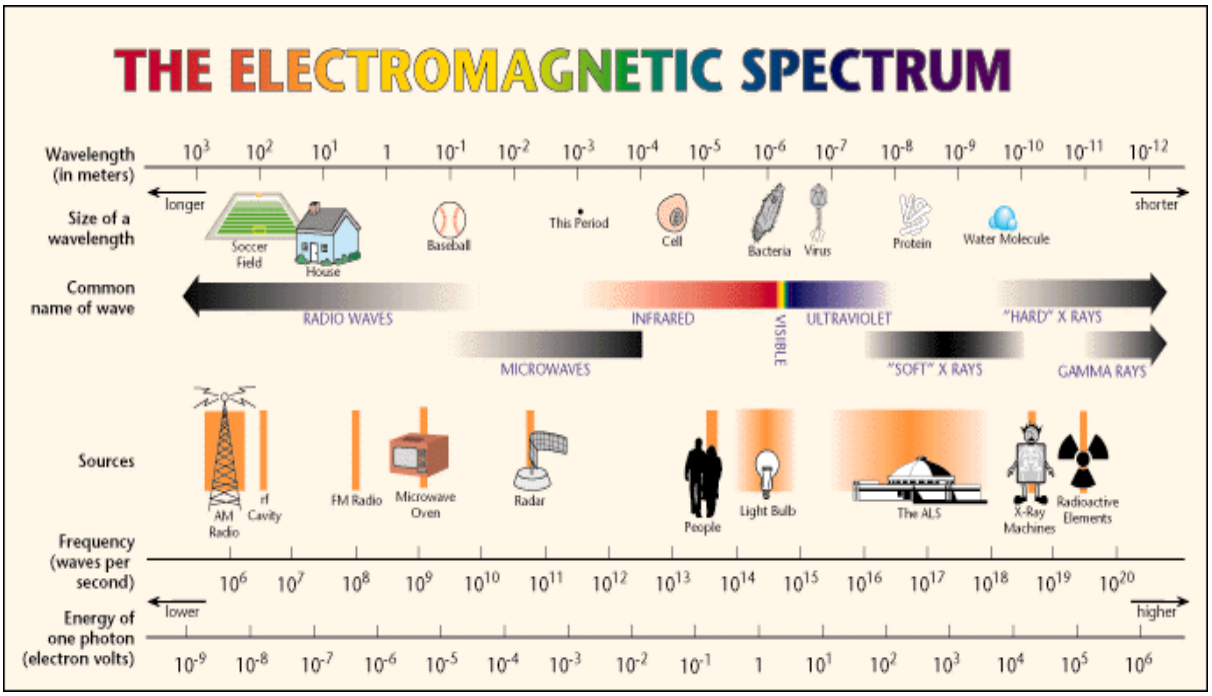

Figure 1. 1: The electromagnetic spectrum [7]

Electromagnetic wave applications are extensively used from a number of centimeters to meters, where the atmospheric window is totally transparent. Since technological approaches evolve with lower wavelengths and higher frequencies are beneficial. Therefore, Electromagnetic wave applications in mm - a range of wavelengths, where the atmosphere is semi-transparent has its potential.

1.2.1. Wave Transparent Applications

Microwave band is classified as electromagnetic waves ranging from the frequency range of 300 MHz to 300 GHz. Resultant wavelengths are ranging from 1 mm to 1m as shown in Figure 1.1. High frequency and low wavelength devices for engineering applications are potential in the high performance and precision microwave band. Numerous applications are radar for airport traffic control, missile tracking radar, long-range weather radar and military communications gains from microwaves. Depending on the microwave frequencies and applications these bands are classified into several types. According to IEEE standard 521 - 2002, radar band designations and their usual applications are provided in Table 1.1.

Table1. 1: Radar frequency(RF) bands and related applications [8]

Range of Frequency	***Band Designation***	***Band Name***	***Applications***
30-300 MHz	VHF	Very High Frequency	A very long range surveillance
300-1000 MHz	UHF	Ultra High Frequency	A very long range surveillance
1-2 GHz	L	Long wave	Long range surveillance en route traffic control
2-4 GHz	S	Shortwave	Moderate range surveillance terminal traffic control & long range weather
4-8 GHz	C	Compromise between S and X	Long range tracking airborne weather detection
8-12 GHz	X	Used in WW II for fire control, X for cross	Short range tracking missile guidance mapping, marine radar airborne intercept
12-18 GHz	Ku	Kurz-under	High-resolution mapping satellite altimetry
18-27 GHz	K	Kurz (German for "short")	Little used (water vapor absorption)
27-40 GHz	Ka	Kurz-above	Very high-resolution mapping airport surveillance
40-100+ GHz	Mm or G	Millimeter	Experimental

Most of the devices have been operated in everyday life at microwave frequencies. Thus the problem of electromagnetic interference is probable to develop as high frequency applications are common. So as to meet the necessities of the devices working at different frequencies, a development of protective material or absorbing material is essential.

The missiles are classified as air to air missiles mounted on board aircraft, moreover aimed to destroy targets. Air to surface missiles also mounted on board aircraft also configured to destroy targets on the water and surface. Surface to air missiles placed on open platforms or mobile containers is intended to destroy long-range missiles and also aircraft. Corresponding to the improvements in missile technology, the effort was on developing precision guidance systems so as to possibly direct to its goal independently of the weather conditions or the position of the launching area.

1.2.2. Radome

The antenna housing, namely (Radome) is one of the most significant parts of the guided missile radar. A radome is a weatherproof, structural enclosure that protects a microwave or radar antenna and is made of a material that receives the electromagnetic signal from the antenna. This is done because it controls the aerodynamic performance of the missile, determines the accuracy with which the missile is guided to the target, and is resistant to thermal and mechanical loads on a missile during maneuvers. The main function of a radome is to protect an antenna from environment destructions, like wind, snow, ice and freezing temperatures to rain, sun and even lightning. The Radome materials are compelled to work in severe environments with lightweight, low dielectric constant, low tangential loss, high flexural strength to withstand handling, aerodynamic and thermal stresses, high thermal shock resistance, minimal moisture absorption, high rain erosion and a high modulus of elasticity to maintain the thin walls of the radomes due to buckling. The demands of the radome and its basic material have become essential as the speed and maneuverability of missiles have amplified. Figure 1.2 shows the photograph of the sintered and machined $Si_4Al_2O_2N_6$ radome.

Figure 1. 2: Photograph of sintered and machined $Si_4Al_2O_2N_6$ radome [9]

Various types of missiles moving at speeds in the range of 5 to 12 Mach number and the surface temperature of the radome may reach up to 2000^0C with the mechanical loads up to 10 tons[10]. Radomes are typically made of dielectric materials that are illustrated by a

dielectric constant, tangent loss factor and other electrical factors. Several configurations used to reduce radomes Radio frequency reflections. The configuration for a specific application depends on operating frequency and mechanical constraints. Ceramic radomes are typically attached to the front part of rockets. The research is carried out for manufacturing of ceramic radomes for high-speed missiles.

1.3. Near net shape techniques

Near Net Shape Manufacturing can be classified into dry shaping techniques such as uniaxial pressing, isostatic pressing, wet colloidal shaping techniques such as slip casting, tape casting, gelcasting and plastic shaping process such as injection molding, extrusion etc., as shown in Figure 1.3. Dry shaping technique needs a reasonably dry feed, usually, contains ceramic powder with < 5v/v% binder.

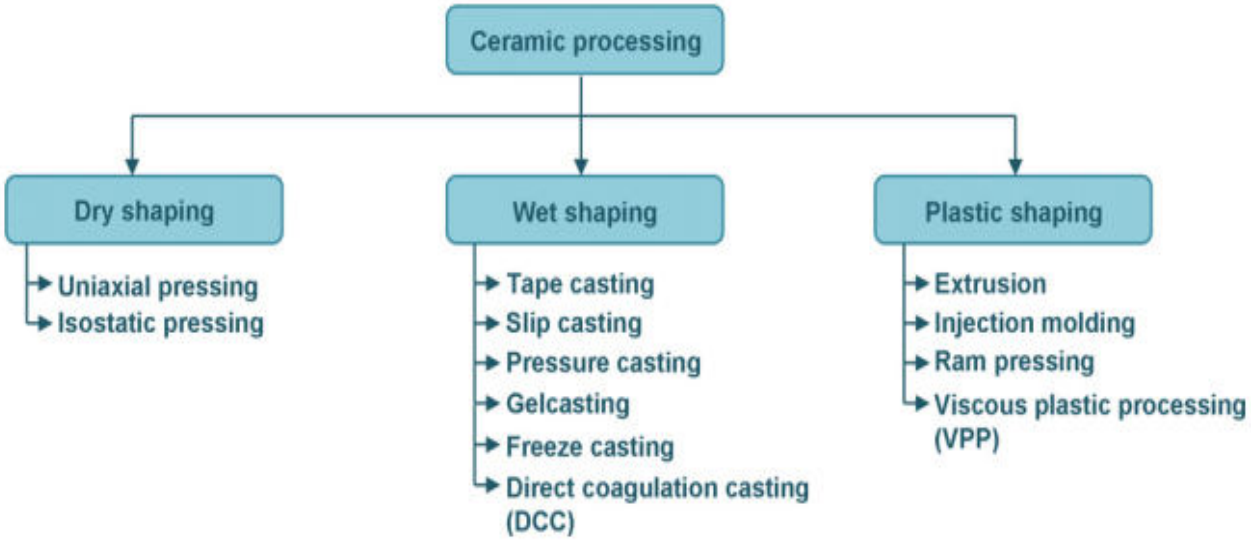

Figure 1. 3: Classification of Ceramic Processing

The reliability of ceramic dry processing is restricted by flaws caused by agglomerates. This problem can be avoided by wet processing techniques. Generally, wet colloidal processes are restricted, in the case of complex workpieces with altogether thick and thin cross-sections because of the density gradients in a green body. The wet processing techniques offer an opportunity of breaking agglomerates but creates other problems in the starting powders for instance differential sedimentation as a result of particle size distribution.

There are various methods to get rid of this problem, for instance, the use of flocculated sludge or frozen systems [11]. The disadvantages of this method are that coagulated and flocculated systems with more open structures and lower densities lead to green bodies that higher sintering temperatures require to reach theoretical density. Further details are discussed in the following sections with respect to dry and wet forming techniques. Since the ceramic processing has continuously increased significantly and new methods are initiated constantly, it is not the intention of the thesis to discuss all existing methods in detail and so few of the wet processing techniques were discussed in Appendix I.

1.4. Process principle of Gelcasting

The step by step procedure of gelcasting process is reviewed in Figure 1.4. It consists of four ingredients such as ceramic powder, solvent, organic monomers, and dispersant. The ceramic powder certainly, for which specific properties are carefully selected. In some cases, few sintering aids are also required. The process is enormously flexible and it is independent of the nature of the materials used. For the solvent, either aqueous or non-aqueous can be employed, the most commonly used is water due to the convenience of use, low cost, non-toxicity, and incombustibility. Non-aqueous solvents pose low boiling point and prevent hydration of ceramic material, however, needs particular attention related to toxicity and inflammability.

These solvents attain uniform green strength and retain viscosity even after long span storage but the slurry becomes volatile and sturdy. The monomers are the third categories of ingredients, which include a mono-functional monomer, used to form a linear polymer and di-functional monomer to perform as the cross linker, which has at least two double bonds. Monofunctional monomers should form water-soluble polymers; this gives a high possibility that the polymer will form a gel with water when it is cross-linked. When monomers are polymerized by free radical initiators, a strong crosslinked polymer solvent gel is formed. The last category of ingredients includes a dispersant, which covers the ceramics powder and maintains stability in the suspension due to steric and electrostatic repulsion. An ideal dispersion will generate chemically stable slurries with low viscosity, high volume fraction, and long shelf life.

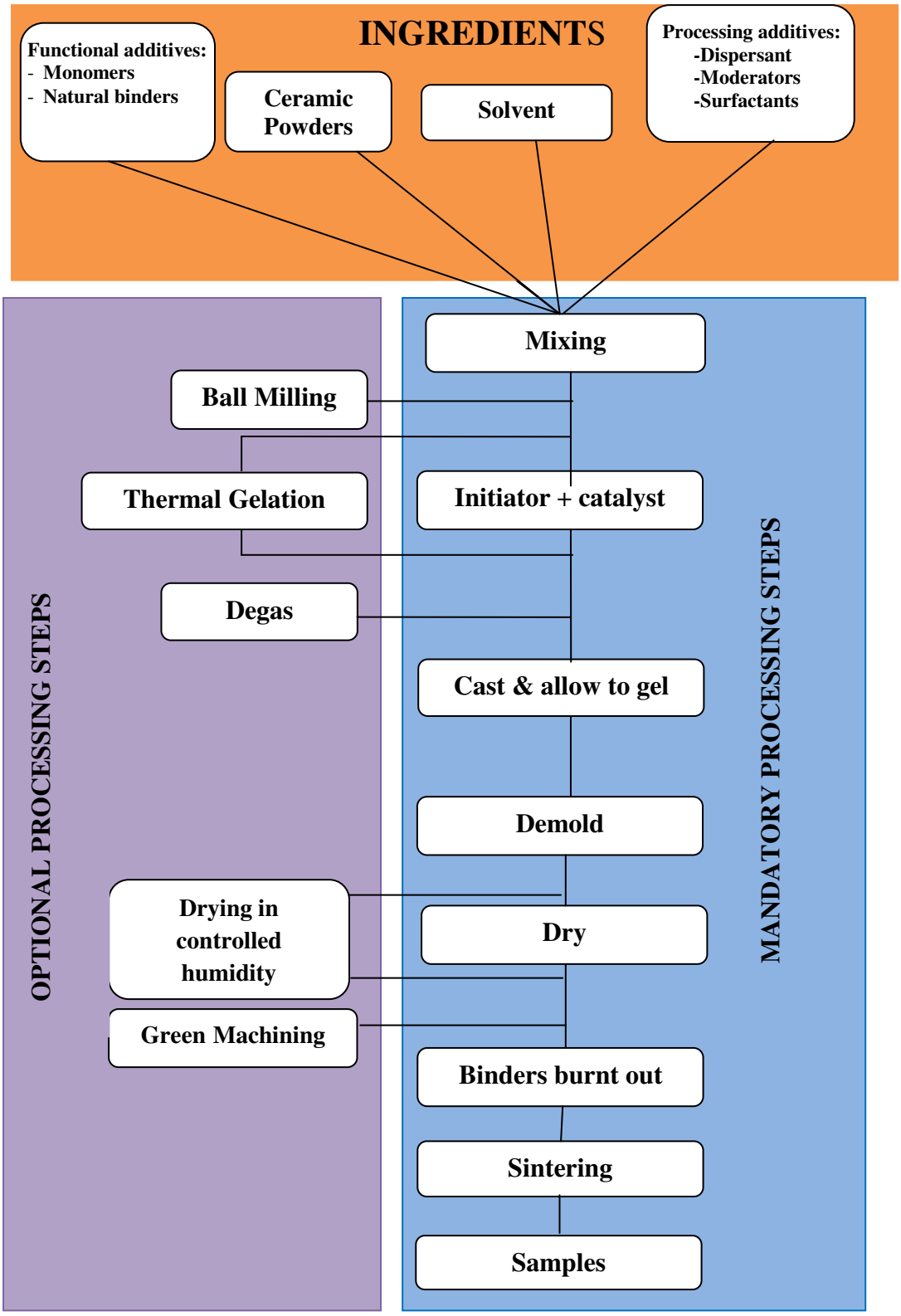

Figure 1. 4: Processing steps of Gelcasting process

The ceramic powders, an organic monomer, a solvent and a dispersant are mixed thoroughly to form the homogeneous slurry with a low viscosity and a high solid loading. Deairing is an essential step if high quality defect free parts are to be acquired. The mixture is deaired in a partial vacuum to remove air from the slurry. The oxygen in monomer solutions will precipitate the radical polymerization by forming a peroxide group at the end of a monomer chain. The presence of adequate oxygen in the suspension forms a weak gel and in some time gelation will not occur at all [12]. The catalyst and the initiator are mixed to the slurry to initiate the polymerization and the mixture is poured into a non-porous mold to cast it into the required shapes. The catalyst traps the water that causes the monomer to form a large crosslinked polymer and forms a rubbery polymer water gel. The gel completely halts the ceramic particles in the required shape by the molds. Figure 1.5 shows the mechanism of polymerization of acrylamide (AM) and methylenebisacrylamide (MBAM) using ammonium persulfate (APS) and tetramethylethylenediamine (TEMED) as polymerization initiator and catalyst, respectively. After the mixture is poured, the slurry is converted to a gel holding ceramic particles in the shape. The mold is removed and the part is dried to remove the solvent in a controlled atmosphere, favorably at a high relative humidity usually above 90%RH to reduce cracking and warping. The organic monomers are then burned and the sample is sintered to form a dense portion [13].

An advantage of gelcasting is a very small amount of polymer is sufficient to make the part of complex form generally below 5 wt%, which is readily burned without manufacturing flaws. Highly concentrated, low viscosity suspensions are attuned with gelcasting additives directed to a high green packing strength and full densification during sintering [14]. At present, water-based gelcasting can be used to produce low-polymer green compacts, which are homogeneous and have high strength. This method has been significantly affected and used in the formation of many kinds of ceramic materials.

Few common rules that can be deduced for the slurry preparation are, (i) the ratio between the monomers and ceramic powder should be maintained as low as possible; (ii) the amount of solvent must be set at a nominal to sustain a uniform suspension; (iii) the dispersant amount should be minimum to maintain the slurry in the stable condition, (iv) the slurry should be of low viscosity and high solid loading, (v) simple and low-toxic monomers should

be chosen and (vi) increase the solid loading content in turn to decrease the drying and sintering shrinkage.

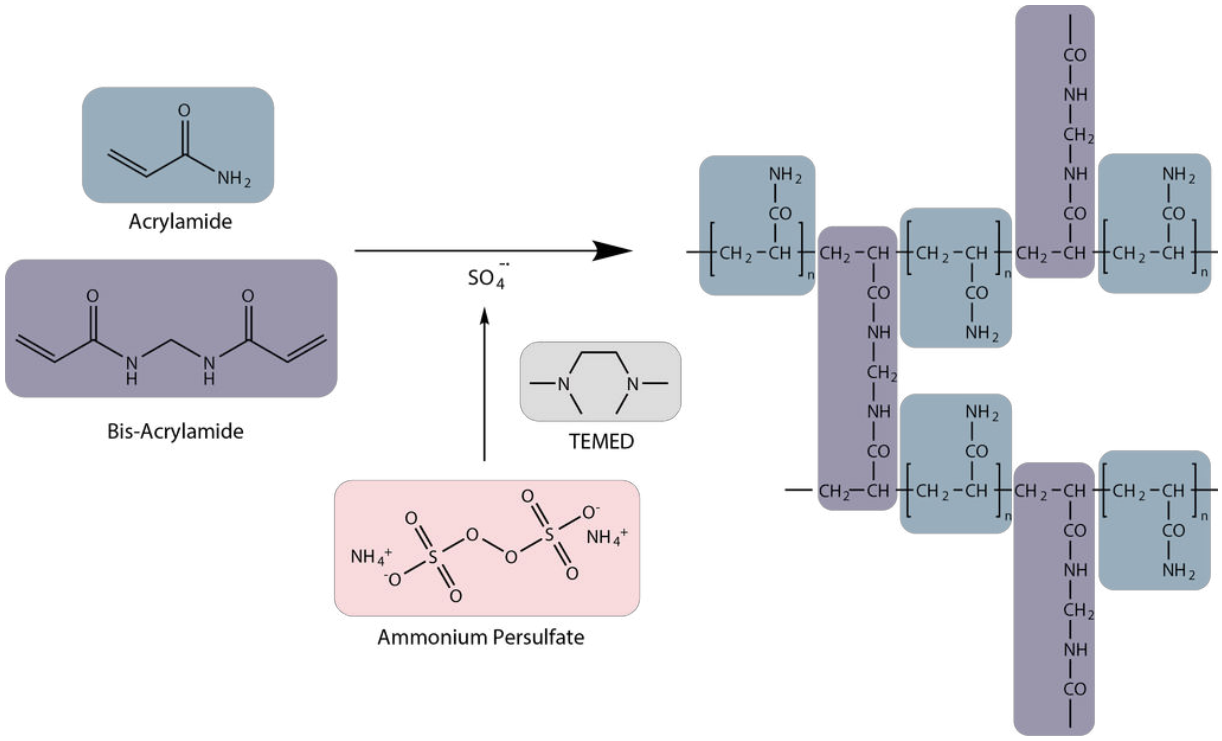

Figure 1. 5: Mechanism of acrylamide polymerization.

1.4.1. Rheology of ceramic slurry for gelcasting process

For acceptable properties of the final product and good strength of the blank is the need to comply with a proper content of the ceramic powder in the slurry. This content should be at least 50 vol%. The more we have ceramic powder in the slurry, thereby increasing the viscosity of the suspension. However, it is important that the concentration of powder has not reached such boundaries; the suspension will be so viscous that it would be impossible to pour into the mold. Conversely, high content of ceramic particles reduces shrinkage and deformation of the blank during drying increases the final density after sintering.

1.4.2. Monomers

The most commonly used monomers in gelcasting are acrylamides such as methacrylamide (MAM), methylenebisacrylamide (MBAM) and hydroxymethyl acrylamide (HMAM) with initiator and catalyst as ammonium persulfate (APS) and

tetramethylethylenediamine (TEMED) respectively. The existence of oxygen impulsively stops radical polymerization by a peroxide group at the end of the polymer chain. In this work, the use of methacrylamide and methylenebisacrylamide as a gel forming agent in gelcasting of silicon nitride and silicon nitride based ceramic composites were examined. A research on the use of these low toxic monomers seems ecologically promising and is a better choice for applications to be a gelcasting complex shaped ceramics.

1.4.3. Solvents

Most commonly used solvent is water. It has a low viscosity. Addition of suitable ceramic powder and a dispersant into water produces a highly liquid suspension with low viscosity. This is probably one of the biggest advantages of using water as a solvent. Another advantage is the ease of drying water, and optionally prevention of subsistence problems associated with the environment when disposing of residues of organic solutions. Non-aqueous gelcasting uses organic solvents. The solvent used must be completely miscible with the monomers and should have low viscosity and low vapour pressure at the reaction temperature. Organic solvents include phthalate esters, petroleum solvents with high boiling point, dibasic esters, and long chain alcohols and pyrolidones.

In addition, attention was paid to the selection of the dispersant, it must be such that it is suitable for the combination of the solvent and monomers. Monomers influence as dispersant interacts with the system ceramic powder -solvent - monomer. Additionally, the dispersant may react negatively to the initiator system - monomer, which may lead to the acceleration or slow down the polymerization process. Most commonly used initiator for polymerization is ammonium persulfate (APS). Most commonly used catalyst is tetramethylethylenediamine (TEMED).

1.4.4. Drying, Binder burnt-out, and sintering

Drying of gels is a critical step in ceramic forming process. Too rapid drying of gelled bodies can cause non uniform shrinkage, resulting in cracking or warpage. There are a number of cause for warpage during drying. One of the most important is the moisture gradient throughout the green body. To minimize the development of flaws, the gelcast ceramic bodies are usually dried in a series of high humidity chambers. Unlike the slip cast parts or pure gels,

there is no constant rate period in the drying of gelcast parts. The drying time depends on the humidity and temperature.

The big advantage of the method of gel casting is a small amount of polymer remaining in the ceramic blank for the drying process. Removal of binders is guaranteed only at the temperatures of 700^0C. The temperature of the binder removal is greatly dependent on their type and composition. After removal of organic components, the body holds the ceramic particles together due to the influence of secondary Vander Waals forces. The compaction of the ceramic body occurs subsequent sintering.

1.5. Genetic Programming

Genetic programming (GP) was introduced by Koza [15], belongs to a group of evolutionary algorithms based on the concept of natural selection and genetics. Genetic programming is comparatively new to a group of other evolutionary algorithms, evolutionary programming [16], evolution strategies[17] and genetic algorithms [18]. An evolutionary algorithm (EA) is a part of the evolutionary computation, in turn, a part of artificial intelligence. GP is a technique for generation of genetic mathematical models introduced by Koza[15, 19].Koza proposed GP as a generalization of GA. The genetic programming method is mainly applied to non-linear regression problems to create mathematical expressions that associate among a set of dependent parameters and independent parameters to provide a good fit[20].

1.5.1. Concept of Genetic Programming

Genetic programming (GP) is an addition of the genetic algorithm (GA) in which the genetic population of computer programs exists. GP is used to model while GA is used for optimization. And also, GP differs from GA by utilizing the tree structure and chromosomes of variable length rather than GAs chromosomes of fixed length and structure. The genetic algorithm output is one set, while the genetic programming output is another computer program. The chromosome in a certain way the problem is coded, it can be carried out usually in its current form instead of binary strings. Therefore, in this approach, members of the population may be represented themselves in a particular problem being solved. For an instance, to undertake a regression problem, the members of the population can be symbolized as a mathematical expression with a tree structure.

1.5.2. Execution of GP

The procedure of GP comprises the following basic steps[15]:

i. Identification of functional set and terminal set, together with fitness measure.
ii. Generation of the initial random population of functional and terminal sets.
iii. On the basis of the fitness value, estimate the fitness of each individual.
iv. Application of the selection operators. The higher the fitness values of an individual, the greater the probability that the individual is selected, and leads to the next generation (survival of the strongest). This population is called as the mating pool.
v. Based on the crossover probability, pairs of individuals from the mating pool are selected and the crossover is carried out.
vi. The next step is to apply a mutation operator, depending on the mutation probability, helps the mutation to ensure that no point in the individual search space stays unexplored.
vii. Copy the individuals to a new population.
viii. Repeat steps (iii) to (vii) for a determined number of iterations or until or until a specified fitness value is achieved.

These steps are discussed with an emphasis on the relevance of modelling with the genetic programming.

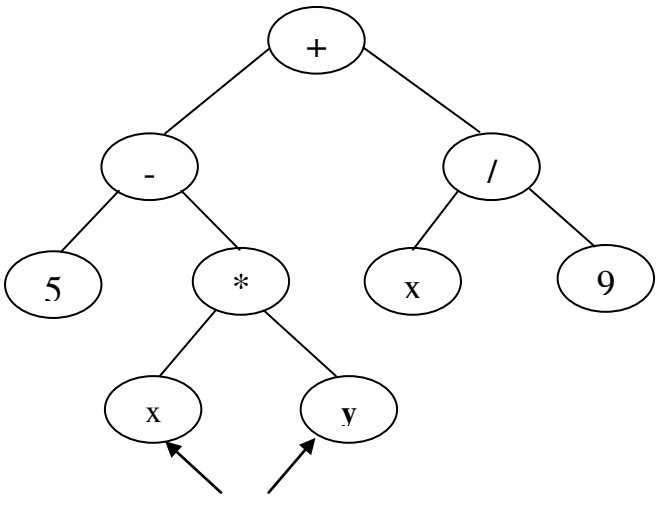

$f = (5\text{-}xy) + x/9$

Figure 1. 6: General tree representation of Genetic Programming

The models are presented as a tree structure, and generate a large population of these models. Each model consists of a functional and a terminal set. The functional set comprises of basic mathematical operators (+, -, ×, /), trigonometric functions (sin, cos, tanh etc.,), exponential functions and boolean algebra operators (eg AND and OR).The problem of the input variables is represented by a terminal set[21].

The representation of a functional tree is shown in Figure 1.6. The connection points are shown as nodes in the tree. The nodes are classified based on their position in the tree. The inner nodes in the tree are called functions. They may be Arithmetic operations, Boolean operations, Mathematical functions etc…The ending nodes (leaf nodes) are called terminal nodes. Here the "+", "*", "/" functions have two sub-trees. The right subtree is (x / 9). Similarly, Figure 1.6 shows f = (5-xy) + x/9.

For a GP model, there are four essential elements that need to be designed:

i. ***Create random initial population*:** The first step is to create random GP population. The random individuals here are random trees. These trees are created by selecting and combining terminal and functions in the trees.

ii. ***Fitness evaluation**:* Designing a fitness function which can determine the ability of a model to solve the problem is an important step in GP. Based on the error between actual data and the model induced by GP a numerical value is obtained. This numerical value is fitness. Each individual in GP will have a fitness value.

iii. ***Selection:*** The individuals with higher fitness values must be selected over the process of lower fitness values for reproduction. This is ensured by the process of selection. The probabilities of choosing a model for reproduction are directly proportional to its fitness value. There are a number of ways of selecting models. Roulette wheel selection, truncation selection, tournament selection, fitness proportionate selection, Ranking selection etc. are some of them.

ii. ***Genetic operators*:** After selecting an individual from the population three genetic operators reproduction, mutation and crossover are used.

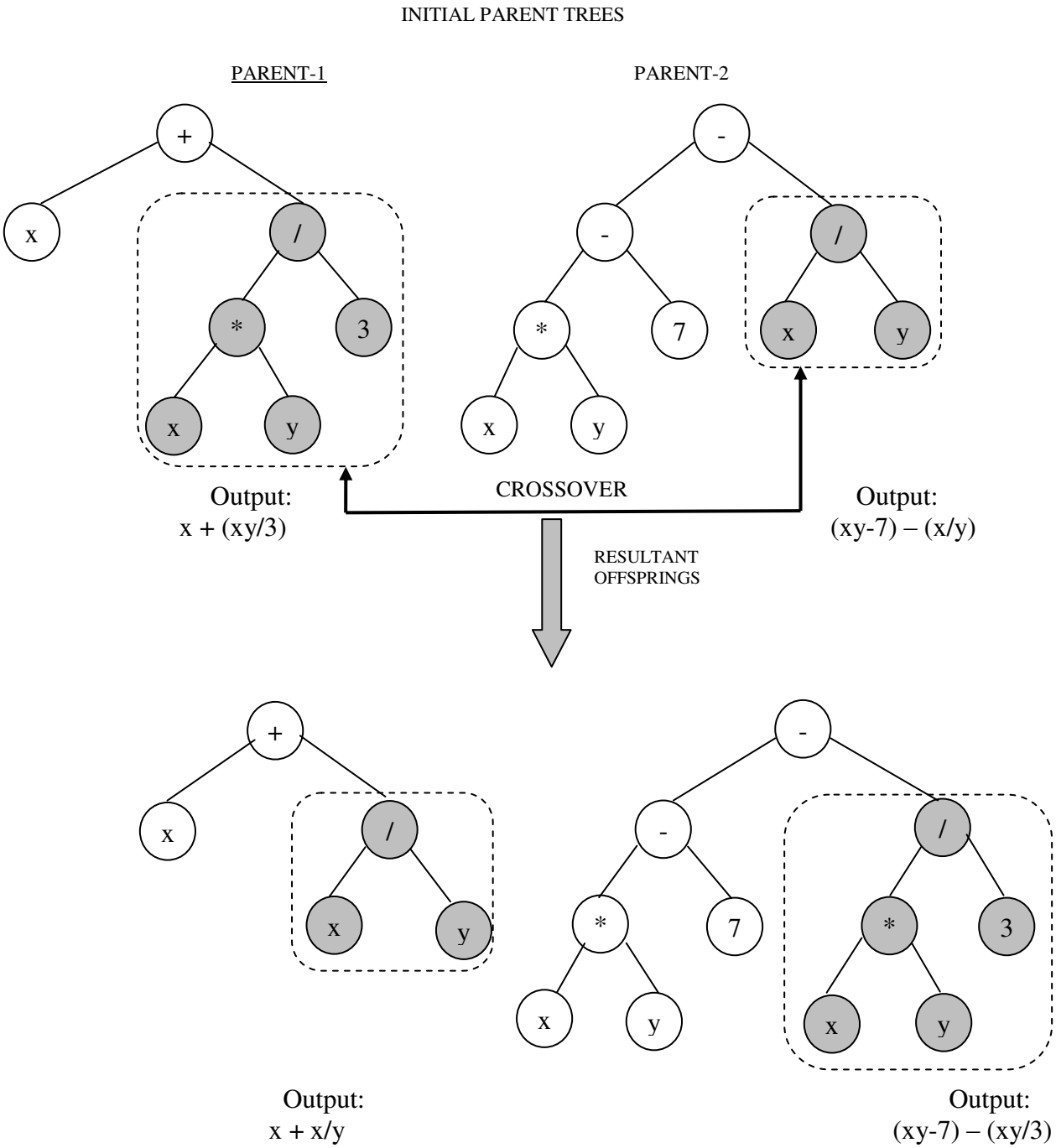

Figure 1.7: Crossover operator

a. *Reproduction* is where selected individual copies itself into the new population. Elitism is a special reproduction operator. Elitism ensures that the superior individual is always selected.

b. *Crossover* is the primary genetic operator for modifying the program structures. With the help of information gathered from parents and by combining them crossover is

carried out. Thus by combining the important information from two parents, a more superior individual is formed. This is done in GP by swapping the subtrees in them as shown in Figure 1.7.

c. *Mutation* is considered as a secondary genetic operator for modifying program structures. Unlike crossover here, there is no involvement of two parent individuals. In GP mutation of an individual is made by selecting a subtree of that individual and replacing it with a newly created subtree as shown in Figure 1.8.

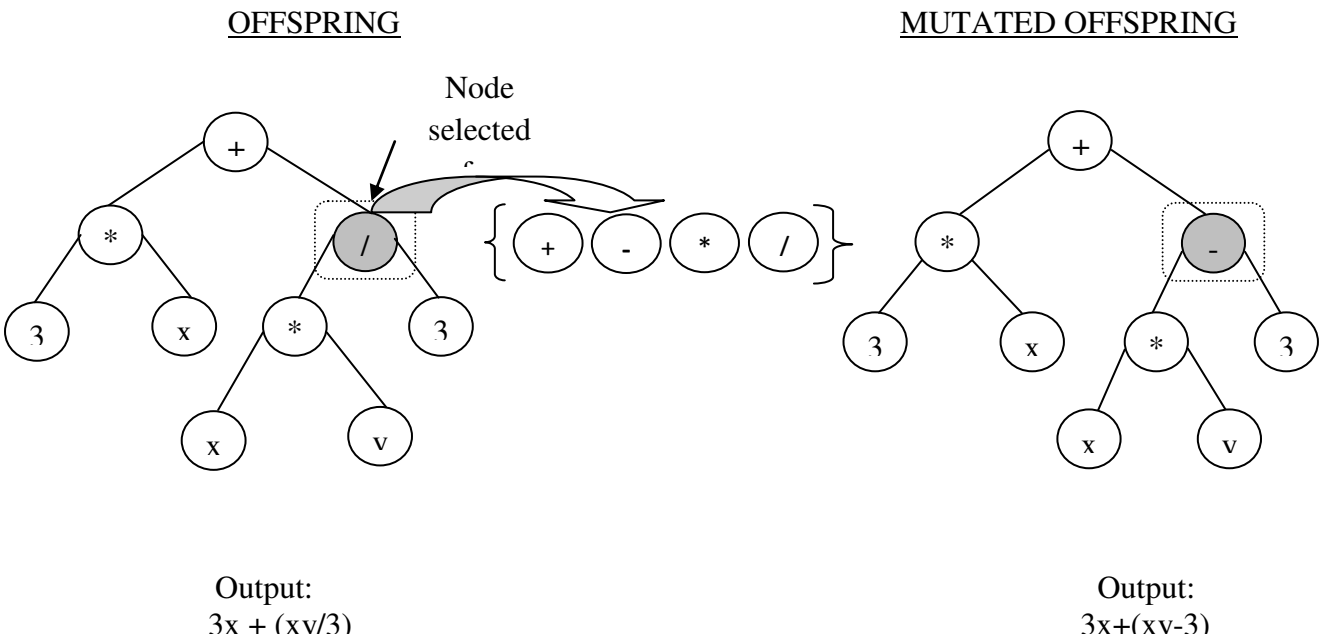

Figure 1. 8: Mutation operator

1.5.3. Multi Gene Genetic Programming

Multi Gene Genetic Programming (MGGP) is a newly developed method of genetic programming[22]. It mainly helps in the improvement of precision of GP. MGGP mainly differ from GP in the number of trees that can be used in MGGP. GP mainly uses single trees whereas MGGP uses a combination of trees. The advantage of multi gene genetic programming process based on previous models is that it is a data-driven method based on data which depends on experimental data to develop models. This avoids errors by reason when building a model of the differential equation is used.

In MGGP the final structure of the target model is made in a linear form by combining two or more non-linear gene. The general form of a MGGP model is:

$$y = a_0 + a_1 Gene_1 + a_2 Gene_2 + \cdots + a_n Gene_n \qquad (1.4)$$

Where, y is the output, $a_0$is the bias term, $Gene_i$are the non-linear genes, $a_i$is the coefficient of related genes, n is the number of genes.

The outline of MGGP algorithm is[23]:

---

i. Define the problem

ii. MGGP Algorithm

Begin

a. Set terminal set and function set, the genetic operators , the population size, number of generations and the maximum number of genes

b. Generation of genes initial population

c. The models are generated by joining the set of genes by the least squares method

d. Evaluation of models performance based on RMSE

e. Employ the genetic operators and create new population

f. Checking the performance of the models according to the termination criteria and, if not satisfied,

GO TO Step ii(e).

End;

END;

A model formulated using MGGP algorithm. Then the method of least squares is used in the MGGP algorithm to find the coefficients $a_0, a_1 \ldots a_n$.

1.5.4. Execution of MGGP

The effective implementation of MGGP algorithm is mainly determined by the parameter settings. These parameter settings are selected by the trial and error method. The problem complexity determines the size of the population and the number of generations.

Based on literature review [24, 25] large size of the population and a large number of generations are to be avoided in case of large number of data samples and this helps in avoiding the problem of over-fitting. The size of the search space and number of models are influenced by a maximum number of genes and the maximum gene depth.

The study of the GP of processing applications and Tai Garg indicates that the population size and the number of generations must be attached to a high number for the smallest amount of data or data, of higher dimensions. The size and the different forms of the model for the space of the global solutions are evaluated by the values of the maximum number of genes and the depth of the genes[26].

The performance of the individual in the initial population from the fitness function, ie the mean square error (RMSE) given as follows:

$$RMSE = \sqrt{\frac{\sum_{i=1}^{n} |G_i - A_i|^2}{n}} \qquad (1.5)$$

Where G is the predicted value data of the i-th sample of the MGGP model, A_i is the real value of the data of the i-th sample, and N is the number of training samples.

GA and GP are similar in almost every aspect, except that the playback operator cut a tree view. In the process of structural adjustment GP population of computer programs is hierarchical. The GP procedures are most commonly used to model the complex system, but also a system can be used effectively for modeling

1.6. Concept of Optimization

Optimization is a method of making things superior. Optimization is a modification of input parameters to obtain the minimum or maximum output(s). The input parameters are the variables, the process or function is called an objective function or cost function and the output is fitness value or cost [27]. Optimization techniques that have reached a maturity level in recent years, come in a variety of industries, including automotive and aerospace manufacturing industries, chemical energy. Optimization refers to the search for one or more possible solutions, extreme values or more goals. The need to find a solution to the problem of this nature is above all the ultimate goal of a solution with a minimum cost of production for

maximum reliability. Due to these extreme properties of optimum solutions, optimization methods of great practical importance, especially in engineering design, experiments and business decisions of the company.

1.6.1. Single Objective Optimization

In single objective optimization, it is the only best solution that is generally the global minimum or maximum based on the type of optimization problem [28]. If there are multiple conflicting objectives, there doesn't exist one solution that is best compared to all targets. It cannot be an optimal combination of parameters in practice for all objectives. The parameters influence them differently. There is, therefore, a need for a multi objective optimization method to the present problem to arrive at the optimal solutions[29].

1.6.2. Multi Objective Optimization

Optimization is the most important method to find an optimal solution. An optimization process consists of three basic elements: variables, objective function and constraints. This process is to minimize or maximize the objective function to satisfy constraints. The problem is based on many variables and therefore must have different combinations of values of the variables are reviewed by the optimism of the objective function [30]. Sometimes many contradictory criteria such as cost, performance, capacity and reliability should be considered at the same time. It is very difficult to decide which is best for the selection criteria because the criteria can conflict with each other. This is also known as the multi-objective optimization problem.

Many real world design problems involve simultaneous optimization of multiple objectives. In the case of multiple objectives, there cannot be a solution that is best (global minimum or maximum) of all objectives. In a typical multi-objective optimization problem, there are a number of superior solutions for the rest of the solutions in the search space if all valid objectives, but are lower than other solutions in space in one or more goals. These solutions are known as non-dominated solutions or Pareto optimal solutions [31]. The rest of the solutions are identified as dominated solutions. The choice of a solution to another problem requires knowledge and a series of factors related to problems. Therefore a solution that can be chosen by a designer may not be acceptable for another designer or in a modified

environment. Therefore, it may be useful for the multi-objective optimization problem to know Pareto optimal solutions.

In the case of multiple conflicting objectives, there is no solution that is best with respect to all objectives. In practice, it may not be a single optimal combination parameter for both flexural strength and porosity. The parameter influences them differently. Therefore, there is a need for a multi-objective optimization method to arrive at solutions to this problem. In the case of several contradictory objectives, there is no solution that is best for all targets.

The multi-objective problem was designed as follows:

Minimization \ Maximization

$F(x) = [f_1(x), f_2(x),\ldots\ldots\ldots..,f_k(x)]$

Subjected to $g_j(x) \leq 0$ where $j = 1,2,3,4,\ldots\ldots..,j$

$h_k(x) = 0$ where $k = 1,2,3,4,\ldots\ldots.,k$

where $f_1(x)$, $f_2(x)\ldots\ldots\ldots..f_k(x)$ are the objective functions. The objective function can be of minimization or maximization type. In multi-objective optimization, preferably an attempt has to be made in obtaining a set of trade–off optimal solution by considering all objective to be significant. The objective function can be minimized or maximized. In the multi-objective optimization, preferably an attempt has to be made in obtaining a set of trade–off optimal solution by considering all objective to be significant.

1.6.3. Concept of dominance and pareto optimality

Multi Objective Optimization uses a dominance concept by comparing two solutions. If a feasible solution is not dominated by any other possible solution to the problem of multi-objective optimization, it is said that a solution is a non-dominated solution. The following procedure can be adopted to find a set of non-dominated solutions. x (1) dominates x (2) if x (1) is not worse than x (2) all targets and x (1) is strictly better than x (2) in at least one target.

It is said that the solution x (1) dominates x (2) or x (1) is dominated by x (2), if the two above conditions are true [29].

There is no single solution to a multi-objective optimization problem, but a set of mathematically equal solutions of good optimal solutions known as non-dominated Pareto solutions. These solutions are strongly based on the concept of domination, where one element dominates another if it is better than the other in at least one target and not a bad function in relation to all other objectives. Pareto front depicts the tradeoffs among competing objectives and recognizes non-dominated solutions. It consists of members of the population, for whom there is no solution, which is better in criteria than the Pareto set member. The ability to characterize the Pareto front can focus on inspection and compensation for conflicting variables. The representation of the Pareto front can be quickly used to find promising solutions to large populations of expressions and focus the efforts of subsequent analysis of these solutions.

Although several conventional methods for obtaining solutions are available for multi-projection problems, they have some disadvantages of conventional methods of min-max optimization, weighted sum, distance function methods. These methods change the multi-objective problem to a single objective, in which the respective weights are based on relative performance. These methods have the disadvantage that the deep knowledge of the meeting manufacturer must have a thorough knowledge of the classification of the objective functions. The methods fail if the objective functions are discontinued. On the other side of the non-dominant genetic algorithm (NSGA) has the advantage that it does not require gradient information and inherent parallelism and thus provides a robust adaptive optimization technique.

1.7. Organization of the Thesis

The structure of the thesis is as follows:

Chapter I present a brief introduction to the electromagnetic spectrum and their applications. Various near net shaping techniques especially wet processing techniques are discussed. This chapter also discussed the gelcasting procedure in detail. This chapter briefly introduces the concept and development of a mathematical model of multi gene genetic programming

(MGGP) and also multi objective optimization using NSGA-II. This chapter also gives an overview of the content of this thesis.

Chapter II focused on literature review, which consists of five sections. In the first section, review on wave transparent materials using different processing techniques was discussed. In the second section, the analysis of the influence of process parameters on structure, mechanical and dielectric properties in the gelcasting process are discussed. In the third section, different methods for improving dielectric properties of Si_3N_4 ceramics are presented. Review on modeling and multi objective optimization were presented in the fourth section. Finally, in the fifth section, literature gaps are identified and analyzed. Research objectives are projected and a work plan is developed to attain the research objectives.

Chapter III summarizes the description of materials and equipment utilized to measure the performance characteristics. Experimental setup used in this work is described in this chapter. This chapter also provides the details of sample processing and their characterization for different silicon nitride based composites. It identifies experimentally the appropriate ceramic slurry system and processing routes of porous Si_3N_4, Si_3N_4–BN, Si_3N_4–SiO_2 and Si_3N_4–SiO_2-BN ceramic composites using the gelcasting method, measurement and analysis methods for related properties. The challenges in each ceramic composite are discussed and solutions are subsequently provided through preliminary experimentation.

Chapter IV deals with the characterization of porous Si_3N_4, and Si_3N_4–SiO_2-BN ceramic composites by varying monomer content, the ratio of monomers and solid loading. The results of mechanical, dielectric properties and microstructural analysis of the sintered Si_3N_4–SiO_2 and Si_3N_4–BN ceramic composites were presented. The effect of process parameters on performance characteristics of Si_3N_4–SiO_2-BN ceramic composite was discussed.

Chapter V generates the regression models for flexural strength and porosity for porous Si_3N_4 and flexural strength and dielectric constant for porous Si_3N_4–SiO_2-BN ceramics using Multi gene genetic programming (MGGP) considering the experimental data in Chapter IV. This chapter also presents the multi-objective optimization of porous Si_3N_4 and Si_3N_4–SiO_2-BN ceramic composites. The responses are simultaneously optimized and the optimal levels of the process parameters are determined.

Finally, the main findings and conclusions of this investigation are summarized in Chapter VI. Also, at the end, a few suggestions for future work on the related topics have been enumerated.

Summary

This chapter presents a brief introduction to the electromagnetic spectrum and their applications. Various near net shaping techniques were discussed. This chapter also discussed the gelcasting procedure in detail. This chapter briefly introduces the concept and development of a mathematical model of multi gene genetic programming (MGGP) and also multi objective optimization using NSGA-II. This chapter also gives an overview of the content of this thesis

CHAPTER 2

LITERATURE REVIEW

2.1. Overview

This chapter is categorized as follows. In the first section, review on wave transparent materials using different processing techniques was discussed. In the second section, the analysis of the influence of process parameters on structure, mechanical and dielectric properties in the gelcasting process are discussed. In the third section, different methods for improving dielectric properties of Si_3N_4 ceramics are presented. Review on modeling and multi objective optimization were presented in the fourth section. Finally, Literature gaps are identified and analyzed. Research objectives are projected and a work plan is developed to attain the research objectives.

2.2. Review on Wave Transparent Materials

A brief review of the state-of-art papers published related to various materials used for wave transparent applications was presented in this section.

In a study, Gilde *et al* (1997) fabricated a silicon oxynitride (Si_2N_2O or SiON) nanocomposite by calcining α-Si_3N_4 powder at 1700^0C in an open-air atmosphere followed by sintering. It has performed in a nitrogen atmosphere at >1800°C. However, in this process the final product could not be prepared repeatedly with consistent properties.The dielectric constant is about 4.78 at 25^0C, 5.0 at 1000^0C and a loss tangent of about 0.0014 [32]. Hongjie Wang et al. (2010) prepared a porous Si_3N_4 ceramics with a porosity of 45–60%, with flexural strength 57–176 MPa, dielectric constant of 2.35–3.39, 8–18 GHz range of frequency, and dielectric loss of 1.6–3.5 x 10^{-3} at room temperature. α- Si_3N_4 powder prepared using Al_2O_3 andY_2O_3 as sintering aids at 1600-1800^0C in N_2 atm by low molding pressure (10MPa) & pressureless sintering[33].

Yong Li et.al. (2010) used 20 wt% naphthalene powder as the pore-forming agent and 9 wt% yttria (Y_2O_3) as the sintering additive to prepare ceramic radome arbitrary porous silicon nitride (Si_3N_4) through sintering cold isostatic pressing and gas pressure sintering. The improved mechanical properties are due to the grain growth during sintering and phase transformation from α- Si_3N_4 to β- Si_3N_4, which leads to significantly improved mechanical properties [34].

Yiguang Wang and Jinling Liu (2009) synthesized $AlPO_4$–SiO_2 powder through sol–gel technique with a composition of Al:P:Si=1.5:1:0.1 (aluminum nitrate, phosphate acid, and tetraethoxysilane) and found that the $AlPO_4$–mullite composites sintered at 1250^0C has high strength and good dielectric properties at 10 GHz, was a suitable material for the radome application[35]. The silica boron nitride and silica fiber reinforced -based composites (SiO_2-BN/SiO_2f) were prepared through the sol-gel method by Li Duan et al. (2012). The composites show excellent dielectric properties with the dielectric constant being 3.22, which indicates that the oxidation treatment is ineffective to improve the properties of SiO_2f/SiO_2-BN composites[36]. Table 2.1 shows the summary of flexural strength and dielectric constant of various wave transparent materials with different processing techniques.

In a study, Aluminium phosphates/Aluminium borate whisker composites were prepared using normal pressure sintering technique. It was found that after sintering at 1050^0C for 1 h, the dielectric constant, flexural strength, and loss tangent of the composites with 30 vol% aluminium borate whisker addition reached, 4.23, 215.3 MPa and 0.0024 at 10 GHz respectively [37]. In another study, Xiaoming Duan et.al.(2012) found that $CaHPO_4$ can promote the densification of ceramics, phase transformation from α- Si_3N_4 to β-Si_3N_4 as well as the development of elongated columnar β-Si_3N_4 grains [38].

Table 2. 1: Summary of properties of various wave transparent materials with different processing techniques

Ref. No	**Author**	**Year**	**Method**	**Material**	**Flexural Strength (MPa)**	**Dielectric constant**	**Tan δ**
[32]	Glide et al.	1997	Calcination N_2 O_2,	Si_2N_2O		4.78	0.0014
[39]	Longjie Zhou et al.	2002	Cold isostatic pressing/ Gas Pr. Sintering	Si_3N_4	944.7 Bending		
[36]	Li Duan et al.	2012	Sol-gel	SiO_2f/SiO_2-BN	113.9	3.22	0.0039
[38]	Xiaoming Duan et.al	2012	Gelcasting	Si_3N_4 ,agarose,$CaHPO_4$	265.5	5.5	
[37]	Lu ZhenYu et al	2008	pressure sintering	Aluminium borate whisker/aluminium phosphates	215.3	4.23	0.0024
[34]	Yong Li et al	2010	Gas Pressure Sintering	porous Si_3N_4, Y_2O_3, Naphthalene	226 bending		
[33]	Hongjie Wang et al.	2010	cold-pressed pressureless sintering	porous Si_3N_4 , agarose	176	3.39	0.003
[40]	Juanli Yu et al.	2010	Gelcasting	Si_3N_4	130		
[41]	Ibram Ganesh et al.	2008	Gelcasting	β-$Si_4Al_2O_2N_6$	226	7.22	
[40]	Ganesh etal .	2010	Gelcasting	β-$Si_4Al_2O_2N_6$ –SiO_2	199	6.32	0.002
[42]	Shengjin Wang et al.	2012	Gelcasting	Si_3N_4-BN	128	4.1	
[43]	Chunrong Zou	2013	Gelcasting	Porous Si_3N_4	108.3 to 235.1	2.65 to 3.68	
[5]	Xuejin Yang et al.	2016	Gelcasting	Porous Si_3N_4	146.0	4.03	
[44]	Shengin Wang et al.	2013	Gelcasting	Si_3N_4-BN with PMMA	71.6 to 105.2	3.35 to 3.8	

Table 2. 2: Summary of Comparison of Dry Pressing(DP), Slip Casting (SC), Gelcasting(GC), Hydrolysis assisted Solidification (HAS) and Hydrolysis induced aqueous gelcasting (GCHAS) along with properties

Dielectric constant	**Green Stren**	**WA (%)**	**AP (%)**	**BD g/cm3**	**GD g/cm3**	**Hardness (Kg/mm^2)**	**Flexural Strength (MPa)**	**Sintering Tempe**	**Solid Loading**	**Process**	**Material**	**Reference**
5.7							200	1400	30%	DP	**SiO_2-AlN**	[45]
6.32		1	1	3.13	1.75	1356	199	1750	48%	GC-7Y	**β-$Si_4Al_2O_2N_6$-0.5**	[46, 47]
	20.25				1.8					GCHAS		
7.206		0.01	0.01	3.07	1.87	1317	206			CDPP	**β-$Si_4Al_2O_2N_6$**	[48, 49]
		0.16	0.47	3.12	1.73	1571				HAS		
		0.01	0.01	3.15	1.96	1495				GCHAS		
7.22		0.04	0.12		1.75	1423	226		50%	GC		
	0.25	0.018	0.064	3.5	1.665	811.36	173	1650		DP	**MAS (Magnesium Aluminate Spinel)**	[50-52]
	7	0.785	1.034	3.39	1.623	656	153			SC		
	15.64	0.083	0.275	3.524	1.635	800	183		45%	GC		
	21	0.076	0.256	3.37	1.638	1197	169		45%	GCHA5		
	11	0.055	0.132	3.36	1.617	1192	112		45%	HAS		
	<0.25	0.045	0.185	3.88		1536	142	1600		DP	**ALUMINA**	[53]
	18.5	0.002	0.213	3.89		1544	153		50%	GC		
	7.1	0.058	0.244	3.63		1394	129		50%	HAS		
	22.4	0.046	0.312	3.76		1476	138		50%	GCHAS		

Ibram Ganesh et.al.(2008) in their paper presented the characteristics of differently formed β-$Si_4Al_2O_2N_6$ ceramics. Dense β-$Si_4Al_2O_2N_6$ ceramics were obtained from α-Al_2O_3, α-Si_3N_4, Y_2O_3, and AlN upon sintering (for 4 h at 1675^0C) green bodies consolidated by a conventional dry powder processing and an aqueous gelcasting route[41]. Dense β-SiAlON–SiO_2 ceramic composites were prepared with a SiO_2 weight percentage of 20, 40, 50, 60, 80 by Ibram Ganesh and Sundhararajan (2010) from fused silica and β-$Si_4Al_2O_2N_6$ by sintering at 1500^0–1750^0C for 3–4 h. The Si_2N_2O formed from a powder mixture of 40 wt% fused silica and 60 wt% β-$Si_4Al_2O_2N_6$ at 1750^0C for 3 h exhibited a flexural strength of >140 MPa [54]. Table 2.2 shows the comparison of Dry Pressing (DP), Slip Casting (SC), Gelcasting(GC), Hydrolysis assisted Solidification (HAS) and Hydrolysis induced aqueous gelcasting (GCHAS) process along with their acquired properties. By comparing the Table 2.2, samples processed with gelcasting process possess high mechanical properties due to uniform microstructure.

2.3. Review on Structure and Properties of gelcasted ceramics

2.3.1. Physical properties

2.3.1.1. Density

The results of the several investigations [13, 55-58] concerning the density of the gelcast ceramic samples can be summarized as follows: high solid loading content aids to high density materials and the low viscosity improves slurry mobility and benefits the homogeneity of the green and sintered ceramic bodies. The final sintered densities are also closely related to the homogeneity obtained in the green body.

Li et al. reported the density of the dried green SiC bodies with PEG (polyethylene glycol) were lower than that without PEG, but it is high enough to permit inexpensive green machining of the green bodies into more complex shapes[59]. The increase in sintering temperatures leads to inflated grain growth with no substantial improvement of density. The densities of the non-aqueous gelcasted BSTM ceramics are inferior but homogeneous compared to dry pressed BSTM ceramics[60].

Zou et al. prepared initially Porous Si_3N_4 ceramics by gelcasting and amorphous SiO_2 was introduced into porous Si_3N_4 frames by sol–gel infiltration[61]. The increase of density

and the formation of well-distributed micro-pores with both uniform smooth pore wall and pore size, they achieved a high mechanical strength and low dielectric constant.

2.3.1.2. Shrinkage

When solid loading increased, the sintering shrinkage decreased while the sintered relative densities increased [62, 63].This phenomenon is because of the packing behavior in the slurry. Higher packing density, higher green strength and lower shrinkage during sintering are obtained by a large distribution of particle sizes.

Yu et al. found that the shrinkage rates of the green sample decrease with increasing monomer content and the decrease in monomer ratio. The uniform distribution of ceramic particles and compact gel network forms the damping motion of homogeneous ceramic particles, which promotes a reduction in the warpage during the drying of the green ceramic body[64].

Prabhakaran and Pavithran experimentally examined the linear shrinkage of 55 vol% alumina suspension was 1.4%and 17% during drying and sintering to 97% theoretical density[63]. Wang et al. observed a decrease in the sintering linear shrinkage as well as green density by the addition of more Boron Nitride (BN) content, while the porosity increases. The observations indicated that BN cannot be sintered due to its relatively high sintering temperature, which leads to increased porosity in BN/Si_3N_4 ceramics when more BN content was added[42].

2.3.2. Mechanical Properties

2.3.2.1. Green strength

The commonly employed acrylamide (AM)[65-69] monomer can have high green strength in the gelcasting bodies, but the problems like neurotoxicity and sensitivity to oxygen bound its applications. Numerous alternative gelling agents were developed such as Methacrylamide (MAM) [54, 57, 66, 70-72], methoxy polyethylene glycol mono methacrylate (MPEGMA)[73], n - vinylpyrrolidone (NVP)[54, 63, 73, 74], 2-hydroxyethyl methacrylate (HEMA)[75], Hydroxymethylacrylamide (HMAM)[76], polyvinyl alcohol [77] and also natural monomers such as gelatine[78, 79], agarose [38, 80], epoxy resin [81], glycerol

monoacrylate [82] and sodium alginate etc.,. A detailed review on these low toxicity monomers was found in references[14, 83, 84].

The gelcasted ceramic body has the poor mechanical strength of the absence of sufficient cross linking of the polymer by gelation of low concentration suspensions. Accordingly, it was necessary to improve the degree of polymerization by free radical polymerization of monomers using an initiator[73]. The green strength samples depend on a number of factors, such as the solid loading, the chemical nature of the monomers, a number of monomers in the suspension, the weight ratio of monomer ratio to crosslinker temperature of polymerization and the chemical nature of the monomer Initiator and its concentration, etc.

The contribution of several researchers regarding the effect of different monomers content on flexural strength of green gelcast Al_2O_3 ceramics is reported in Figure 2.1. Tong and Chen [85] showed that the addition of 2,4,6,8 and 10 wt% AM (Acrylamide) led to the high green strengths of Al_2O_3, typically ~45 MPa. Kasgoz et al. (2005) found that the addition of 2-8wt% PAM (Polyacrylamide) increased green strength of gelcasted Al_2O_3 ceramics to over 42 MPa [86].

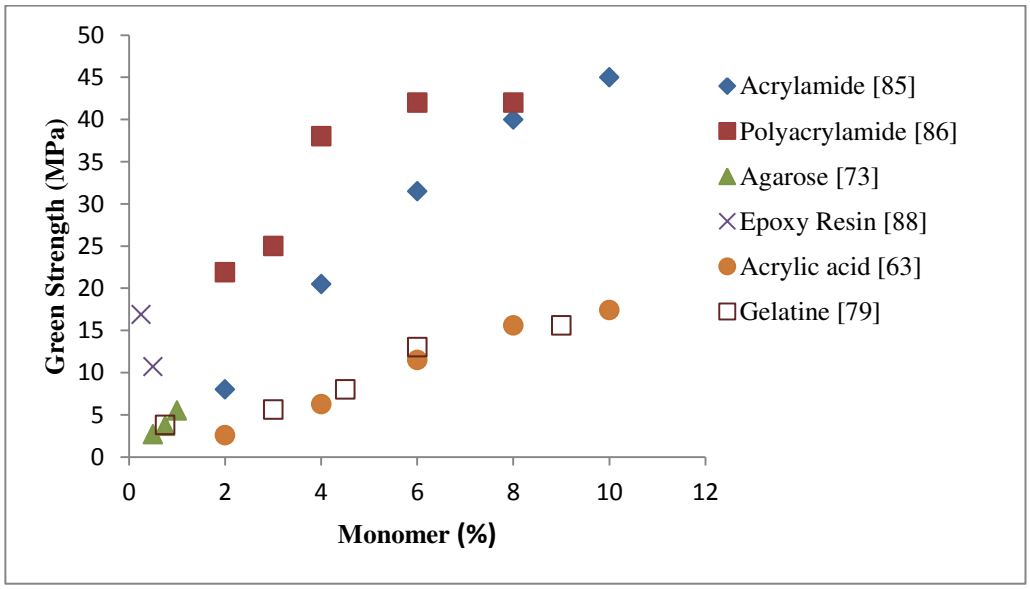

Figure 2. 1: Green strength versus percentage of different monomers for gelcast Al_2O_3 ceramics

Ma et al. reported the decreased green strength with the addition of moderator due to relaxation of the harder polymer chain by incorporating a short chain molecule of the moderator, the polymer network strength is decreased [87]. Mao et al. prepared alumina foams by a soluble epoxy resin combined with water as a binder with a polyamine curing by the gelcasting process[88].The adhesion of polymers network between particles is related to the green strength of the ceramics. As the solids loading of slurry increases, a number of ceramic particles increases, which hinders the connection between monomers and diminishes the strength of polymer networks. So, when solids loading is more the green strength reduces [67]. The bending strength of the green ceramic is maximum, as the ratio of the monomer has an optimum value. The green strength decreases because the three dimensional lattice structures of polymer gels are rough to reduce the tenacity of lattice structures when the ratio of the monomer is too low[64]. At the same time, when the ratio of the monomer is too high, the three dimensional structures in lattices are loose and lead to a heterogeneous distribution of the ceramic particles in the body, which in turn reduces the green strength.

Oxygen-containing atmospheres, such as air and vacuum, were unsuitable for gelcasting as the strong binder networks formed by polymerization are stopped in the exterior surface area, ensuring surface exfoliation of the ceramics. This problem can be avoided with the atmosphere of N_2. The green strength of the gelcasted ceramic was measured as 30.8 MPa, which was almost 22 times superior to that of slipcasted ceramics[89]. Li et al. studied the role of polyethylene glycol in silica carbide gelcasting with AM and MBAM to remove surface exfoliation from silicon carbide green bodies. The addition of polyethylene glycol has no evident effect on the colloidal behavior of the silicon carbide in aqueous suspension but decreased the green strength of the bodies, which helps in green machining before sintering. The addition of Polyacrylamide can, in particular, improve the flexural strength of the green Si_3N_4 body[59].

Jian et al reported an increase in the amount of initiator (ammonium persulfate), polymerization time and polymerization temperature, increases the green strength of the body and then decreases. The higher the APS amounts, the more the crucial radicals decompose from the APS, which leads to an increase in the active points of chain propagation and a reduction in the length of the polymer chains[90]. The polymerization rate progresses slowly and the polymerization time is too lengthy, which directs the sedimentation of the AlN

particles at low temperatures. At high temperature, the polymerization rate is high and the temperature gradient is high in the suspension, resulting in stress and defects in the green ceramic bodies [87].

2.3.2.2. Flexural strength

The researchers attributed that the increase in flexural strength to the decreased porosity and the increased solid loading of the ceramic material. Zou et al. reasoned the increase the flexural strength of sintered ceramics to the increased solids loading. As the Solid loading increased from 30 to 45vol%, the porosity of the ceramic was reduced from 57.6% to 36.4%, and the flexural strength was linearly increased from 108.3 MPa 235.1 MPa[43]. Huang et al. showed that the coating of silicon nitride with oxides improved the bending strength of the sintered gelcast sample[68]. Wang et al. fabricated Si_3N_4 porous ceramic produced by a pressureless sintering process without any pore forming agents with high flexural strength[33].

Yong Li et al. reported the bending strength and the porosity initially increased and then decreased with the increase in sintering temperature due to a transformation of phase from α-Si_3N_4 to β-Si_3N_4 initially and later governed by both grain growth and densification of elongated β-Si_3N_4[34]. Stampfl et al. studied the effect of mold surface quality on the flexural strength of Si_3N_4 and reported as 414 and 950 MPa for unpolished and polished samples, respectively[91]. Hu et al. fabricated porous yttria stabilized zirconia (YSZ) ceramics by tertbutyl alcohol based gelcasting and observed that compressive strength increases (3-27Mpa) with increasing of sintering temperature (1350^0C-1550^0C)[92].

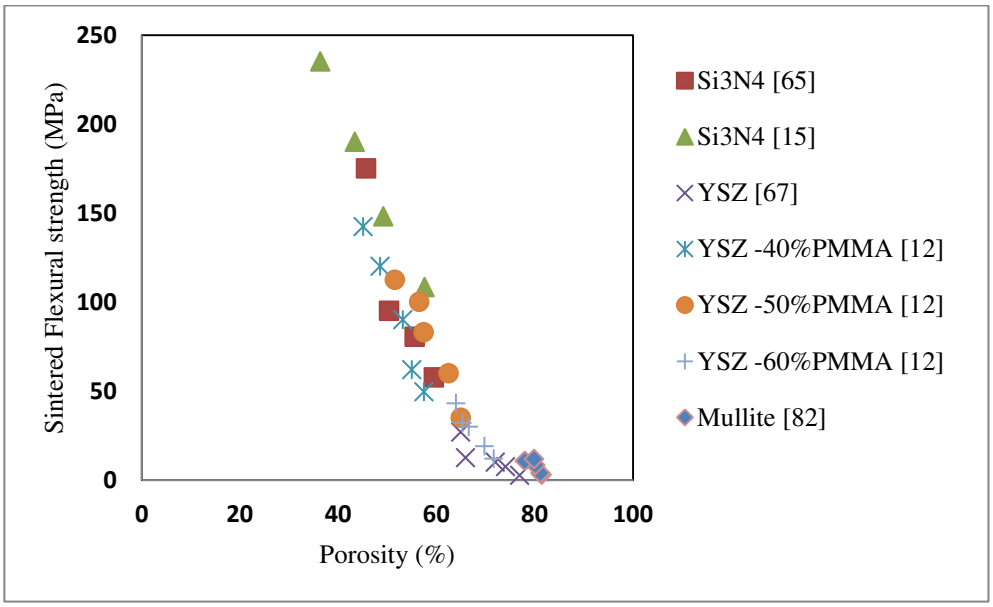

Figure 2. 2: Porosity versus sintered flexural strength from literature

Figure 2.2 is a plot of sintered flexural strength as a function of the porosity for different ceramics. [33] and [43] described that the sintered flexural strength decreased with increase in the porosity for gelcasted Si_3N_4 ceramics. The variation in the flexural strength of gel-cast Si_3N_4 possibly due to particle size and its distribution, monomers used, test condition, sample size etc.

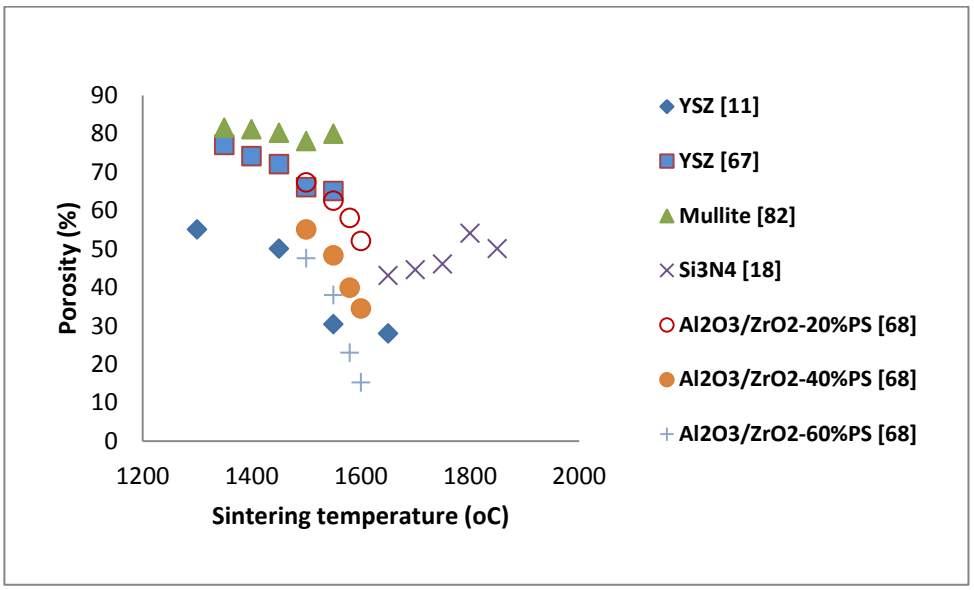

Figure 2. 3: Porosity as a function of sintering temperature for various ceramics

Figure 2.3 is a plot of porosity as a function of sintering temperature. From figure 2.3, it is evident that with the rise in sintering temperature porosity decreases. But, the porosity at first increased after that decreased as the increase in sintering temperature, which leads to phase evolution. In Si_3N_4 ceramics, the sintering process is governed by α-Si_3N_4 phase transformation into β-Si_3N_4, when the sintering temperature is in the range of 1650^0–1750^0C which leads to an increase in porosity. As the sintering temperature is >1750^0C, the phase transformation is finished and dominated by grain growth to densification, which results to decrease porosity [34, 93].

2.3.2.3. Fracture toughness

The fracture toughness of porous Si_3N_4 ceramics increased promptly as the porosity decreases, which leads to an increase in density and the growth of the elongated interlocked β-Si_3N_4 grains to facilitate crack deflection and bridging. Several authors [41, 55, 94] reported the increased fracture toughness to the increase in solid loading of suspensions.

2.3.3. Dielectric properties

2.3.3.1. Dielectric constant and loss tangent

Increasing the sintering temperature leads to a reduction in the lattice defects, the densification, and the crystallizability, this leads to an increased dielectric constant. Since the particles of the ceramic are more compact and uniform by aqueous gelcasting, they are used for mass transfer in the sintering process[95].

Porous silicon nitride ceramics were prepared using benzoic acid as blowing agent and the samples were formed with a porosity of 34.1% to 59.2%. The dielectric constant of the ceramic decreases as the porosity increases. The results show that the α-Si_3N_4 crystal phase exists in the samples while the main crystal phase of the samples is β-Si_3N_4, indicating that the α/β transformation occurs during sample preparation and the transformation is incomplete[96]. The microstructure consists of a dense matrix containing cavities with needle-like and large pores and flocculent β-Si_3N_4 grains distributed therein.

Wang et al. found that the addition of 0-15 vol% BN decreased the tangent loss of Si_3N_4 and dielectric constant ceramics[42]. Wu et al. prepared BSTM ceramic samples by

non-aqueous gelcasting have higher dielectric constant, loss tangent and more uniform than that of the dry pressed BSTM ceramics[60]. Zhou et al. prepared BNBT6 ceramic by gelcasting and the dipping pre-treatment have a more uniform microstructure and high relative density of 97% with optimal dielectric properties[97]. The microwave properties like dielectric constant (ε_r), quality factor (Q), the temperature coefficient of resonant frequency (τ_f), and microstructure of the gelcasted samples are determined with those that were die pressed. It was found that the gelcasted samples showed slightly better results than die pressed ones. This may be due to their micro structural difference[98]. Guo et al. also found that the Na + element present in the sodium salt of the polyacrylic acid entered the phase of the PZT specimen and caused a curing effect which decreased the dielectric properties but other organic dispersants have no effect on the dielectric properties[99].

The dielectric properties of ZTM ceramics [90% by weight (0.75; $ZnAl_2O_4$ - $0.25TiO_2$) - 10% by weight of $MgTiO_3$] prepared by aqueous gelcasting were studied. The ZTM ceramics prepared had the microwave dielectric constant of 12.25 while that of the dry pressed ZTM made by dry pressing was 11.77. Due to weak pores, uniform and more dense ceramics were attained by gelcasting compared to conventional dry pressure at a certain sintering temperature range [97, 98].

2.3.3.2. Electrical conductivity

Takahashi et al. proposed to combine a new process for producing electrically semiconducting alumina for the electrostatic shielding of applications by a gelcasting method and a reducing sintering process. The process is similar to the conventional gelcasting except for amounts of content of methacrylamide monomers varied to 2.83, 5.50 and 8.04% by weight, based on the weight of the slurry[100].

Luo et al reported that the electrical conductivity then remained very low below the sintering temperature of 600°C., the electrical conductivity increases quickly with the increase in the sintering temperature. The reason for this is that the parties MCMB (mesocarbon microbeads) do not form a sufficient carbon network to form electrons when the sintering temperature is below 600°C. By means of carbonization process, the carbon network can be finally formed at a higher temperature [101].

2.3.4. Thermal Properties

Aluminum nitride (AlN) ceramics were made by nonaqueous gelcasting with polyglycidyl ether of sorbitol and tetraethylenepentamine as gelling, curing and sintering agents in a nitrogen atmosphere. After sintering at 1800 ° C for 4 h, AlN ceramics were prepared with a thermal conductivity of 200 W. $(m.K)^{-1}$ [56]. AlN / CBC exhibited a flexural strength of 54 MPa and a thermal conductivity of 136 W (mK) -1, which is two and four times greater than that of the conventional material produced by the ball milling process. The AlN network at 20% by volume enhanced the thermal conductivity of AlN / CBC[102].

Chen et al. experimented AlN / CBC at sintering temperatures of 1600-1900°C, 30 MPa for 5 min by Spark plasma sintering (SPS). Large AlN grains benefit from thermal conductivity in dropping phonon diffusion[103]. Yang et al. demonstrated that an increase in sintering temperature from 1350 to 1550°C, increases the thermal conductivity increased from 0.14 to 0.35 $W.(m.K)^{-1}$ of a porous gelcasted mullite ceramics [104]. Zhou and Wang reported that porous YSZ ceramics prepared by TBA-based gelcasting with a pore-forming agent and states that as the porosity increased from 45.1% to 71.6%, the thermal conductivity of the YSZ porous ceramic was increased from 0.17 to 0.65 $W.(m.K)^{-1}$ [105].

2.4. Review of Different Methods for improving dielectric properties

Silicon nitride (Si_3N_4) ceramics are known for its high strength, fracture toughness, strength at elevated temperatures, excellent ablation resistance, and chemical resistance, which makes them suitable as radome material, but a relatively higher dielectric loss tangent and dielectric constant at elevated temperatures limits its applications as a wave transparent materials[106-108]. SiO_2 ceramics has rather low-dielectric constant, high chemical stability and extremely low coefficient of thermal conductivity and thermal expansion than Si_3N_4 ceramics[109]. However, it has the low flexural strength (less than 80 MPa), and poor rain erosion resistance, which cannot meet the requirements of radome used in high speed missiles. Compared to Si_3N_4, BN has a better thermal shock resistance and dielectric properties. In order to improve the dielectric properties of Si_3N_4 ceramics at pores and elevated temperatures or hexagonal boron nitride (h-BN) particles were introduced as second-phase dispersion into the Si_3N_4 matrix. Wu et al. reasoned the increase in sintering temperature leads to a reduction

of crystal lattice defects, crystallizability, and densification, which could result in increased dielectric constant. Because particles in the ceramics prepared by aqueous gelcasting are more uniform and compact, it is helpful for the mass transfer in the sintering process[110].

Wang et al. fabricated porous silicon nitride ceramics using Benzoic acid as a pore-forming agent, and the samples are produced with porosity from 34.1% to 59.2%. The results showed that the α-Si_3N_4 crystalline phase exists in the samples while the main crystalline phase of the samples is β-Si_3N_4, indicating that the *α/β* transformation happens during the preparation of samples and the transformation is incomplete[96]. Liu et al. prepared silicon dioxide fiber-reinforced silicon nitride matrix (SiO_2/Si_3N_4) composite by chemical vapour infiltration (CVI) process using the $SiCl_4$-NH_3-H_2 system [111]. Li *et al.* developed a process combining sol–gel infiltration-sintering and oxidation-bonding to fabricate Si_3N_4–SiO_2 ceramics. The ceramic with a porosity of 23.9% attained a Vickers hardness of 4.1GPa, the flexural strength of 120MPa, the dielectric constant of 3.80, and fracture toughness of 1.4MPam$^{1/2}$, with a tangent loss of 3.11×10^{-3} at a resonant frequency of 14GHz[112]. Recently, they also studied the effect of infiltration time on mechanical and dielectric properties.

Qi et al developed three-dimensional quartz fiber-reinforced silicon nitride composites using infiltration and pyrolysis method by polyhydridomethylsilazane[113] and perhydropolysilazane[111]. They observed the formation of silicon oxynitride in the fiber/matrix interfaces showing a high flexural strength of 114.5 MPa and a non-brittle failure behavior. Wang et al. fabricated porous silicon nitride ceramics using Benzoic acid as a pore-forming agent, and the samples are produced with porosity from 34.1% to 59.2%. The results showed that the α-Si_3N_4 crystalline phase exists in the samples while the main crystalline phase of the samples is β-Si_3N_4, indicating that the *α/β* transformation happens during the preparation of samples and the transformation is incomplete[96].

Huang et al. reported that coating of silicon nitride with oxides improved the bending strength of the sintered gelcast sample[114].Wang et al. fabricated porous Si_3N_4 ceramics with high flexural strength by pressureless sintering process without any other pore forming agents[33]. Li et al. reported the increase in sintering temperature increased the bending and the porosity initially increased and then decreased due to a phase transformation from α-Si_3N_4

to β-Si_3N_4 initially, and later dominated by both the elongated β-Si_3N_4 grain growth and the densification[34].

Yuchen et al. prepared Si_2N_2O–Si_3N_4 in situ composites by the gelcasting process, the composite attained flexural strength 230.46 ± 13.24 MPa and dielectric constant varies from 4.34 to 4.59 from room temperature to elevated temperature (1150 ^{0}C). Pei Yuchen et al (2009) prepared Si_2N_2O Si_3N_4 composites by liquid pressureless sintering process used sintering additives Yb_2O_3 and Al_2O_3 powders. The gelcasting samples were shown no critical temperature difference as well as macroscopic cracks upto 1400^{0}C. [115, 116]. Guanglei et al. fabricated porous SiO_2 -Si_3N_4 ceramic composites with high porosity and excellent mechanical properties by pressureless sintering at a relatively low temperature of 1500^{o}C using diatomite as pore forming agent. The study shows that the flexural strength and fracture toughness reaches 78.04 MPa and 1.25 MPa·m$^{1/2}$, respectively for SiO_2 -Si_3N_4 ceramic with 10% diatomite. As the porosity increases, the dielectric constant decreased from 3.65 to 2.95[117].

Liu et al. prepared Si_3N_4-BN composites fabricated through die-pressing, pyrolysis (PIP) and precursor infiltration route using borazine as the precursor. Using starch as pore forming a substance, the Si_3N_4 preform was prepared from the liquid precursor borazine. With 20 wt.% starch and drawn Si_3N_4 preform from borazine before curing the porosity, density, elastic modulus and flexural strength of the composites were 29.78%, 1.70 g.cm^{-3}, 32.45GPa, and 48.05MPa respectively. The loss tangents and dielectric constants were 0.48~3.42×10 -3 as well as 4.20~4.44 at the frequency 7~ 18GHz[118]. Feng.Y et al. prepared porous BNp/Si_3N_4 ceramics by gas pressure sintering method as a candidate wave-transparent material. Specifically, when 10% BN particles were added, the porous BNp/Si_3N_4 has the permittivity and a porosity of 20.5% and dielectric loss were 5.14 and 0.0085 respectively with a fracture toughness of 4.16 MPa.m$^{1/2}$ and bending strength of 190.1 MPa which meets the required value of wave transparent materials[119].

2.5. Review on Modelling and Multi Objective Optimization

Myong-Il Kim has developed a mathematical model to predict the influence of the drill point angle on the cutting forces in drilling with the twist drills, which was used to optimize the angle to reduce drilling forces. The effectiveness of the proposed model was verified by

comparison with published data. It was observed that the proposed model corresponded well with the experimental data and was useful for improving the performance of twist drill [120]. Juanli Yu et al. developed empirical models for the performance of Si_3N_4 porous ceramic prepared by gel casting process using an artificial neural network (ANN). The developed ANN model was used to obtain the influence of the composition on the performance of Si_3N_4 porous ceramics[121].

Garg and Tai compared the performance of MGGP with partial regression of the least squares and ANN in solving multicollinearity studies[26]. It has been observed that the ability of MGGP is to remove unnecessary variables automatically. Garg et al also compared and found that the performance of classification driven GP (C-GP) model is similar to the ANN model. The performance of the SVR model is worse than the ANN and C-GP models. June Li et al. developed empirical models of the service life, the residual stress and the surface roughness by regression analysis and optimal grinding parameters to control NSGA-II using technical applications[122].

Metin Kök et al. proposed to an empirical model for the prediction of surface roughness processing AWJ 7075 alloy Al-Al2O3 particles with the programming of gene expression (GEP). In the developed models, material properties such as the size and the weight fraction of the reinforcement and the depth of the cut particles were considered as variables in the model[123]. Jeyapaul A. et al reported on the use of the genetic algorithm and method ANOVA Taguchi to optimize the gear milling process with several performance characteristics. They have shown that several response optimization problems effectively address genetic algorithms[124].

SH Yang et al. tried two evolutionary algorithms, i.e., the differential development of the methodology and the permissive-II gene classification algorithm to determine the optimal set of parameters for multicriteria optimization problems, ie to minimize wear on the tool and the metal removal rate in the surface temperature and roughness constraints to maximize [125].

Previous literature shows that the implementation of the more gene genetic programming modeling and Pareto optimization genetic algorithm in various other processes than gelcasting. However, very little about the effects of modeling parameters reported on the

performance properties of gelcasting, namely, the flexural strength and porosity of the ceramic materials.

2.6. Gap Analysis

There is a wide variety of research carried out in the gelcasting area with different monomers, ceramic material. There is also a considerable amount of work in the processing of wave transparent materials. However, there is no much research work on the combination of this two.Hence the proposed work aims at investigating in the research of gelcasting of silicon nitride based ceramics by using different combinations of SiO_2 content, BN content, precursor amounts, solid loadings, monomers and its contents etc., and to identify the best suitable material for wave transparent applications.

Wave transparent materials are required for radomes of missiles. Based on the thorough Literature survey, the gap is identified and formulates the problem on processing and characterization of Si_3N_4 based composites using a gelcasting method by varying precursor amounts, solid loadings, monomers and its contents and to identify the best suitable material for wave transparent materials. Silicon dioxide (SiO_2) and Boron nitride (BN) powders were added to silicon nitride to improve the dielectric properties. Effect of various process parameters of gelcasting on mechanical and dielectric properties are to be studied on these Si_3N_4 based ceramic composites. A new composite of Si_3N_4, SiO_2 and BN for wave transparent applications which has got excellent properties was processed.

A very few research work has been reported on modeling and multi objective optimization for flexural strength and dielectric constant of gelcast ceramics. Hence, an attempt has been made to apply multi gene genetic programming (MGGP) and multi objective optimization of gelcasted Si_3N_4 based ceramic composites. The present work also lays emphasis on the use of a statistical tool for minimizing the number of trials involved in sample preparation with more number of variable parameters. This minimizes not only the number of trials but also minimizes the wastage of money, material and time. The present work determines the optimum processing conditions involving a conflict between maximizing flexural strength and minimizing dielectric constant using multi objective optimization.

2.7. Research Objectives

The main objective of this study is to manufacture radomes(wave transparent materials) with ceramic materials like Si_3N_4, BN and SiO_2 with best of its properties for flexural strength/ dielectric constant. The other objectives being proposed in this study are:

- To study the rheological behavior of the Si_3N_4 suspensions by varying dispersant content, pH value, solid loading, ball milling time.
- To select a suitable dispersant and its concentration to produce the maximum volume% of Si_3N_4 particles with low viscosity.
- To develop an appropriate slurry system to fabricate Si_3N_4 ceramics and Si_3N_4 based ceramics. The systems are to be tested including water, dispersant content to identify the best system in terms of low viscosity and zeta potential values.
- Gelcasting of Si_3N_4–BN and Si_3N_4–SiO_2 ceramic composites and evaluation of mechanical, dielectric properties and microstructure analysis.
- To identify the best combination of ceramic materials varying solid loadings, monomer content and the ratio of monomers, dispersant & solvents etc., on gelcasting of porous Si_3N_4 ceramics and Si_3N_4–SiO_2–BN ceramic composite.
- An attempt is made to develop empirical models for prediction of flexural strength and porosity of porous ceramics from the experimental data using multi gene genetic programming (MGGP). The existing models were then used for process optimization. A set of Trade of solutions were obtained between flexural strength and porosity as they are conflicting in nature, using multi-objective optimization by Genetic Algorithm approach to obtain the multiple optimal sets of input variables.
- MGGP developed models were used as objective functions and multi objective optimization has to perform using the non-dominated sorting genetic algorithms-II (NSGA-II).
- Non-dominated Sorting of genetic algorithms-II (NSGA-II) is also used to simultaneously optimize the conflicting objectives of Flexural strength and dielectric constant.

2.8. Work Plan

Experiments were conducted to effectively manufacture Si_3N_4 ceramic composites suitable for wave transparent application. The detailed work plan is schematically presented in Figure 2.4.

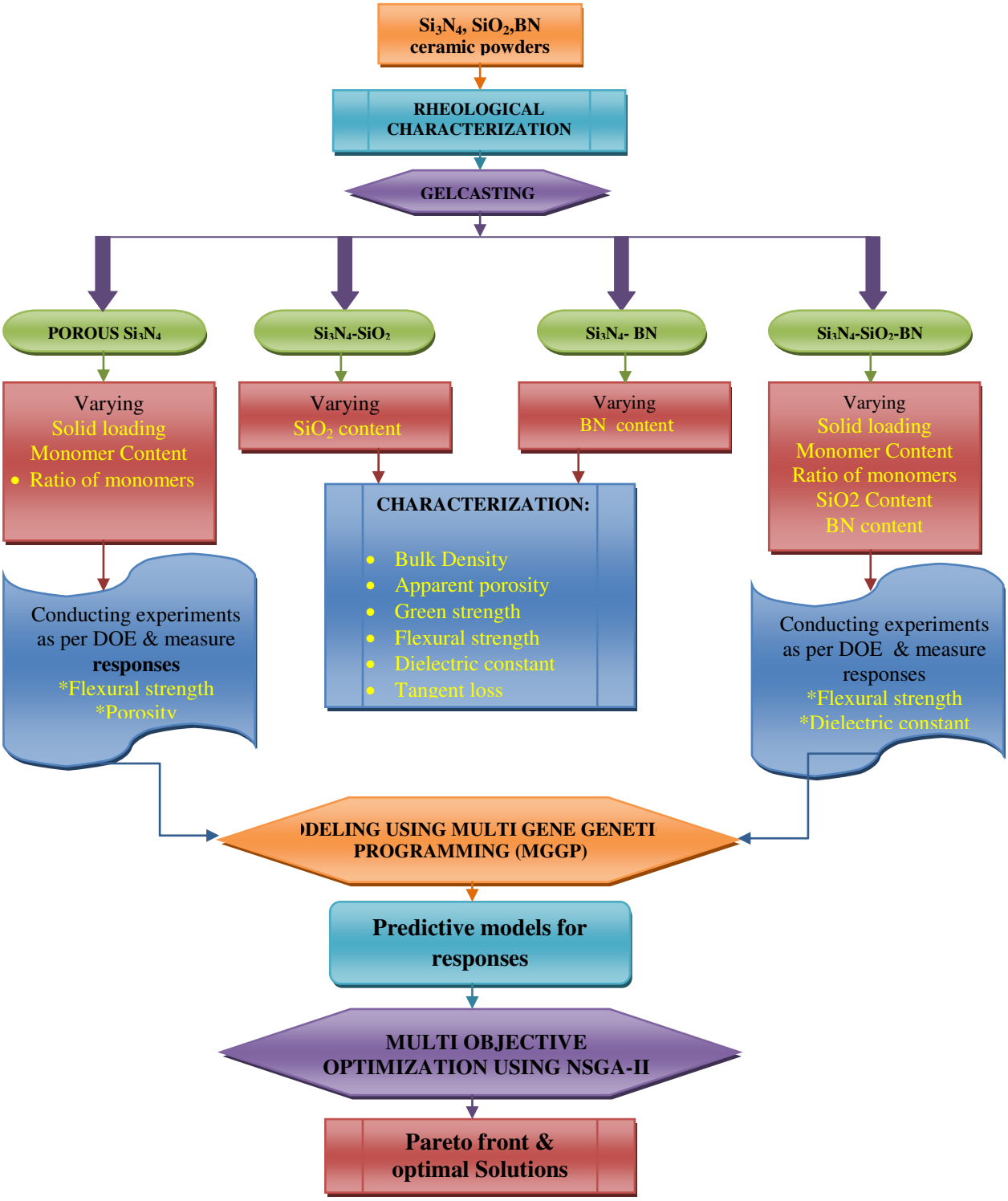

Figure 2. 4 Total Work plan

Summary

A thorough literature review is presented in this chapter dealing with a review on wave transparent materials using different processing techniques. The analysis of the influence of process parameters on structure, mechanical and dielectric properties in the gelcasting process is also discussed. In this chapter, different methods for improving dielectric properties of Si_3N_4 ceramics and also modeling and multi objective optimization were presented Finally, Literature gaps are identified and analyzed. Research objectives are projected and a work plan is developed to attain the research objectives. This research work has been investigated the influence of SiO_2 and BN on Si_3N_4 ceramic composite properties and to explore the possibility of a new composite material for near net shaped ceramic part with enhanced properties for a wave transparent application. Hence, a problem related to gelcasting of Si_3N_4, Si_3N_4–SiO_2, Si_3N_4–BN and Si_3N_4–SiO_2–BN ceramic composites is formulated to develop porous Si_3N_4 based ceramic composites.

CHAPTER 3

MATERIALS AND METHODS FOR PROCESSING OF CERAMIC GELS AND SAMPLES

3.1. Introduction

This chapter describes the details of the materials and various equipments used during processing of ceramics. The chapter provides techniques to prepare samples for phase and micro structural analysis. This chapter also provides the details of sample processing and their characterization for different silicon nitride based composites. It identifies experimentally the appropriate ceramic slurry system and processing routes of porous Si_3N_4, Si_3N_4–BN, Si_3N_4–SiO_2 and Si_3N_4–SiO_2-BN ceramic composites using gelcasting method, measurement and analysis methods for related properties. The challenges in each ceramic composite are discussed and solutions are subsequently provided through preliminary experimentation.

3.2. Materials Used

3.2.1. Silicon Nitride

Silicon nitride (Si_3N_4) ceramics are known for its high flexural strength, high fracture toughness, strength at elevated temperatures, high thermal shock resistance, excellent ablation resistance, chemical resistance and low thermal expansion coefficient, which makes the material suitable as radome material [126], but a relatively higher dielectric constant and dielectric loss tangent at elevated temperatures limits its applications as a wave transparent materials. These materials are densified with the addition of sintering aids at high temperatures under pressureless sintering conditions. Y_2O_3 and Al_2O_3 are the sintering aids most widely used for processing of Si_3N_4 ceramics. Table 3.1 shows the various ceramic materials and other additives used in the present work along with the supplier details and properties.

3.3. Slurry preparation

Slurry based systems are considered as an effective methodology to filling the mold and obtaining high green strength parts and thus the sintered parts. To attain this goal, the characterization of the ceramic materials and addition of additives to the homogeneous ceramic slurry is important. When ceramic materials, dispersants, monomers and other additives do not have the appropriate characteristics, it is difficult to get the optimum properties. The objective of the experimental study was to examine various suspension systems of Si_3N_4 ceramic and an optimal composition for the manufacture of near net shape ceramic components.

A premix solution was prepared by mixing Methacrylamide (MAM) and N, N'-Methylenebisacrylamide (MBAM) in distilled water with a dispersant. Ceramic powders and sintering aids were added to premix solution maintaining the proper solid loading of the suspensions. In order to break down agglomerates and to achieve good homogeneity the suspensions were mixed in magnetic stirrer. Hydrochloric acid and ammonia were used to adjust the pH value and measured using pH meter. The resultant suspension was deaired for 5-10 min using dessicator connected to a vacuum pump and an initiator (10wt% aqueous solution of ammonium persulfate, APS) and catalyst (tetramethylethylenediamine, TEMED) was introduced into it. Immediately, the suspension was cast into a nonporous mold and dried under controlled humidity with oven. The samples were binder burnt out and sintered in the N2 atmosphere, followed by natural cooling in High temperature Muffle furnace.

3.3.1. Rheological measurement

The viscosity of the suspensions is measured with a rotational rheometer (Physica MCR 51, Anton Paar GmbH) as shown in Figure 3.1 The configuration used for measurement is cone and plate type (41, 40 mm and 1 mm gap) and the flow measurements carried out from 0.1 to $400s^{-1}$ at 25^0C constant temperature. Concentric cylinder (CC27) attachment was also used with a gap between the inner and outer cylinder walls of 1.33mm. The measuring cup requires a sample volume of 22 ml. To prevent the adverse effect of different slurry processing methods, a homogenous fresh sample was prepared through preshearing with 100 s^{-1} for 2 min and kept stable further 3 min prior to rheological measurement. Rheometer,

which is a computer controlled apparatus with RheoPlus software and specifications were given in Table 3.2 .

Table 3. 1: Raw Materials used for processing throughout the work

S.No.	Material (Chemical Formula)	Function	Supplier	Density (g/cm^3)	Melting point (^0C)	Dielectric constant
1	Silicon Nitride(Si_3N_4)	Ceramic powder	Ube Industries, Japan, APS 0.5µm	3.44	1900	α-5.6/β-7.5
2	Alumina (Al_2O_3)	Sintering aid	Alfa aesar,USA, APS 100 nm	3.98	2072	8.5
3	Yttria (Y_2O_3)	Sintering aid	Alfa aesar,USA, APS 50 nm	5.01	2425	12
4	Silicon Dioxide (SiO_2)	additive	Sigma Aldrich,USA, APS1-5µm	2.65	1600	3.4
5	Boron Nitride (BN)	additive	Sigma Aldrich, USA, APS1µm	2.29	2973	7.1
6	Methacrylamide CH_2-$C(CH_3)CONH_2$	Monomer (MAM)	Sigma Chem. Co., USA	1.235	106-110	
7	N N'-Methabisacrylamide (MBAM) ($C_7H_{10}N_2O_2$)	Cross linker	Sigma Chem. Co., USA	1.24	>300	
9	Dolapix A 88	Dispersant	Zschimmer & Schwarz GmbH	0.95		pH-11
10	Polyethylenimine (PEI)	Dispersant	Sigma Aldrich, USA	1.030	250(bp)	pH-12
11	Distilled water	solvent				
12	Ammonium persulfate (APS) $H_8N_2O_8S_2$	Initiator	Sigma Aldrich, USA	1.982	120	
13	Tetramethylethylenediamine (TEMED) $C_6H_{16}N_2$	Catalyst	Sigma Aldrich, USA	0.775	120(b.p)	

Table 3. 2: Specifications of Rheometer

Specification	**Value**
Speed	0.01 to 1200 /min
Torque	0.2 to 75 mNm
Shear stress range	5 to 30 x 10^3 Pa
Shear rate range	0.01 to 4000 /s
Viscosity range in m pascals	1 to 10^9
Temperature range in °C	-20 to 180
Angular resolution in micro radians	2
Dimensions in millimetres	W=300, H=720, D=350

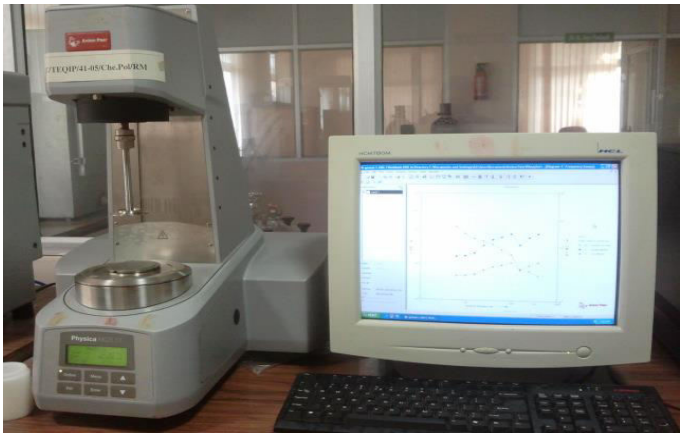

Figure 3. 1: Rotational Rheometer

3.3.2. Zeta potential

Zeta potential implies the degree of repulsion between the dispersed particles with similar charge. zeta potential is correlated to the stability of the colloidal dispersion. Highly stable suspensions can overcome van der Waals attraction and inhibit aggregation by producing strong repulsive forces between the particles. To achieve a high zeta potential for the consolidation of electro statically stabilized aqueous ceramic suspensions is important. The surface properties (and thus also the zeta potential) of the powder in suspension were controlled by the H + ions and OH^- ions adsorption on the surface. Adsorption of ions was restricted by altering the suspension pH value. On the other hand, a dispersant for controlling the surface charges of the particle by establishing an electrostatic or steric barrier effects or both. A slight variation in the pH value or the concentration of the dispersant can drastically affect the surface charge of the particles and thus provide the stability to suspension [127].

The stability of the particles in a suspension is measured by Zeta potential Analyzer (Zetasizer Nano ZS, Malvern, UK).

3.3.3. Slurry Mixing

A magnetic stirrer (REMI 5 MLH) is used for mixing the suspension to produce a stable and homogenous dispersion of ceramic powders. A DC (PMDC) motor provides high torque and retains speed constancy in the magnetic stirrer even in case of variation in volume or viscosity. The magnetic stirrer's specifications are given in Table 3.3. The pH value of all the suspensions are measured by pH meter as shown in Figure 3.2.

Figure 3.2 (a) Magnetic stirrer (b) pH meter

Table 3.3: Specifications of the Magnetic stirrer

Specification	Value
Power	500 W
Maximum stirring quantity	5 litres
Motor rating	10W
Speed range	100-1500 rpm
display resolution	1 rpm
Heating power	500W
Temperature Range	Up to 340°C maximum

3.3.4. Deairing

The suspension used in gelcasting process must be flowable in nature. The air trapped in the suspension leaves pores in the molded parts, which reduces mechanical properties and leads to defects. Thus, Deairing is carried out before casting. Excessive deairing can lead to solvent loss by evaporation and influence the properties of the suspension. After intimate mixing with a magnetic stirrer, the suspension undergoes deairing for 20 min before gelation takes place. Deairing is done using a desiccator which was connected to a vacuum pump as shown in Figure 3.3.

Figure 3. 3: Dessicator

3.3.5. Casting and Gelation reaction

Initiator and catalyst were added to the suspension before casting. The slurry was then cast into moulds as shown in Figure 3.4(a) and gelled for about 20min after casting. This allows retaining a reasonable amount of time (10 min) at ambient temperature after adding initiator and catalyst to the suspension for deairing and molding filling. This prevents premature gelation, which destroys the usefulness of the slurry. After gelation, few samples were cut in green state as shown in Figure 3.4(b).

Figure 3. 4: (a) Moulds and (b) samples cutting after gelation process

3.3.6. Drying

In gelcasting process, the green sample is produced without removal of the liquid phase of the suspension after polymer gel reaction. In other words, the wet gelcasted bodies contain almost as much water as the initial suspension. This water must be removed by a consequent drying phase, which is the most important in the gelcasting process. The gelled wet body was detached from the mold after gelation. Drying should be conducted out under a well controlled temperature and humidity using Controlled Humidity Oven (Thermospectrum Instruments Pvt. Ltd, India) shown in Figure 3.5. Gelcast green bodies were first dried under high moisture: 90% RH and 40 ° C in the ambient chamber to remove 40 to 50% water content. From there, the humidity was reduced to 30% relative humidity, and the temperature rose to 90^0C to accelerate drying. The specifications of humidity oven are given in Table 3.4.

Table 3. 4: Specifications of Controlled-Humidity Oven

Specification	**Value**
Temperature range	10 to 90°C
Humidity range	25 to 95% RH
Accuracy	±0.1°C or ±2% RH
Resolution	0.1 °C or 1% RH
Controller	PID control Microprocessor
Temperature sensor	PT – 100
RH sensor	Direct capacitance type

Figure 3. 5: Controlled-Humidity Oven

3.3.7. Binder burnout and sintering

Subsequent to drying, the samples were dealt in a traditional way. The organic monomers (MAM & MBAM) content is only approximately 5-15 wt% of the silicon nitride powder. The binder was removed in a separate step or conducted out immediately in a sintering furnace. The samples are sintered in a High-Temperature Tube Furnace (Bionics Scientific Technologies, New Delhi) (Figure 3.6) connected with an N_2 cylinder for gas purging. The specifications of the furnace are given in Table 3.5. The Sintering atmosphere was N_2 gas. The heating and cooling cycles were instructed by means of the PID controller in the furnace. The cooling phase was done naturally inside the furnace.

Table 3. 5: Specifications of High-Temperature Muffle Furnace

Specification	**Value**
Model	**BST/MF/1800**
Maximum Temperature	1800°C
Working Temperature	1700°C
Heating Element	($MoSi_2$) Molybdenum di Silicide
Temperature Accuracy	+/- 1°C

Temperature Controller	PID controller
External Chamber Construction	304 Grade Stainless Steel
Internal Chamber Construction	Ceramic Refractory Chamber of size 200x200x100 mm^3
Power Supply	220 / 440 Volts

Figure 3. 6: High-Temperature Muffle Furnace

3.4. Property Characterization

3.4.1. Relative density and porosity measurement

The density of all samples was measured using Archimedes principle. First, the weight of the dry sample (W_1) was measured by means of weighing balance (accuracy of 0.1 mg), before it was immersed in water in vacuum for 5 min. After that suspended weight of the sample (W_2) was measured. Finally, wet weight of the sample was measured ($W_{3)}$ after removing from water and covered with a tissue paper for 1 min to remove residue of water on the surface. This method was repeated to ensure reliability of weighing. Then porosity and bulk density was calculated using measured values as described in ASTM Standard C914 – 09 using equations 3.1, 3.2 and 3.3..

$$True\ volume\ of\ the\ sample = \frac{W_{1-}\ W_2}{\rho_w} \qquad (3.1)$$

$$Bulk\ density\ of\ the\ sample = \frac{W_1\rho_w}{W_3 - W_2} \qquad (3.2)$$

$$open\ porosity = \frac{W_3 - W_1}{W_3 - W_2} \qquad (3.3)$$

Where, W_3 is saturated weight of the sample, W_2 is suspended weight of the sample and W_1 is dry weight of the sample.

3.4.2. Linear Shrinkage Measurement

The determination of linear shrinkage before and after sintering was performed by measuring the change in dimensions of the specimen before (l_0) and after sintering (l) and dividing by the initial diameter as in equation 3.4. The dimensions were measured by digital vernier callipers of least count of 0.01 mm.

$$Shrinkage = \frac{l_0 - l}{l} x\ 100 \qquad (3.4)$$

3.4.3. Mechanical properties

3.4.3.1. Preparation of samples for mechanical testing

For mechanical testing, the large gelcasted sintered samples were cut by Diamond saw into rectangular bars of dimensions 3mm x 4mm x 40mm and re-machined until they met fineness requirement. High-speed diamond cut-off saw Preparing samples for three point bending test is very tiresome and difficulty job. A few samples were broken at some point during cutting into small test samples. However, at the end an adequate number of test samples were acquired. The cut samples were then grinded and polished using 240, 600, 800 and 1200 grits SiC paper simultaneously to obtain a plain surface on the sample.

Figure 3. 7: High-speed diamond cut-off saw

3.4.3.2. Flexural strength measurement

The gelcasted samples were cut into small bars in sizes 3 x 4 x 45 mm in according with ASTMC1161-94 for a three point bending test according to ASTM (C1161-94) standard. For the flexural strength of sintered test specimen was measured universal testing machine (Dak systems, Bangalore) with a load cell of 1 kN. The span length and crosshead speed were 20 mm and 0.05 mm min^{-1} respectively. All corners and edges of the samples were beveled with SiC abrasive paper, to avoid stress concentration. The flexural strength was calculated from the following equation 3.5.

$$flexural\ strength = \frac{3PL}{2WD^2} \qquad (3.5)$$

Where P = maximum load; L = Span length; W = width of the sample; D = depth or thickness of the sample.

Table 3. 6: Universal Testing Machine Specifications

Specifications	Value
Capacity in KN	50
Clearance between columns in mm	1000
Load cells in KN	10, 5, 2.5, 1, 0.5, 0.25, 0.1, 0.05, 0.01, 0.005
Maximum crosshead Travel in mm	1100

Maximum speed at capacity in mm/min	500
Testing speed Range in mm/min	0.001 to 1000
Capacity at Maximum speed in KN	5
Jog speed in mm/min	0.001 to 1000
Return speed in mm/min	0.001 to 750

Figure 3. 8: Universal Testing Machine

3.4.4. Dielectric constant

The dielectric constant (ε) is described as the ratio of amount of capacitance of a capacitor packed with a dielectric material to amount of capacitance of identical capacitor measured with vacuum as a dielectric means. The dielectric constant depends on the frequency and the range of optical frequency. Electronic polarization is the main contribution due to the orientation of polarizations and cannot react to this time scale. At lower frequencies, where the devices (of the order of several hundreds of MHz) are actuated, the three polarizations will be a factor to the dielectric constant (ε). The value ε is correlated to the polarizability, and number of chemical bonds in a material. Therefore, ε depends strongly on chemical structure and density [128]. The dielectric constant of gelcasted sintered ceramic > 1 mm thickness was measured by an impedance analyzer (MTZ-35, Biologic Sciences

Instruments Pvt. Ltd., France), as shown in the Figure 3.9, in the frequency range of 50 Hz to 35 MHz.

Figure 3. 9: Impedance Analyzer set up

3.4.5. X-ray Diffraction

The analytical method used to characterize the ceramic powders and sintered samples was X-ray diffraction (XRD). The diffraction patterns were measured using a X-ray Diffractometer (Panalytical X'Pert powder, Netherlands), as shown in Figure 3.16. The purity of the phases was determined by X-ray diffraction with a Cu Ka-radiation operating at 10-15 kV and 20 mA. All measurements were performed using a 0.020 progressive scan in 2-regime recording from 10 to 80^0 for 30 minutes. comparison of identified patterns with the X'Pert high-score software patterns were performed by ICDD (International Centre for Diffraction Data) data files.

Figure 3. 10: XRD Machine

3.4.6. Scanning Electron Microscopy (SEM) observations

The morphology of as received ceramic powders and microstructure of gelcasted specimens were examined by Scanning Electron Microscope (VEGA3, Tescan,Czech Republic) as shown in Figure 3.11. All samples were sputtered using a Au/Pd for a minimum of 50 seconds target to ensure high conductivity during the electron microscopy and secured to an SEM stub using carbon tape prior to imaging. Operating voltage used in SEM was between 10-20kv.

Figure 3. 11: Scanning electron Microscopy machine

3.5. Processing of porous Si_3N_4 ceramics

3.5.1. Pilot Experimentation

Through pilot experiments, 0.8 wt% of Dolapix A88 was found to be highly effective dispersant[129]. From the literature review, the sintering temperature for the gelcasting of porous silicon nitride ceramics was chosen as 1700^0C after the selection of the proper dispersant. Preliminary experimentation ware conducted to determine suitable ranges for the processing parameters. From the pilot experimentation, the amount of solid loading was varied from 30 to 60 vol%, the monomer content is varied between 5 and 20 wt% relative to the amount of solid loading while the ratio of monomers varied from 1:5 to 1:20. Preliminary experiments indicates the damage to green ceramic bodies occurred because of adding 1.5 wt% of polymerization initiator as shown in the Figure 3.12. The amount of APS (initiator) and TEMED (catalyst) were chosen as 1wt% of monomer content and 0.8 % of monomer content respectively.

Drying was carried out under controlled humidity and temperature. It has been determined that the drying operation is carried out in two steps: first at high humidity (90% RH) and low temperature (40°C) in the first few hours, it is necessary to prevent the cracking of the samples. The second phase of the process begins at the time when water content of 25-30% was removed. Then, the temperature can be increased to 80 to 100°C, and humidity at 30% RH is lowered to accelerate this until process fill the end of drying operation. Thus, the total drying time can be reduced to one third of the time required under constant conditions.

Figure 3. 12: Images of damaged samples

3.5.2. Rheological measurement

This technique involves looking at the viscosity of a suspension as a function of added amount of Dolapix A88 and Si_3N_4 powder (35 Vol%), Distilled water and varying amounts of Dolapix a88 (ranging from 0.3wt% to 1.0 wt%, based on dry Si_3N_4 powder) were milled with alumina media. In a Planetary Mill (Retsch PM 100, GmbH, Germany) at 120rpm for 1 hour. The milling jar is made out of alumina. After milling, the pH values were checked and adjusted to 10.5 using ammonium hydroxide. The flow measurements were performed with shear rate between 0.1 and 400 s^{-1} at room temperature (25^0C). Bubbles were removed by slowly stirring the suspension before the viscosity measurements were carried out. To prevent the adverse effect of different slurry processing methods, a homogenous fresh sample was prepared through preshearing with 100 s^{-1} for 2 min and kept stable further for 3 min prior to rheological measurement.

3.5.3. Zeta potential Measurement

In the experimentation explained below, dilute ceramic suspensions with a 0.05 wt% concentration were prepared and dispersant was added. Silicon Nitride along with sintering additives Y_2O_3 and Al_2O_3 are milled in a planetary ball mill and termed as a mixed powder. A suspension was made at 25 vol% solid loading. The suspension was aged for 24 hrs with stirring. 2 ml of above suspension was then diluted to 1000 ml to give a final working solution with a solid loading of 0.05% for analysis. The zeta potential value of the as-received Silicon Nitride particles, mixed powder and mixed powder in the presence of dispersant by varying pH value was measured using Zeta Potential Analyzer (Zetasizer Nano ZS, Malvern, UK) to estimate the effect of dispersant on the surface charges present. The pH levels of the suspensions were adjusted to the preferred value. To adjust the pH value, hydrochloric acid and sodium hydroxide solutions were used and the zeta potential was determined as a function of pH. The suspension was ultrasonically dispersed for five minutes before measurements to improve dispersion and to remove small air bubbles, which possibly will influence the accuracy of the measurements.

3.5.4. Experimental design

As discussed in the literature review, a large number of variables are involved in the gelcasting process and virtually all these variables affect the performance characteristics, considering all of them for steady will result in unmanageable work. Therefore, only major and important control processes parameters such as solid loading, monomer content and ratio of monomers were considered in this study. Experimental design comprises of determining the factors, their levels and performance characteristics on which the factors influences and lastly type of design. From the preliminary experimentation, three factors namely, solids loading of silicon nitride powder, monomer content and ratio of monomers are considered for measuring the performance characteristics of ceramic composite. Two performance characteristics nearly flexural strength and porosity are measured. Table 3.7 shows different levels of the parameters used in the experiment and the same data were used in further modeling runs.

Table 3. 7: Gelcasting parameters and their level used in experimentation

Variables	**Notation**	**Levels**			
		1	**2**	**3**	**4**
Solid Loading (Vol%)	x_1	30	40	50	60
Monomer content (wt%)	x_2	5	10	15	20
Ratio of monomers	x_3	1:5	1:10	1:15	1:20

3.5.5. Experimental Procedure

A solution of premixed monomer was prepared using 5- 20 wt% of monomers dissolving in distilled water. The linear monomer used is Methacrylamide (MAM) made by Sigma Aldrich Chemie, Germany and N, N'-Methylenebisacrylamide (MBAM) (Sigma Aldrich Chemie, Germany) The ratio of Methacrylamide to the N,N- Methylenebisacrylamide is ranged from 3:1 to 10:1. Silicon nitride along with alumina and yttrium oxide were used as sintering aids which are dispersed in a premix solution to obtain a suspension with powder

solid loading of 30 - 60 vol% using a magnetic stirrer. Each experiment contains 3wt% of Y_2O_3 and 2wt% of Al_2O_3 as sintering aids. Dolapix A88 (Zschimmer & Schwarz, Germany), being used as stabilize ceramic particles in each experiment. Ammonium persulfate (APS, 99.99%, Aldrich) and tetramethylethylenediamine (TEMED, 99%, Aldrich) were added to the suspension as a catalyst and an initiator, respectively.

The ceramic suspensions were mixed for 6 h earlier to the addition of initiator and catalyst. 5 wt% water solution of APS was added to the suspension. The APS solution was always prepared as and when we use such that the pH of the solution was around 11 [129]. TEMED is also used as a 5 vol% water solution for dilution. A flow chart of the gel-casting process is shown in Figure 3.13. Thus the aim of ceramic powder after formulation gel was cast into nonporous molds and dried the samples under controlled humidity till burnout of binder, which is carried out at 550^{o}C for 2 h, with a heating rate of 20 ^{o}C/min. The samples were further sintered at temperature of 17000C for 2h in Nitrogen atmosphere, followed by cooling cycle as shown in Figure 3.14. Various suspensions prepared throughout the work along with processing conditions and supplier details are tabulated in Table 3.8.

Two performance characteristics are measured, namely the flexural strength and porosity as described in section 3.4.3.2. Flexural strength was measured using three point bending test on specimens of 40 mm x 4 mm x 3 mm using a three-point bend fixture with a span of 35 mm and a crosshead speed of 0.5 mm/min. Porosity was determined by the Archimedes technique by means of distilled water as the medium as described in section 3.4.1..

Table 3. 8: Gelcasting Suspensions made throughout the work

Slurry	SN	SNS	SNB	SNSB
Material make up	90wt% Si_3N_4 6wt% Y_2O_3 4wt% Al_2O_3	80-95 vol% Si_3N_4 0-15 vol% SiO_2 3vol% Y_2O_3 2vol% Al_2O_3	80-95vol% s Si_3N_4 0-15 vol% BN 3vol% Y_2O_3 2vol% Al_2O_3	75-90vol Si_3N_4 0-10vol% BN 0-10vol% SiO_2 3vol% Y_2O_3 2vol% Al2 O3
Supplier	Denka Kogaku,Japan,d50~4.2µm Alfa Aesar USA(APS 50nm) Alfa Aesar USA (APS100nm)	Denka Kogaku,Japan,d50~4.2µm S5631,sigma Aldrich, ~99% 0.5-10µm Alfa Aesar USA(APS 50nm) Alfa Aesar USA (APS100nm)	SNE10 Ube Indus tries Ltd Japan 255475 sigma aldrich Co. ~1µm,98% Alfa Aesar USA(APS 50nm) Alfa Aesar USA (APS100nm)	SNE10 Ube Indus tries Ltd Japan 255475 sigma aldrich Co. ~1µm,98% S5631,sigma Aldrich, ~99% 0.5-10µm Alfa Aesar USA(APS 50nm) Alfa Aesar USA (APS100nm)
Solid loading	30-60	50	40	30-40
Dispersant	Dolapix A88 0.8wt% of S.L	Dolapix A88 0.8wt	Polyethylene mine (PEI) 1wt%	Polyethylene mine 1wt%
Monomer canter (MAM+MBAM)	5-20wt%	10wt%	10wt%	5-15wt%
Ratio of Monomers(MBAM:MAM)	(1:5 to 1:20)	1:10	1:10	1.5 to 1:15
Others		0-15vol% Silicon dioxide	0-15VOL% BN	0-10vol% SiO2 0-15vol% Bal
APS	0.8wt%	1wt% MC	1wt% MC	0.8wt% MC
TEMED	2-3 drops	1wt% M.C	1wt% M.C	2-3 drops
Binder burnt out & Sintering Condition	500^0c 2hr 1700^0c 2hr N atom	550^0c 2hr (2^0c/min 1550^0c 2hr N2	550^0c 2hr 1700^0c 2hr N2	550^0c 2hr 1550^0c 2hrs N2

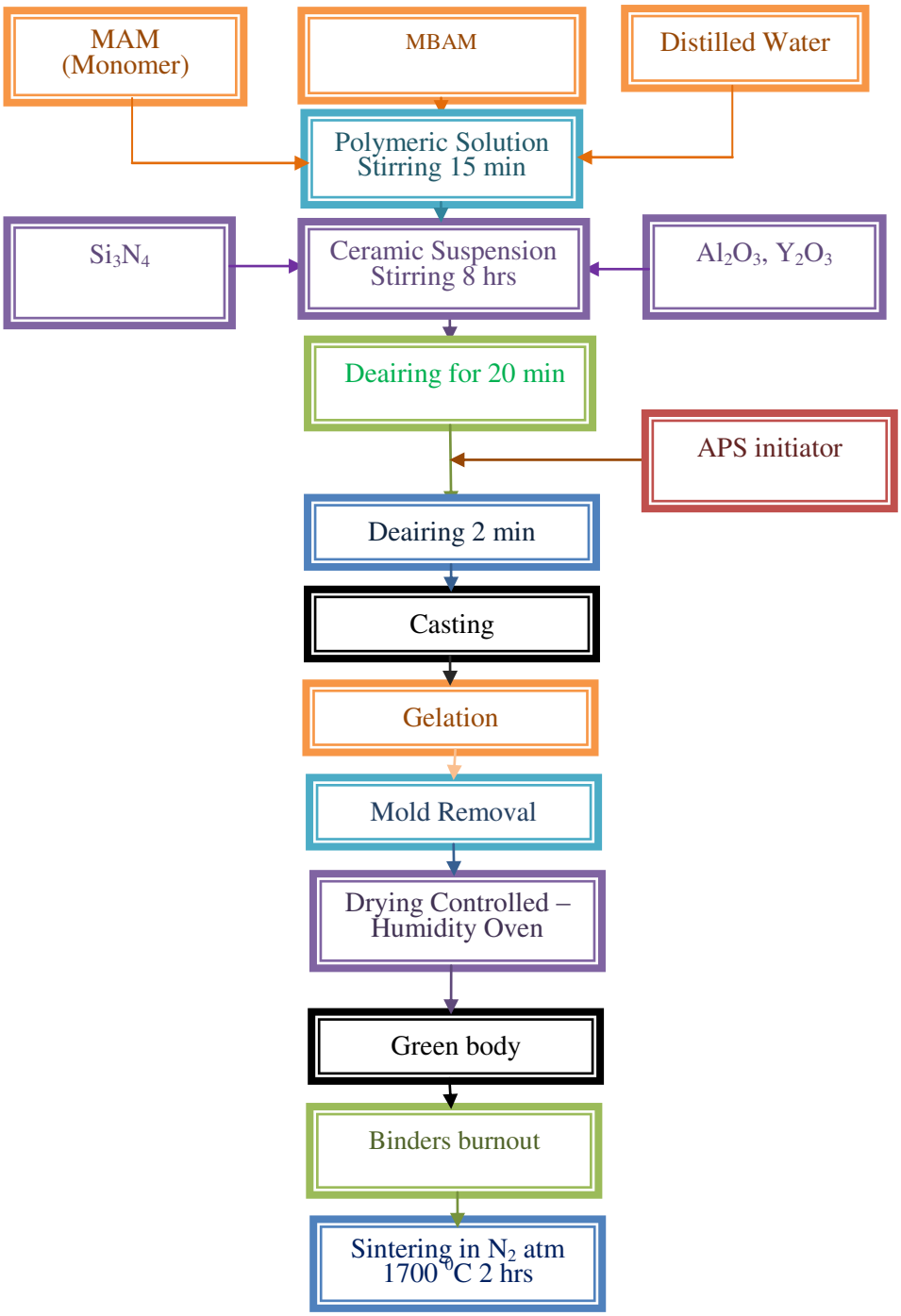

Figure 3. 13: Gelcasting procedure

Table 3. 9: Fixed parameters used in the experimentation

S. No.	Material	Amount
1	Al_2O_3 (aluminium Oxide)	2 vol% of solid loading
2	Y_2O_3(Yttrium Oxide)	3vol % of solid loading
3	DISPERSANT (Dolapix A 88)	0.8 wt% of solid loading
4	APS	0.8wt% of monomer content
5	TEMED	1 wt% of monomer content

Three input process parameters: solid loading (x_1), Monomer content (x_2), and Ratio of monomers (x_3), having values at four levels were considered. The fixed conditions in which the experiments are performed are shown in Table 3.9. The values were established on the basis of detailed preliminary tests. The experiments were carried out according to Table 3.10. The Flexural strength and the porosity measured for each experiment and discussed in detail in next chapter.

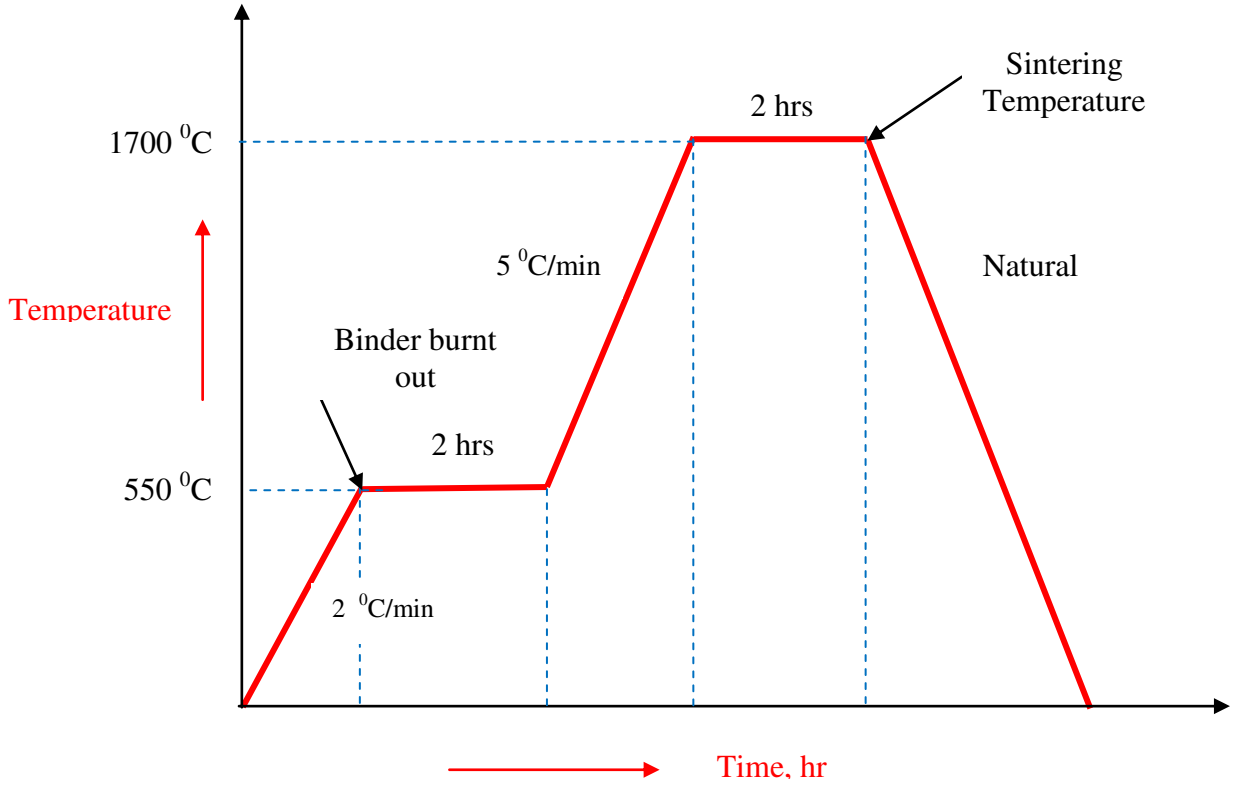

Figure 3. 14: Graphical representation of sintering for all green gelcast samples

Table 3. 10: List of experimental details with performance values

	Input parameters			**Output parameters**	
S.No	Solid Loading (Vol%) (x_1)	Monomer Content (wt%) (x_2)	Ratio of monomers (x_3)	Flexural strength (M.Pa)	Porosity (%)
1	30	5	0.2	85.69	43.75
2	30	10	0.1	82.16	42.23
3	30	15	0.067	114.43	38.29
4	30	20	0.05	123.89	36.29
5	40	5	0.1	116.74	38.84
6	40	10	0.067	159.74	33.21
7	40	15	0.05	150.72	34.28
8	40	20	0.2	74.82	41.23
9	50	5	0.067	149.51	35.24
10	50	10	0.05	174.39	34.92
11	50	15	0.2	139.71	40.11
12	50	20	0.1	85.69	40.15
13	60	5	0.05	92.82	40.85
14	60	10	0.2	57.40	44.28
15	60	15	0.1	55.27	45.96
16	60	20	0.067	54.86	43.68

From the Table 3.10, experiment number 13, 14, 15 and 16 had given a difficulty because of the high solid loading. The suspensions of these experiments were high viscous and observed agglomerations, which may be the reason for less flexural strength.

3.6. Processing of Si_3N_4-SiO_2 ceramic composites

3.6.1.Preliminary Experiments

From the pilot experimentation, we found that 0.8 wt% of Dolapix A 88 is an effective dispersant with low viscosity and high solid loading same as processing of Si_3N_4 ceramics. Trails were carried out to investigate the sintering temperature required for Si_3N_4-SiO_2 ceramics composites and we also experienced that, the final sintering temperature was modified and examined at 1500^oC. A Si_3N_4-SiO_2 sample was failed at 1600 ^oC sintering such as shown in Figure 3.15 (a) and Figure 3.15 (b) shows a photograph of samples that are to be sintered in muffle furnace.

Figure 3. 15: (a) Damaged Samples (b) Samples before sintering

3.6.2. Experimental Procedure

All samples used in this experiment were fabricated by gelcasting from Si_3N_4 and SiO_2.Premix solution was prepared by mixing Methacrylamide (MAM) and N, N'-Methylenebisacrylamide (MBAM) in distilled water with a 0.8 wt% of Dolapix A88 [130]. The premixed aqueous solution contained 10 wt.% monomer content, and the MAM to MBAM ratio were set as 5:1. Ceramic powders were added to premix solution maintaining the solid loading of the suspensions as 50 vol%. The fixed conditions in which the experiments are performed are shown in Table 3.11. The Material Code are listed in Table 3.12, S0 ,S5, S10, and S15 denote the SiO_2 is added 0vol. %, 5vol. %, 10vol. % and 15vol. %. In each experiment

3% of Y_2O_3 and 2% of Al_2O_3 were used as sintering aids. Hydrochloric acid and ammonia were used to adjust the pH value to approximately 10.5. The resultant suspension was de-aired for 5-10 min and an initiator (10 wt% aqueous solution of ammonium persulfate, APS) and catalyst (tetramethylethylenediamine, TEMED) is introduced into it. Immediately, the suspension was cast into a nonporous mold and dried under controlled humidity. For the binder burnout a temperature of 550^0C was chosen, with a heating rate of 2^0 C/min for 2 h and then, the samples were sintered at 1500 ^{0}C for 2h in the N_2 atmosphere, followed by natural cooling. Gelcasted components of a variety of shapes and sizes were fabricated as shown in the Figure 3.16(a). Figure 3.16 (b) shows a green radome after gelcasting process.

Table 3. 11: Fixed conditions of the gelcasting of Si_3N_4-SiO_2 ceramics composites

S. No.	Material	Amount
1	Solid Loading	= 50vol%
2	Monomer Content(MAM+MBAM)	= 10wt% of Solid loading.
3	Ratio of Monomers (MBAM: MAM)	= 1:5
4	Dispersant (Dolapix A88)	= 0.8 wt% of Solid Loading
5	APS(initiator)	= 1wt% of Monomer Content
6	TEMED	= 1 wt% of monomer content

Figure 3. 16: (a) Typical shaped samples (b) A green radome after gelation in the mould.

3.6.3. Characterization

The bulk densities of green and sintered ceramic samples were determined by Archimedes displacement method and XRD; Rigaku, D/max2550HB +/PC is used for determining the composition of sintered samples and SEM; JEOL, JSM-6460LV is used for the study of the microstructure. In order to determine flexural strength of the samples, the three-point bending test at room temperature was carried out following the ASTM D-143 (1996) standard on the specimen with dimensions of 40mm×4mm×3 mm at a crosshead speed of 0.5 mm/min on an Electronic Universal Testing Machine (Dak Systems, India. The loss tangent and dielectric constant are measured using an impedance analyzer (MTZ-35, Biologic Science Instruments, France) in the frequency range of 0.1~35 MHz.

Table 3. 12: The Composition Ratio of Si_3N_4-SiO_2 ceramic composites

Sample codes	Si_3N_4 (vol%)	SiO_2 (vol%)	Y_2O_3 (vol%)	Al_2O_3 (vol%)
S0	95	0	3	2
S5	90	5	3	2
S10	85	10	3	2
S15	80	15	3	2

3.7. Processing of Si_3N_4-BN ceramic composites

3.7.1. Preliminary Experimentation

From the preliminary experimental work, it was observed that the gelcasting of Si_3N_4/BN ceramic composite with Dolapix A 88 as dispersant lost its flowability and became inconvenient for gelcasting. Many kinds of literature on the colloidal process of Si_3N_4 are available [131, 132] but the colloidal process of Si_3N_4/BN composites has not been reported much. The addition of BN content decreased the slurry fluidity and increased the viscosity of the slurry. The reason for the decrease of slurry fluidity with BN content addition is specific surface area of flake BN was larger, so more water was needed to wet the particle surface when more BN were added[133]. On the other hand, The low surface energy of BN is a major drawback for its use in aqueous media, because it is not easily dispersed[134]. Thus, Polyethylenimine (PEI) a strongly cationic branched polymer was used as the dispersant [135] [136]. Si_3N_4/BN suspension is a complex system in which many factors have significant effect

on its rheological behaviors such as pH value, dispersant and its content, solid loading etc.,. From the preliminary experimentation, 1 wt% of dispersant was used to prepare a Si_3N_4–BN aqueous suspension with a high solid loading and low viscosity.

3.7.2. Rheological properties measurement

A Rotational rheometer (Physica MCR 51, Antonpaar GmbH) was used to evaluate the rheological behavior of the Si_3N_4– BN suspensions at room temperature. In order to avoid the undesirable effect of various mechanical histories, the fresh samples were homogenized before measurement by an identical shear rate of 100 $s^{-1}$for 2 min and left standing for an additional 3 min. The measuring configuration implemented was a cone and plate (4^0, 40 mm, and gap 1 mm), and the flow measurements were performed from 0.1 to 400 s^{-1} at a constant temperature 25^0C. Prior to carrying out the measurement of viscosity, bubbles were removed from the suspensions by slow speed stirring. The effects of concentration of PEI, pH value on the dispersion of Si_3N_4 and BN in water, and rheological behavior of Si_3N_4–BN aqueous suspensions were discussed in detail in next chapter.

3.7.3. Zeta potential measurement

Initially, the dispersion of Si_3N_4 and BN ceramic powders in water was examined by measurement of zeta potential. Zeta potential of Si_3N_4 and BN in PEI dispersant were measured as a function of pH. To produce slurries, powders were mixed with various amounts of PEI (0.4–1.5wt.%) as a dispersant. The pH of slurries was also set 10. To investigate the effect of pH on Si_3N_4–BN suspension properties, slurries with were prepared. To adjust the pH value of the suspension, hydrochloric acid and sodium hydroxide solutions were used. Zeta potential measurements of Si_3N_4 and BN in the presence of PEI were carried out separately as a function of pH (in the range of 2 –12) through the Zeta potential analyzer (Zetasizer Nano ZS, Malvern, UK) using very dilute suspensions (0.01 vol%). The ionic strength was altered with 0.001M KCl solutions.

3.7.4. Experimental procedure

Processing of Si_3N_4-BN ceramic composite procedure is based on the proposed procedure presented in the previous section 3.6.2., except the SiO_2 content was replaced by BN ceramicpowder. Fixed conditions of the gelcasting of Si_3N_4-BN ceramics composites were taken from Table 3.13. The sample codes are presented in Table 3.14. SB0 SB5 SB10, and SB15 represents the BN ceramic powder is added in 0vol.%, 5vol.%, 10vol.% and 15vol%, respectively. These samples have been sintered at the temperature of 1700^0C for 2 hours in N_2 atmosphere, followed by natural cooling. The characterization of samples was also same as the previous section 3.6.3.

Table 3. 13: Fixed conditions of the gelcasting of Si_3N_4-BN ceramics composites

S. No.	Material	Amount
1	Solid Loading	= 40vol%
2	Monomer Content(MAM+MBAM)	= 10wt% of Solid loading.
3	Ratio of Monomers (MBAM: MAM)	= 1:5
4	Dispersant (Polyethylenimine)	= 1 wt% of Solid Loading
5	APS(initiator)	= 1wt% of Monomer Content
6	TEMED	= 1 wt% of monomer content

Table 3. 14: The Composition Ratio of Si_3N_4-BN ceramic composites

Sample codes	Si_3N_4 (vol%)	BN (vol%)	Y_2O_3 (vol%)	Al_2O_3 (vol%)
SB0	95	0	3	2
SB5	90	5	3	2
SB10	85	10	3	2
SB15	80	15	3	2

3.8. Processing of Si_3N_4-SiO_2-BN ceramic composites

Compared to Si_3N_4, BN has a better thermal shock resistance and dielectric properties. SiO_2 has a dielectric constant and dielectric tangent losses even lower, which makes silica widely used as wave transparent materials. Therefore, Si_3N_4-SiO_2-BN ceramic composites can combine the advantages of individual phases of Si_3N_4, BN and SiO_2 and have better dielectric and mechanical properties, which have been considered as capable materials for wave transparent applications. However, it has been proven that addition of SiO_2 into Si_3N_4 and also BN into Si_3N_4 could significantly decrease the dielectric constant of the materials. This research work has been investigated the influence of SiO_2 and BN on Si_3N_4 ceramic composite properties and to explore the possibility of a new composite material for near net shaped ceramic part with enhanced properties for a wave transparent application.

3.8.1. Preliminary Experiments

It was observed from preliminary experimental work that the gelcasting of Si_3N_4-SiO_2-BN with Polyethylenimine (PEI) as dispersant has lost its ability to flow and became tiresome for gelcasting above 42 vol% of solids loading. As a result, levels of solid loading parameter 30-40 vol% were chosen. It was also observed that the excess amount of monomer content causes serious problems in mixing of the suspension and leads to poor homogeneity. Also the slurry was not suitable for casting due to its high viscosity. Therefore, the limit for monomer content was chosen as 15 wt% of ceramic powders. Preliminary experimentation was done to determine suitable ranges for the processing input parameters. All of the Si_3N_4-SiO_2-BN samples were sintered at a maximum temperature of 1550^{o}C in Nitrogen atmosphere.

3.8.2. Experimental design

Preliminary experimentation was carried out to determine suitable ranges for the gelcasting of the Si_3N_4-SiO_2-BN ceramic composite. The amount of BN and SiO_2 varied from 0 to 10 wt% relative to the amount of solid loading used, the monomer content varied between 5 and 15 wt% and the ratio of monomers from 1:5 to 1:15,while the solid loading is varied from 30 to 40 vol%. The upper limit of the solid loading was restricted to 40 vol% because of high viscosity due to the addition of BN content. In addition the upper and lower limits of monomer content and ratio of monomers were selected in order to ensure the

solubility of monomers in the solution. Table 3.15 shows the gelcasting parameters and their levels used in the experimentation.

Table 3. 15 Gelcasting parameters and their level used in experimentation

Factors	**Levels**	**Responses**
Solid Loading(vol%) (x1)	30	Flexural Strength
	35	
	40	
Monomer Content (wt%) (x2)	5	
	10	
	15	
Ratio of Monomers (x3)	1:5	
	1:10	
	1:15	
SiO_2 Content (vol%) (x4)	0	Dielectric Constant
	5	
	10	
BN Content (vol%) (x5)	0	
	5	
	10	

3.8.3. Materials Used

Commercially available Si_3N_4, SiO_2 and BN ceramic powders are used in this study. Distilled water is used as a solvent. Commercially available dispersant Polyethylenimine (PEI) is used as dispersant for dispersing ceramic particles in slurries with high solid loading and low viscosity. In this work, Methacrylamide and N,N^{l}- Methylenebisacrylamide are used as the monomer and cross-linker respectively. Ammonium persulfate (APS) and N,N,*N′*,*N′*-Tetramethylethylenediamine (TEMED) are used as the initiator and catalyst. Fixed parameters used in the experimentation were tabulated in Table 3.16.

Table 3. 16: Fixed parameters used in the experimentation

S. No.	Material	Amount
1	Al_2O_3 (aluminium Oxide)	3 vol% of solid loading
2	Y_2O_3(Yttrium Oxide)	3vol % of solid loading
3	DISPERSANT (Polyethyleneimine,PEI)	1wt% of solid loading
4	APS	0.8wt% of monomer content
5	TEMED	1 wt% of monomer content

3.8.4. Experimental Procedure

Premix solution was prepared using and mixing linear monomer (Methacrylamide (MAM)) and cross linking (N,N-methylenebisacrylamide (MBAM)) in distilled water with a 1 wt% of PEI. The premixed aqueous solution is having 10 wt.% monomer content, and 5:1 ratio of monomers. Ceramic powders such as SiO_2 and BN were added to premix solution maintaining the solid loading in the suspensions as 50 vol%. Suspensions were ball milled for a period of 24 h in a plastic bottle to minimize the agglomerates and to have the uniformity in size. Diluted Nitric acid and ammonia solution is used to maintain the PH value to 10.5.

Figure 3. 17 Sintered Si_3N_4-SiO_2-BN samples for flexural strength measurement

Table 3. 17: List of experimental details with performance values

	INPUT PARAMETERS					**OUTPUT PARAMETERS**	
Exp. No.	**Solid loading (vol%)**	**Monomer content(wt%)**	**Ratio of Monomers**	**SiO2(vol%)**	**BN (vol%)**	**Flexural strength (MPa)**	**Dielectric constant@ 30 MHz freq**
1	30.00	5.00	0.2	0.00	0.00	118.67	6.35
2	30.00	5.00	0.1	5.00	5.00	105.28	4.16
3	30.00	5.00	0.067	10.00	10.00	79.05	3.09
4	30.00	10.00	0.1	5.00	5.00	116.92	3.67
5	30.00	10.00	0.067	10.00	10.00	78.61	3.1
6	30.00	10.00	0.2	0.00	0.00	125.7	5.4
7	30.00	15.00	0.067	10.00	10.00	85.23	3.1
8	30.00	15.00	0.2	0.00	0.00	127.73	3.9
9	30.00	15.00	0.1	5.00	5.00	116.56	3.56
10	35.00	5.00	0.2	5.00	10.00	117.27	3.7
11	35.00	5.00	0.1	10.00	0.00	121.82	5.31
12	35.00	5.00	0.067	0.00	5.00	139.37	5.42
13	35.00	10.00	0.1	10.00	0.00	134.82	4.56
14	35.00	10.00	0.067	0.00	5.00	147.2	5.21
15	35.00	10.00	0.2	5.00	10.00	120.83	3.89
16	35.00	15.00	0.067	0.00	5.00	148.69	4.64
17	35.00	15.00	0.2	5.00	10.00	119.35	3.83
18	35.00	15.00	0.1	10.00	0.00	132.9	3.8
19	40.00	5.00	0.2	10.00	5.00	129.63	5.12
20	40.00	5.00	0.1	0.00	10.00	164.74	4.52
21	40.00	5.00	0.067	5.00	0.00	152.99	5.9
22	40.00	10.00	0.1	0.00	10.00	149.94	4.5
23	40.00	10.00	0.067	5.00	0.00	160.97	6.3
24	40.00	10.00	0.2	10.00	5.00	135.56	5.1
25	40.00	15.00	0.067	5.00	0.00	162.21	5.6
26	40.00	15.00	0.2	10.00	5.00	133.73	4.83
27	40.00	15.00	0.1	0.00	10.00	165.38	4.68

The final suspension was degassed for a period of 5-10 min then 0.8 wt% of initiator (Ammonium Persulfate, APS) and a Catalyst (tetramethylethylenediamine, TEMED) is used. Afterward, the ceramic get is casted into the nonporous molds and dried under controlled humidity and the binder was burned out at 550^{o}C for 2 h, with the increment of 20oC/min. Then the samples have been sintered at the temperature of 1700^{o}C for 2h in Nitrogen atmosphere, followed by natural cooling. Sintered samples of Si_3N_4-SiO_2-BN ceramic composites for flexural strength measurement were shown in Figure 3.17. A total of 27 experiments were carried out with the parameters shown in Table 3.17.

Summary

In this chapter, the details of the materials used for fabrication of porous Si_3N_4 based Si_3N_4-SiO_2, Si_3N_4-BN and Si_3N_4-SiO_2-BN ceramic composites are presented. The various equipment used for slurry preparation with their specifications are presented in this chapter. This chapter also present equipment used in this work for property characterization namely mechanical properties, dielectric properties, XRD analysis, and SEM analysis.

It identifies experimentally the appropriate ceramic slurry system and processing routes of porous Si_3N_4, Si_3N_4–BN, Si_3N_4–SiO_2 and Si_3N_4–SiO_2-BN ceramic composites using gelcasting method. The levels of input factors solid loading, monomer content, ratio of monomers and SiO_2 and BN content were fixed based on the results of preliminary experimentation. In this chapter, the challenges in each ceramic composite were discussed and solutions have been achieved through preliminary experimentation. The difficulties in addition of BN ceramic powder to Si_3N_4 were discussed and resolved by changing dispersant. Preliminary experiments were conducted and the sintering temperature was fixed as 1550 °C for sintering all the Si_3N_4-SiO_2-BN ceramic composites.

CHAPTER 4

RESULTS AND DISCUSSIONS

4.1. Introduction

This Chapter first deals with the characterization of Si_3N_4, SiO_2 and BN raw materials. Chapter also deals with a characterization of ceramic suspensions prepared using different pH values, solid loadings and concentration of the dispersant, which changes the colloidal behavior. In order to obtain very stable suspensions, zeta potential and rheological characterization were obtained to determine optimum dispersant and pH concentration. Based on the slurry results and optimizing the dispersant and the monomer content, the resulting gelcast ceramic bodies were characterized. The results of the mechanical, dielectric and microstructure analysis of Si_3N_4–SiO_2 and Si_3N_4–BN sintered ceramic composites were presented. The effect of process parameters on performance characteristics of Si_3N_4–SiO_2-BN ceramic composite was discussed.

4.2. Characterization of Raw Materials

4.2.1. Characterization of Si_3N_4 powder

A Scanning Electron Microscope micrograph has been done on as received Si_3N_4 powder (SN-E10, Ube Industries, Japan). Figure 4.1 shows the SEM image. It can be seen that the powders have an irregular morphology with an average particle size of about 0.5 micrometers. Figure 4.2 shows the X Ray diffraction analysis results of the silicon nitride powder. Comparing the X-ray diffraction patterns with the JCPDS standards (No.98-005-9091), the diffraction peaks can be indexed as particles of Si_3N_4, which is consistent with the manufacturer's data. The secondary phase was found. The crystallite size of Si_3N_4 powder is found to be around 0.42 µm using Debye- Scherrer's formula as given below.

$$D_x = \frac{0.9\,\lambda}{\beta\,cos\theta}$$

Where D_x is average crystalline size, λ is the X-ray wavelength used, β is the line broadening at half the maximum intensity (FWHM), θ is the bragg angle.

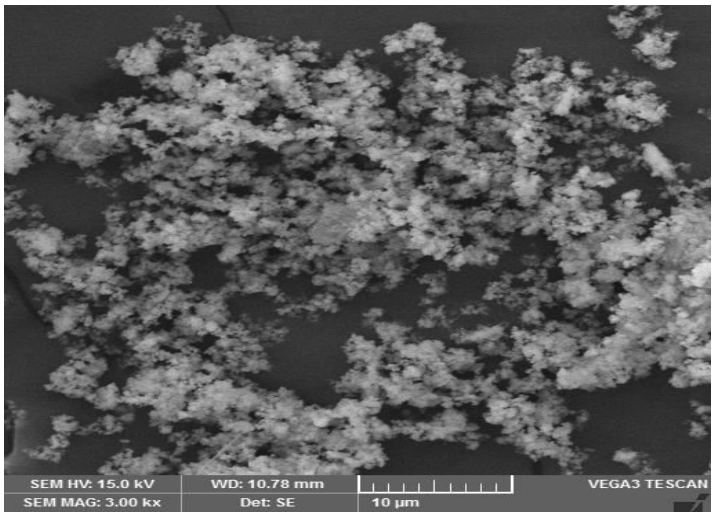

Figure 4. 1: SEM Microstructure of as- received Si_3N_4 powder

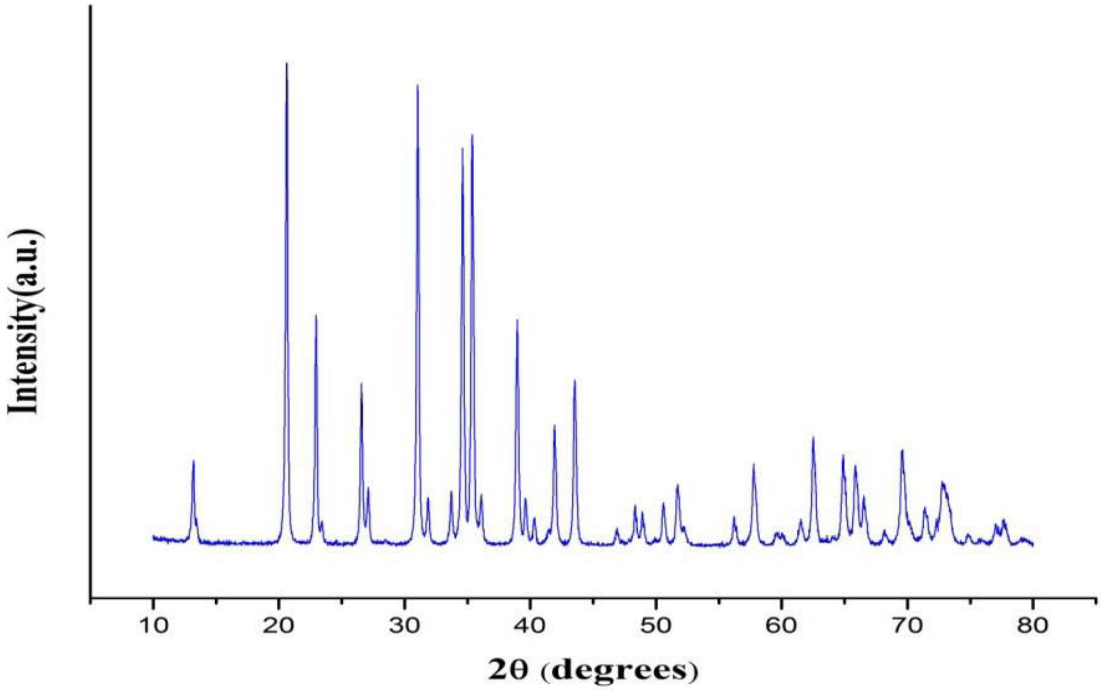

Figure 4. 2: XRD analysis of as- received Si_3N_4 powder.

4.2.2. Characterization of BN powder

The X-ray diffraction pattern of the as-received BN ceramic powder is shown in Figure 4.3. By comparing these XRD pattern with JCPDS standards, the diffraction peaks can be indexed as pure BN, as noted on the data sheet received from Sigma Aldrich, USA. SEM micrograph of the as received BN ceramic powder (255475, Sigma Aldrich, USA) used in this study is shown in Figure 4.4.

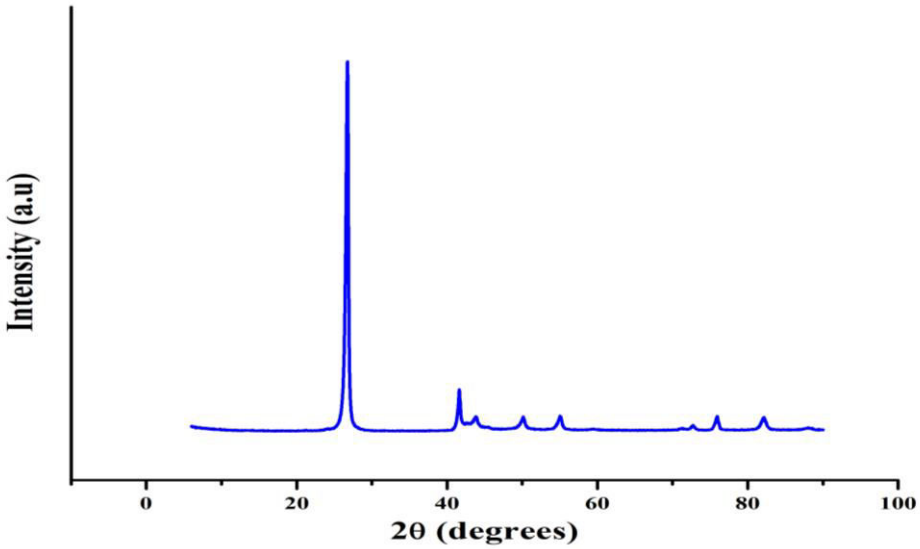

Figure 4. 3: XRD analysis of as- received BN powder.

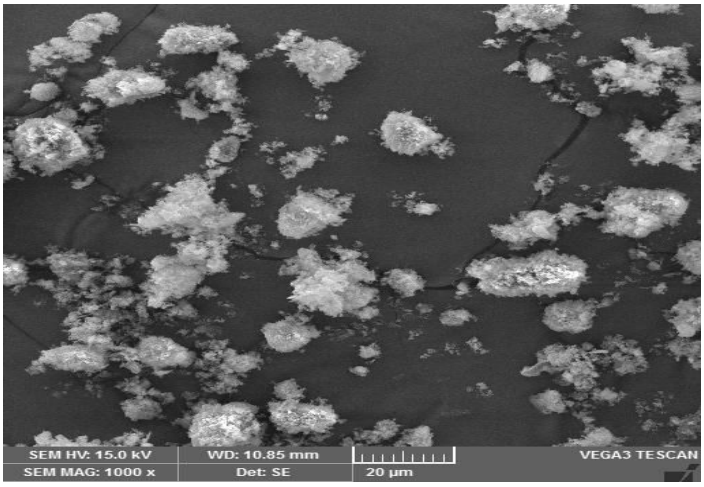

Figure 4. 4: SEM Microstructure of as- received BN powder

4.2.3. Characterization of SiO_2 powder

Figure 4.5 shows the SEM image of the as-received SiO_2 powder. It can be seen that the powders have an irregular morphology with an average particle size of 5 microns. Figure 4.6 shows the results of XRD analysis of the SiO_2 powder. When comparing the diffraction pattern of X-ray particles with JCPDS standards, diffraction peaks can be indexed as SiO_2, which is reliable with manufacturer data.

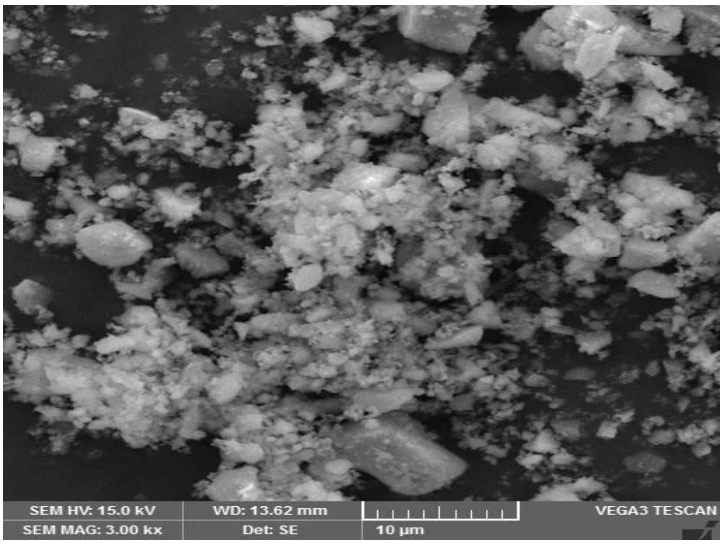

Figure 4. 5: SEM microstructure of as received SiO_2 powder

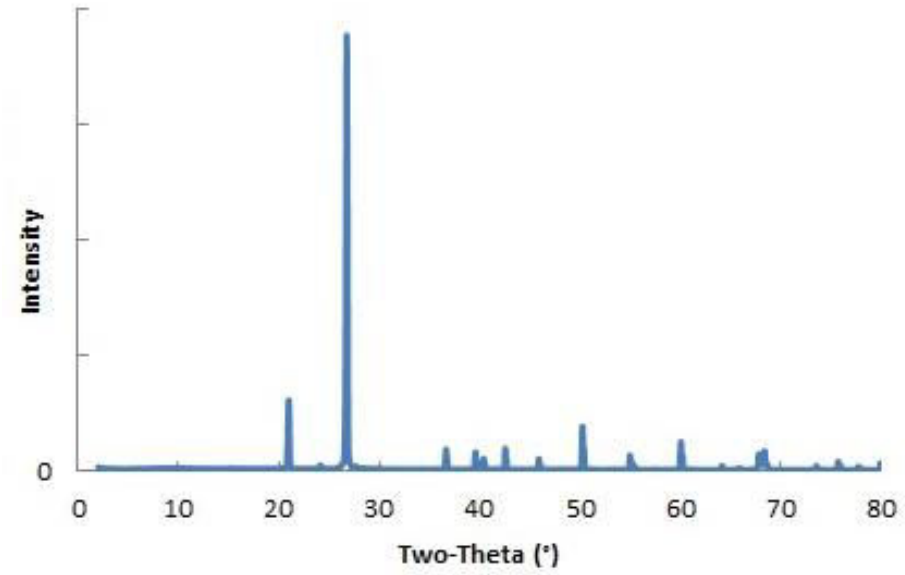

Figure 4. 6: XRD Pattern of as- received SiO_2 powder

4.3. Characterization of Porous Si_3N_4 Ceramics

The processing of porous Si_3N_4 ceramics prepared by gelcasting method has been elaborated in section 3.5.5. The rheological characterization of the slurry and properties of the sintered porous Si_3N_4 ceramics are discussed in the following sections.

4.3.1. Optimization of slurry preparation and Rheological Characterization

In a ceramic colloid, the ceramic particles are uniformly dispersed in a continuous phase in the presence of a suitable dispersant. The resulting colloid may be a suspension or a slurry or a dilute suspension in the form of suspended particles. Ceramic particles have a significant influence on surface chemistry. The colloidal processing has many benefits on the other techniques. It is possible to solve the problems of heterogeneity or defects associated with the drying process. Heterogeneity develops from agglomerates and inclusions, such as binders, dispersants in the dry powder [87]. In this section, the characterization of ceramic suspensions with different pH values, solid loadings and dispersant concentration of the slurry was investigated, which can change the colloidal behavior.

4.3.1.1. Rheological properties

In this section, the results of zeta potential as a function of pH value for bare Si_3N_4 powder and Si_3N_4 powder with the addition of Dolapix A88 are presented.

4.3.1.2. Effect of Dispersant Content on the Viscosity of the Si_3N_4 Slurry

The addition of effective dispersant can dramatically reduce the viscosity of slurries with very high solids loading. Dispersion of ceramic powders in a aqueous medium is explained by an electro- static or static mechanism, or a combination of both[137]. The addition of a polyelectrolyte as dispersing agent helps for stabilization is achieved by electrostatic as well as static mechanisms. In an aqueous-based system, PH value of the medium can also be used as a parameter to control dispersion. This is widely used for processing of ceramic polymer composites [138, 139].

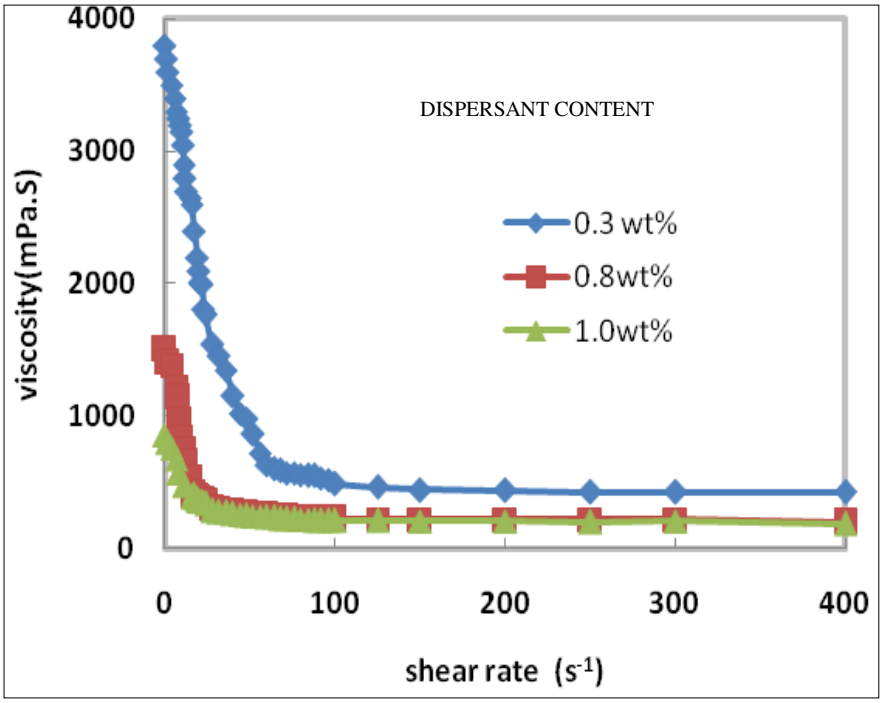

Figure 4. 7: Effect of dispersant concentration on the viscosity of Si_3N_4 suspensions

The effects of dispersant content on the rheology of slurries are presented in Figure 4.7. For each group, the flow curve deviates from Newtonian behavior, the viscosity decreases as the shear rate increases, which is known as shear thinning behavior[140] .In addition, It has been found that the viscosity of the slurry decreases with the% weight increase of dispersant, in particular when the amount of the dispersant is less than 0.8 wt%. If the amount of dispersant is even higher, ie, above 0.8wt.%, the viscosity increases. Accordingly, 0.8wt.% is established as an appropriate dispersant concentration for the processing of Si_3N_4 slurries in this work.

4.3.1.3. Effect of Ball milling on the Viscosity of the Si_3N_4 Slurry

Low viscosity and high solid loading are beneficial for both mixing and casting in slurry processing. It is, therefore, important to maintain slurry fluidity while optimizing solid loading. Figure 4.8 depicts the typical plots of viscosity various shear rate at various ball

milling times. The study had been performed on suspensions containing 50 vol.% of composite powders. When the milling time was shorter than 24 h, the viscosity of slurries decreased gradually as the time of milling increased. It showed that the absorption of the dispersant on particles did not reach equilibrium and the suspension was unstable until the ball milling time is equal to or more than 24 h. After 24 h milling, the viscosity of the suspension tended to be consistent. Therefore, the ball milling time should be equal to or more than 24 h to obtain a stable suspension at equilibrium.

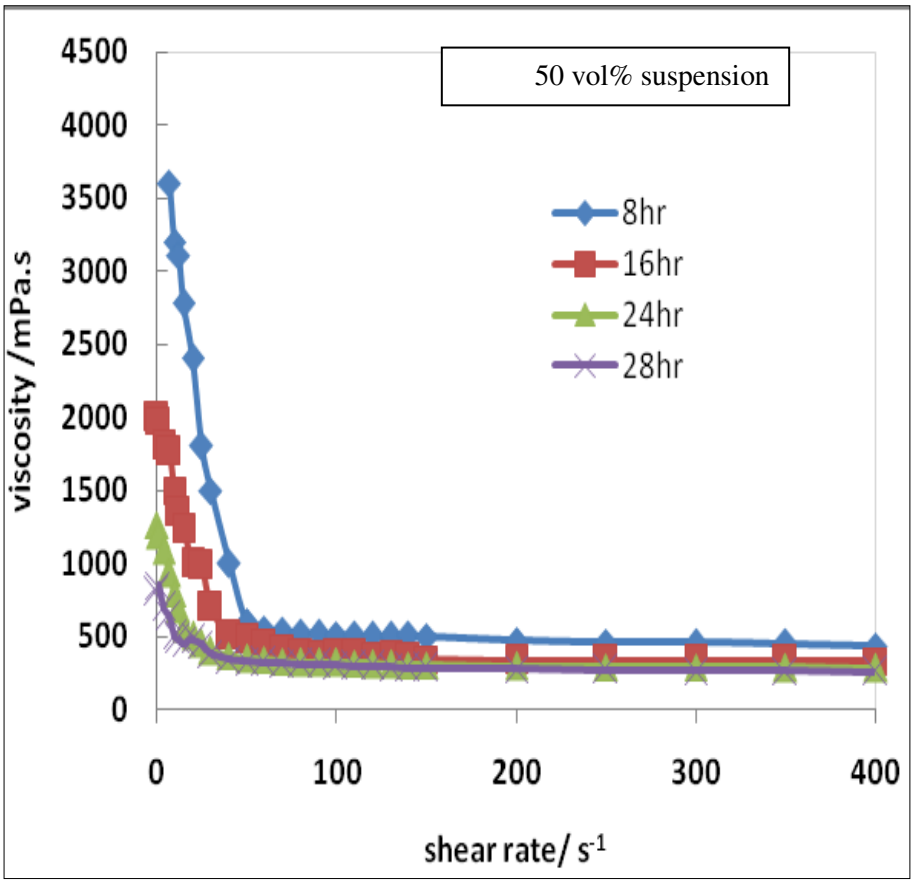

Figure 4. 8: Effect of ball milling time on the viscosity of 50 vol% Si_3N_4 suspensions

4.3.1.4. Effect of pH on Zeta potential of suspensions

Stability of colloidal suspensions is also measured by Zeta potential. Suspensions having at pH values close to pH_{iep} tend to flocculate rapidly and in sufficient to overcome the

van der Waals forces. The rate of flocculation should be slower. Figure 4.9 shows the variation of zeta potential verses pH for Si_3N_4, mixed powder (Si_3N_4+Al_2O_3+Y_2O_3) and mixed powder in the presence of Dolapix A88.

The isoelectric points (pHiep-value) of Si_3N_4, mixed powder (Si_3N_4+Al_2O_3+Y_2O_3) and mixed powder in the presence of Dolapix A88 were 6.9, 6.3 and 4.5 respectively, as shown in Figure 4.9. At low value of pH, far from the pHiep-value of either powder, only the silicon nitride particles have a high positive zeta potential and the suspension is colloidally stable. Around pHiep, the particles have a low zeta potential which may be either positive (pH<pHiep)or negative (pH>pHiep); suspensions prepared in this region are colloidally unstable and consist of large agglomerates that are likely to result in a porous gelcast ceramics. Finally, far high pH values of pH_{iep} of two powders, the particles have a high negative zeta potential are colloidal stability[10][11]. The pH_{iep} of mixed powder shifted from 6.3 to a much acidic value 4.5 in the presence of dispersant. For suspensions, a dispersant, a zeta potential is relatively high, about 61 mV at a pH of 11, the optimum pH conditions being dispersed for stable suspensions

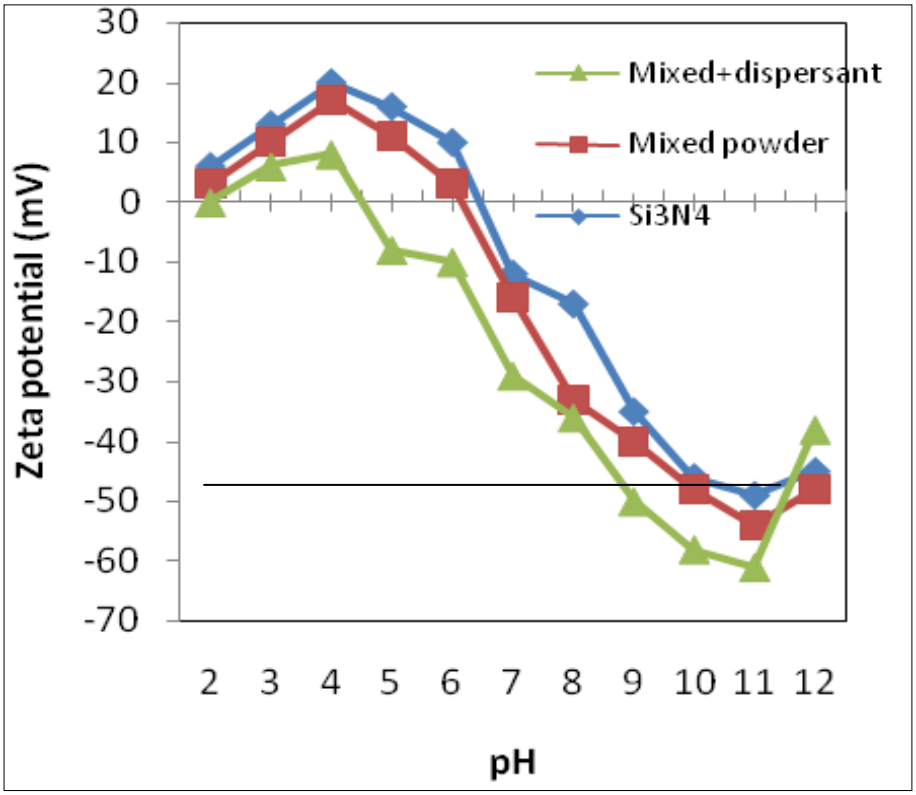

Figure 4. 9: Zeta potential of Si_3N_4 and mixed powder (Si_3N_4+Al_2O_3+Y_2O_3) as function of pH.

4.3.2. Properties of green samples

The Flexural strength and the porosity obtained for the porous Si_3N_4 ceramics are shown in Table 3.10. From the Table 3.10, experiment number 13, 14, 15 and 16 had given a difficulty because of the high solid loading. The suspensions of these experiments were high viscous and observed agglomerations, and thus these samples have less flexural strength.

4.4. Characterization of Si_3N_4-SiO_2 Ceramic Composites

Silicon nitride (Si_3N_4) ceramics are known for its high strength, fracture toughness, strength at elevated temperatures, chemical resistance, and excellent ablation resistance, which make them suitable as radome material, however Si_3N_4 has a relatively higher dielectric constant and loss tangent properties at elevated temperatures limits its applications as a wave transparent materials[9, 141] . SiO_2 ceramics has rather low-dielectric constant, high-chemical stability and extremely low coefficient of thermal expansion and thermal conductivity than Si_3N_4 ceramics [109, 142].

However, it has low flexural strength (less than 80 MPa), and poor rain erosion resistance, which cannot meet the requirements of radome used in high speed missiles. Thus, the Si_3N_4-SiO_2 ceramic composites may have excellent properties because of combined benefits of both the materials. Here, the SiO_2 ceramic powders were introduced with the Si_3N_4 ceramic powders in order to improve dielectric properties. A traditional gelcasting process was used to obtain the Si_3N_4- SiO_2 ceramics, (described in detail in Chapter 3.6.).

4.4.1. Mechanical Characterization

4.4.1.1. Density and porosity

Figure 4.10 shows the variation of bulk density and porosity of Si_3N_4-SiO_2 composite ceramics with SiO_2 content. With the increase of SiO_2 content, the density of composited decreases while the porosity is found increased. It is due to the formation of the crystalline Si_2N_2O, so the transformation of α-Si_3N_4 into β-Si_3N_4 and densification are

obstructed. From the rule of mixture, the density of SiO_2 was lower than Si_3N_4.This also the reason for decreasing the bulk density as the SiO_2 content increases.

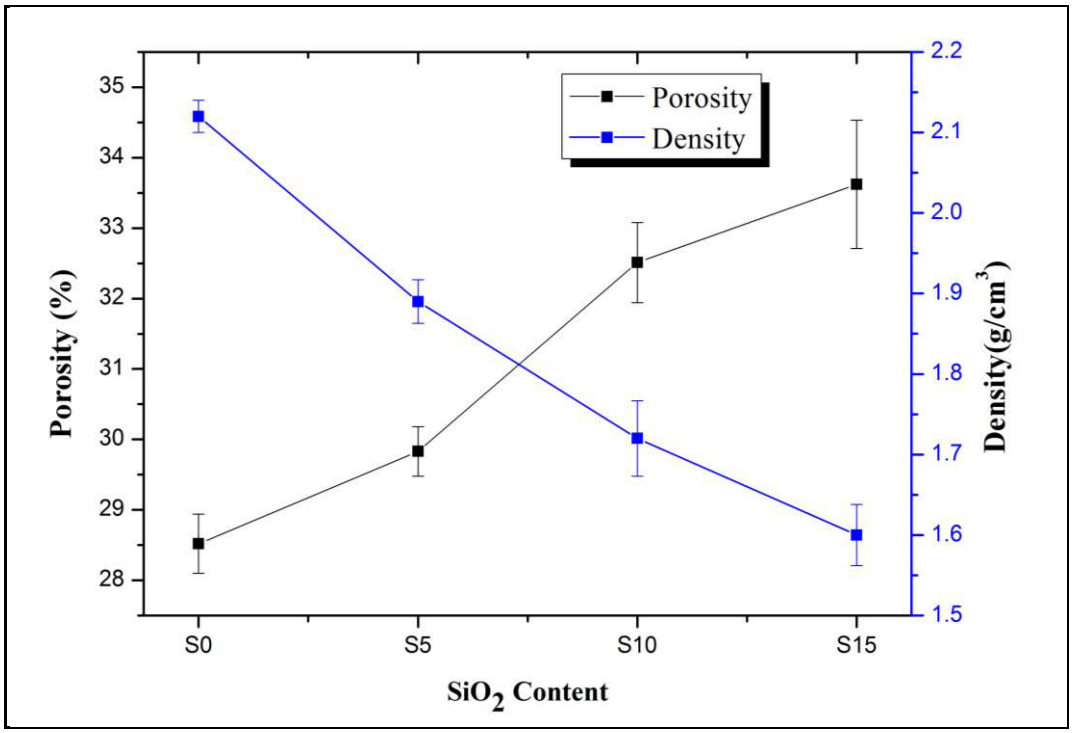

Figure 4. 10: Porosity and bulk density of ceramics as a function of SiO_2 content

The sintered densities of the composites were measured using the Archimedes method. From Table 4.2, it is evident that decrease in density increases the porosity and it can be seen that the maximum porosity and minimum porosity achieved at 15 vol% SiO_2 content and 0 vol % SiO_2 content, respectively.

Table 4. 2: Density, porosity and Flexural strength of Si_3N_4–SiO_2 ceramic composites.

Sample	Actual density (g/cm^3)	Porosity (%)	Flexural strength (MPa.)
S0	2.14	28.6	179.56±9.35
S5	1.93	29.6	117.83±5.91
S10	1.78	32.3	89.32±3.82
S15	1.61	33.5	60.24±9.74

4.4.1.2. Flexural Strength

The sintered materials exhibit a brittle fracture and the fracture surface has not obvious grain pull-out, while performing three point bending test. Micro pores are seen when the amount of SiO_2 reaches 15vol%. This may be due to the obstruction of densification and hence decrease in flexural strength. Hardness and flexural strength are tested on all the prepared samples with varying with respect to size of particle. The effect of SiO_2 powders on the flexural strength is shown in Figure 4.11.

The flexural strength decreases with the increase of SiO_2 powder and as SiO_2 is softer than Si_3N_4 matrix. Figure 4.11 shows the flexural strength of the Si_3N_4-SiO_2 composite ranges from 60.59 to 178.47 MPa. The effective loading across the section of the material has been found reduced due to presence of pores in the ceramic composite. Therefore, the more is the porosity, the less is the strength. Due to large mismatch of Coefficients of thermal expansion between Si_3N_4 and cristobalite formed, induces the formation of micro cracks, which may also leads to decrease in flexural strength[143].

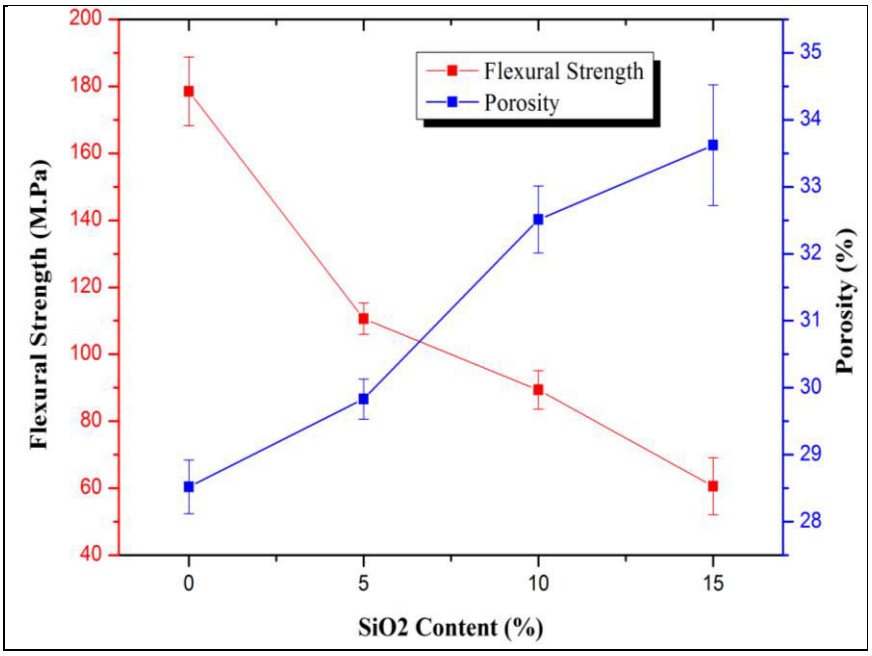

Figure 4. 11: Flexural strength and porosity of Si_3N_4-SiO_2 ceramic composite as a function of sio_2 content

4.4.1.3. Phase Evolution of the Sintered Samples

The XRD Patterns of Si_3N_4-SiO_2 ceramics are shown in Fig. 1 and the main crystal phase of the composites is β-Si_3N_4, Si_2N_2O and small amounts of SiO_2, cristobalite and $Y_2Si_2O_7$. The diffraction intensities of Si_2N_2O increase with an increase in SiO_2 content. The formation of micro cracks due to the presence of cristobalite can be the major reason for decreased strength of Si_3N_4- SiO_2 ceramics compared to other Si_3N_4 matrix composites. The presence of Si_2N_2O in the monolithic ceramic (i.e. Fig 1 a), can be explained from the following reaction which occurs during the sintering process between Si_3N_4 and SiO_2 as [144]

$$SiO_2(l) + Si_3N_4(s) \rightarrow 2Si_2N_2O \qquad (4.1)$$

The existence of Si_2N_2O in the monolithic ceramic (i.e. Fig 1 a), can be explained by the following reaction which occurs during the sintering process when the temperature reaches 1600 ^{0}C [145]:

$$2Si_3N_4(s) + 1.5O_2(g) \rightarrow 3Si_2N_2O(s) + N_2(g) \qquad (4.2)$$

When the temperature is higher than 1650 ^{0}C, the reversible reaction occurs and the amount of Si_2N_2O decreases:

$$2Si_2N_2O(s) \rightarrow Si_3N_4(s) + SiO(g) + 0.5O_2(g) \quad (4.3)$$

Hence it is revealed that Si_3N_4 as well as Si_2N_2O phases exist. Actually, amorphous SiO_2 starts to crystallize and forms cristobalite at temperature more than 1300 ^{0}C, and its nucleation is heterogeneous [146], it may appear from the surface of SiO_2 and extends inwards. From Figure 4.12, we can also see the peak of cristobalite when SiO_2 is added and becomes strong as the SiO_2 content increases, and it means that an extensive crystallization of SiO_2 occur[147].

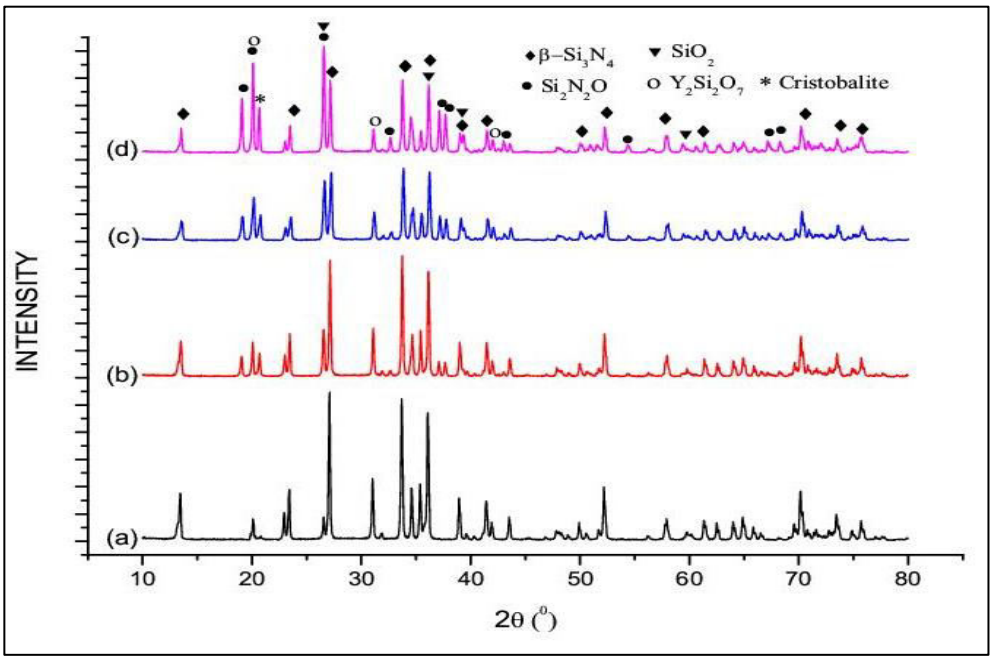

Figure 4. 12: XRD patterns for different SiO_2 content a) S0; b) S5; c) S10; d) S15

4.4.2. Dielectric Characterization

The dielectric loss and dielectric constant (ε) are two important and complimentary properties of a dielectric material. If the material possesses a low dielectric loss then it is an excellent material for radome as it has the ability to convert the absorbed electromagnetic energy into heat. Figure 4.13 and Figure 4.14 shows dielectric constant and loss tangent of the Si_3N_4-SiO_2 ceramic composites with the various wt.% SiO_2 content with respect to frequency.

The ε value of porous Si_3N_4 is highly influenced by the porosity, Si_3N_4, and phase of Si_2N_2O and cristobalite. It can also be seen that in Figure 4.13. The ε value of composite

decreases to the maximum extent when the porosity is 1. When SiO_2 content increases from 0 to 15wt. %, the ε of porous Si_3N_4-SiO_2 ceramic decreases from 6.8 to 3.2.

Porosity is the major influencing factor for the ε of porous ceramics. SiO_2 ceramics are having lower dielectric properties compared to Si_3N_4 ceramics. Thus, the Si_3N_4-SiO_2 ceramic has a relatively lower ε than that of Si_3N_4 ceramics. Porosity is the dominating factor for the dielectric constant of porous ceramics. Pure SiO_2 ceramics can have lower dielectric properties than Si_3N_4 ceramics. Thus, the Si_3N_4-SiO_2 ceramic may have low dielectric constant compared to the pure Si_3N_4 ceramics. Also, due to the increase of porosity, the dielectric constant is low and due to this we can treat porous phase as a phase whose dielectric constant is 1. The dielectric constant does not have great variation with increasing frequency due to the polarization mechanism remains unchanged in this area.

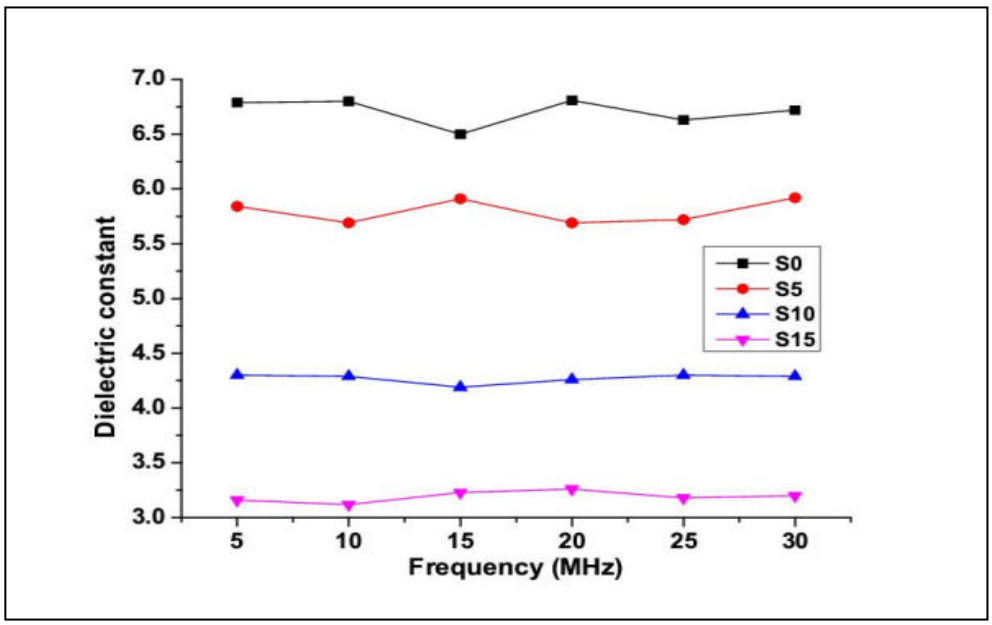

Figure 4. 13: Dielectric constant of Si_3N_4-SiO_2 ceramic composite as a function of SiO_2 content

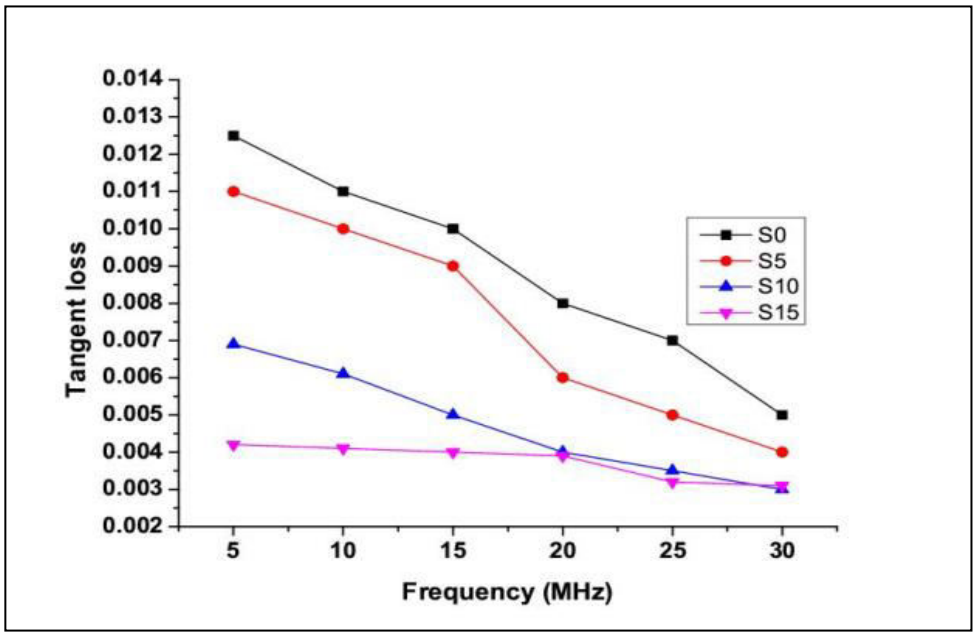

Figure 4. 14: Tangent loss of Si_3N_4-SiO_2 ceramic composite as a function of SiO_2 content

Also, the ε could be lower due to the increase of porosity, because of which we can treat pore as phase with a unit dielectric constant. It is also observed that the polarization mechanism is unchanged with frequency and hence the ε does not vary with increasing frequency.

4.4.3. Microstructure of the Sintered Samples

The fracture morphology as observed by SEM for Si_3N_4-SiO_2 composites are shown in Figure 4.15 for various SiO_2 content. It can be seen that SiO_2 and Si_3N_4 are arranged homogenously in the composite and also in the pores. It is also observed that the pores are evenly distributed in the matrix and with an average size of 4μm. A uniform microstructure and the small amount of β-Si_3N_4 due to its elongated grains are also observed in SEM micrograph, from Figure 4.15a-15d.

Through microstructure analysis, it can be observed that the samples consisted of bonded particles and minor columnar grains with high aspect ratio, indicating a few α/β phase transformations, and this is well consistent with the XRD analysis. It also can be seen that the pores distribute uniformly in the matrix, and the connected open pores are formed by stacking Si_3N_4 particles.

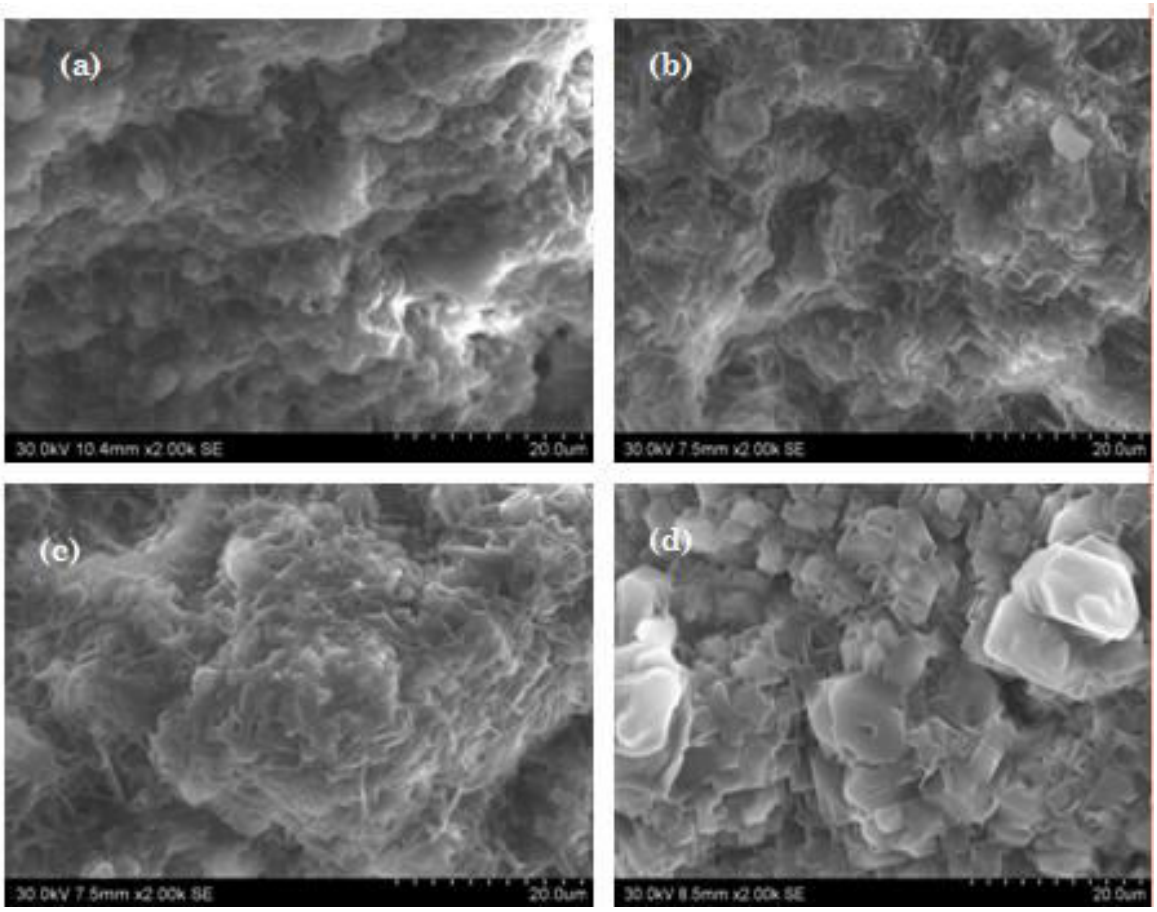

Figure 4. 15: Fracture morphology of Si_3N_4-SiO_2 ceramic composite of different SiO_2 content. a) S0; b) S5; c) S10; d) S15.

The microstructure (Figure 4.15) reveals that the samples contain trace of micropores, probably due to the distribution of organic binders. It is thermodynamically possible to form Si_2N_2O from SiO_2 and α-Si_3N_4 or β-Si_3N_4 according to the reaction. The formation of Si_2N_2O indeed proceeds in a liquid phase. The Si_2N_2O crystal structure is built up by distorted [SiN_3O] tetrahedral, whereas α- and β -Si_3N_4 are composed of [SiN_4] tetrahedron is replaced by an oxygen atom, a tetrahedral [SiN_3O] structural unit of Si_2N_2O is formed. Therefore, the Si_2N_2O nuclei are formed in the liquid phase at the sintering temperature[147]. After the Si_2N_2O nucleation occurs, Si_2N_2O grain-growth rate is very high. Si_2N_2O grew via a solution precipitation process in the presence of a large amount of SiO_2- rich liquid phase. Obviously, the liquid phases were largely consumed with the formation of the crystalline Si_2N_2O, so the transformation of α-Si_3N_4 into β-Si_3N_4 and densification are obstructed. This also may be the reason for increasing the porosity as the SiO_2 content increases.

4.5. Characterization of Si_3N_4-BN Ceramic Composites

From the preliminary experimental work, it was observed that the gelcasting of Si_3N_4/BN ceramic composite with Dolapix A 88 as dispersant lost its flowability and became inconvenient for gelcasting. Many kinds of literature on the colloidal process of Si_3N_4 are available [131, 132] but the colloidal process of Si_3N_4/BN composites has not been reported much. The addition of BN content decreased the slurry fluidity and increased the viscosity of the slurry. The reason for the decrease of slurry fluidity with BN content addition is specific surface area of flake BN was larger, so more water was needed to wet the particle surface when more BN were added[133, 148]. On the other hand, The low surface energy of BN is a major drawback for its use in aqueous media, because it is not easily dispersed[134]. Thus, Polyethylenimine (PEI) a strongly cationic branched polymer was used as the dispersant [135] [136]. Si_3N_4/BN suspension is a complex system in which many factors have significant effect on its rheological behaviors such as pH value, dispersant and its content, solid loading etc.,. From the preliminary experimentation, 1 wt% of dispersant was used to prepare a Si_3N_4–BN aqueous suspension with a high solid loading and low viscosity.

4.5.1. Optimization of slurry preparation

4.5.1.1. Effect of Dispersant Content on the Viscosity of the Slurry

As discussed earlier, the zeta potentials of Si_3N_4 and BN particles shown stronger inter- particle forces exhibits stronger repulsions at lower and higher pH values. Hence, the variations in zeta potentials able to affects the rheological behaviour of Si_3N_4– BN suspensions. Figure 4.16 exhibits the viscosities of Si_3N_4– BN suspension as a function of shear rate with various concentrations of PEI.

The rheological behaviour of the Si_3N_4– BN aqueous suspensions is completely dependent on the quantity of PEI added. The addition of 1 wt% PEI to the suspension was shown the lowest viscosity. 1 wt% of PEI has been found as the optimum concentration to disperse the Si_3N_4– BN powder mixture in aqueous media. It was also shown the less viscosity value (as shown in Figure 4.16) and high zeta potentials. For every group, the flow curve deviates from a Newtonian behaviour, its viscosity becomes lower as the shear rate is increased, which is known as shear-thinning in rheology [149]. Besides, it was observed that

the viscosity of slurry reduces with increase of dispersant dosage and an optimum value of the dispersant dosage was found.

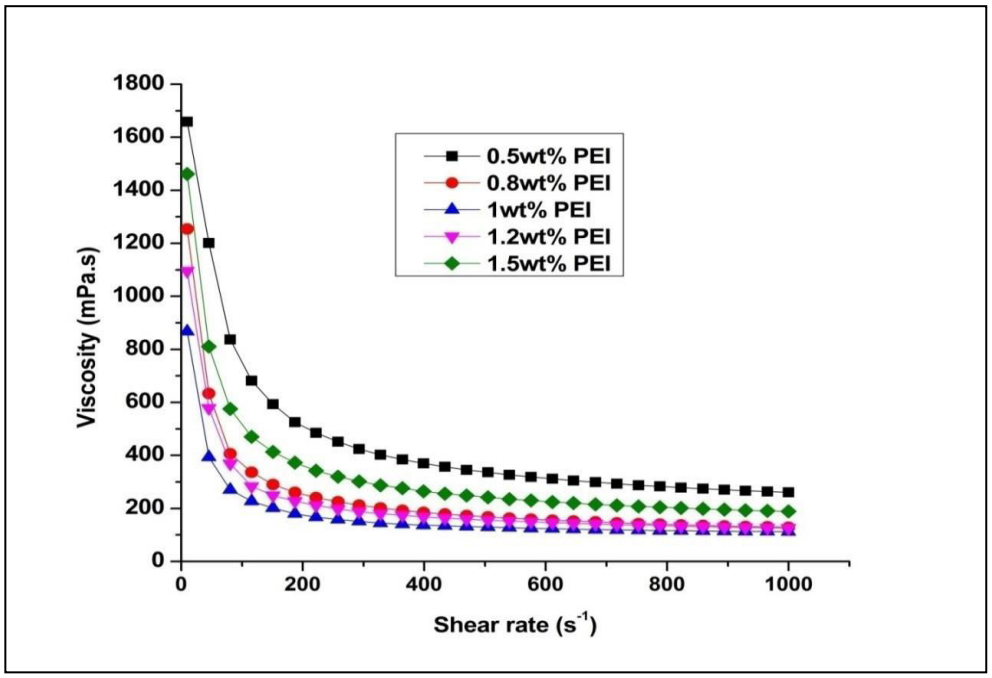

Figure 4. 16: Effect of concentration PEI on the viscosity of 40 vol% SiN4-BN suspension

4.5.1.2. Effect of pH Value on the zeta potential of the Slurry

Electrostatic stabilization is widely used to stabilize the ceramic suspensions by the repulsive forces of net surface charges between the particles. Figure 4.17 shows the Zeta potential of Si_3N_4 or BN powders as a function of pH. The isoelectric point (iep) for Si_3N_4 and BN powder with PEI locates at the pH value of 6.5 and 3.7 respectively. Increasing of pH value from 2 to 12, Zeta potential was also increased negatively up to -55.3mV for Si_3N_4 and -51.2mV for BN powders, respectively.

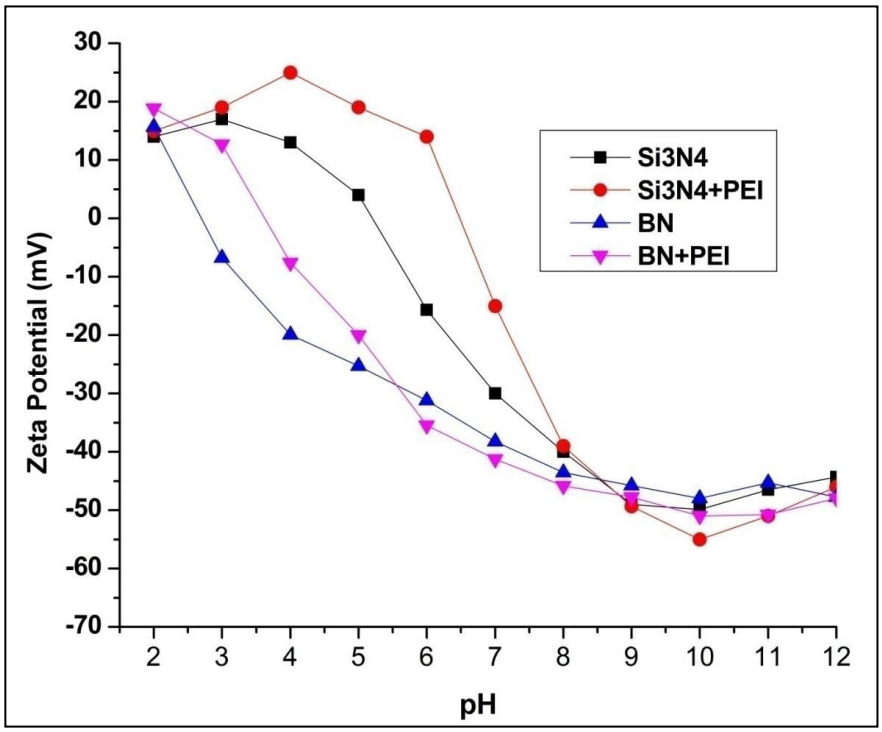

Figure 4. 17: Effect of pH on the zeta potential of Si3N4 and BN with and without 1wt% PEI concentration

Addition of 1wt% PEI into the suspensions, made the pHiep of both the powders transferred to basic region and Zeta potential attains more negative value, especially whenever the suspensions pH>7.It was observed that the changes in Zeta potential value and pHiep of each particles of powder is mainly caused by the addition of dispersant, creates the positive charge on the surfaces or maximize the negative charges on the surfaces of the particles. The cationic PEI has higher affinity to the negatively charged surface hence the stronger effect of the dispersant on the particle surface charge was observed in lower pH region.

Table 4. 1: Zeta potential of suspension at pH 11

Suspension	**Zeta potential (mV)**
Si_3N_4 + Dolapix A88	-59.4
Si_3N_4 +Al_2O_3+Y_2O_3+ Dolapix A88	-61.4
Si_3N_4 +SiO_2 + Dolapix A88	-61.0
Si_3N_4 +BN+ Dolapix A88	-43.7
Si_3N_4 +SiO_2+BN+ PEI (0.5 wt%)	-51.5
Si_3N_4 +SiO_2+BN+ PEI (1 wt%)	-59.8
Si_3N_4 +SiO_2+BN+ PEI (1.5 wt%)	-57.3

As Table 4.3 further reveals, the Si_3N_4 +Al_2O_3+Y_2O_3 suspension has a higher zeta potential value than Si_3N_4 suspension produced from individual powder. It is also observed that Si_3N_4 suspension becomes unstable by adding BN powder because of its positive surface charges. As Table 4.3 further reveals, 1 wt% of PEI gives an optimal value of zeta potential.

4.5.1.3. Effect of pH Value on the Viscosity of the Slurry

For making the Si_3N_4– BN composite, the following operational parameters such as rheological properties, pH, solid loading as well as low viscosity of the suspension is very important. In order to find the optimum pH value of stable suspensions, the pH of the suspensions were readjusted to observe the viscosities of the Si_3N_4– BN suspensions containing 40 vol% of solids loading, as shown in Figure 4.18. The viscosity of the suspension decreases whenever the pH increase from 5 to 10, and also observed that viscosity slightly increase whenever pH increases from 10 to12 [58]. It was observed that lower viscosity were attained at pH=10. These results are agreed well with the results of zeta potential analysis, it was conformed that optimum pH of Si_3N_4– BN aqueous suspension was 10.

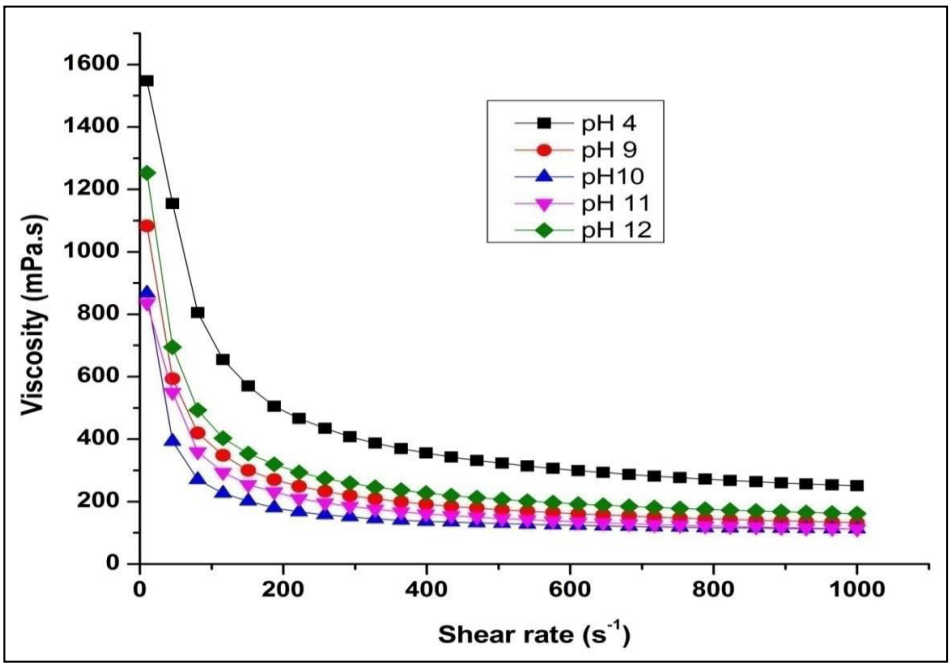

Figure 4. 18: Effect of pH on the viscosity of 40 vol% Si_3N_4-BN suspension with the addition of 1 wt% PEI

4.5.2.Mechanical Characterization

4.5.2.1. Mechanical Properties

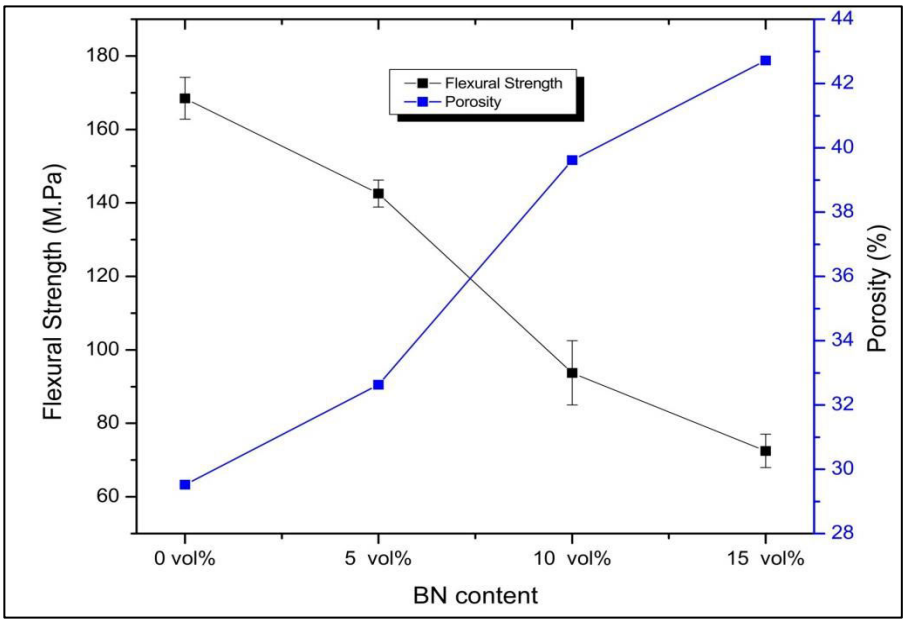

Figure 4. 19: Flexural Strength of Si_3N_4-BN ceramic composite as a function of BN content

Figure 4.19 shows the mechanical properties of the Si_3N_4-BN ceramics as a function of BN content. The flexural strength decreases with the increase of BN content as BN is a weaker phase than Si_3N_4 matrix. Figure 4.19 shows the flexural strength of the Si_3N_4-BN composite ranges from 71.93± 5.23 MPa to 169.23±6.74 MPa. The changes of the mechanical properties for the composites are also related to their microstructures. The interlocking microstructure formed by rod-like β-Si_3N_4 grains was in favor of enhancing the flexural strength of the ceramic, but increase in BN content hinders the transformation of α-Si_3N_4 to β-Si_3N_4 and densification is obstructed which leads to decrease in flexural strength.

4.5.2.2. Phase Evolution of the Sintered Samples

Figure 4.20 shows the XRD patterns of the obtained h-BN/Si_3N_4 composite ceramics with different BN contents. The XRD Pattern indicates that the main crystal phase of the composites is β-Si_3N_4, α-Si_3N_4 and h-BN. Al_2O_3 and Y_2O_3 was not detected in the XRD patterns, which was due to their amounts being too small to be detected. The diffraction intensity of h-BN increases with increasing BN content, signifying that the h-BN did not

participate in any reaction during the sintering process, but the transformation to β-Si_3N_4 was hindered as the BN content increases[150].

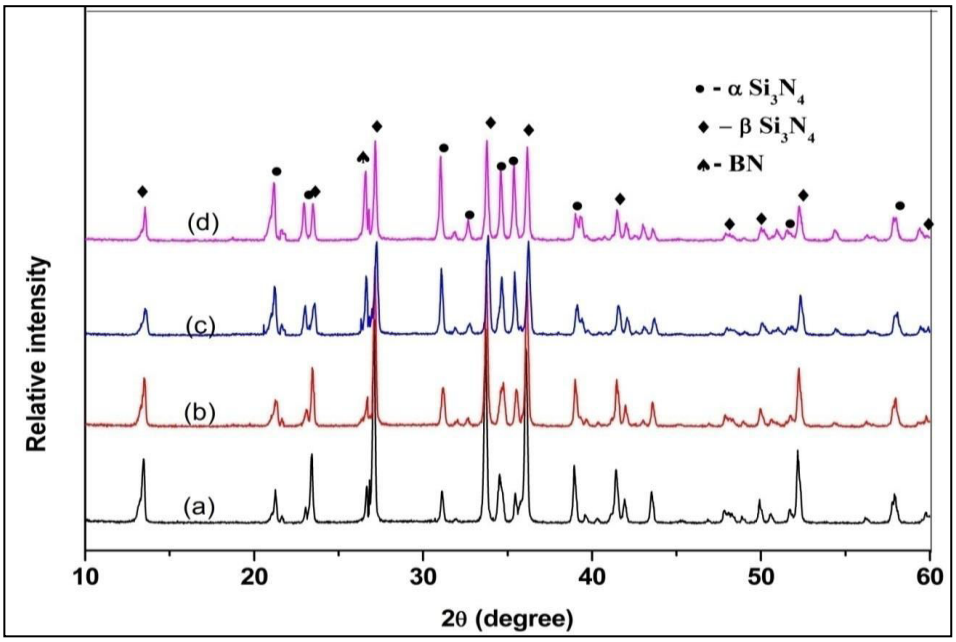

Figure 4. 20: XRD patterns of different BN content ceramic composites a) SNB0; b) SNB5; c) SNB10; d) SNB15.

4.5.3. Dielectric Characterization

Effect of BN content on dielectric constant of a Si_3N_4-BN ceramic is shown in Fig.4.21. Dielectric constant decreases with the increase of BN content in Si_3N_4-BN ceramic composites. This is because as the addition of BN powder hinders the β-Si_3N_4 transformation. The dielectric constant of α- Si_3N_4 was 5.6 where as the β- Si_3N_4 was 7.5.

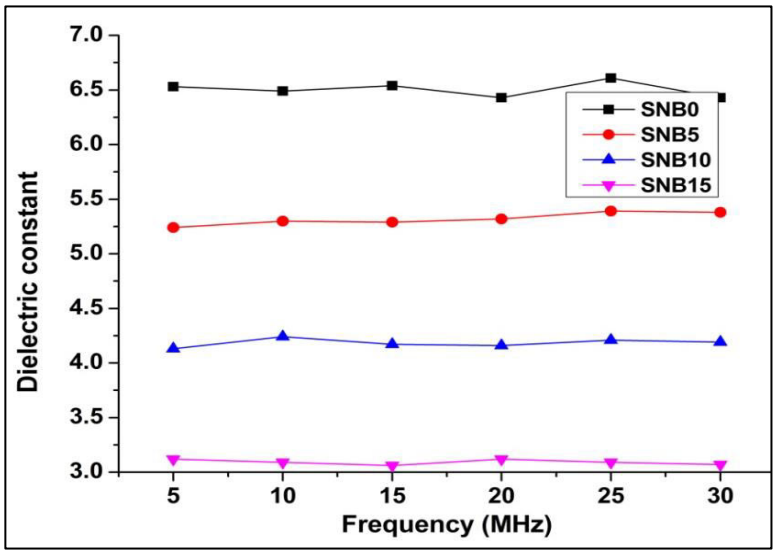

Figure 4. 21: Dielectric constant of Si_3N_4-BN ceramic composite as a function of BN content

Also the increasing porosity with increasing BN content further decreases the dielectric constant of the composite ceramics. The dielectric constant of the ceramic composite was expressed as follows in equation 5.2. The dielectric constant of air is around 1, so increasing the porosity decreases the dielectric constant considerably.

$$ln\varepsilon_o = \sum v_i ln\varepsilon_i \qquad (4.4)$$

$$\varepsilon = \varepsilon_o^{1-p} \qquad (4.5)$$

Where ε_0 is dielectric constant of the dense composite ceramic, ε_i is the dielectric constant of the i phase, v_i is the volume fraction of the i phase, and ε is dielectric constant of the porous ceramic composite, and p is the porosity of the porous material.

4.5.4. Microstructure of the Sintered Samples

Si_3N_4-BN composites samples having fracture surfaces were observed by SEM analysis. From Figure 4.22, one can observe that BN and Si_3N_4 are homogenously distributed in the pores of the composite. The pores are distributed evenly. It was found that the microstructures are homogeneous, and the small amount of β-Si_3N_4 could be identified in the SEM micrograph due to the elongated grains. From Figure, it can be seen that the amount of long-bar-shaped β-Si_3N_4 reduces while increase of BN content[150].

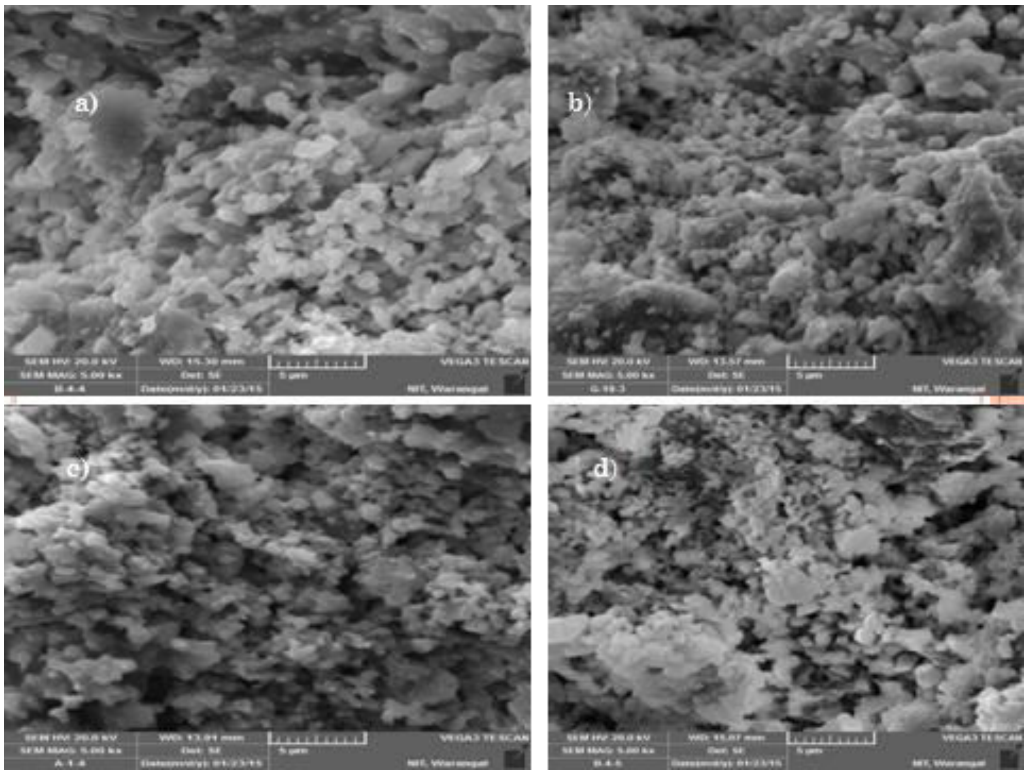

Figure 4. 22: Fracture morphology of Si_3N_4-BN ceramic composite of different BN content. a) SNB0; b) SNB5; c) SNB10; d) SNB15.

From the microstructure analysis, it could be observed that the samples composed of bonded particles and very less columnar grains with more aspect ratio, exhibiting few α/β phase transformation, and XRD analysis are well consistent with these results. It was also observed that the pores distributed homogeneously in the ceramic matrix, and the connected open pores are generated by stacking Si_3N_4 particles. After sintering, the interlocking microstructure formed by rod-like β-Si_3N_4 grains was in favor of improving the flexural strength, but increasing in BN content hinders the transformation of α-Si_3N_4 to β- Si_3N_4 and densification is obstructed which leads to a a increase in porosity and decrease in flexural strength.

4.6. Characterization of Si_3N_4-SiO_2-BN Ceramic Composites

Compared to Si_3N_4, BN has a better thermal shock resistance and dielectric properties. SiO_2 has a dielectric constant and dielectric tangent losses even lower, which makes silica widely used as wave transparent materials. Therefore, Si_3N_4-SiO_2-BN ceramic composites can combine the advantages of individual phases of Si_3N_4, BN and SiO_2 and have better dielectric and mechanical properties, which have been considered as capable materials for wave transparent applications. However, it has been proven that addition of SiO_2 and also BN into Si_3N_4 could significantly decrease the dielectric constant of the materials. This research work has been investigated the influence of SiO_2 ,BN and also gelcasting process parameters on Si_3N_4 ceramic composite properties and to explore the possibility of a new composite material for near net shaped ceramic part with enhanced properties for a wave transparent application.

4.6.1. Experimental Design

27 experiments were conducted based on the orthogonal array. The samples were binder burnt out at 550^0C for 2 hrs with heating rate 2^0C/min, then sintering at 1550^oC for 2 hr with heating rate 10^0C/min in N_2 atmosphere and finally natural cooling. Table 3.17 gives the list of experimental conditions along with performance characteristics (i.e., flexural strength and dielectric constant) of a Si_3N_4-SiO_2-BN ceramic composites.

4.6.2. Effect of gelcasting process parameters on Flexural Strength

To better understand the effect of the process parameters on the performance characteristics (i.e., flexural strength and dielectric constant), 3D surface plots were generated from the experimental data in Table 3.17.

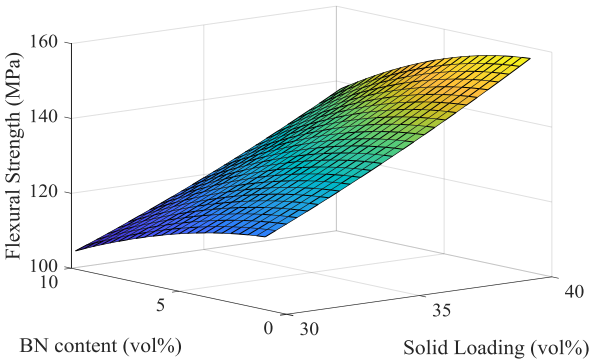

(a)

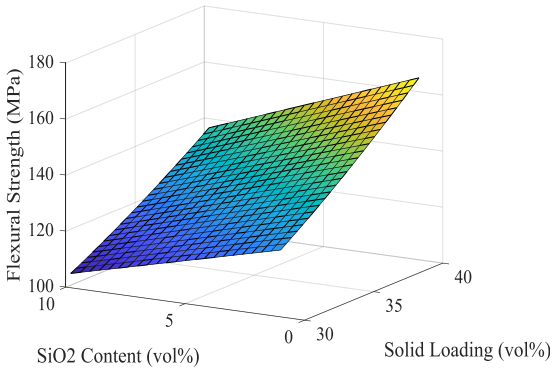

(b)

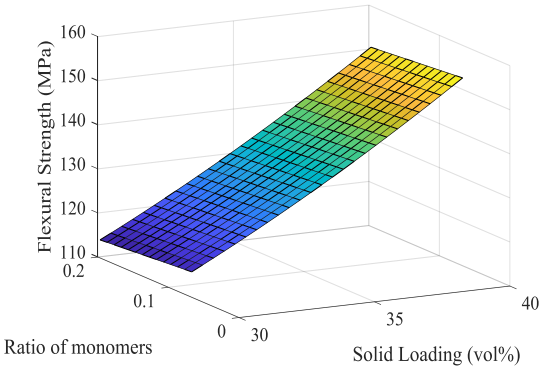

(c)

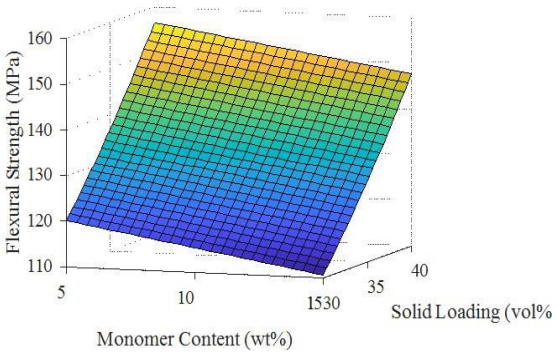

(d)

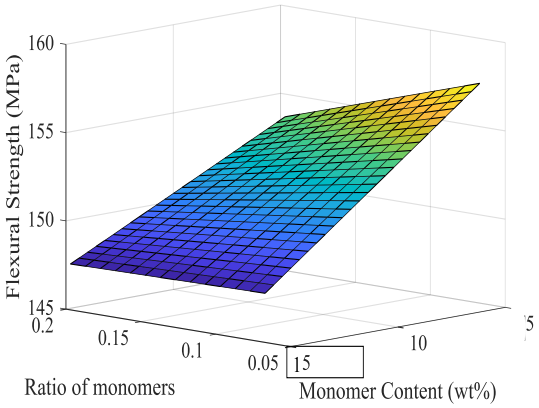

(e)

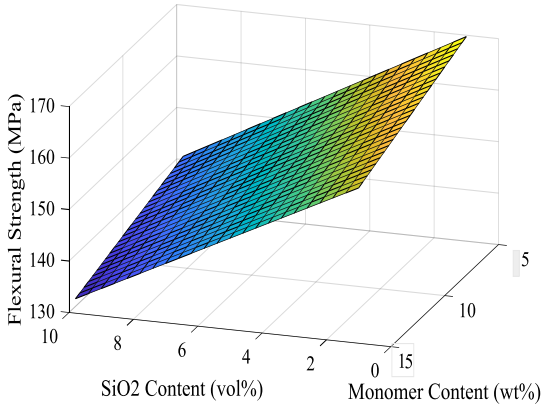

(f)

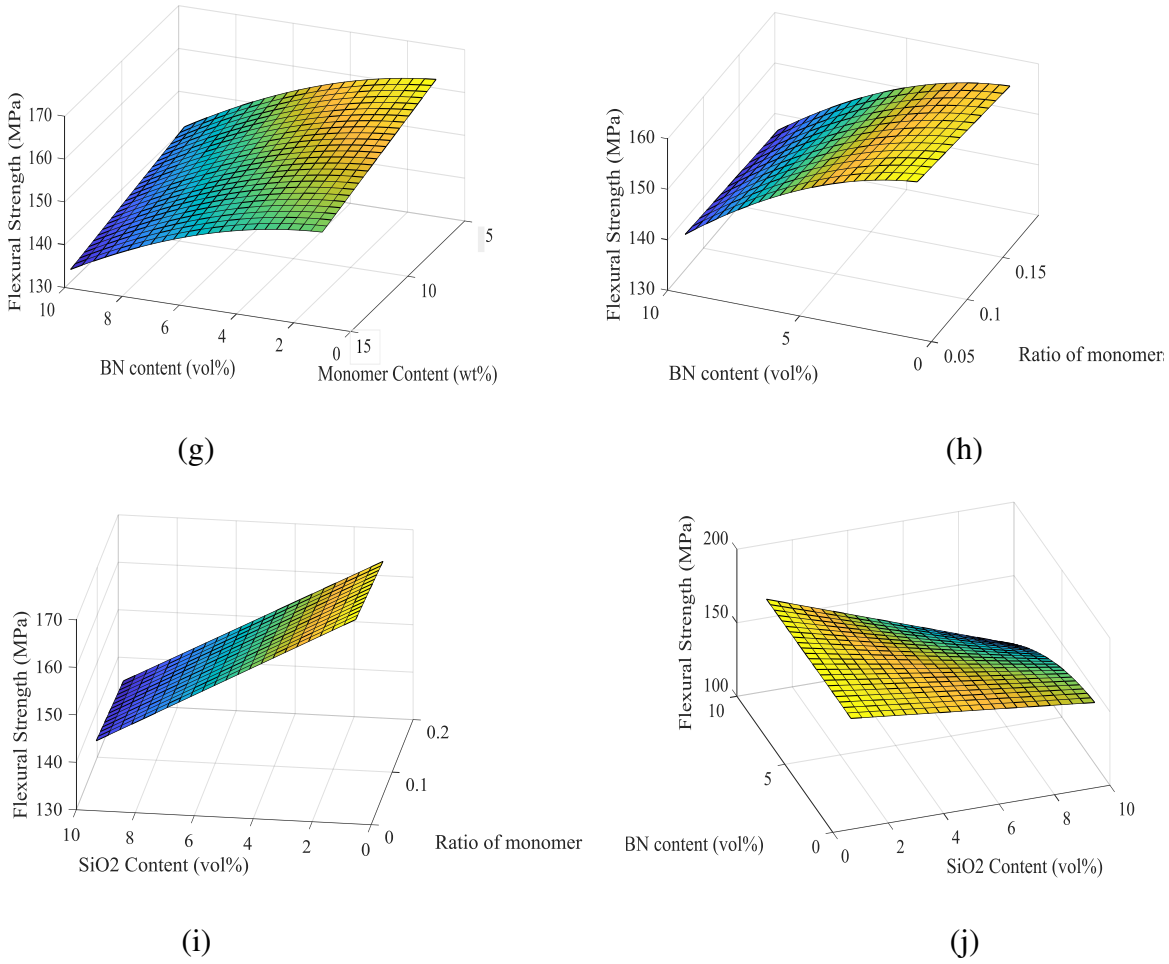

Figure 4. 23: 3D surface plots of Flexural Strength

Surface plots are plotted to investigate the effect of the process parameters on the flexural strength and is shown in Figure 4.23(a)-(j). Figure 4.23 shows increasing trend with increasing solids loading, monomer ratio, and at the same time it decreases with increasing monomer content, SiO_2 content and BN content. Figure 4.23 (a),(b),(c),(d) shows that the flexural strength increases as the solids loading increases. When the effect of two parameters is plotted, the other three parameters are kept constant. The hold values are Solid loading 40vol%, Monomer content 10 wt%, ratio of monomers is 1:10, SiO_2 Content is 5 vol% and BN content is 5vol%.

From the Figure 4.23, it is observed that a high flexural strength of the sample is obtained with a high solids loading and a low monomer content. With increasing solid

loading, density of samples increases leads to an increase in flexural strength. When the solid loading decreases, the space between the suspended particles is large, resulting in increased drying and sintering contraction, and the possibility of formation of microcracks increases in a green body. Figures 4.23 (e), (f) and (g) show a decrease in flexural strength with the monomer content increases. During sintering, the gel network polymer is completely burned by increase in monomer content, leaving large pores in the ceramic structure, which can reduce the flexural strength. As the monomer content increases, the porosity increases and the flexural strength decrease monotonically. Figures 4.23 (h) and (i) show that the flexural strength of the sintered body increases with increase in ratio of the monomers.

When the ratio of monomers is low, the gel structures are unstable and fragile, and therefore the flexural strength is reduced. By increasing the ratio of monomer to the cross linking gel points becomes more, making the cross-linked network structures compact in three-dimensional polymer gels and then the distribution of the ceramic particles in the gel network become more uniform. Therefore, the probability of occurrence of micro cracks in drying the green body decreases, and ultimately increases the flexural strength of the sintered ceramic body. Large ratio of monomers owing to detachment of the gel network structure in three dimensions leads to a significant decrease in the density and strength of the network molecular gel and finally the agglomerated particles and the non uniform distribution leads to a decrease in flexural strength. Therefore, there is an optimum ratio of monomers wherein the gel network structures are very homogeneous is more stable and provide an improved distribution of ceramic powder and the likelihood of low internal stresses in the drying step.

Figure 4.23 (h)shows the effect of the ratio of monomers and BN content various flexural strength. It confirms that a higher flexural strength is achieved at 1:10 ratio of monomers and without BN content. When the monomer content is low, the gel density is poor after gelcasting process, and the stability and uniformity of the green ceramic body is reduced. The increase in the monomer content builds a three-dimensional network structures compact which increases the green strength of the ceramic but decreases the flexural strength of sintered ceramic composite.

Figure 4.23(j) shows the effect of SiO_2 content and BN content on flexural strength (MPa). The Highest value of flexural strength is found at 0% SiO_2 content and 0% BN

content. As the SiO_2 Content and BN content increases the flexural strength decreases. The flexural strength decreases with the increase of SiO_2 powder as SiO_2 is softer than Si_3N_4 matrix. The transformation of α-Si_3N_4 into β-Si_3N_4 and densification are obstructed due to formation of the crystalline Si_2N_2O. Thus the porosity increases as the SiO_2 content increase, which leads to decrease in flexural strength. Due to large disparity in coefficients of thermal expansion between Si_3N_4 and cristobalite induces the formation of micro cracks, which can also lead to decreased flexural strength[143]. After sintering, the interlocking microstructure formed by rod-like β-Si_3N_4 grains was in favor of improving the flexural strength, but increasing in BN content hinders the transformation of α-Si_3N_4 to β- Si_3N_4 and densification is obstructed which leads to a decrease in flexural strength.

4.6.3. Main effects of Flexural strength

The influence of process parameters like Solid loading, Monomer content , ratio of monomers, SiO_2 Content, BN content has significant effect on flexural strength, as shown in main effect plot for flexural strength in Fig 4.24. From Figure 4.24, it is observed that as the solid loading increases from minimum to maximum, flexural strength initially increases and then decreases. Too low ratio of monomers makes the three-dimensional network structures of cross- linked polymer gels incomplete. With the increase of monomer content, the porosity monotonically increases and then decreases, and the flexural strength decreases. The pores of sintered body mainly originate from the residual micro-space of the organic processing aids in the green body during organic binder burnout. Therefore, the porosity monotonically increases with the increase of monomer content[40].

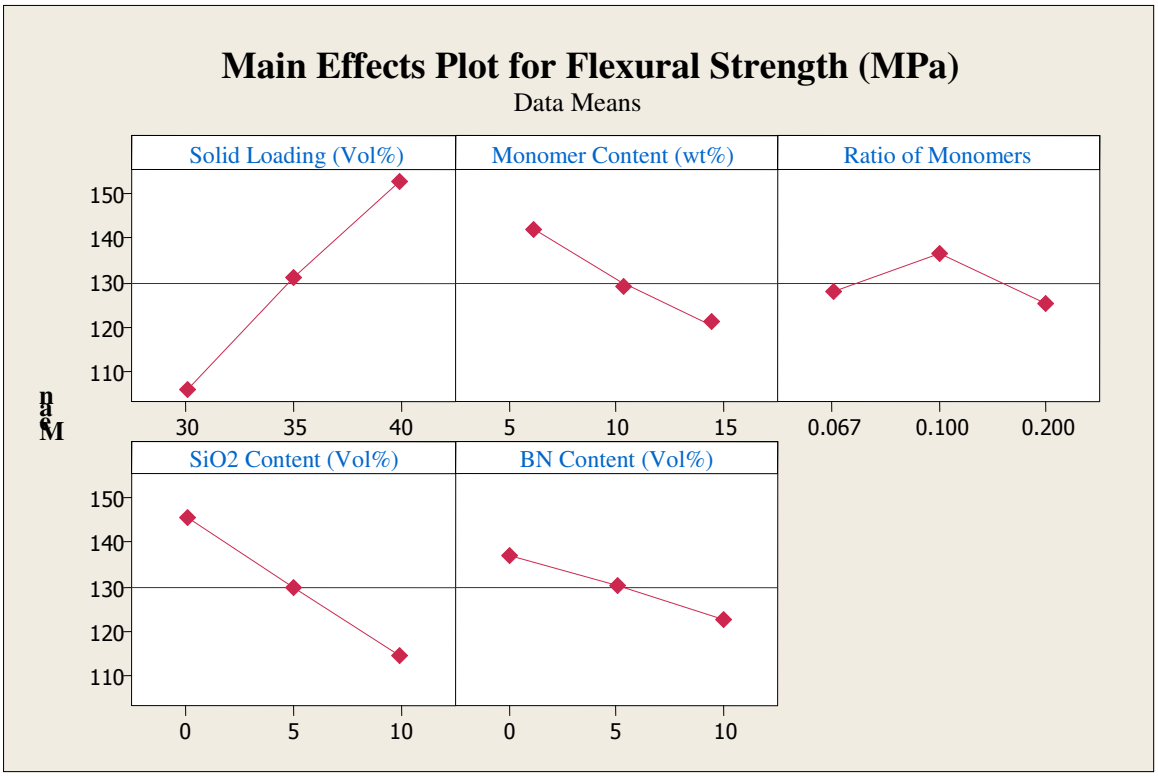

Figure 4. 24: Main effects of Flexural strength

With the increase of ratio of monomers, the flexural strength first increases, reaches maximum value, and then decreases. The results indicate that the ratio of monomers has an optimum value where the flexural strength of green body is highest. In the study, by merely increasing the monomer content in the slurry without other organic additives during the gelcasting preparation, monomer and cross linker herein not only can form macromolecular gel network to hold the ceramic particles together, but also can play a leading role of pore formation. The homogeneity of cross linking points in the gel body is mainly dependent on the ratio of monomers, and increasing the ratio of monomers makes the three-dimensional network structures of gel loose[64].

As the SiO_2 Content and BN content increases the flexural strength decreases. The flexural strength decreases with the increase of SiO_2 powder as SiO_2 is softer than Si_3N_4 matrix. The transformation of α-Si_3N_4 into β-Si_3N_4 and densification are obstructed due to formation of the crystalline Si_2N_2O. Thus the porosity increases as the SiO_2 content increase, which leads to decrease in flexural strength. Due to large disparity in coefficients of thermal expansion between Si_3N_4 and cristobalite induces the formation of micro cracks, which can

also lead to decreased flexural strength[143]. After sintering, the interlocking microstructure formed by rod-like β-Si_3N_4 grains was in favor of improving the flexural strength, but increasing in BN content hinders the transformation of α-Si_3N_4 to β- Si_3N_4 and densification is obstructed which leads to a decrease in flexural strength[151].

4.6.4. Effect of gelcasting process parameters on Dielectric constant

Surface plots are plotted to investigate the effect of the process parameters on the dielectric constant and is shown in Figure 4.25. Figure 4.25 shows increasing trend with increasing solids loading and at the same time it decreases with increasing monomer content, ratio of monomers,SiO_2 content and BN content. Figure 4.25 (a),(b),(c),(d) shows that the dielectric constant increases as the solids loading increases. The hold values are same as discussed previously. The dielectric properties and material density are closely related.

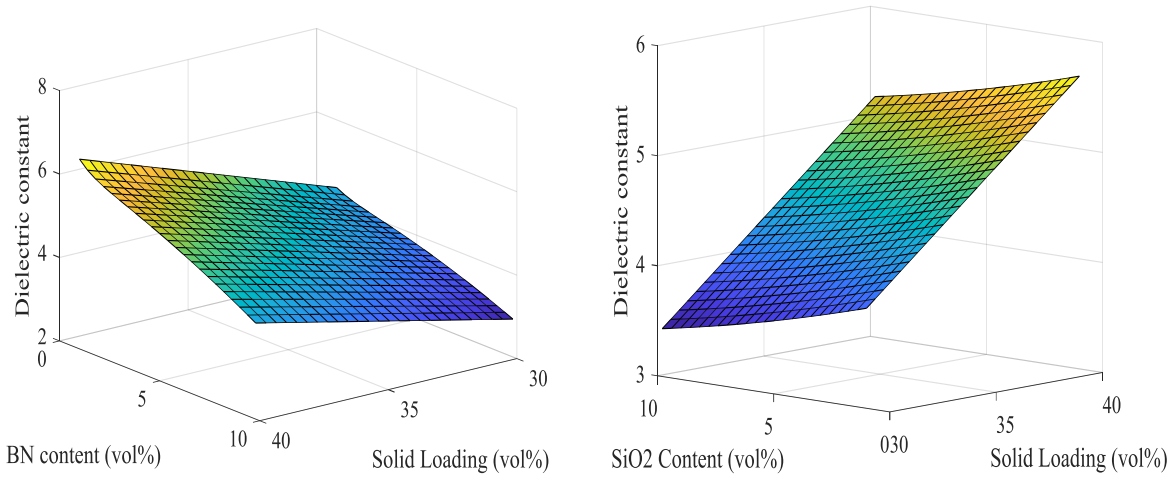

(a) (b)

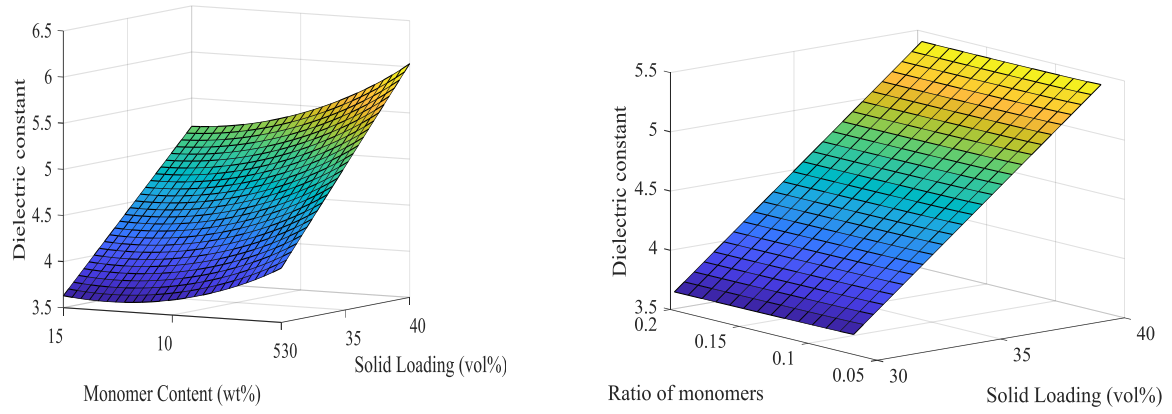

(c) (d)

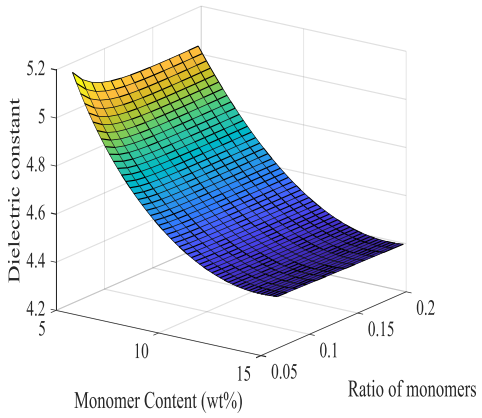

(e)

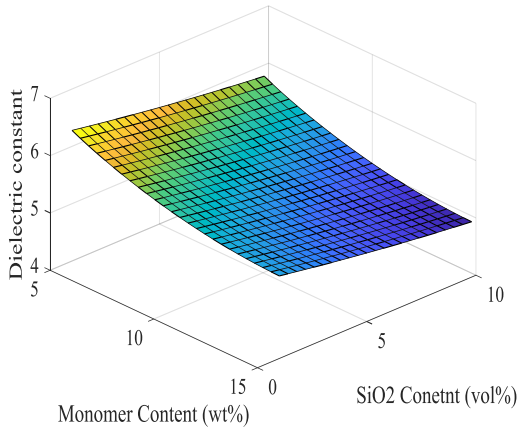

(f)

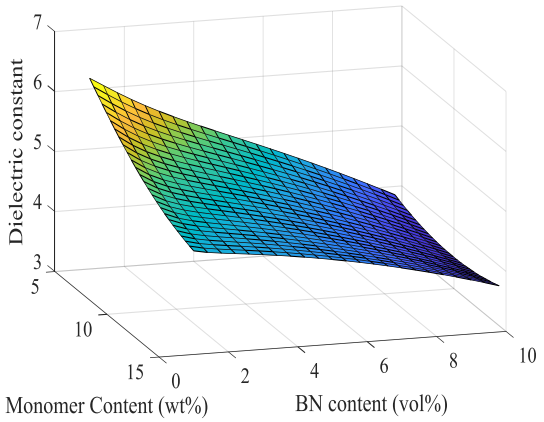

(g)

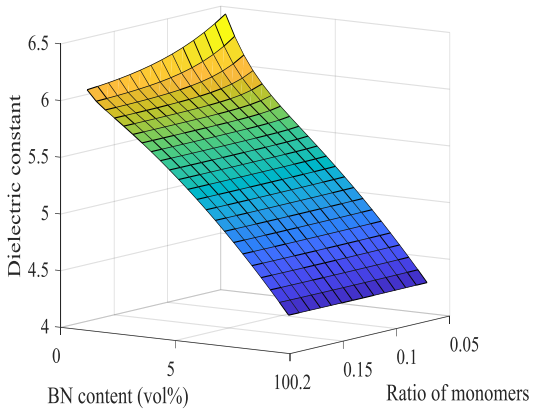

(h)

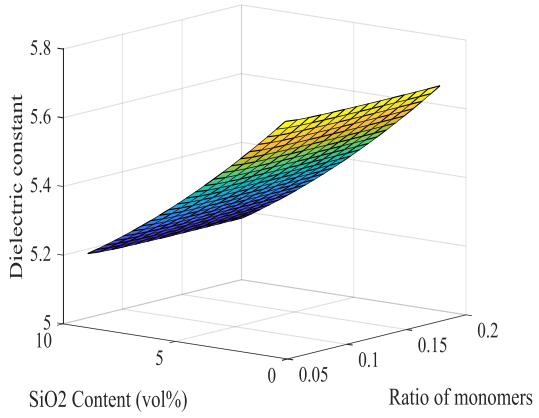

(i)

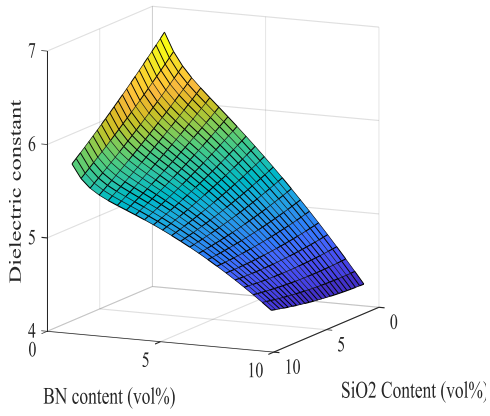

(j)

Figure 4. 25: Response surface plots of dielectric constant

As shown in Figure 4.25(a) (b) (c) and (d) with the increase of solid loading, the increase in density of ceramic composites will lead to the increase of dielectric constant. Figures 4.25 (e), (f) and (g) show a decrease in dielectric constant with the increase in monomer content. The increase in monomer content decreases the density of sintered ceramic due to the formation of large pores during binder burn out. Thus more the monomer content lowers the density and lower the dielectric properties.

Figures 4.25 (h) and (i) show that the dielectric constant of the sintered body decreases slightly with increase in ratio of the monomers. Dielectric constant is predicted to be decreasing with increase in ratio of monomers. At a given monomer content, increasing the ratio of monomers means the decrease of cross linker. Therefore, increasing the ratio of monomers makes the crosslink density of cross-linked polymer gels decrease, and the three-dimensional network structures of gel become loose. This decreases density of ceramic material and thus decreases dielectric constant.

Figure 4.25 (j) shows the effect of SiO_2 content and BN content on flexural strength (MPa). The effect of SiO_2 and BN content have similar effect on dielectric constant as on flexural strength. SiO_2 ceramics are having lower dielectric properties compared to Si_3N_4 ceramics. Thus the increase of SiO_2 content decreases the dielectric constant. The transformation of α-Si_3N_4 into β-Si_3N_4 and densification are obstructed due to formation of the crystalline Si_2N_2O leads to porosity. Due to the increase of porosity, the dielectric constant could be lower as the dielectric constant of pore is 1. With the increase in BN content, the transformation of α to β -Si_3N_4 was inhibited which results in a decrease in dielectric content. As the dielectric constant of α- Si_3N_4 and β- - Si_3N_4 are 5.6 and 7.5 respectively. Also, densification was obstructed which leads to increase in porosity.

4.6.5. Main effects of Dielectric Constant

The influence of process parameters like Solid loading, Monomer content , ratio of monomers, SiO_2 Content, BN content has significant effect on dielectric constant, as shown in main effect plot for flexural strength in Figure 4.26.

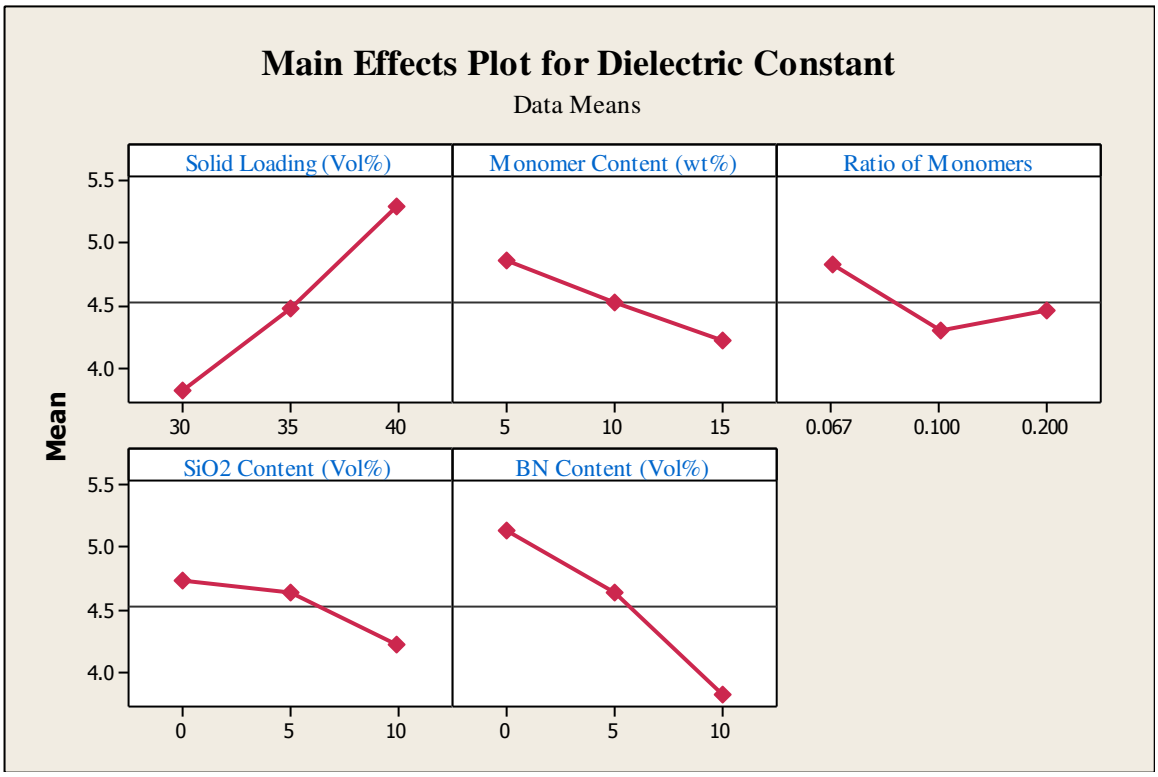

Figure 4. 26: Main effects of Dielectric constant

The dielectric properties and the density of the material are closely interrelated. As shown in Figure 4.26, with a increase of solid loading, the increase in density of ceramic leads to an increase in the dielectric constant. Density begins to decline when the solids loading increases beyond a certain value due to the increase in pore surface area, or a ceramic powder agglomeration followed by the formation of micro cracks. From the Figure 4.26, as the monomer content increases monotonically, the dielectric constant decreases. The monomer content decreases progressively to the density of the sintered ceramics due to the formation of large pores during binder burn out. Thus, the increase in monomer content decreases the density and dielectric properties[43].

It is anticipated that the dielectric constant decreases with the increase in the monomer ratio. At a given monomer content, increasing the ratio of monomers means the decrease of cross linker. Therefore, by the proportion of the monomers decreased an increase in the crosslinking density of the crosslinked polymers gels and three-dimensional network structures become loose gel. This reduces the density of the ceramic material and thus the dielectric constant [152].

SiO_2 ceramics have dielectric properties lower with respect to the Si_3N_4 ceramic. Therefore, the dielectric constant decreases with increase in SiO_2 content. In addition, it is possible to thermally form Si_2N_2O from SiO_2 and α- Si_3N_4. Obviously, the liquid phases have been consumed to a large extent on the formation of Si_2N_2O, so the transformation to β- Si_3N_4 hinders and leads to increased porosity. Due to the increased porosity, dielectric constant can be less as the dielectric constant of the pore is 1. With the increase in the BN content, α-Si_3N_4 to β-Si_3N_4 transformation was hindered and results in decrease in dielectric constant as α-Si_3N_4 and β- Si_3N_4 have dielectric constant of 5.6 and 7.5, respectively. Furthermore, densification was obstructed which leads to increase in porosity.

Summary

This chapter first deals with the characterization of Si_3N_4, SiO_2 and BN raw materials. The chapter also deals with a characterization of ceramic slurries prepared using different pH, solid loadings and dispersant concentration of the slurry which alters the colloidal behaviour. To achieve highly stable suspensions zeta potential and Rheological characterizations were obtained to decide the optimal dispersant concentration and pH level. Based on the slurry results, and by optimizing dispersant and monomer content, the resulting green Si_3N_4 ceramic bodies were characterized. Compared to Si_3N_4, BN has a better thermal shock resistance and dielectric properties. SiO_2 has a dielectric constant and dielectric tangent losses even lower, which makes silica widely used as wave transparent materials. The effects of SiO_2 or BN content on the microstructures, mechanical and dielectric properties of the Si_3N_4–BN, Si_3N_4–SiO_2 composites are investigated. The effect of process parameters on performance characteristics of Si_3N_4–SiO_2-BN ceramic composite was discussed. Therefore, Si_3N_4-SiO_2-BN ceramic composites can combine the advantages of individual phases of Si_3N_4, BN and SiO_2 and have better dielectric and mechanical properties, which have been considered as capable materials for wave transparent applications. However, it has been proven that addition of SiO_2 and also BN into Si_3N_4 could significantly decrease the dielectric constant of the materials.

CHAPTER 5

MODELING AND MULTI-OBJECTIVE OPTIMIZATION

5.1. Introduction

This chapter deals with the generation of regression models for flexural strength and porosity for porous Si_3N_4 ceramics using Multi Gene Genetic Programming (MGGP) by considering the experimental data from chapter V. This chapter also deals with prediction of flexural strength and dielectric constant f porous Si_3N_4–SiO_2-BN ceramics using Multi gene genetic programming (MGGP) model. This chapter also presents the multi-objective optimization of porous Si_3N_4 and Si_3N_4–SiO_2-BN ceramic composites using genetic algorithm. These responses are simultaneously optimized and the optimal levels of the process parameters are determined by Pareto front.

5.2. Modelling of Porous Si_3N_4 Using Multigene genetic Programming (MGGP)

5.2.1. MGGP Implementation

In this work, the software tool GPTIPS' is used to develop appropriate MGGP models to predict the flexural strength and the porosity of the gelcasted Si_3N_4 ceramic [23].This software is a new code written by "Genetics and Regression Symbolic Programming" on the basis of multi gene genetic programming by means of MATLAB[20]. MGGP method is applied to the dataset of Table 3.10 in chapter 3. This study aims to determine the flexural strength and the porosity of the ceramic Si_3N_4 and develop a model for prediction of flexural strength and porosity of the gelcast Si_3N_4 ceramics based on the MGGP. Figure 5.1 shows the architecture of the modeling concept for predicting the Flexural strength and porosity.

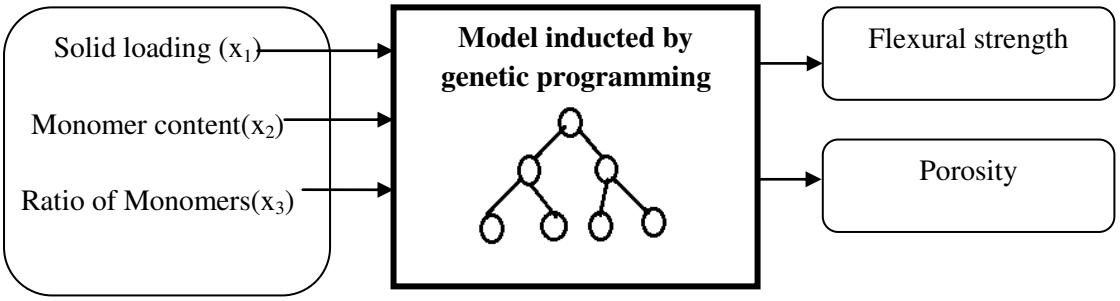

Figure 5. 1: architecture of the modeling paradigm to predict the Flexural strength and porosity

GPTIPS has the ability to prevent limitations to the arising of bloating. Bloating is explained as the redundant growth of the tree model without any considerable development in the fitness value[120, 153]. This can be prevented when initial parameters were set to certain boundaries, such as a maximum number of nodes per trees, maximum depth of genes, trees, and a maximum number of genes. The tournament selection used was lexicographic, which is an effective method for controlling the bloating of the model[154]. The authors examined the value of Root mean square error (RMSE) for evaluating the fitness function. Other initial parameters were established for the implementation of GPTIPS is given in the Table 5.1 [155].

5.2.2. Setting of parameter for implementation of MGGP

Table 3.10 in chapter 3 shows the 16 experimental data set values. The experimental data were divided into two groups: the testing dataset as well as the training dataset. The training dataset was employed to compute the equation with input parameters for each response (output parameters) and the testing data was used to verify the developed model and to ensure the widespread implementation of the model for the invisible cases. Selection of testing and training data set has an effect on training models. In this work, about 80 % of the experimental data was chosen randomly for training model while the other 20% of data is used as testing data. The selection is such that the minimum, maximum, mean and standard deviation of the training and testing data sets were reliable. MGGP's best model is based on a minimum RMSE value.

Table 5. 1: Initial factor settings for MGGP

Parameters	**Values assigned**
Population size	150
Number of generations	100
Runs	10
Size of the tournament	2
Maximum depth of the tree	4
Maximum genes	5
Functional Set	(Plus, minus, multiply, tanh, sin, cos, exp)
Terminal Set	(x_1, x_2, x_3, [−10 10]) x_1-Solid Loading x_2-Monomer Content x_3-Ratio of monomers
Crossover probability(%)	0.85
Mutation probability (%)	0.05
Reproduction probability(%)	0.10

Basic arithmetic operators, trigonometric and exponential functions are used to obtain optimal MGGP models. The size of the population controls the number of equations in the population. The numbers of levels used by algorithms at end of the run were set by the number of generations. The appropriate number of generation and population always depends on a number of the problem complicity and feasible solutions.

A good number of generations and population were thoroughly tested to obtain accurate models for minimum error. The program is executed until the run inevitably completed. The maximum depth of the tree and the maximum number of genes in an individual affects the number of solutions dealt with the search space and the size of the search space. In this case, both complexities of the function and the speed of the developed algorithm decrease simultaneously. The permissible number of genes and the depth of the tree are each set to the optimal values of 5 and 4 as shown in the Table 5.1.

There were several tests performed with different initial parameters of MGGP and the performance of developing equations was calculated for every run. Finally, the best

mathematical models were selected for the prediction of flexural strength and porosity according to performance evaluation criteria.

5.2.3. MGGP model for Flexural strength

The best model for Flexural strength formulated by MGGP using experimental data given in Table 4.3 is

$$\boldsymbol{Flexural\ strength} = \mathbf{181.2} \times \boldsymbol{tanh}\left(\frac{x_2}{x_1}\right) - \mathbf{0.0351} \times \boldsymbol{x_1} + \mathbf{91722} \times \boldsymbol{tanh}(\mathbf{0.1238} \times \boldsymbol{x_1}) + \left(\frac{\mathbf{181.2} \times (\boldsymbol{x_2} + \mathbf{1.176})}{(\boldsymbol{x_2} + \mathbf{6.481})}\right) - \mathbf{0.0351} \times \boldsymbol{x_1} \times \boldsymbol{x_2} - \mathbf{0.0351} \times \boldsymbol{x_1^2} \times \boldsymbol{x_2} \times \boldsymbol{x_3} + \left(\frac{\mathbf{18.36} \times \boldsymbol{x_1} \times \boldsymbol{x_3} \times (\boldsymbol{x_2} - \mathbf{1.176})}{\boldsymbol{x_2}}\right) - \mathbf{91700} \quad (5.1)$$

The accuracy of the equation 5.1 is shown by plotting the Flexural strength against training and testing data with predicted values as shown in Figure 5.2. The determination of the coefficient (R) and root mean square error (RMSE) are equal to 0.9983 and 1.4391 for training sets are 0.9733 and 6.6957, for testing sets as shown in Figure 5.3(i) and (ii), respectively. There is a good correlation among the predictions from MGGP and the measured values.

A comparison of the errors for the training and testing with experimental data is performed using MGGP and experimental results are shown in Figure 5.2. As can be seen, the training set that includes results of 11 samples and testing set comprising samples of 5 results. It has been observed that the MGGP model can predict the flexural strength with a high degree of precision and high variance (99.83% for training and 97.33% testing data) and the root mean square error (RMSE).

Smaller absolute error is better in the GP model, the error found to be is decreased with the increase of number of nodes and thus a MGGP model is more complex. Figure 5.3 shows the actual versus predicted values of flexural strength of training data and testing data Due to this computational difficulty, model was run for the tree depth limited to 4 as shown in Table 5.1. MGGP model was run for 100 times in the same conditions (Table 5.1).This MGGP model is capable of predicting objective (Flexural strength) of gelcasting process with high accuracy. The fitness value (log scale) and the mean fitness values with the number of

generations are shown in Figure 5.4. From this Figure 5.4, we found that the root mean square error (RMSE) value decreases by enhancing the number of generations. The best fitness value was found to be at 149th generation (RMSE= 1.4391).

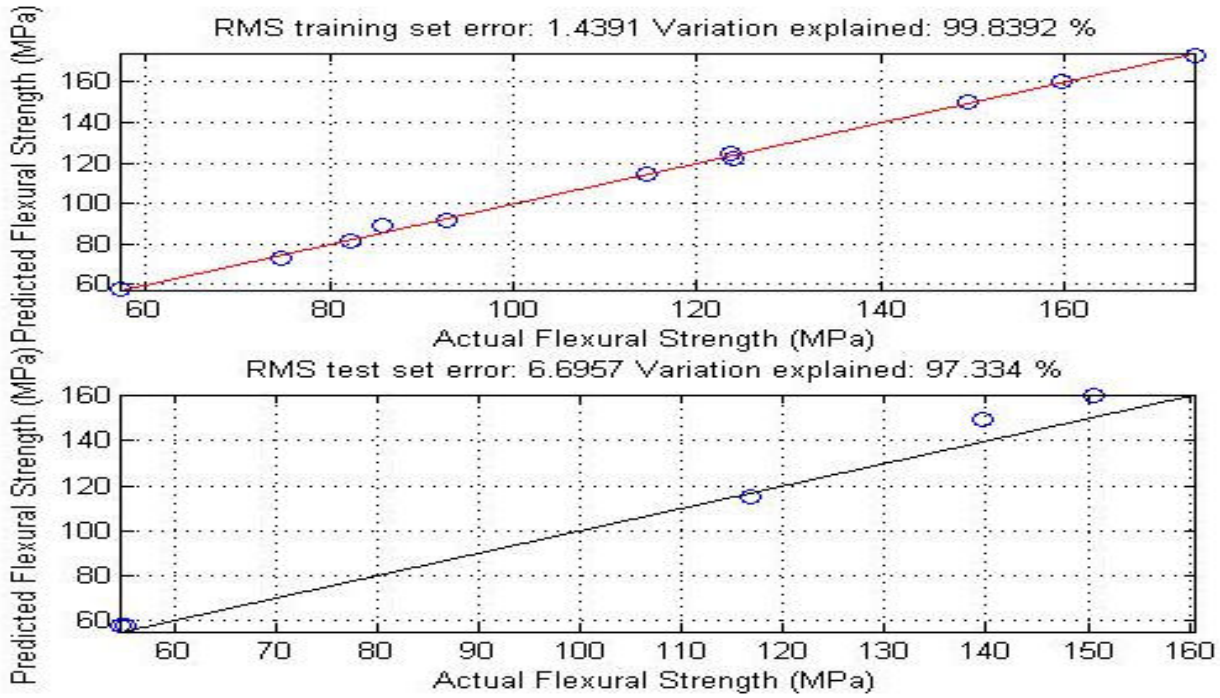

Figure 5. 2: Comparison of experimental results and the MGGP model prediction of flexural strength for (i) training data and (ii) testing data

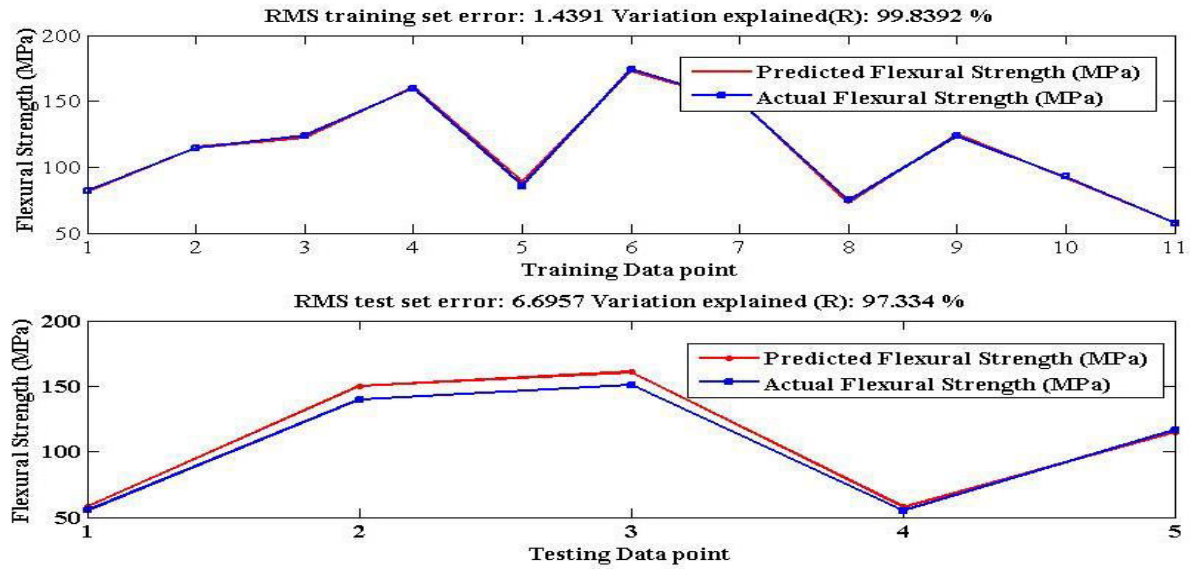

Figure 5. 3: Actual versus predicted values of flexural strength (i) training data and (ii) testing data

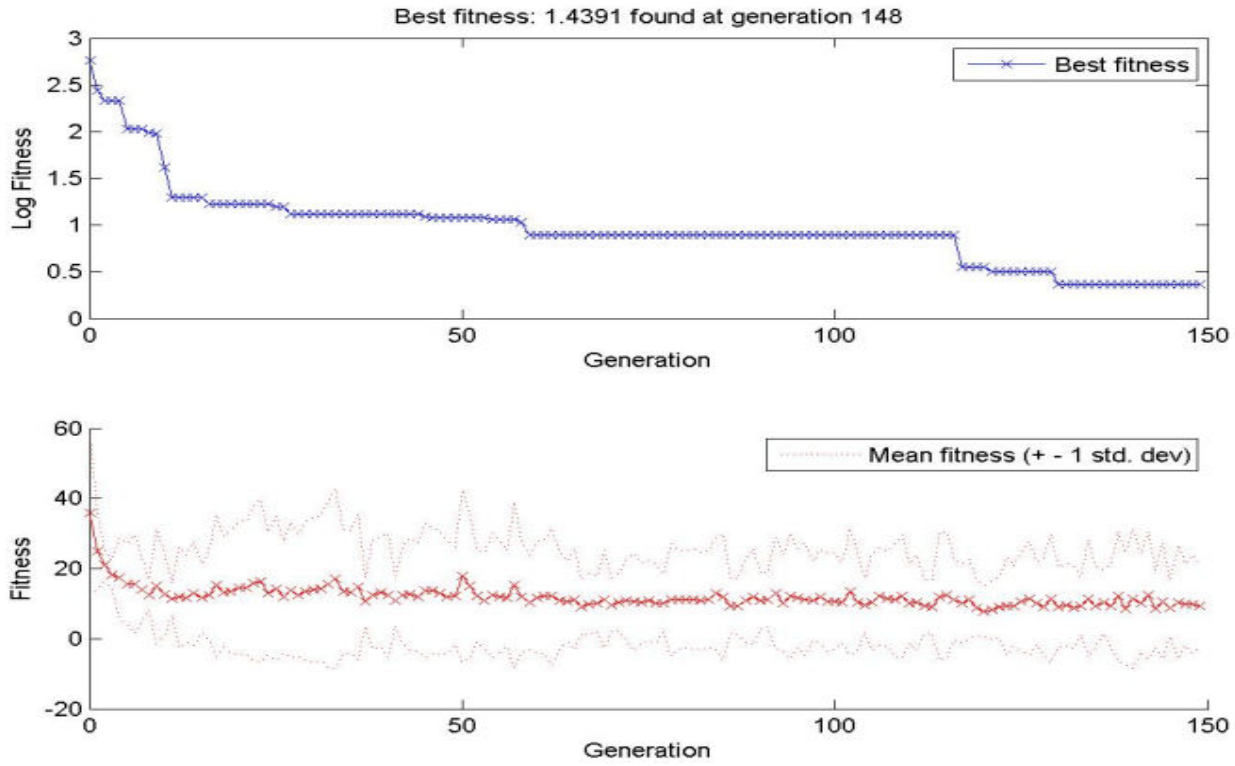

Figure 5. 4: Variation of fitness with number of generations of flexural strength

The surface plot of the predicted model of flexural strength is shown in Figure 5.5 for a value of x_2 (monomer content) = 10 wt%. The factor x_2 (monomer content) has less influence on flexural strength compared to x_1 (Solid loading) and x_3 (Ratio of monomers) as discussed in section 4.6.3.

Figure 5.5 shows the effect of solid loading and ratio of monomers on flexural strength of gelcast porous Si_3N_4 ceramics. It indicates that a high flexural strength sample is obtained with high solid loading and high ratio of monomers. With the increase of solid loading, the increase in density of ceramics is beneficial for the increase of flexural strength. When the solid loading decreases, the space between the suspended particles is large, which results in an increase in drying and sintering contractions, and the possibility of occurrence of micro cracks in a green body is increased.

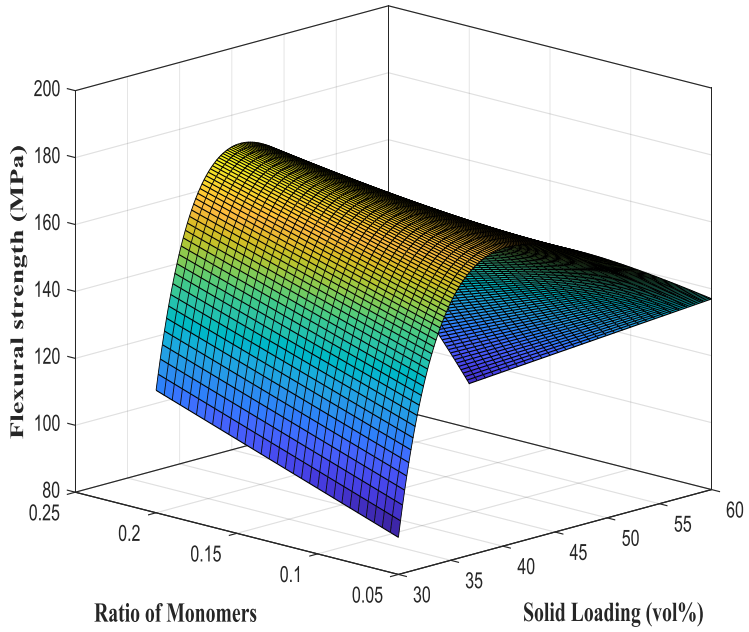

Figure 5. 5: Response surface plot showing the effect of Solid loading and Ratio of monomers on flexural strength with 10wt% monomer content

As a result, the flexural strength of the Si_3N_4 ceramic composite was low. The preparation of the suspension is almost impossible due to increase of viscosity by increasing the solids loading upto 60 vol%. Therefore, the maximum flexural strength of the sintered body is at most by 46 vol% solid loading from the Figure 5.5.Also the flexural strength increases to increase the ratio of the monomers. When the ratio of monomers is low, the gel structures are unstable and fragile and so flexural strength decreases. Increasing the ratio of monomer to cross linker, the cross linking gel points becomes more, making the cross-linked network structures compact in three-dimensional polymer gels, and then the distribution of ceramic particles in the gel network will be more uniform and finally the flexural strength of Si_3N_4 ceramic increases. The surface plot reflects the nonlinear variation of flexural strength with the solid loading and ration of monomers.

5.2.4. MGGP model for Porosity

The best model for porosity formulated by MGGP was as follows:

$$Porosity = 1.537 \times x_1 - 53.2 \times x_3 + 93.91 \times \tanh(8.888 \times x_3) + 172.4 \times \tanh\left(\frac{17.19}{x_1}\right)$$

$$+\left(\frac{1.537 \times tan(x_1)}{x_3}\right) - \mathbf{1.537 \times x_1 \times x_3} - \left(\frac{814.7 \times x_3}{(x_1 - 7.613)}\right) + \mathbf{3.7 \times x_2 \times x_3^2} - \mathbf{161.6} \quad (5.2)$$

The precision of the developed equation is examined by plotting the values of Coefficient of correlation (R) and root mean square error (RMSE) for training datasets are 0.9859 and 0.4138, respectively, and for testing datasets 0.9728 and 0.7198, respectively as shown in Figure 5.6,. The accuracy of developed equation is analyzed by plotting the measured porosity value against the predicted porosity values for training and testing sets as shown in Figure 5.7. The values of R and RMSE values are shown as 0.9859 and 0.4138, respectively, for the training set and are 0.9728 and 0.7198, respectively, for the testing data. The R value was low because the same conditions of flexural strength have been used to compare both the results. There is a good correlation between the predictions from multigene genetic programming (MGGP) and the measured data.

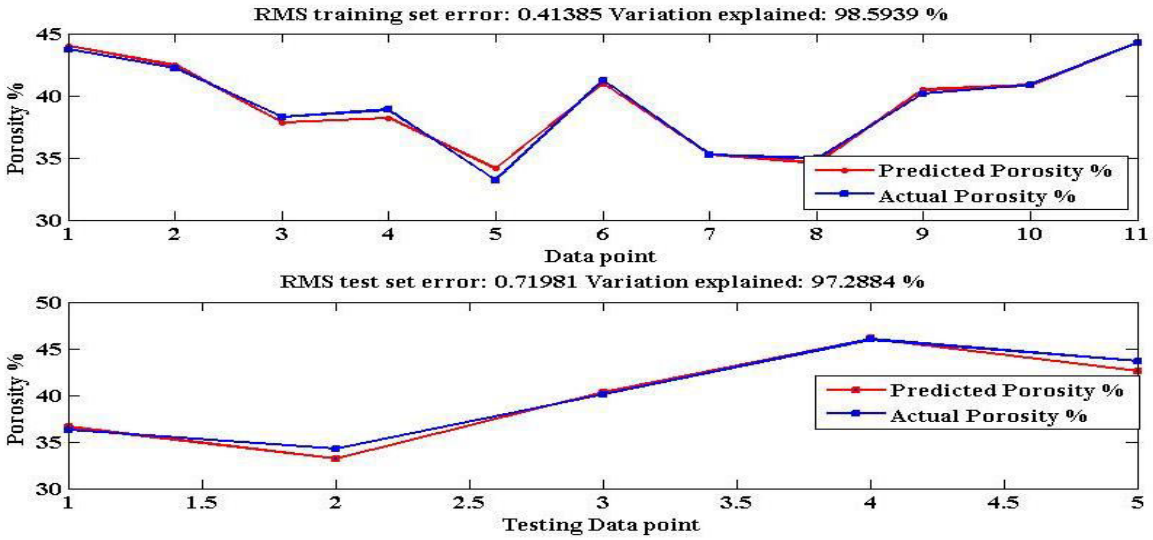

Figure 5. 6: Comparison of experimental results and the MGGP model prediction of Porosity for (i) training data points and (ii) testing data points

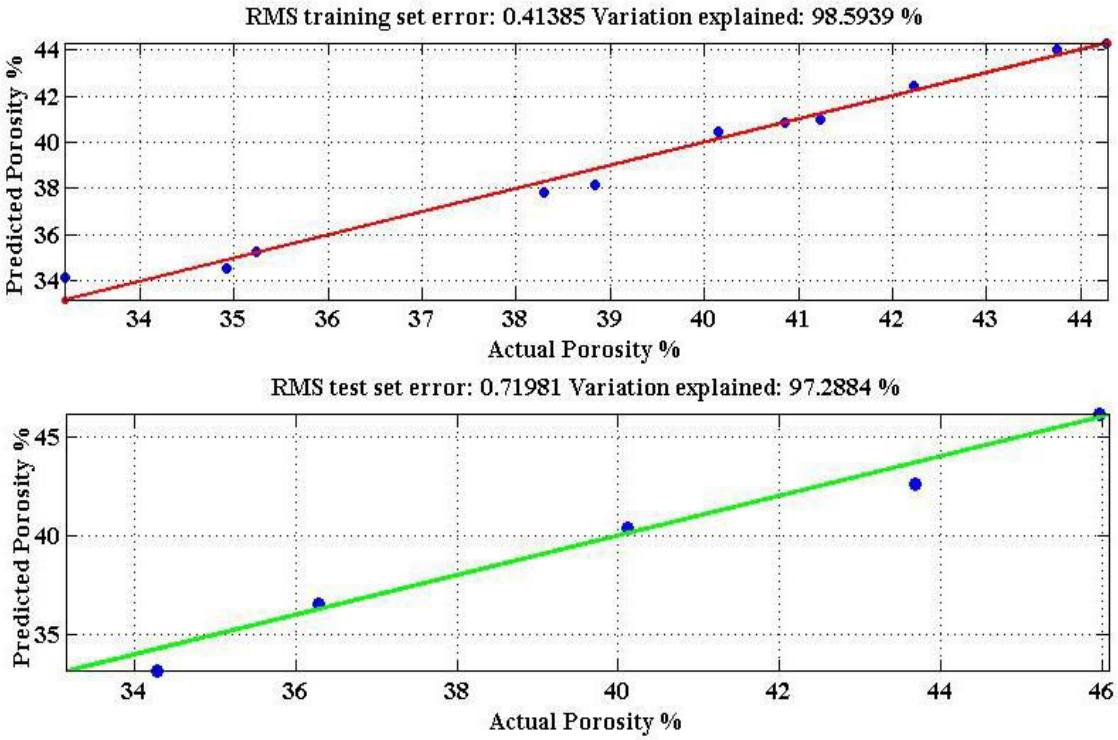

Figure 5. 7: Actual versus predicted values of Porosity (a) training data and (b) testing data

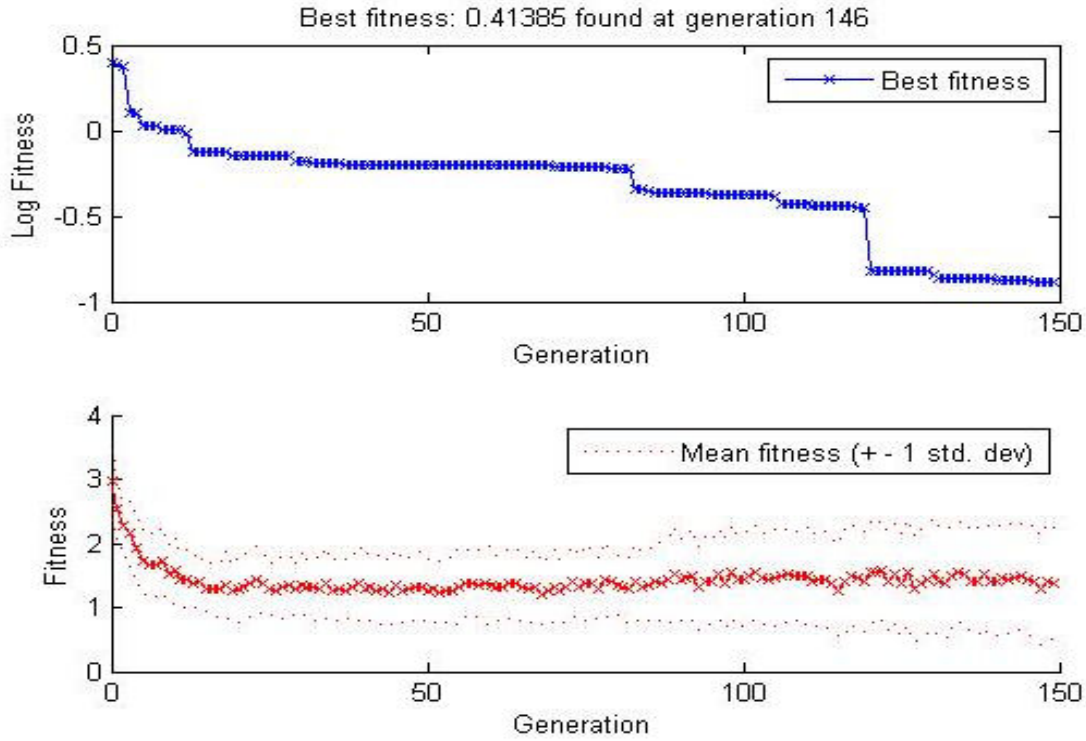

Figure 5. 8: Variation of fitness value with the number of generations of porosity

The error between the calculated values of MGGP model and experimental results of the training and test data are shown in Figure 5.6. The variation explained is 98.59% and 97.28% for the training and testing data. Figure 5.8 (a) and (b) depict the variation in the best fitness value (log values) and the mean fitness with the number of generations. The best fitness value (RMSE) of 0.41385 was found at 146^{th} generation).

5.3. Formation of multi objective optimization problem

In this work, two objectives were considered, they were namely flexural strength and porosity. It is observed that the increase in porosity, the flexural strength decreases, and also vice versa. However, our goal is to maximize both. Thus generation of mono optimal solution will not serve the purpose, as the objectives are contradictory to each other. The simultaneous optimization of flexural strength and the porosity comes into multi objective optimization problem. There cannot be a single optimal solution to a problem of multi objective optimization. Thus, a set of equally reliable solutions being called as non-dominated or pareto set of optimal solutions were obtained. These optimal solutions are clearly based on the concept of dominance, where it is said that one element dominates another if it is better than the other in at least one objective and not a bad function with respect to all other objectives. The pareto front depicts tradeoffs among challenging objectives and recognizes non-dominated solutions. It consists of population members, for whom there is no solution that is better than the Pareto member criteria.

5.3.1. Genetic algorithm for optimal pareto front

MATLAB toolbox for optimization (R2013a) is used to create the Pareto optimal front for flexural strength and porosity using with 'gamultiobj' function. The initial population for the genetic algorithms generated randomly by default. The elitism process gives emphasis to the best solutions in subsequent generations. The next generation of the population is based on the non-dominated rank. The rank is calculated as crowding distance of individuals in the current pool. The algorithm stops after execution of 100 iterations.

5.3.2. Problem Formulation

In this work, objectives are to maximize the flexural strength and porosity. These objectives are conflicting in nature. So as to convert two objectives for minimization, it is appropriately modified. The optimization problem is stated as follows:

Objective 1 = 1/1+Flexural Strength

Objective 2 = 1/1+Porosity

Subject to

30>Solid Loading> 60

5> Monomer Content > 20

0.05> Ratio of Monomers > 0.2

where objective 1 and objective 2 are taken from Equation 5.1 and 5.2, respectively.

The flexural strength and porosity to be maximized were negated in the vector valued fitness function as 'gamultiobj' minimizes all objectives. Ranges of experimental values were used as constraints for the input variables as stated above. In Table 5.2 gives the options and parameters for the optimization of the genetic algorithm. The algorithm is executed again and again for more number of points in the Pareto optimal front.

Table 5. 2: GA parameters and options

Population type: Double vector type
Population size: 100
Function for selection: Tournament
Tournament size: 2
Reproduction crossover fraction: 0.8
Crossover: Scattered function
Mutation : Constrained dependent function
Migration factor: 0.2
Migration interval : 20
Migration direction: Forward

Distance function: Crowding
Pareto population fraction: 0.5

5.3.3. Pareto front and optimal solutions

The change in weighted average of fitness function value was employed as a criterion to stop the algorithm. A pareto front after 127 iterations as the best multi objective optimized solution, which is shown in Figure 5.9. The concave curve in Figure 5.9 show that, there is no pareto optimal solution that is better than any other solution since they are all non dominated solutions. The choice of the solution depends on the requirement of the process. The Pareto optimal solutions with corresponding decision variables were given in Table 5.3. Each point on the pareto front represents a group of decision variables. The choice of set of flexural strength and porosity values can be obtained from the Figure.4.8 and the corresponding decision variables were taken from Table 5.3.

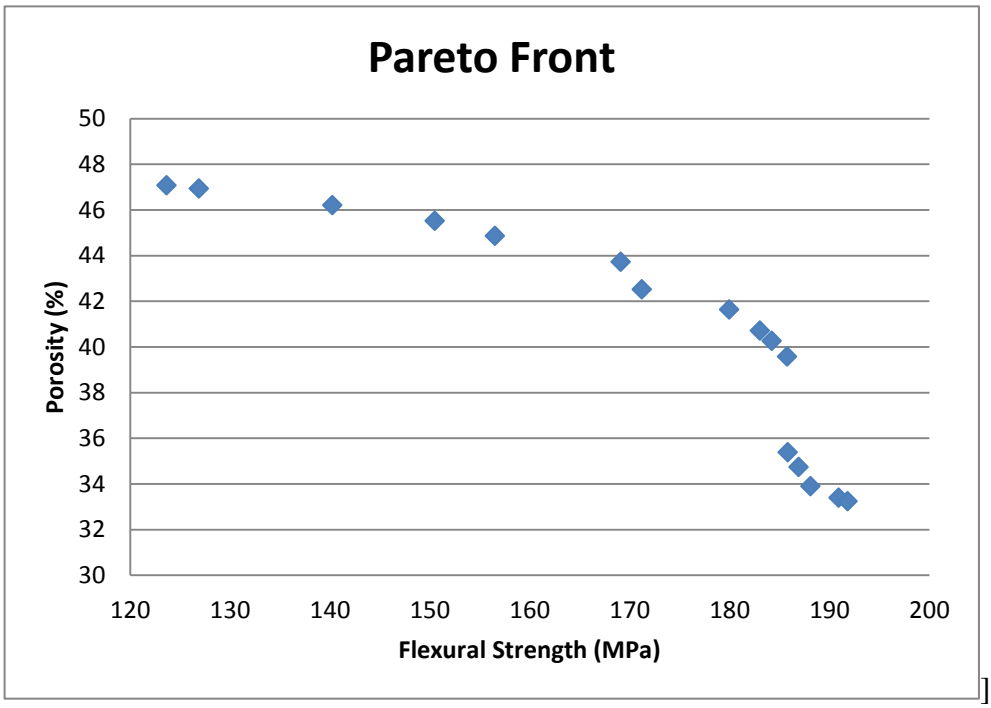

Figure 5. 9: Optimal Pareto front

Table 5. 3: Set of gelcasting parameters along with the Pareto optimal solutions for gelcasting of porous silicon nitride.

	INPUT PARAMETERS			OUTPUT PARAMETERS	
	Solid Loading (Vol%)	Monomer content (wt%)	Ratio Of Monomers	Flexural Strength (M.Pa)	Porosity (%)
1	38.04	8.787	0.194	184.23	30.26
2	*30.02*	*19.83*	*0.161*	**123.65**	**46.07**
3	36.26	19.62	0.074	185.85	34.38
4	*36.71*	*19.54*	*0.07*	**186.93**	**33.73**
5	36.37	18.84	0.063	188.1	32.89
6	34.62	16.65	0.158	169.11	42.72
7	32.59	18.11	0.172	156.51	43.86
8	30.19	19.76	0.16	126.88	45.93
9	38.05	9.269	0.188	183.05	39.7
10	36.79	19.82	0.058	190.92	32.39
11	31.02	19.28	0.163	140.26	45.2
12	31.73	17.44	0.159	150.49	44.51
13	35.63	19.49	0.128	171.22	41.52
14	36.6	9.874	0.181	179.99	40.63
15	39.06	8.532	0.2	185.77	38.58
16	39.93	9.81	0.165	191.84	32.23

For example, when a manufacturing engineer has a component with 40% porosity, the set of decision variables can be chosen from the fourteenth row of Table 5.3. As a result, the flexural strength of 179.99 MPa would be attained. To illustrate the advantage of the proposed method, two examples are explained below. From the experimental results of Table 3.10 in Chapter 3, the variables listed in the fourth row are given as a porosity value of 36.29% and the flexural strength is 123.89 MPa. After optimization, it can be seen that the porosity is increased to 46.07% for the same flexural strength (Sl No. 2, Table 5.3), with an increase of 27 percent porosity. In another case, from Table 3.10 in chapter 3 sixth row, the set of input

parameters leads to the flexural strength of 159.74 MPa and the porosity of 33.21%. After optimization, the flexural strength increases to 186.93 MPa (Sl No. 4, Table 5.3) with almost the same porosity value.

5.4. Modeling of Si_3N_4-SiO_2-BN ceramic composite using multi-gene genetic programming (MGGP)

5.4.1. Settings of parameter for implementation of MGGP

Table 3.17 from chapter 3 shows the 27 experimental data sets used for modeling flexural strength and dielectric constant of the gelcasted Si_3N_4-SiO_2-BN ceramic composite. The experimental data were divided into a training dataset and testing dataset as discussed in section 5.2.2. In this work, 21 experiments are chosen randomly selected as the training data while the other seven experiments are used as testing data. MGGP's best model is based on a minimum fitness value (RMSE) selected in the training data of all test runs.

The permissible maximum number of genes and the maximum tree depth are each set to 6 and 4 as shown in Table 5.4.There were several tests performed with different initial parameters of MGGP and the performance of developing equations was calculated for every run. Finally, the best MGGP models were chosen based on the performance evaluation criteria for the prediction of flexural strength and porosity, independently. This study aims to develop a model for the prediction of flexural strength and the dielectric constant of the Si_3N_4-SiO_2-BN ceramic composite using MGGP. The authors examined the value of RMSE for evaluating the fitness function. Other initial parameters were established for the implementation of GPTIPS is given in the table[155]

Table 5. 4: Initial parameter settings for MGGP

Population size	250
Max. generations	150
Input variables	5
Tournament size	25
Elite fraction	0.7

Max. genes	6
Max. tree depth	4
Max. total nodes	Inf
Crossover probability	0.84
Mutation probabilities	0.14
Complexity measure	Expressional
Function set	TIMES, MINUS, PLUS ,TANH ,MULT3, ADD3

5.4.2. MGGP model for flexural strength

The best MGGP model for Flexural strength was as follows.

$$Flexural\ strength = 4.87\,x1 + 0.294\,x2 - 2.75e4\,x3 - 3.18\,x4 - 1.45\,x5 + 5.61e4\,\tanh(x2) + 2.8e4\,\tanh(x3) - 5.61e4 \quad (5.3)$$

Where x_1-Solid Loading (vol%), x_2-Monomer Content (wt%), x_3-Ratio of Monomers, x_4-SiO_2 Content (vol%) and x_5-BN Content (vol%) .

The determination of the coefficient values (R) and RMSE are equal to 0.9979 and 1.6361 for training sets 0.9839 and 6.6957, for testing sets as shown in Figure 5.10 a and b, respectively. A comparison of the errors for the training and testing with experimental data is performed using MGGP and experimental results are shown in Figure 5.10. As can be seen, the training set that includes results of 21 samples and testing set comprising samples of 6 results. It has been observed that the MGGP model can predict the flexural strength with a high degree of precision and high variance (99.41% for training and 97.15% test) and the lowest average square error (RMSE (1.7524 for testing and 4.797 for testing data). As can be seen, the MGGP model is capable of predicting objectives with high accuracy.

There is a good correlation among the predictions from MGGP and the measured values. The accuracy of the equation is shown by plotting the measurement against for training and test predicted as in Figure 5.11. Figure 5.11 shows that the fitness of the optimal

GP model improves and the complexity changes as they develop GP models in the training phase. Because of the smaller the absolute error the better the GP model, the absolute error decreased and the number of nodes shows a rising trend, which means that the GP model will become more complex as it evolves. The depth of the tree is limited to below 4 according to the conditions in Table 5.4. Because of the more the absolute error, the more the GP model. Decreasing the absolute error and the number of nodes shows an upward trend, which means that the GP model becomes more complex as it develops. The depth of the tree is limited to below 4 according to the conditions in Table 5.4 below.

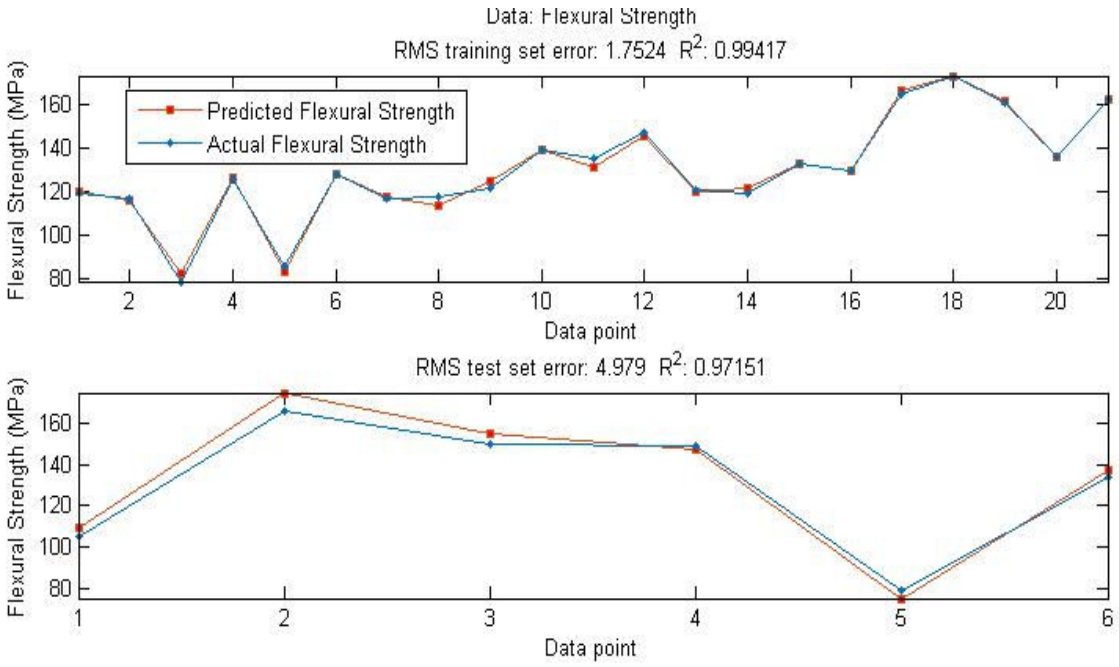

Figure 5. 10: Comparison of experimental results and the GP model prediction of flexural strength for (a) training data and (b) testing data

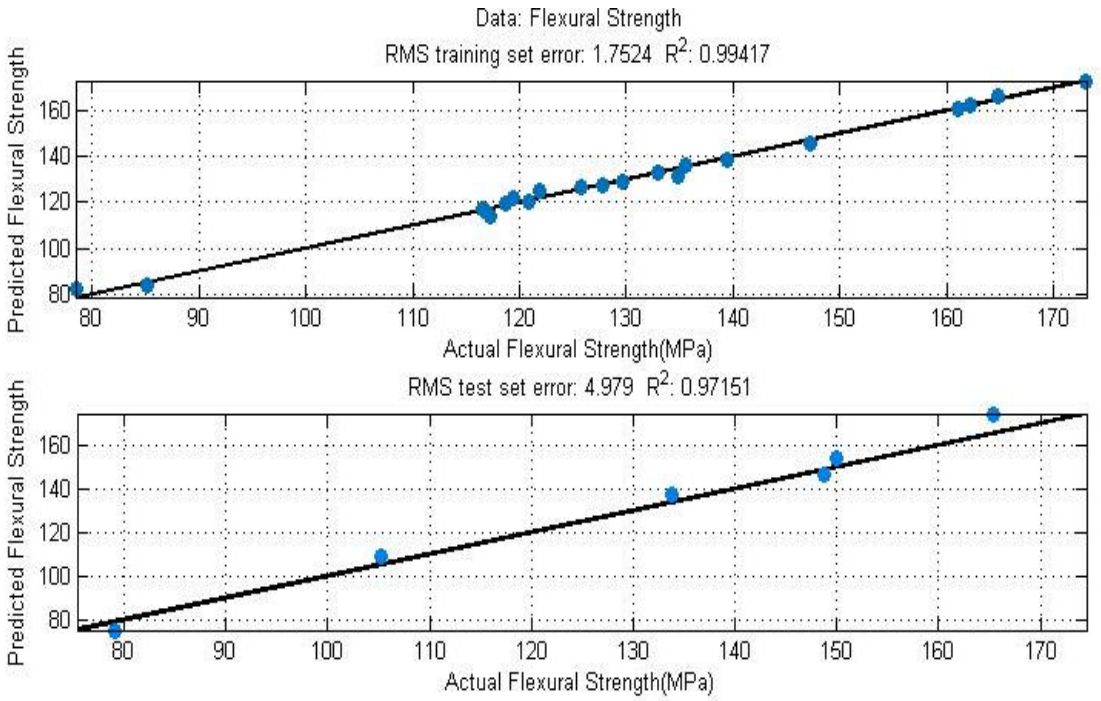

Figure 5. 11: Measured versus predicted values of flexural strength (a) training data and (b) testing data

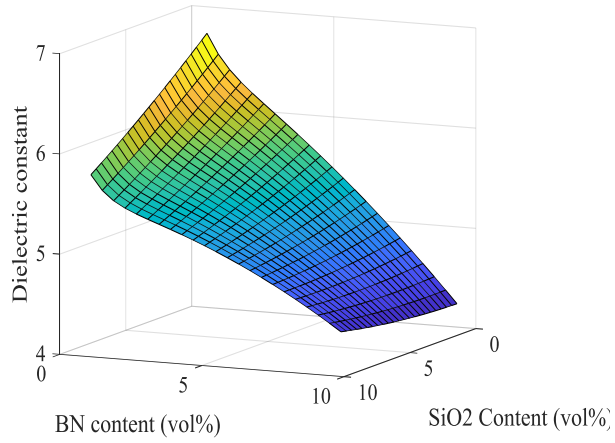

Figure 5. 12: Response surface plot showing the effect of SiO_2 Content and BN Content on flexural strength with 40vol% solid loading, 10wt% monomer content and 1:10 ratio of monomers

The surface plot of the predicted model of flexural strength is shown in Figure 5.12 for 40vol% solid loading, 10wt% monomer content and 1:10 ratio of monomers. Figure 5.12 shows the effect of SiO_2 Content and BN content on flexural strength of gelcast porous Si_3N_4-SiO_2-BN ceramic composite. It indicates that a high flexural strength sample is obtained with low SiO2 content and low BN content, which was discussed earlier in section 4.6.2.4.

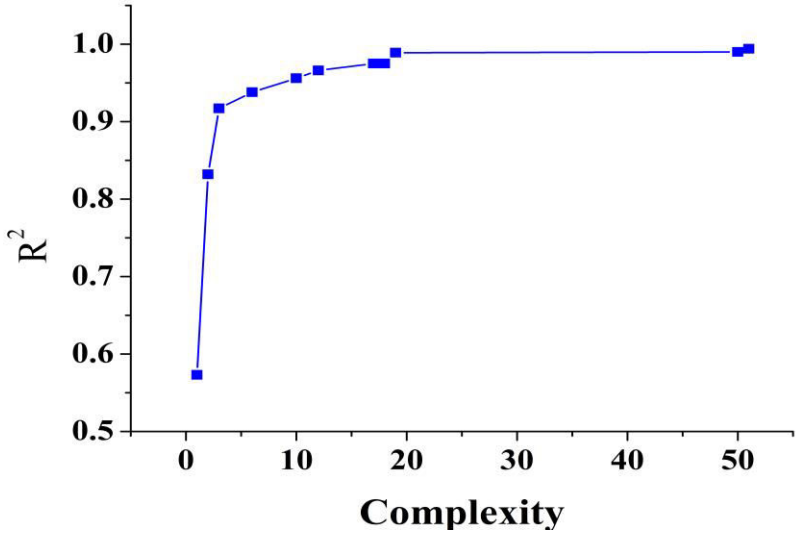

5. 13: Effect of complexity on Goodness of Fit (R^2)

Table 5. 5: Report shows the expressional complexity/performance characteristics (on training data) of symbolic models for flexural strength

Model ID	Goodness of fit (R^2)	Model complexity	Model
1843	0.994	51	$4.87\ x_1 + 0.294\ x_2 - 2.75e^4\ x_3 - 3.18\ x_4 - 1.45\ x_5 + 5.61e^4 \tanh(x_2) + 2.8e^4 \tanh(x_3) - 5.61e^4$
994	0.99	50	$6.32\ x_1 + 0.802\ x_2 - 2.69e^4\ x_3 - 3.18\ x_4 + 2.74e^4 \tanh(x_3) - 0.287 \tanh(x^2)\ (5.0\ x_1 + 5.0\ x_3 + 5.0\ x_5) - 58.6$
14356	0.989	19	$4.79\ x_1 + 0.783\ x_2 - 2.7e^4\ x_3 - 3.27\ x_4 - 1.52\ x_5 + 2.75e^4 \tanh(x_3) - 54.2$
278	0.975	18	$3.04\ x_1 + 0.967\ x_2 - 95.9\ x_3 - 2.21\ x_4 - 14.8\ x_5 + 0.382\ x_1\ x_5 + 44.4$
2727	0.975	17	$4.69\ x_1 - 2.57e^4\ x_3 - 3.06\ x_4 - 1.48\ x_5 + 2.62e^4 \tanh(x_3) - 41.3$
14761	0.966	12	$4.12\ x_1 - 1.49\ x_4 - 17.6 \tanh(x_3) - 0.00957\ x_1\ x_4\ x_5 + 4.0$
6551	0.956	10	$3.98\ x_1 - 55.3\ x_3 - 1.58\ x_4 - 0.0308\ x_4^2\ x_5 + 12.4$

6962	0.938	6	$4.92\ x_1 - 3.0\ x_4 - 1.57\ x_5 + 8.39e^4 \tanh(x_2) - 8.39e^4$
3771	0.917	3	$4.76\ x_1 - 2.88\ x_4 - 1.59\ x_5 - 13.7$
233	0.832	2	$4.65\ x_1 - 2.87\ x_4 - 17.2$
113	0.573	1	$4.43\ x_1 - 23.9$

Table 5.5 shows that the improvement GP model of optimal fitness value and expressional complexity changes as the developed GP models in the training phase. Figure 5.13 shows as the complexity of the model increases the R^2 (Coefficient of Determination) which leads to an increase in processing time.

5.4.3. MGGP model for Dielectric Constant

The best MGGP model for dielectric constant was as follows.

$$\text{Dielectric constant} = 0.251\ x_1 - 0.143\ x_2 - 0.101\ x_4 + 0.515\ x_5 - 0.0214\ x_1\ x_5 - 0.00372 \tanh(x_3 + x_4)\ (2.0\ x_1 + x_3 + x_4 + x_1\ x_3 - 5.0) + 2.4e^{-5}\ x_2\ x_5\ (x_2 + x_4)\ (x_1 - 1.0\ x_5) - 1.48 \quad (5.4)$$

Where x_1-Solid Loading(vol%), x_2-Monomer Content (wt%), x_3-Ratio of Monomers, x_4-SiO_2 Content (vol%) and x_5-BN Content (vol%).

The accuracy of the extended equation is examined by plotting the measured against predicted values for training and testing sets as shown in Figure 5.14. The values of R and RMSE are equal to 0.9859 and 0.4138, respectively, for training sets are 0.9728 and 0.7198, respectively, for testing sets. There is a good correlation between the predictions from multigene GP and the measured data. The error between the predicted values of MGGP and experimental results of the training and test data are shown in Figure 5.15. The variation explained is 98.59% and 97.28% for the training and testing data.

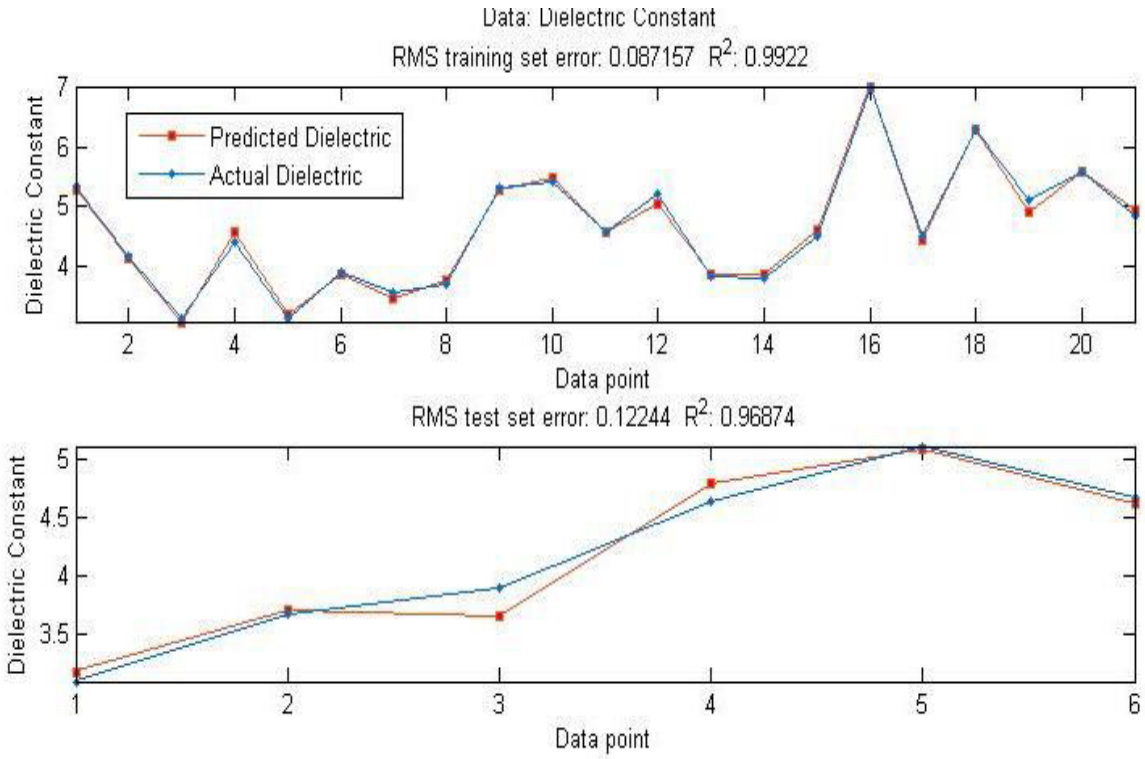

Figure 5. 14: Comparison of experimental results and the MGGP model prediction of dielectric constant for (a) training data and (b) testing data

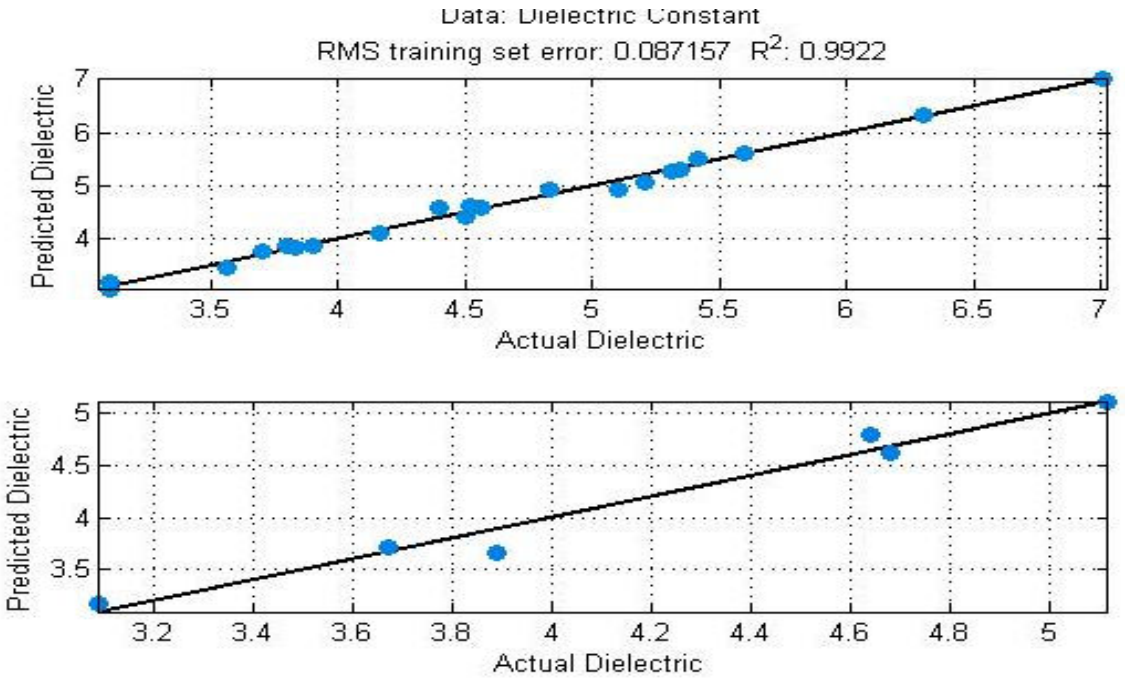

Figure 5. 15: Measured versus predicted values of dielectric constant for (a) training data and (b) testing data

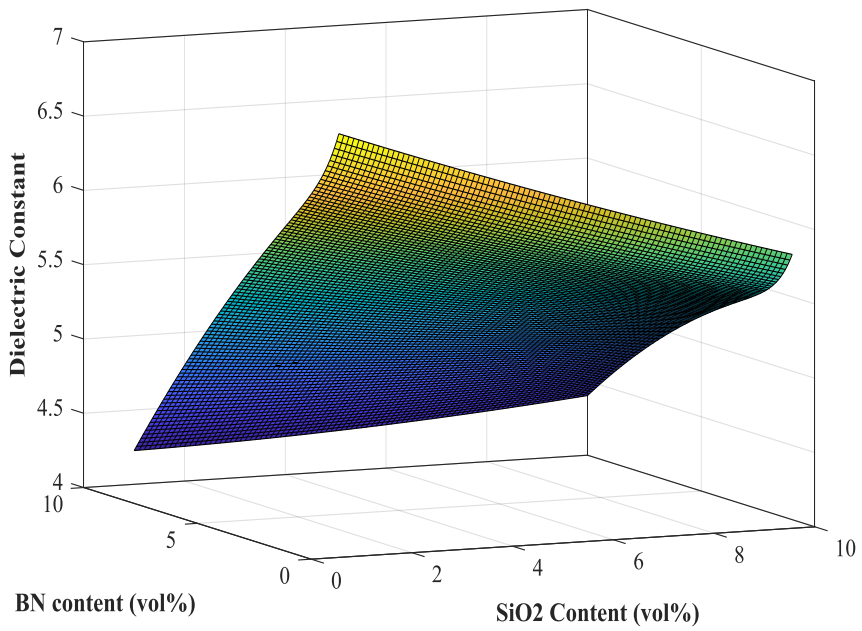

Figure 5. 16: Response surface plots showing the effect of SiO_2 content and BN content on dielectric constant with 35vol% solid loading, 10wt% monomer content and the ratio of monomers 1:10.

Figure 5.15 represents the 3D response surface plots of dielectric constant with solid loading at 35vol%, monomer content 10wt% and the ratio of monomers 1:10. Figure 5.16 shows the effect of SiO_2 content and BN content on flexural strength (MPa). Higher flexural strength values are found at 0% SiO_2 content and 0% BN content. As the SiO_2 Content and BN content increases the flexural strength decreases. The reasons were discussed in section 4.6.4.4 and 4.6.4.5 in chapter 4.

5.5. Formulation of multi-objective optimization problem

In this section, two objectives were considered the namely flexural strength and dielectric constant. It is observed that as the porosity increases, dielectric constant decreases and flexural strength also decreases, but our goal is to maximize flexural strength and minimize dielectric constant for a wave transparent material. Here, the single optimal solution will not serve the purpose, as these objectives are contradictory in nature. The simultaneous optimization of flexural strength and the dielectric constant falls in the area of multi-objective optimization. There is no single solution to a problem of multi objective optimization, but a

set of mathematically equal good solutions known as non-dominated or Pareto optimal solutions were obtained.

5.5.1. Genetic algorithm for optimal pareto front

The MATLAB function of "gamultiobj" is used to generate a pareto front for flexural strength and dielectric constant, this function uses a kind of controlled elitist genetic algorithm that dominates the fitness value and ranks individuals in objective function space based on the degree of non domination. The elitist selection process gives emphasis to the best solutions in following generations, without any operator.

5.5.2. Problem formulation

For a wave transparent application, the material has to exhibit high flexural strength and need a low dielectric constant. These objectives are conflicting in nature. Therefore, in the present work, the purpose of the multiobjective optimization of the gelcasted Si_3N4-SiO_2-BN ceramic is to maximize flexural strength and minimize dielectric constant simultaneously subject to the feasible bounds of control variables.

Maximize objective 1 and minimize objective 2

Objective 1 = 1/1+Flexural Strength

Objective 2 = Dielectric Constant

Subject to

30>Solid Loading> 40

5> Monomer Content > 15

0.067> Ratio of Monomers > 0.2

0> SiO2 content > 10

0> BN content > 10

where objective 1 and objective 2 are taken from MGGP modeled equation 5.3 & 5.4 respectively.

Experimental ranges were placed as constraints on the three input variables in the limit were preferred in the initial population. In Table 5.6, the options required for the optimization

of the genetic algorithm are used. The algorithm ran again and again for more number of points in the pareto optimal front.

Table 5. 6: GA parameters and options

Population type: Double vector
Population size: 200
Selection function: Tournament
Tournament size: 2
Reproduction crossover fraction: 0.8
Mutation function: Constrained dependent
Crossover function: Scattered
Migration Direction: Forward
Migration fraction: 0.2
Migration interval: 20
Distance measure function: Crowding
Pareto-front population fraction: 0.5

5.5.3. Pareto front and optimal solutions

The algorithm found the pareto optimal of the conflicting objective functions with good diversity of the solutions as shown in Figure 5.17. As the graph shows, no solution in Pareto optimal front is better than any other because they are non dominated solutions. The optimal input variables and their relative objective function values are presented in table… in Appendix A. By analyzing the pareto front, some decisions could be taken, depending upon specific requirements of the process. For example, at point 1(extreme left corner point), a specimen has low dielectric constant but with low flexural strength. On the other extreme of the front, i.e. at point 2 (extreme right corner point), high strength specimen can be achieved but it will have high dielectric constant. All the other points are in between cases. For example, if a ceramic processing engineering chooses to process a Si_3N_4-SiO_2-BN ceramic material using gelcasting method with a strength of 180 MPa, one can select the set of input

variables from the table… given in Appendix. To attain optimal operating conditions based on the desired flexural strength and dielectric constant may be obtained from the Figure 5.17.

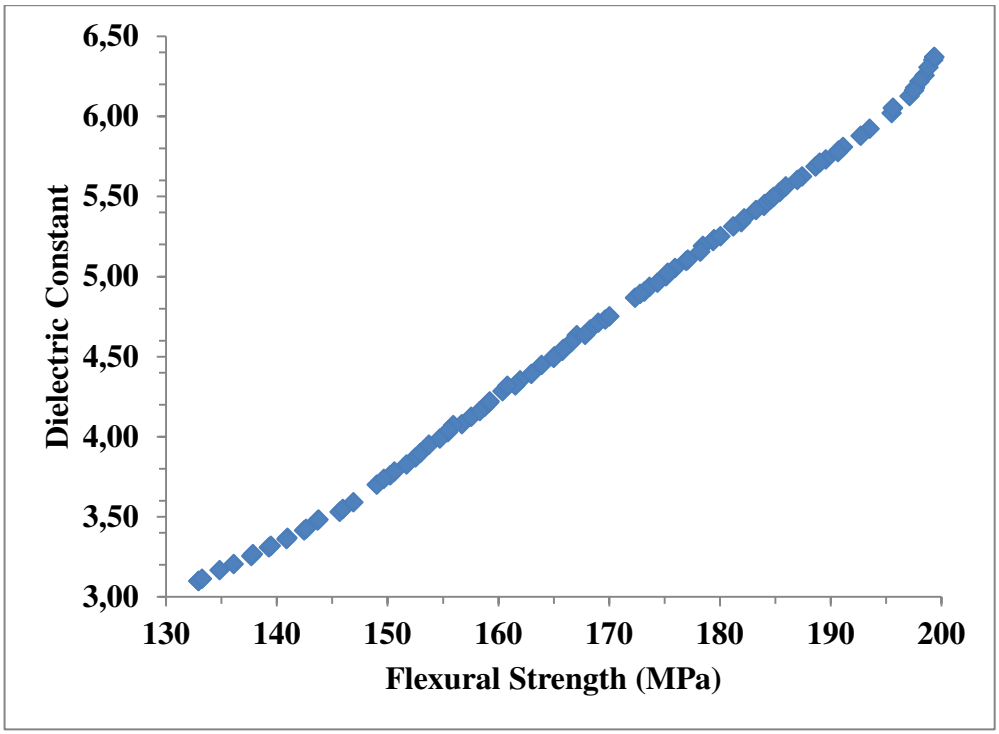

Figure 5. 17: Pareto optimal front obtained from multi-objective optimization

5.6. Comparison of Si_3N_4, Si_3N_4-SiO_2, Si_3N_4-BN and Si_3N_4-SiO_2-BN ceramic composites

The experimental conditions of Si_3N_4, Si_3N_4-SiO_2, Si_3N_4-BN and Si_3N_4-SiO_2-BN ceramic composites along with the sample codes are tabulated in Table 5.7. The values of flexural strength and dielectric constant of Si_3N_4 and each composite i.e., Si_3N_4-SiO_2, Si_3N_4-BN and Si_3N_4-SiO_2-BN with various combinations (Table 5.7) are presented in Figure 5.15 and Figure 5.16, respectively. Composite S1 to S8 indicates the experimental values whereas S9 to S11 indicates the optimized values after modeling and multi objective optimization.

Table 5. 7: Description of all Samples

Sample Code	**Solid Loading (vol%)**	**Monomer Content (wt%)**	**Ratio of Monomers**	**SiO_2 Content (vol%)**	**BN Content (vol%)**
S1	50	5	0.05	0	0
S2	30	10	0.1	0	0
S3	50	10	0.2	0	0
S4	50	10	0.2	5	0
S5	50	10	0.2	15	0
S6	40	10	0.1	0	0
S7	40	10	0.1	0	5
S8	40	10	0.1	0	15
S9	39.93	9.81	0.165	0	0
S10	39.72	10.26	0.19	2.35	3.58
S11	30.06	14.98	0.13	4.56	5.23

For a wave transparent application, the material has to exhibit a high flexural strength and requires a low dielectric constant. It is observed that the increase in flexural strength decreases porosity and forms a dense ceramic which leads to an increase in dielectric constant.

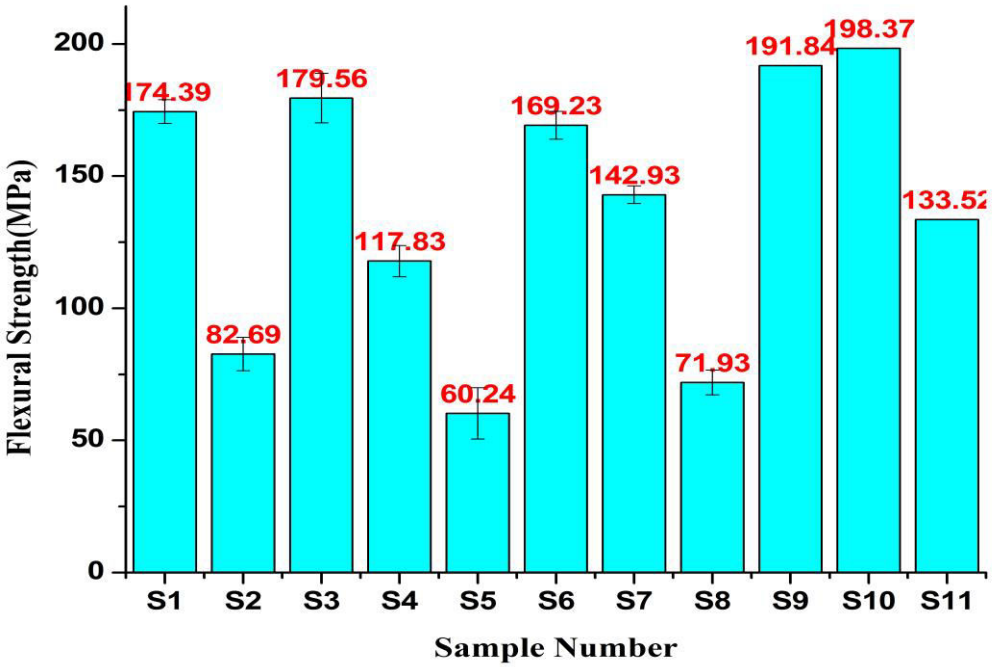

Figure 5. 17: Comparison of flexural strength achieved for various ceramic composites.

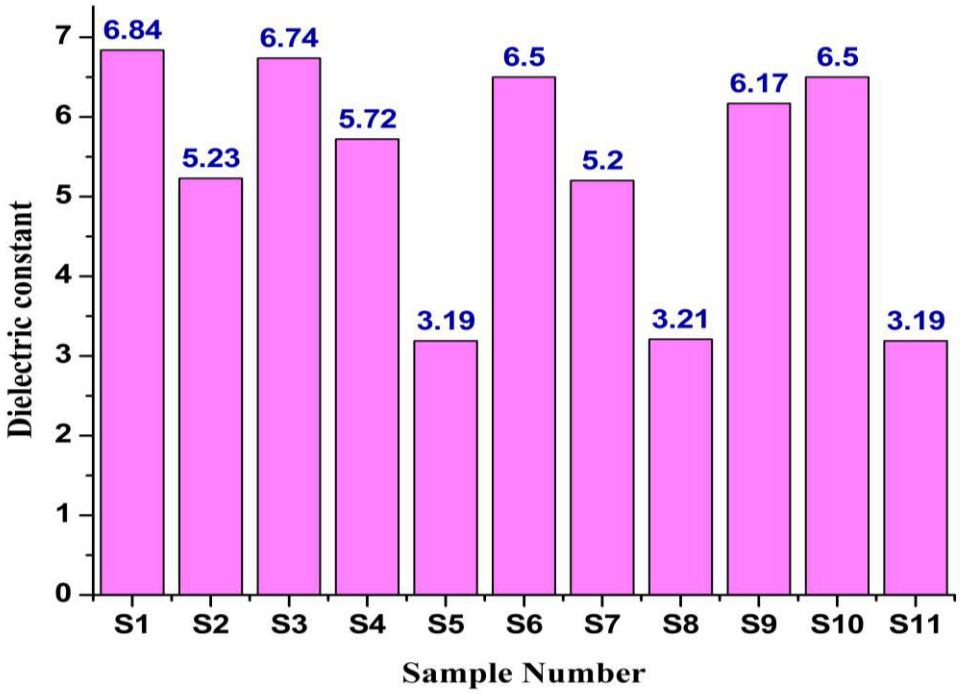

Figure 5. 18: Comparison of dielectric constant achieved for various ceramic composites.

The flexural strength and dielectric constant of ceramic composite S4 (5vol% SiO_2) are 117.83 MPa and 5.72 and for S7 (5vol% BN) are 142.93 MPa and 5.2, respectively, which indicates the flexural was low for S4 composites due to the less flexural strength of SiO_2 ceramic powder. Composite S5 and S7 indicates the maximum addition of 15 vol% of SiO_2 and BN ceramic powder, which was decreasing dielectric constant but also decreasing the flexural strength. It is well known that SiO_2 content and BN content are mainly responsible for decreasing the dielectric constant.

Composite S9 indicates the one of the pareto optimal solutions after modeling and multi objective optimization. Thus the Si_3N_4-SiO_2-BN ceramic composite has the maximum flexural strength of 198.37 MPa with a dielectric constant of 6.5. Hence it is further concluded that if maximum flexural strength is the preference, then the combination of S10 (Si_3N_4-SiO_2-BN)is best and if dielectric constant is preferred then a combination of S11 (Si_3N_4-SiO_2-BN) ceramic composite is best. Upon comparison of the maximum values of flexural strength and dielectric constant, one has to take trade-off decision for selecting appropriate and best wave transparent materials among various composites.

Table 5. 8: Confirmation Test results

	Optimal Experimental Combination					Experimental Value		Model Valiue		Prediction error (%)	
No. of Experiments	Solid loading (vol%)	Monomer Content (wt%)	Ratio of Monomers	SiO2 Content	BN content	Flexural Strength (MPa)	Dielectric Constant	Flexural Strength (MPa)	Dielectric Constant	Flexural Strength (MPa)	Dielectric Constant
1	39.72	10.26	0.19	2.35	3.58	185.84	6.67	198.37	6.5	6.31%	2.61%
2	30.06	14.98	0.13	4.56	5.23	126.48	3.4	133.52	3.19	5.27%	6.58%

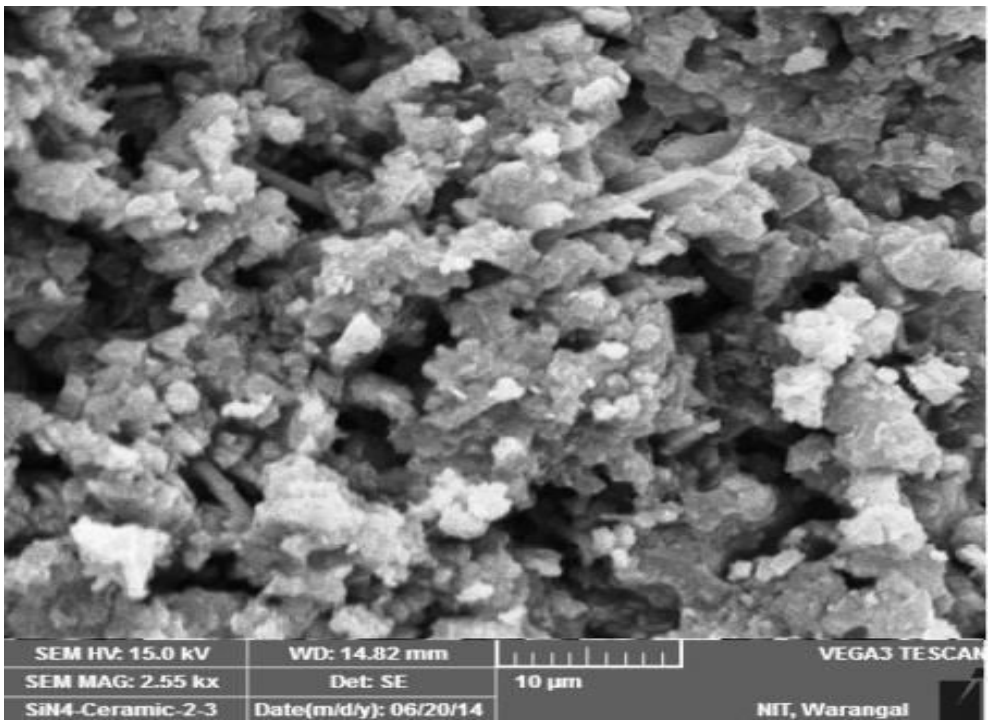

Figure 5. 19: SEM micrograph of Sample S10(Si_3N_4-SiO_2-BN)ceramic composite

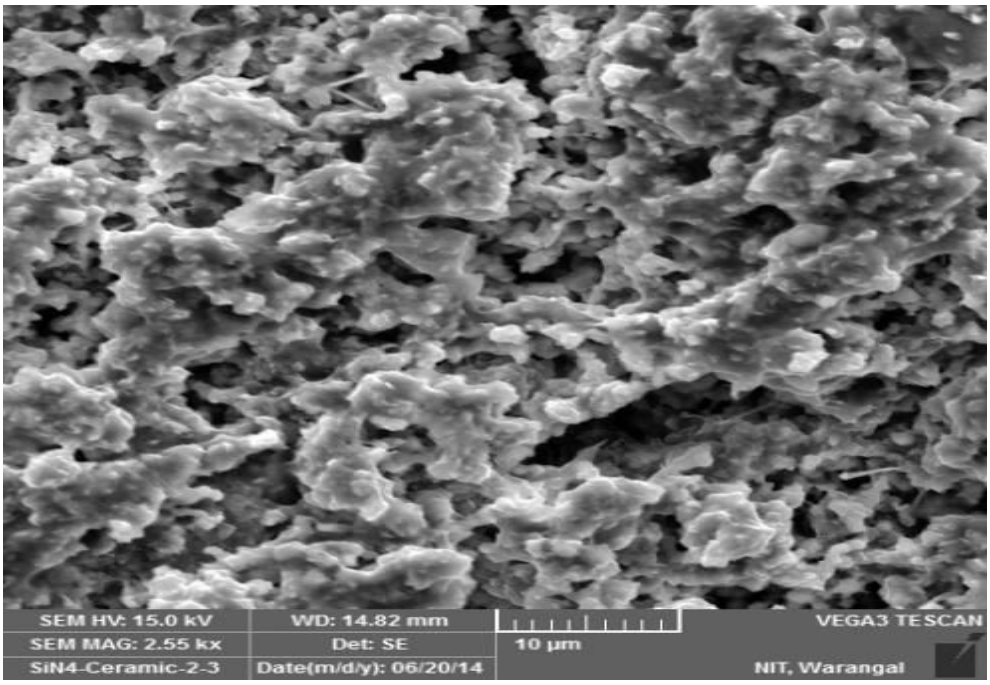

Figure 5. 20: SEM micrograph of Sample S11(Si_3N_4-SiO_2-BN)ceramic composite

5.7. Confirmation Test

The final step after selecting the optimal parameter is to verify with the selected optimum processing conditions. Confirmation experiment at the selected optimum processing conditions for sample code S10 and S11 were performed. A fine agreement was obtained between the predicted and the actual machining performance. Table 5.8 shows that there was good agreement between the experimental and predicted results as the prediction error found is very small.. A prediction error of 6.31% and 2.61% for flexural strength and dielectric constant of sample S10 and an error of 5.27% and 6.58% for flexural strength and dielectric constant of sample S11, respectively, were observed.

Sample S10 and S11(Si_3N_4-SiO_2-BN)ceramic composite with the processing conditions in Table 5.7 are processed by gelcasting method. Flexural strength and dielectric constant of the samples are measured and tabulated in Table 5.8. Figure 5.19 and Figure 5.20 shows the SEM micrograph of Sample S10 and S11 composite, respectively. It can be clearly seen, some needle like structure are observed, which represents β-Si_3N_4 transformation from α- Si_3N_4. The transformation is less in sample S11 than in S10, because more amount of SiO_2 and BN content were added in sample S11.

Summary

This chapter deals with the generation of regression models for flexural strength and porosity for porous Si_3N_4 ceramics using Multi Gene Genetic Programming (MGGP) by considering the experimental data from Chapter IV. This chapter also deals with the prediction of flexural strength and dielectric constant of porous Si_3N_4–SiO_2-BN ceramics using Multi gene genetic programming (MGGP) model. This chapter also presents the multi-objective optimization of porous Si_3N_4 and Si_3N_4–SiO_2-BN ceramic composites using a genetic algorithm. These responses are simultaneously optimized and the optimal levels of the process parameters are determined by the Pareto front.

A comparison of flexural strength and dielectric constant were made among Si_3N_4, Si_3N_4–SiO_2, Si_3N_4 –BN and Si_3N_4–SiO_2-BN ceramic composites and presented. Empirical models for the chosen performance measures were developed using MGGP. The models obtained were truly reliable and shows very good generalization capability. Higher values of multiple regression coefficients for flexural strength and dielectric constant (i.e. 99.41% and 99.22% respectively) reveal that better prediction of physical phenomenon is possible with the developed models. The Pareto-optimal set was found out by using non-dominated sorting genetic algorithm II and optimal values of solid loading, monomer content and the ratio of monomers can be selected for desired value of flexural strength and porosity from the Pareto-optimal set. The optimum processing parameters for gelcasting of SiO_2–Si_3N_4–BN composites for a wave transparent application are 35.9vol% solid loading, 9.81wt% monomer content, 0.19 ratio of monomers, 2.56 vol% SiO_2 content and 5.24 vol% BN content. The obtained flexural strength and dielectric constant are approximately 166.72 MPa and 4.5, respectively.

CHAPTER 7

CONCLUSIONS AND FUTURE SCOPE OF WORK

This chapter exhibits the major conclusions obtained from the research work reported in this thesis. There are also few issues dealt in this study which needs further investigation, thus, some recommendations for future work are also suggested.

7.1. Conclusions

Si_3N_4 based ceramic composites such as Si_3N_4-SiO_2, Si_3N_4-BN, and Si_3N_4-SiO_2-BN have been successfully produced using the gelcasting method. In this study, MGGP models were developed for the prediction of flexural strength and porosity of ceramics prepared by the gelcasting process. Later, a multi objective problem was formulated to obtain optimum parameter combination for maximization of both flexural strength and porosity to find the multiple sets of optimal solutions for ease of use by a ceramic processing engineer's to save time, effort and cost. The following conclusions are drawn from critical observation of results obtained:

- Si_3N_4 and Si_3N_4-SiO_2 gelcast slurries have been carefully prepared by Dolapix A 88 as a dispersant. The optimum amount of dispersant was determined to be 0.8wt% of solid loading of ceramic powders through rheology and zeta potential measurements. A simple step by step slurry formulation process was evolved with minimal steps to help increase process casting time and efficiency.
- Zeta potential measurements were done to determine the stability of the addition of 0.8wt% Dolapix A 88 at pH 10.5. It was concluded that 0.8wt% dispersant creates a large potential barrier resulting in a stabilized disperse suspension. The zeta potential was determined to be -55mV, large enough to stabilize the silicon nitride slurry. At this pH, the Si_3N_4 has a strong negative charge. Zeta potential measurements and interaction potential calculations were also conducted on alumina with no dispersant at pH 9.2. Here, it was seen that there was weak electric double layer repulsion, resulting in an undesirable coagulated suspension.

- The isoelectric points (pH_{iep}-value) of the as-received Silicon nitride particles, mixed powder and mixed powder in the presence of the Dolapix A88 were 6.9, 6.3 and 4.5 respectively. It was found that isoelectric point of mixed powder shifted from 6.3 to a much acidic value 4.5 in the presence of a dispersant.
- Silicon nitride suspension exhibited a shear thinning behavior, which is beneficial for the casting and gelation process. The solid loading of the slurry reaches as high as 50 vol% solid loading with the dispersant concentration (Dolapix A88) of 0.8 wt%,
- The formation of the crystalline Si_2N_2O will consume a large amount of liquid phase, so the transformation of α-Si_3N_4 into β-Si_3N_4 and densification are obstructed. This may be the reason for increasing the porosity as the SiO_2 content increases. The mechanical properties are found to be lower with the increase of SiO_2 content. The dielectric properties may be improved by the addition of SiO_2 powder.
- The microstructures of the Si_3N_4-SiO_2 ceramic composite are found to be with an even distribution of pores. When the wt.% of SiO_2 content in the range of 0% to 15%, it is found that the flexural strength is 60.6-178.5MPa and dielectric constant of Si_3N_4-SiO_2 composites are in a range of 60.6-178.5MPa and 3.2-6.8, respectively.
- Microstructures of Si_3N_4-SiO_2 composite ceramics with uniform pore distribution were formed. As the weight of % SiO_2 content increase from 0% to 15%, the flexural strength decrease from 179.56 ± 9.35 MPa to 60.24±9.74 MPa and the dielectric constant decreases from 6.74 to 3.19 of Si_3N_4-SiO_2 ceramic composites.
- Polyethylenimine (PEI) was selected as the dispersant for the aqueous dispersion of Si_3N_4–10vol%BN powder mixture. The zeta potential values for the Si_3N_4 and BN powders are more negative with the pH increase from 2 to 12 or by the addition of 1wt% of PEI. Well- dispersed Si_3N_4 suspension and BN suspension was obtained by using 1 wt% PEI at pH 10.
- The slurry with 42 vol% of Si_3N_4–BN was found to have low viscosity and exhibited a shear thickening behavior and at 45 vol% slurry has a higher viscosity and showed more obvious shear thickening behavior. Finally, a high solids loading (42% vol), low viscosity (380 mPa.s at $100s^{-1}$) Si_3N_4-BN slurry was prepared with 1% PEI at a pH of 10. It was observed that the suspensions exhibited shear thinning behavior with relatively low viscosity for ease of the gelcasting process.

- For Si_3N_4-BN ceramic composites the flexural strength and dielectric constant decreases with increase in the BN content. The monolithic Si_3N_4 sintered at 1700°C exhibited a maximum strength of 169.23±5.23 MPa, while the strength of Si_3N_4- 5 vol% BN and Si_3N_4-15vol% BN ceramic are 142±3.34 and 71.93±4.63 MPa, respectively.
- For Si_3N_4-SiO_2 ceramic composites the flexural strength and dielectric constant decreases with increase in the SiO_2 content. The Si_3N_4 sintered at 1550°C exhibited a maximum strength of 179.23±9.35 MPa, while the strength of Si_3N_4- 5 vol% SiO_2 and Si_3N_4-15vol% SiO_2 ceramic are 117.83±5.91 and 60.24± 9.74 MPa, respectively.
- It was concluded that, Si_3N_4-SiO_2 ceramic composite fabricated using 50 vol% solid loading, 10 wt% MAM content , ratio of monomer (MAM:MBAM) 1:10 and 5vol% SiO_2 sintered at 1550°C has bulk density of 1.93 g/cm^3, porosity of 42.3 %, flexural strength of 117.83±5.91 MPa and dielectric constant of 5.72. On the other hand, Si_3N_4-BN fabricated using 40 vol% solid loading, 10 wt% MAM content, ratio of monomer (MAM:MBAM) 1:10 and with 5 vol% BN sintered at 1680°C has bulk density of 1.85g/cm^3, porosity of 32.34 %, flexural strength of 142.93±3.34 MPa and dielectric constant of 5.2. .

- Empirical models for the chosen performance measures were developed using MGGP. The models obtained were truly reliable and shows very good generalization capability. Higher values of multiple regression coefficients for flexural strength and dielectric constant (i.e. 99.41% and 99.22% respectively) reveal that better prediction of physical phenomenon is possible with the developed models.
- The Pareto-optimal set was found out by using non-dominated sorting genetic algorithm II and optimal values of solid loading, monomer content and the ratio of monomers can be selected for desired value of flexural strength and porosity from the Pareto-optimal set.
- The optimum processing parameters for gelcasting of SiO_2–Si_3N_4–BN composites for a wave transparent application are 35.9vol% solid loading, 9.81wt% monomer content, 0.19 ratio of monomers, 2.56 vol% SiO_2 content and 5.24 vol% BN content. The obtained flexural strength and dielectric constant are approximately 166.72 MPa and 4.5, respectively.

- The developed approach provides many combinations of process parameters which give higher flexural strength and low dielectric constant in comparison to experimental values, which indicates that the proper selection of process parameters enhance the process efficiency.

Thus, the proposed work enables ceramic processing engineers to select optimal values depending on their requirements. The proposed MGGP model efficiently incorporates the effects of several parameters representing the nonlinear behavior. A major advantage of MGGP lies in its powerful ability to generate compact models.

7.2. Future Scope of Work

The results of the present work have commenced the following prospects that can be considered as future work:

- Fabrication of Si_3N_4 based ceramic composite for wave transparent applications using gelcasting process has been thoroughly investigated in the present work and still, there is a scope for further investigation of materials to biomedical applications, porous materials etc.,
- Effect of SiO_2 and BN nanopowders on the gelcasting of Si_3N_4 ceramics can be studied further.
- In this work, dielectric properties were measured in a frequency range of MHz using impedance analyzer. Further, the Network analyzer can be used to measure dielectric properties in a frequency range of GHz.
- Use of various pore forming agents in the gelcasting process can also be studied.

.

Appendix A

1. Wet colloidal Processing Techniques

1.1 Direct Coagulation Casting

Direct coagulation casting (DCC) is the solidification process for aqueous slurries introduced by a group of scientists from ETH, SF[156]. DCC method is a unique near net shape method of homogeneous suspensions of particles with high solids loading on the green ceramic body [157]. The basic principle of the DCC process of a coagulated stable suspension is poured into a non-porous mold to use a time-delayed chemical reaction in the suspension results in a destabilization and a dense, homogeneous green body. Consolidation of the high dense suspension is controlled by a coagulant to increase the pH to the isoelectric point (IEP) of the suspension and / or to move the ion concentration in the suspension it is used. Such species double-layer repulsive forces minimize by compression or collapse of the double-layer.

This process is rooted in destabilization of slurry by means of chemical reactions to reduction of surface charge in particles circulated through a change in pH or ionic concentration is increased in the slurry. If the charge of the surface of the particles is high and is of the same sign, dominate the repulsion force in Van der Waals attraction, and low viscosity stable slurry is formed. When the repulsive forces displacing the pH in the direction of the isoelectric point (IEP) or with increase in ionic concentration, the attraction force among the particles is eliminated, flocculation or coagulation of the suspension is formed and a rigid solid is formed and damp. This process can result with high green density and homogeneous microstructures. At a high solids concentration in the liquid to solid transition and through the drying, no linear shrinkage occurs for green body and after the sintering step, exact sizes of the component can be expected [158]. DCC is particularly suitable for the production of complex parts with large and small cross sections in the same part.

1.2. Slip Casting

Slip casting is an appropriate and reliable technology for production of dense and uniform ceramics [159, 160]. In fact, this shaping process improves the packaging structure of ceramic

particles in the green body with low porosity and a fine distribution of pore size to a large extent. Slip casting is essential to attain thick slurry of highly deflocculated powder having a high volume fraction. For this purpose, a high repulsive force between the ceramic particles can be attained with modification in surface characteristics of the powder. By the way, the repulsion force is greater than the attractiveness. This was attained by electrostatic repulsion, which arises as of overlapping the electric double layers (ζ- potential) or from steric hindrance, resulting as of the adsorbed molecules of the solvent or dispersant type. [161]. Through specific control of the above said factors, ceramics with high density and a homogeneous microstructure could be produced. Slip casting is an appropriate method to achieve homogeneous microstructure and high green density materials, permitting the production of complex shaped components.

1.3. Hydrolysis-Assisted Solidification

Hydrolysis-assisted solidification (HAS) is an innovative method for net-shaping green ceramic components from aqueous ceramic suspensions in nonporous molds. This method utilizes thermally activated and/or accelerated hydrolysis of aluminium nitride (AlN) powder, which was added into ceramic suspensions. The solidification process supports hydrolysis has been developed by Kosmacˇ and co-workers at Josef Stefan Institute in Ljubljana, SI [162]. This method is a sort of cross between the curing of the cement products and offer of gelation by certain advantages. The method is based on thermal and thermally activated aluminum nitride (AlN) ceramic bonded suspensions with high concentration. During the hydrolysis of AlN, the water is consumed. The solid loading is increased because the water is bound to metal hydroxide and ammonia is formed, which increases the pH of the slurry (the pH value is shifted towards the isoelectric point (IEP) of alumina). The two means, consumption of water and pH change can be used for the solidification of a ceramic aqueous suspension in a matrix. In addition, the aluminum hydroxide would get a reaction product further away from the hydrolysis of AlN gels; the heating which will further aids the solidification process and increase the green strength of the molded body [163, 164]. The advantages of this method are outstanding rheological properties, high solidification rate and a high density. Disadvantages include a limited duration and temperature stability.

$$AlN + 2H_2O \rightarrow AlO(OH)_{am} + NH_3 \qquad (1.1)$$

$$NH_3 + H_2O \rightarrow NH_4OH \quad (1.2)$$

$$AlO(OH) + H_2O \rightarrow Al(OH)_3 \quad (1.3)$$

From the above reactions (1.1), water is consumed throughout the hydrolysis of AlN powder, (1.2) ammonia is produced and (1.3) AlN particles are suspended to form aluminum hydroxides. The first reaction increases the solids loading and the second has a significant impact on the pH value of the slurry, electrokinetics and thus affects its rheological properties. Resolution of the AlN ceramic particles can affect the ionic and precipitation phases formed by the reaction can lead to an increased solids surface area or a change in the rheological properties of the liquid medium. It was clear that all of these reactions can alter the rheological properties of the ceramic slurry significantly and therefore the involvement of each effect in this study was investigated[165].

1.4. Freeze Casting

Freeze casting was developed as a near net shape wet processing technique, which gives dense ceramic component with fine replica of the mould shape[166]. The first Fukasawa works on this method and [166, 167] discovered the potential of the porous ceramics and considerable efforts were then placed. Freezing is a simple technique for the production of complex ceramics or a porous molding polymer parts[168]. In this method, ceramic suspension is poured into a mold and frozen. Temporarily, the solvent freezing acts as a binder to hold the workpiece for removal. Thereafter, component is directed to freeze drying to sublimate the solvent in vacuum. The limitations of drying and shrinkage is avoided that can cause cracks and deformation during normal drying. Subsequent to drying, the samples are sintered to produce a high strength and stiff porous material with required porosity. The result is a component with a complex porous microstructure and often generated during the freezing[169]. it is possible to impose a preferential orientation for the porosity by controlling the growth direction of the ice crystals in the final component.

1.5. Tape casting

Tape casting is near net shape method to be employed for mass production of ceramic substrates and multilayer structures [161, 170]. A suspension comprising ceramic powder in a

solvent with the addition of dispersing agents, binders and plasticizers is poured into a fixed or movable surface. The cast strip having a typical thickness of the order of 100 to 300 µm is dried followed by sintering to acquire a required form. A variety of non-aqueous organic solvents such as alcohols, ketones or hydrocarbons are commonly used to produce highly concentrated suspensions exhibiting repeated rheological properties and drying behaviour depending on the ceramic powder composition.

These days, the ecological and healthiness features of the tape casting method have attracted particular attention. As a result, in the literature the formulation of suspension appeared with water as solvent in place of organic liquids. The starting suspension for tape casting generally includes the mixture of ceramic powder depending on the phase, solvents, additives (antifoam agent, dispersant, surfactant, etc.), Binder, and one or more plasticizers. so as to obtain complete dissolution of the hydrocolloid, the suspension is heated to a particular temperature. After degassing, the suspension is poured with a doctor blade on a support film. The properties of organic binder wire to easy-to-use tapes. In next steps, the tape is removed from the carrier sheet, followed by drying, heat treatment, to remove the organic compounds from the green body, and sintering process. If necessary, further shaping, calendering or rolling between drying and calcining may take place[171].

1.6. Gel casting

The gelcasting method was initially developed in Ceramic Processing Group at Oak Ridge National Laboratory (ORNL), USA by Janney and Omatete [172]. The homogeneous suspension having a high solids loading and a low viscosity mixture was prepared with ceramic powders, organic monomers, solvents and dispersants, with careful mixing. The polymerization begins with the addition of an initiator and a catalyst to the suspension, and into a non-porous form for molding into the desired shapes. After removal from the mold, the organic monomers are combusted and the sample forms a sintered dense component. It is a near net shaping process applied for different ceramic materials in making complex shaped and high quality ceramic parts. This method assures lower cost for manufacturing ceramics than conventional forming techniques[13]. Gel casting forming processes is one of the quasi-net, which is in the production of complex shapes of great importance because the costly operations after the sintering treatment are reduced. In addition, the aqueous method also

provides a number of economic and environmental benefits. Figure 1.4, shows the schematic diagram of gelcasting process.

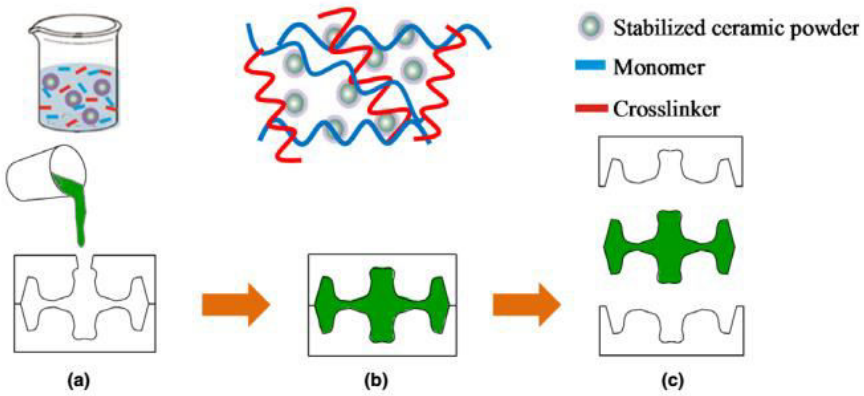

Figure 1: Schematic diagram of gelcasting process (a) slurry with polymer and ceramic powders (b) initiation of polymerization c) formation of green body

Appendix - B

2.1. Physical properties

2.1.1. Density

Density is a physical property that reflects the characteristics of ceramics. The density of a pure ceramic possibly determined from lattice parameters measurements. For hexagonal lattice structure, the volume of unit cell is:

$$V = \sqrt{(3/2)a^2 c} \qquad (2.1)$$

Where a and c are the individual lattice parameters. The theoretical density of a material can also be determined from:

$$\rho_{th} = \frac{M_z}{N_A V} \qquad (2.2)$$

Here z is the number of formula units per unit cell, M is the molar mass, N_A is Avogadro's number, and V is the volume of the unit cell, The theoretical density possibly employed as an approximate of bulk density of extremely low porosity polycrystalline ceramics with the lack of intragranular solid solution formation or momentous secondary phases[173]. Green density can be calculated by Archimedes method, by measuring the dimensions and mass of the original specimen experimentally.

2.1.2. Linear shrinkage

The linear shrinkage of sintered samples be governed by the following equation:

$$Shrinkage = \left[\frac{l_g - l_s}{l_g}\right] \times 100\% \qquad (2.3)$$

where l_g and l_s are the length of green and sintered samples. The measured bulk density of sintered sample can be calculated from the mass of the sample and dimensions using

Archimedes principle. The relative density was attained from the ratio of measured bulk density to the theoretical density.

Both causes of shrinkage in the process gelcasting form shrinkage due to a slight contraction in the polymerization process and the other due to moisture drying shrinkage. To facilitate the shrinkage reduction of a green sample, a firm high solid loading in the slurry is preferably in the gelcasting process. On the other hand, there is a limit for the solid loading in the suspension to achieve uniformity and preferred viscosity. The wet green body is generally dried gradually in a controlled temperature and humidity and then debindered at a low heating rate to assist control of shrinkage rates. This is not favorable in practice because it leads to more operation time and higher production costs[62].

The shrinkage of the gel is more during drying and sintering makes dimensional control of large samples difficult. Drying is frequently a constraining step for samples with thickness of 1 mm, and the shrinkage in the course of drying and sintering are large. The ability to shape complex shapes by casting the gel combined with moderately low sintering temperature are attractive elements of the route, but cracking during drying and the considerable shrinkage during sintering can present consequential challenges in achieving the desired shape.

2.2. Mechanical Properties

Mechanical properties of ceramics are an intricate function of the microstructure. The property of ceramics depends on composition, porosity, strength and fracture behavior despite these depends on the grain size. Usually, for gelcasted ceramics, the compressive strength is a high and tensile strength is low. This behavior evolves as the flaws in the ceramics are efficiently clogged under compressive stress but rapidly inflamed under tensile stress. From the application perspective, the flexural strength of ceramics is one of the most noteworthy factors. Failure generally occurs on the side under tensile stress, which is initiated from a microstructure, strength-limiting flaw in a three-point bending test. The green and sintered gelcasted ceramics were illustrated for mechanical properties.

2.3. Green strength

The green strength is a critical property of a dried body. Green strength is defined as the mechanical strength of an unsintered dried gelcast sample. George Y. and Onoda's [174]model says that the force required to break the interparticle bonds of green bodies depended on the amount of binder joining the particles at the necks. The green strength of a dried body, σ, can be expressed by the following equation[175]:

$$\sigma = \left[\frac{9\emptyset}{8(1-\sigma)^{1/2}}\right](v_B)^{1/2}\sigma_B \qquad (2.4)$$

Where φ is the packing fraction of the ceramic particles, ν_B is the binder volume fraction relative to the ceramic and σ_B is the strength of the binder. The mechanical behavior of green bodies can be used to assess the processing conditions which the gelcast components were made. The test often used in measuring the green strength of ceramics is either flexural strength [64, 70, 73, 74, 176] or diametric compression test [63, 77, 177]

2.4. Flexural Strength

Sintered strength is defined as the flexural strength of a sintered gelcast sample. It is the capacity of a sample to withstand a failure in three or four point bending. The flexural strength determination is often required as part of the design of structural ceramics. The flexural strength is articulated in "modulus of rupture" in MPa. Typically, the flexural strength is about 10 to 20% of the compressive strength of the ceramic. Nevertheless, the best ratio of specific ceramic materials is acquired experimentally. The flexural strength of the green body and the sintered bodies was determined at three points bending test. The flexural strength was determined according to the standard equation:

$$\sigma_f = \frac{3FL}{2bh^2} \qquad (2.5)$$

Where *F* is the maximum load at fracture, *L* is the span length, *b* is the width of the sample; *h* is the height of the sample[40]. According to Coble and Kingery [178], the strength of porous ceramics decreases exponentially with an increase in porosity, which can be calculated as:

$$\sigma = \sigma_0 \exp(-\beta P) \qquad (2.6)$$

Where σ_0 is the strength at a porosity of 0, β is a structural factor and P is porosity.

2.5. Fracture toughness

Fracture toughness is the resistance of crack propagation. Fracture toughness utilizes a fracture mechanics approach, which takes into account the stress at the tip of the crack. There are three modes of crack propagation (mode I, mode II and mode III). Mode I is called the tensile or opening mode and the most frequently encountered in ceramics such as when undergoing a tensile or flexure test. Mode II is termed the sliding plane mode, while mode III is called the tearing mode. Ceramics generally fail in mode I loading and thus this will be considered further. The fracture toughness was estimated from the equations:

$$K_{IC} = \frac{3PL}{2bh^2} a^{1/2} f\left(a/h\right)$$
$$f\left(a/h\right) = 1.93 - 3.07\left(a/h\right) + 13.66\left(a/h\right)^2 - 23.98\left(a/h\right)^3 + 25.22\left(a/h\right)^4 \qquad (2.7)$$

where a is the depth of the notch, b rectangular bar specimens width, h the height of the specimens, L the span length, and P is the maximum load applied.

2.6. Dielectric constant and loss tangent

In addition to the mechanical properties, the dielectric constant is also an important aspect of performance factor for wave transparent applications. For well dispersed ceramic composites, the dielectric constant can be determined by the mixing law:

$$ln\ \varepsilon = \sum_{i}^{n} V_i ln\varepsilon_i \qquad (2.8)$$

where ε_i and V_i are the dielectric constant and volume fraction of every phase *i*, respectively. The two reasons for the diversity of the dielectric constants are the first is porosity. As the air has a very low dielectric constant close to 1, the ceramic ε increases greatly as the porosity decreases. The other is the disimiliar values of dielectric constant for ceramic materials.

2.7. Electrical conductivity

Electrically conductive ceramics are required in dense and porous shapes depending on the applications, which mean subjecting the ceramic parts to harsh environmental conditions. Dense electrically conductive ceramics are employed for the dissipation of static charges, ceramic heaters, lightning protection, electronic shielding, etc. On the other hand, electrically conductive porous ceramics have aroused great interest in the development of high performance radiators, exhaust for cold start applications of automobiles.

2.8. Thermal conductivity

The purpose of the thermal conductivity of ceramic materials is vital in a number of industrial applications. The thermal conductivity of the gel-cast materials is exaggerated by a number of phases present, the pore size and distribution, the monomer content, the sintering temperature, the solid charge, etc. Above the Debye temperature, the photon-photon contact by lattice vibration of the array is the main process for the conduction of heat in ceramics, and estimated as follows:

$$k = {}^{1}/_{3}\, cv\lambda \qquad (2.9)$$

Where k = thermal conductivity, c= specific heat of the sample, ν = elastic wave velocity or mean velocity and λ= mean free path among interactions.

Appendix- C

3.Applications of Gelcasting process

Because of unique structure and properties attained by gelcasting, it drew attention to a number of diverse applications, even though only a few feature properties figures have been described so far.

3.1. Radomes

A radome is an electromagnetic dome like the transparent structure that covers an antenna. The main function of a radome is to protect an antenna from environment destructions, like wind, snow, ice and freezing temperatures to rain, sun and even lightning. The Radome materials are compelled to work in severe environments with lightweight, low dielectric constant, low tangential loss, high flexural strength to withstand handling, aerodynamic and thermal stresses, high thermal shock resistance, minimal moisture absorption, high rain erosion and a high modulus of elasticity to maintain the thin walls of the radomes due to buckling.

Kirby et al. (2000 and 2001) [179] at the Oak Ridge National Laboratory (ORNL), USA, manufactured successfully β- $Si_4Al_2O_2N_6$ radomes using an industrially obtained water processable AlN powder. In addition, these radomes have been successfully tested for some missile applications after sintering. Ganesh et al. successfully fabricated $Si_4Al_2O_2N_6$and β-$Si_4Al_2O_2N_6$- SiO_2 with near net shape and a high product yield using the gelcasting process [41, 54]. Figure 3.1 (a) shows the photograph of the sintered and machined $Si_4Al_2O_2N_6$ radome. Finally, it was concluded that Si_2N_2O formed at 1750°C from a powder mixture of 60% by weight of β- $Si_4Al_2O_2N_6$ and 40% by weight of fused silica for 3 h had a flexural strength greater than three times of the sintered fused silica and a lower dielectric constant than that of stoichiometric β- $Si_4Al_2O_2N_6$.

Figure 3.1: Photograph of (a)sintered and machined $Si_4Al_2O_2N_6$ radome **[9]** (b) Bipolar plates of proton exchange membrane fuel cell by gelcasting**[180]**

3.2. Solid oxide fuel cells

Lanthanide doped ceria is one of the most potential materials for transitional temperature oxide fuel cells. The ideal material must have high ionic conductivity, the low electric conductivity and a high chemical stability in oxidizing and reducing atmospheres. Doping of the cerium oxide with trivalent cations generates a vacancy by two cations of oxygen doping. Increasing the concentration of intervals increases the oxygen ions conductivity, which is the principal characteristic of fuel cell applications[181].

In a study by Molenda et al., the gelcasting method was employed to the development of ceria membranes from nanopowders obtained from an inverse micro emulsion method in addition to commercial microcrystalline powders. They reasoned on the increase in the surface roughness of the diepressed sintered sample at 1100 ° C., due to the stress induced during the die pressing. Gas resistant membranes are attained when sintering is carried out at normal temperatures[182]. Such a low sintering temperature makes it possible to control the structural and transport properties, thus making it possible to obtain strong and gas proof membranes. Ping et al. succeeded in synthesizing lanthanum silicate oxyapatite, by water-based gel casting as a substitute electrolyte in solid oxide fuel cells[183].

Lin et al have developed a simple and cost effective method for manufacturing proton exchange membrane fuel cells (PEMFCs) using the gel casting and spray technique[184]. Proton exchange membrane fuel cell (PEMFC) bipolar platelets were prepared by mesocarbon microbeads (MCMB) with 66.7% by weight of solid loading in a premix solution of the AM monomer, the MBAM crosslinker and the dispersant (Darvan 821A) in deionized water as shown in Figure 3.1 (b)[101]. They claimed to increase the electrical conductivity at temperatures that MCMB parts can not form a sufficient carbon network for electron transport, if the sintering temperature is below 600 ° C, the carbon network eventually can be developed at a higher temperature in carbonization process.

3.3. Tissue Engineering

Materials and manufacturing technologies are of crucial importance for the engineering of bone tissue in the design of scaffolds, which support the formation of three-dimensional tissues. To facilitate tissue engineering scaffolds with a porous three-dimensional structure favorable to adequate nutrition and therefore the growth of cells in the reconstruction of bone tissue. The pores of the scaffold, however, are subjected to a blockage of cell growth and lead to restriction of nutrients supply[185]. Several biomaterials have been prepared as bone substitute material for bone defects developed and used by trauma and bone tumors. Hydroxyapatite, calcium phosphate, tricalcium-b are used in orthopedic applications because of its excellent biocompatibility. An indirectly deal with a combination of rapid prototyping and gelcasting of beta-tricalcium phosphate (TCP-B) scaffolds together, which are connected to each other have permeable structure and the microchannel array, as shown in figure 3.2[186].

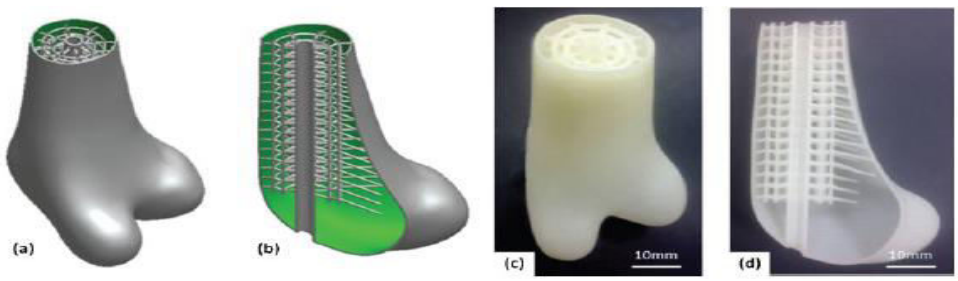

Figure 3.2: The CAD mould and resin mould with microchannels: (a) CAD model of mould, (b) CAD Model of channel network (c) resin mould, (d) vertical section of resin mould [139]

3.4. Construction materials

In gelcasting process, the toxic monomer component can be completely replaced by non toxic gel forming agents. This is an advantage for the manufacture of porous ceramics for the construction of in situ solidification of suspension piled with waste including municipal and industrial waste[187]. Porous ceramic tiles were fabricated by gelcasting method through industrial waste such as glass, low grade silica and alumina powder. Porous ceramics are obtained have high porosities of about 60% with a bending strength of 15 to 45 MPa, which is a sufficient value for the ceramic tile for construction. Fuji et al. (2006), also fabricated construction tiles and tested to examine the influences of various surfactants on the microstructure, sound absorption and thermal conductivity by gelcasting method[188].

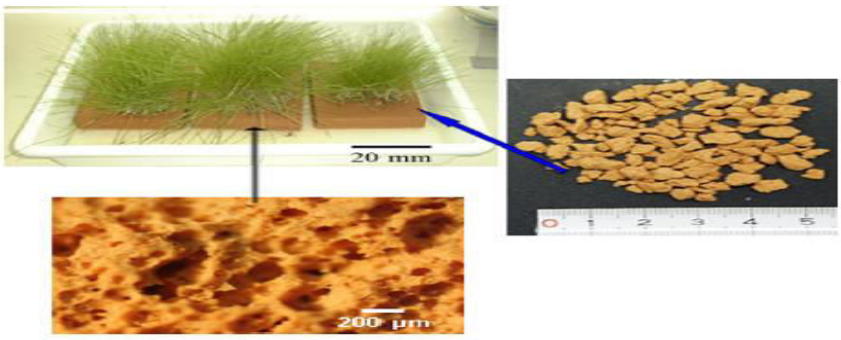

Figure 3.3: Porous ceramic tiles fabricated by gelcasting from waste with grass growing on the surface **[189]**

Figure 3.3 shows grass growing on the porous ceramic substrate while being immersed in the liquid source. The study of the microstructure shows well interconnected pore structures that allow roots to penetrate as natural soil. This material has an interesting role, including the water storage panel, which evaporates in thermal insulation. In addition, as tested, this material is a fascinating roof garden and also wall materials[189].

3.5. Rocket Nozzle

Dense ZrC / W composites were produced at moderate temperatures and ambient pressure by a reactive infiltration process . Porous WC preforms with hourglass shapes were formed by gel casting, while simple rod shaped preforms were produced by uniaxial pressing. Porous preforms were dipped in molten Zr_2Cu at 1200-13000°C and at ambient pressure[190].

The Zr_2Cu fluid quickly penetrates into preforms and undergoes a reaction with WC to give a mixture in greater mass of ZrC and W as shown in Figure 3.4.

Figure 3.4: Photographs of (a) a nozzle shaped WC preform after reactive infiltration with Zr_2Cu(l) and (b) after removal of excess solidified metal on the nozzle surfaces by polishing **[190]**.

This increase induced internal displacement reaction of the solid volume of the first completed pore space of preforms for dense composites ZrC / W. Since the preforms remain rigid during reactive infiltration, final composites retain the outer shapes and dimensions of the initial preforms. This process allows the manufacture of dense refractory metal composites and close to net shapes without densification at high temperatures.

3.6. Replamineform Inspired Bone Structures (RIBS)

A new technology simple, fast and affordable by the manufacture of Replamineform inspired backbone structures (RIBS), which has been producing forms for the creation of complex macro scale geometries with gelcasting technology. Gelcasting of the alumina was made by adding 0 to 10% by weight of carbon volatile particles to attain the porous microstructure. The porous gelcasted alumina filled with carbon was used to build bone structures replicas by a polyurethane mold into several parts automatically generated by a 3D image of a real bone completed as shown in Figure 3.5.

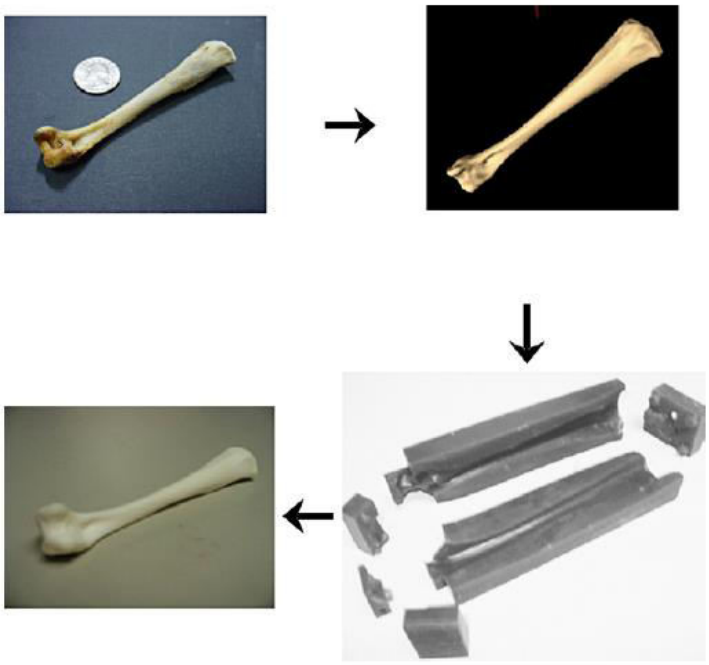

Figure 3.5: Bone generation process using a multi-piece polyurethane mold automatically generated from a 3D image of a real bone using new geometric algorithms to select appropriate cutters for machining the mold **[191]**.

Structural Performance RIBS as shown in the figure was caluculated by performing compression tests on a bone structure with a total porosity of 35% of carbon and another without pore forming agent. The tests showed that the 35% porous charcoal structure had a 1/8 strength, stiffness 1/5, and a total deformation of 40% less than the porous structure 13% without propellant[191].

3.7. High frequency ultrasound devices

High frequency ultrasonic transducers are desired to develop the spatial resolution of realtime biomedical imaging in topics such as dermatology, dentistry, ophthalmology etc. A novel gelcasting method has been used to produce a piezoelectric ceramic polymer composites produced by irregularly shaped pillars. This method contains the polymerization of piezoelectric slurries by water soluble epoxy resin and a polyamine hardener which result in a dense and high strength ceramic component. Soft micro molding was utilized to shape the ceramic parts and micro-pillars. The composite showed a net resonance mode at about 70

MHz and a kerf ~ 0.51, indicating so as to have good electrical properties for ceramic micro-pillars.

Piezoelectric ceramic polymer composites were fabricated using lead zirconate titanate (PZT) powder dispersed in an ammonium salt of polyacrylic acid solution upto 50% solid loading. The ethylene glycol diglycidyl ether, bis (3-aminopropyl) amine and Poly-dimethylsiloxane are employed as epoxy resin, hardener, and mold material respectively. The first model has ellipses with long axis 50 µm and short axis 10 µm, and the second one has radius arcs of20 µm with 8 µm width [192].

REFERENCES

[1] M. Sawitz, "Commercialisation of Advanced Ceramics, Part I," *Am. Ceram. Soc. Bull,* vol. 78, pp. 53-56, 1999.

[2] R. N. Katz, "Opportunities and prospects for the application of structural ceramics," *Structural Ceramics, Treatise on Materials Science and Technology,* vol. 29, pp. 1-26, 2012.

[3] D. W. Richerson, *The magic of ceramics*: John Wiley & Sons, 2012.

[4] S. Schmidt, S. Beyer, H. Knabe, H. Immich, R. Meistring, and A. Gessler, "Advanced ceramic matrix composite materials for current and future propulsion technology applications," *Acta Astronautica,* vol. 55, pp. 409-420, 2004.

[5] X. Yang, B. Li, C. Zhang, S. Wang, K. Liu, and C. Zou, "Fabrication and properties of porous silicon nitride wave-transparent ceramics via gel-casting and pressureless sintering," *Materials Science and Engineering: A,* vol. 663, pp. 174-180,2016.

[6] U. Bakshi and A. Godse, *Analog electronics*: Technical Publications, 2009.

[7] M. Gupta and E. W. W. Leong, *Microwaves and metals*: John Wiley & Sons, 2008.

[8] J. Knott, "Schaeffer and MT Tuley,"" *Racer Cross Section,* vol. 2, 1993.

[9] I. Ganesh, "Development of β-SiAlON based ceramics for radome applications," *Processing and application of ceramics,* vol. 5, pp. 113-138, 2011.

[10] E. I. Suzdal'tsev, "Radio-Transparent Ceramics: Yesterday, Today, Tomorrow," *Refractories and Industrial Ceramics,* vol. 55, pp. 377-390, 2015.

[11] R. W. Rice, *Ceramic fabrication technology* vol. 20: CRC Press, 2002.

[12] O. O. Omatete, M. A. Janney, and S. D. Nunn, "Gelcasting: from laboratory development toward industrial production," *Journal of the European Ceramic Society,* vol. 17, pp. 407-413, 1997.

[13] A. C. Young, O. O. Omatete, M. A. Janney, and P. A. Menchhofer, "Gelcasting of alumina," *Journal of the American Ceramic Society,* vol. 74, pp. 612-618, 1991.

[14] C. Tallon and G. V. Franks, "Recent trends in shape forming from colloidal processing: A review," *Journal of the Ceramic Society of Japan,* vol. 119, pp. 147-160, 2011.

[15] J. R. Koza, *Genetic programming: on the programming of computers by means of natural selection* vol. 1: MIT press, 1992.

[16] H.-P. Schwefel, *Numerical optimization of computer models*: John Wiley & Sons, Inc., 1981.

[17] L. J. Fogel, A. J. Owens, and M. J. Walsh, "Artificial intelligence through simulated evolution," 1966.

[18] D. E. Goldberg and J. H. Holland, "Genetic algorithms and machine learning," *Machine learning,* vol. 3, pp. 95-99, 1988.

[19] J. R. Koza, "Architecture-Altering Operations for Evolving the Architecture of a Multi-Part Program in Genetic Programming," Stanford University1994.

[20] R. Poli, "A Simple but Theoretically-Motivated Method to Control Bloat in Genetic Programming," in *Genetic Programming: 6th European Conference, EuroGP 2003 Essex, UK, April 14–16, 2003 Proceedings*, C. Ryan, T. Soule, M. Keijzer, E. Tsang, R. Poli, and E. Costa, Eds., ed Berlin, Heidelberg: Springer Berlin Heidelberg, 2003, pp. 204-217.

[21] A. Garg, K. Tai, and M. M. Savalani, "Formulation of bead width model of an SLM prototype using modified multi-gene genetic programming approach," *The International Journal of Advanced Manufacturing Technology*, vol. 73, pp. 375-388, 2014.

[22] J. R. Koza, *Genetic programming III: Darwinian invention and problem solving* vol. 3: Morgan Kaufmann, 1999.

[23] D. P. Searson, D. E. Leahy, and M. J. Willis, "GPTIPS: an open source genetic programming toolbox for multigene symbolic regression," in *Proceedings of the International multiconference of engineers and computer scientists*, 2010, pp. 77-80.

[24] A. Garg and K. Tai, "Review of genetic programming in modeling of machining processes," in *2012 Proceedings of International Conference on Modelling, Identification and Control*, 2012, pp. 653-658.

[25] A. Garg and K. Tai, "Selection of a robust experimental design for the effective modeling of nonlinear systems using Genetic Programming," in *2013 IEEE Symposium on Computational Intelligence and Data Mining (CIDM)*, 2013, pp. 287-292.

[26] A. Garg and K. Tai, "Comparison of statistical and machine learning methods in modelling of data with multicollinearity," *International Journal of Modelling, Identification and Control*, vol. 18, pp. 295-312, 2013.

[27] R. L. Haupt and S. E. Haupt, *Practical genetic algorithms*: John Wiley & Sons, 2004.

[28] D. E. Goldberg, *Genetic Algorithms in Search, Optimization and Machine Learning*: Addison-Wesley Longman Publishing Co., Inc., 1989.

[29] N. Srinivas and K. Deb, "Muiltiobjective Optimization Using Nondominated Sorting in Genetic Algorithms," *Evolutionary Computation*, vol. 2, pp. 221-248, 1994.

[30] C. M. Fonseca and P. J. Fleming, "An Overview of Evolutionary Algorithms in Multiobjective Optimization," *Evolutionary Computation*, vol. 3, pp. 1-16, 1995.

[31] G. P. Rangaiah, *Multi-objective optimization: techniques and applications in chemical engineering* vol. 5: World Scientific, 2016.

[32] G. Gilde, P. Patel, C. Hubbard, B. Pothier, T. Hynes, W. Croft, *et al.*, "SiON low dielectric constant ceramic nanocomposite," ed: Google Patents, 1997.

[33] H. Wang, J. Yu, J. Zhang, and D. Zhang, "Preparation and properties of pressureless-sintered porous Si3N4," *Journal of Materials Science*, vol. 45, pp. 3671-3676, 2010.

[34] Y. Li, F. Chen, L. Li, W. Zhang, H. Yu, Y. Shan, *et al.*, "Gas Pressure Sintering of Arbitrary Porous Silicon Nitride Ceramics with High Mechanical Strength," *Journal of the American Ceramic Society*, vol. 93, pp. 1565-1568, 2010.

[35] Y. Wang and J. Liu, "Aluminum Phosphate–Mullite Composites for High-Temperature Radome Applications," *International Journal of Applied Ceramic Technology,* vol. 6, pp. 190-194, 2009.

[36] D. Li, C.-r. Zhang, B. Li, F. Cao, S.-q. Wang, B. Yang, *et al.*, "Effects of oxidation treatment on properties of SiO_2f/SiO_2-BN composites," *Journal of Central South University,* vol. 19, pp. 30-35, 2012.

[37] Z. Lü, H. Geng, M. Zhang, and X. Hou, "Preparation of aluminum borate whisker reinforced aluminum phosphate wave-transparent materials," *Chinese Science Bulletin,* vol. 53, pp. 3073-3076, 2008.

[38] X. Duan, D. Jia, J. Deng, Z. Yang, and Y. Zhou, "Mechanical and dielectric properties of gelcasted Si_3N_4 porous ceramic using $CaHPO_4$ as an additive," *Ceramics International,* vol. 38, pp. 4363-4367,2012.

[39] L. Zhou, Y. Huang, Z. Xie, A. Zimmermann, and F. Aldinger, "Preparation of Si_3N_4 ceramics with high strength and high reliability via a processing strategy," *Journal of the European Ceramic Society,* vol. 22, pp. 1347-1355, 2002.

[40] J. Yu, H. Wang, J. Zhang, D. Zhang, and Y. Yan, "Gelcasting preparation of porous silicon nitride ceramics by adjusting the content of monomers," *Journal of Sol-Gel science and technology,* vol. 53, pp. 515-523, 2010.

[41] I. Ganesh, N. Thiyagarajan, D. C. Jana, Y. R. Mahajan, and G. Sundararajan, "Aqueous Gelcasting Process for β-$Si_4Al_2O_2N_6$ Ceramics," *Journal of the American Ceramic Society,* vol. 91, pp. 3121-3124, 2008.

[42] S. Wang, D. Jia, Z. Yang, X. Duan, Z. Tian, and Y. Zhou, "Effect of BN content on microstructures, mechanical and dielectric properties of porous BN/Si_3N_4 composite ceramics prepared by gel casting," *Ceramics International,* vol. 39, pp. 4231-4237, 2013.

[43] C. Zou, C. Zhang, B. Li, S. Wang, and F. Cao, "Microstructure and properties of porous silicon nitride ceramics prepared by gel-casting and gas pressure sintering," *Materials & Design,* vol. 44, pp. 114-118,2013.

[44] S. Wang, Z. Yang, X. Duan, D. Jia, W. Cui, B. Sun, *et al.*, "Effects of pore size on microstructure, mechanical and dielectric properties of gel casting BN/Si_3N_4 ceramics with spherical-shaped pore structures," *Journal of Alloys and Compounds,* vol. 581, pp. 46-51, 2016.

[45] J.-H. Wu, J.-K. Guo, and B.-S. Li, "Preparation and properties of SiO_2 matrix composites doped with AlN particles," *Journal of Materials Science,* vol. 35, pp. 4895-4900,2000.

[46] I. Ganesh, N. Thiyagarajan, D. C. Jana, P. Barik, and G. Sundararajan, "An Aqueous Gelcasting Route to Dense β-$Si_4Al_2O_2N_6$–0.5SiO_2 Ceramics," *Journal of the American Ceramic Society,* vol. 91, pp. 1566-1571, 2008.

[47] I. Ganesh and G. Sundararajan, "Novel route to β-SiAlON–SiO_2 ceramic composites," *Advances in Applied Ceramics,* vol. 110, pp. 87-94, 2011.

[48] I. Ganesh, "Near-Net Shape β-$Si_4Al_2O_2N_6$ Parts by Hydrolysis Induced Aqueous Gelcasting Process," *International Journal of Applied Ceramic Technology,* vol. 6, pp. 89-101, 2009.

[49] I. Ganesh, "Near-Net Shape β-$Si_4Al_2O_2N_6$ Parts by Hydrolysis Induced Aqueous Gelcasting Process," *International Journal of Applied Ceramic Technology,* vol. 6, pp. 89-101, 2009.

[50] I. Ganesh, G. J. Reddy, G. Sundararajan, S. M. Olhero, P. M. C. Torres, and J. M. F. Ferreira, "Hydrolysis-Induced Aqueous Gelcasting of Magnesium Aluminate Spinel," *International Journal of Applied Ceramic Technology,* vol. 8, pp. 873-884, 2011.

[51] I. Ganesh, "Aqueous slip casting of $MgAl_2O_4$ spinel powder," *Bulletin of Materials Science,* vol. 34, pp. 327-335, 2011.

[52] I. Ganesh, S. M. Olhero, P. M. C. Torres, and J. M. F. Ferreira, "Gelcasting of Magnesium Aluminate Spinel Powder," *Journal of the American Ceramic Society,* vol. 92, pp. 350-357, 2009.

[53] I. Ganesh, G. Sundararajan, S. M. Olhero, P. M. Torres, and J. M. Ferreira, "A novel colloidal processing route to alumina ceramics," *Ceramics International,* vol. 36, pp. 1357-1364, 2010.

[54] I. Ganesh and G. Sundararajan, "Hydrolysis-Induced Aqueous Gelcasting of β-SiAlON–SiO2 Ceramic Composites: The Effect of AlN Additive," *Journal of the American Ceramic Society,* vol. 93, pp. 3180-3189, 2010.

[55] X. Duan, D. Jia, B. Yuan, S. Wang, Z. Yang, and Y. Zhou, "Effect of solid contents on the mechanical properties of SiC–10 wt.%AlN ceramic composites prepared by gelcasting," *Journal of Alloys and Compounds,* vol. 546, pp. 275-279, 2013.

[56] J. Xue, M. Dong, J. Li, G. Zhou, and S. Wang, "Gelcasting of Aluminum Nitride Ceramics," *Journal of the American Ceramic Society,* vol. 93, pp. 928-930, 2010.

[57] C. Takai, M. Tsukamoto, M. Fuji, and M. Takahashi, "Control of high solid content yttria slurry with low viscosity for gelcasting," *Journal of Alloys and Compounds,* vol. 408–412, pp. 533-537,2006.

[58] Q. Zhang and M. Gu, "Rheological properties and gelcasting of concentrated aqueous silicon suspension," *Materials Science and Engineering: A,* vol. 399, pp. 351-357, 2005.

[59] F. Li, H.-y. Chen, R.-z. Wu, and B.-d. Sun, "Effect of polyethylene glycol on the surface exfoliation of SiC green bodies prepared by gelcasting," *Materials Science and Engineering: A,* vol. 368, pp. 255-259, 2004.

[60] J.-M. Wu, X.-H. Wang, Y.-N. Fan, X. Shi, and W.-Z. Lu, "Microstructures and dielectric properties of $Ba0.6Sr0.4TiO_3$–MgO ceramics prepared by non-aqueous gelcasting and dry pressing," *Materials Research Bulletin,* vol. 46, pp. 2217-2221, 2011.

[61] C. Zou, C. Zhang, B. Li, F. Cao, and S. Wang, "Improved properties and microstructure of porous silicon nitride/silicon oxide composites prepared by sol–gel route," *Materials Science and Engineering: A,* vol. 556, pp. 648-652, 2012.

[62] Y. Huang and J. Yang, *Novel colloidal forming of ceramics*: Springer Science & Business Media, 2011.

[63] K. Prabhakaran and C. Pavithran, "Gelcasting of alumina from acidic aqueous medium using acrylic acid," *Journal of the European Ceramic Society,* vol. 20, pp. 1115-1119, 2000.

[64] J. Yu, H. Wang, H. Zeng, and J. Zhang, "Effect of monomer content on physical properties of silicon nitride ceramic green body prepared by gelcasting," *Ceramics International,* vol. 35, pp. 1039-1044, 2009.

[65] L. Zhao, J.-l. Yang, L.-g. Ma, and Y. Huang, "Influence of minute metal ions on the idle time of acrylamide polymerization in gelcasting of ceramics," *Materials Letters,* vol. 56, pp. 990-994, 2002.

[66] D. Zhang, Y. Zhang, R. Xie, and K. Zhou, "Freeze gelcasting of aqueous alumina suspensions for porous ceramics," *Ceramics International,* vol. 38, pp. 6063-6066, 2012.

[67] Z.-Z. Yi, Z.-P. Xie, J.-T. Ma, Y. Huang, and Y.-B. Cheng, "Study on gelcasting of silicon nitride-bonded silicon carbide refractories," *Materials Letters,* vol. 56, pp. 895-900, 2002.

[68] Y. Huang, L. Ma, Q. Tang, J. Yang, Z. Xie, and X. Xu, "Surface oxidation to improve water-based gelcasting of silicon nitride," *Journal of Materials Science,* vol. 35, pp. 3519-3524, 2000.

[69] L. Zhou, Y. Huang, and Z. Xie, "Gelcasting of concentrated aqueous silicon carbide suspension," *Journal of the European Ceramic Society,* vol. 20, pp. 85-90, 2000.

[70] D. Kong, H. Yang, S. Wei, D. Li, and J. Wang, "Gel-casting without de-airing process using silica sol as a binder," *Ceramics International,* vol. 33, pp. 133-139, 2007.

[71] X. Guo, Z. Zhou, G. Ma, S. Wang, S. Zhao, and Q. Zhang, "Effect of forming process on the integrity of pore-gradient Al2O3 ceramic foams by gelcasting," *Ceramics International,* vol. 38, pp. 713-719, 2012.

[72] I. Ganesh, S. M. Olhero, P. M. C. Torres, F. J. Alves, and J. M. F. Ferreira, "Hydrolysis-induced aqueous gelcasting for near-net shape forming of ZTA ceramic composites," *Journal of the European Ceramic Society,* vol. 29, pp. 1393-1401, 2009.

[73] M. Potoczek and E. Zawadzak, "Initiator effect on the gelcasting properties of alumina in a system involving low-toxic monomers," *Ceramics International,* vol. 30, pp. 793-799, 2004.

[74] I. Ganesh, G. Jaganatha Reddy, G. Sundararajan, S. M. Olhero, P. M. C. Torres, and J. M. F. Ferreira, "Influence of processing route on microstructure and mechanical properties of MgAl2O4 spinel," *Ceramics International,* vol. 36, pp. 473-482, 2010.

[75] Y. Li and Z. Guo, "Gelcasting of WC–8wt%Co tungsten cemented carbide," *International Journal of Refractory Metals and Hard Materials,* vol. 26, pp. 472-477, 2008.

[76] F. S. Ortega, R. H. R. Castro, D. Gouvêa, and V. C. Pandolfelli, "The rheological behavior and surface charging of gelcasting alumina suspensions," *Ceramics International,* vol. 34, pp. 237-241, 2008.

[77] F. Chabert, D. E. Dunstan, and G. V. Franks, "Cross-linked Polyvinyl Alcohol as a Binder for Gelcasting and Green Machining," *Journal of the American Ceramic Society,* vol. 91, pp. 3138-3146, 2008.

[78] M. Lombardi, V. Naglieri, J.-M. Tulliani, and L. Montanaro, "Gelcasting of dense and porous ceramics by using a natural gelatine," *Journal of Porous Materials,* vol. 16, pp. 393-400, 2009.

[79] Y. Chen, Z. Xie, J. Yang, and Y. Huang, "Alumina casting based on gelation of gelatine," *Journal of the European Ceramic Society,* vol. 19, pp. 271-275, 1999.

[80] J.-y. Zhang and F. Ye, "Effect of agarose content on microstructures and mechanical properties of porous silicon nitride ceramics produced by gelcasting," *Journal of Zhejiang University-SCIENCE A,* vol. 11, pp. 771-775, 2010.

[81] X. Mao, S. Shimai, M. Dong, and S. Wang, "Gelcasting of Alumina Using Epoxy Resin as a Gelling Agent," *Journal of the American Ceramic Society,* vol. 90, pp. 986-988, 2007.

[82] C. Tallon, D. Jach, R. Moreno, M. I. Nieto, G. Rokicki, and M. Szafran, "Gelcasting of alumina suspensions containing nanoparticles with glycerol monoacrylate," *Journal of the European Ceramic Society,* vol. 29, pp. 875-880, 2009.

[83] M. A. Janney, O. O. Omatete, C. A. Walls, S. D. Nunn, R. J. Ogle, and G. Westmoreland, "Development of Low-Toxicity Gelcasting Systems," *Journal of the American Ceramic Society,* vol. 81, pp. 581-591, 1998.

[84] J. Yang, J. Yu, and Y. Huang, "Recent developments in gelcasting of ceramics," *Journal of the European Ceramic Society,* vol. 31, pp. 2569-2591, 2011.

[85] J. Tong and D. Chen, "Preparation of alumina by aqueous gelcasting," *Ceramics International,* vol. 30, pp. 2061-2066, 2004.

[86] A. Kaşgöz, Z. Özbaş, H. Kaşgöz, and I. Aydin, "Effects of monomer composition on the mechanical and machinability properties of gel-cast alumina green compacts," *Journal of the European Ceramic Society,* vol. 25, pp. 3547-3552, 2005.

[87] M. Rahaman and M. N. Rahaman, *Ceramic processing*: CRC press, 2006.

[88] X. Mao, S. Shimai, and S. Wang, "Gelcasting of alumina foams consolidated by epoxy resin," *Journal of the European Ceramic Society,* vol. 28, pp. 217-222, 2008.

[89] J.-S. Ha, "Effect of atmosphere type on gelcasting behavior of Al_2O_3 and evaluation of green strength," *Ceramics International,* vol. 26, pp. 251-254, 2000.

[90] G. Jian, Q. Tai, Y. Jian, F. Yongbao, Z. Chao, Z. Wenpeng, *et al.*, "Process dependant setting behavior of aqueous gelcast AlN slurries," *Ceramics International,* vol. 38, pp. 2905-2911, 2012.

[91] J. Stampfl, H.-C. Liu, S. W. Nam, K. Sakamoto, H. Tsuru, S. Kang, *et al.*, "Rapid prototyping and manufacturing by gelcasting of metallic and ceramic slurries," *Materials Science and Engineering: A,* vol. 334, pp. 187-192, 2002.

[92] L. Hu, C.-A. Wang, and Y. Huang, "Porous yttria-stabilized zirconia ceramics with ultra-low thermal conductivity," *Journal of Materials Science,* vol. 45, pp. 3242-3246, 2010.

[93] L. Shen, M. Liu, X. Liu, and B. Li, "Thermal shock resistance of the porous Al_2O_3/ZrO_2 ceramics prepared by gelcasting," *Materials Research Bulletin,* vol. 42, pp. 2048-2056, 2007.

[94] X. Liu, Y. Huang, and J. Yang, "Effect of rheological properties of the suspension on the mechanical strength of Al_2O_3–ZrO_2 composites prepared by gelcasting," *Ceramics International,* vol. 28, pp. 159-164, 2002.

[95] J.-M. Wu, W.-Z. Lu, W. Lei, J.-P. He, and J. Wang, "Effects of aqueous gelcasting and dry pressing on the sinterability and microwave dielectric properties of $ZnAl_2O_4$-based ceramics," *Ceramics International,* vol. 37, pp. 481-486, 2011.

[96] J. Yue, B. Dong, and H. Wang, "Porous Si_3N_4 Fabricated by Phase Separation Method Using Benzoic Acid as Pore-Forming Agent," *Journal of the American Ceramic Society,* vol. 94, pp. 1989-1991, 2011.

[97] D. Zhou, H. Li, S. Gong, Y. Hu, and K. Han, "Sodium Bismuth Titanate-Based Lead-Free Piezoceramics Prepared by Aqueous Gelcasting," *Journal of the American Ceramic Society,* vol. 91, pp. 2792-2796, 2008.

[98] Z. X. Xiong, C. Fang, Y. X. Wang, and Z. G. Su, "Gel-casting of ceramic components for wireless communications," *Journal of the European Ceramic Society,* vol. 25, pp. 2071-2074, 2005.

[99] D. Guo, K. Cai, L. Li, and Z. Gui, "Application of gelcasting to the fabrication of piezoelectric ceramic parts," *Journal of the European Ceramic Society,* vol. 23, pp. 1131-1137, 2003.

[100] M. Takahashi, K. Adachi, R. L. Menchavez, and M. Fuji, "Fabrication of semi-conductive ceramics by combination of gelcasting and reduction sintering," *Journal of Materials Science,* vol. 41, pp. 1965-1972, 2006.

[101] Y.-F. Liu, X.-Q. Liu, G. Li, and G.-Y. Meng, "Low cost porous mullite-corundum ceramics by gelcasting," *Journal of Materials Science,* vol. 36, pp. 3687-3692, 2001.

[102] W. Chen, Y. Miyamoto, T. Matsumoto, and T. Tojo, "Preparation of AlN ceramic bonded carbon by gelcasting and spark plasma sintering," *Carbon,* vol. 48, pp. 3399-3404, 2016.

[103] W. Chen, Y. Miyamoto, T. Tojo, and M. Naito, "Densification and properties of AlN ceramic bonded carbon," *Journal of the European Ceramic Society,* vol. 32, pp. 245-250, 2012.

[104] F. Yang, C. Li, Y. Lin, and C.-A. Wang, "Effects of sintering temperature on properties of porous mullite/corundum ceramics," *Materials Letters,* vol. 73, pp. 36-39, 2012.

[105] J. Zhou and C.-A. Wang, "Porous yttria-Stabilized Zirconia Ceramics Fabricated by Nonaqueous-Based Gelcasting Process with PMMA Microsphere as Pore-Forming Agent," *Journal of the American Ceramic Society,* vol. 96, pp. 266-271, 2013.

[106] C. Boberski, R. Hamminger, M. Peuckert, F. Aldinger, R. Dillinger, J. Heinrich, *et al.*, "High-performance Silicon nitride materials," *Angewandte Chemie,* vol. 101, pp. 1592-1601, 1989.

[107] S. Mishra, C. Mallika, P. K. Das, U. K. Mudali, and R. Natarajan, "Development and Characterization of Porous Silicon Nitride Tubes," *Transactions of the Indian Ceramic Society,* vol. 72, pp. 52-55, 2013.

[108] F. Wang, J. Yin, D. Yao, Y. Xia, K. Zuo, H. Liang, *et al.*, "Effects of oil on gelcasting of oil-in-water Si_3N_4 suspensions," *Journal of Alloys and Compounds,* vol. 699, pp. 268-273, 2017.

[109] B. Bergman and H. Heping, "The influence of different oxides on the formation of Si_2N_2O from SiO_2 and Si_3N_4," *Journal of the European Ceramic Society,* vol. 6, pp. 3-8, 1990.

[110] J.-M. Wu, X.-Y. Zhang, and J.-L. Yang, "Novel porous Si_3N_4 ceramics prepared by aqueous gelcasting using Si_3N_4 poly-hollow microspheres as pore-forming agent," *Journal of the European Ceramic Society,* vol. 34, pp. 1089-1096, 2014.

[111] Y. Liu, L. Cheng, L. Zhang, Y. Xu, and Y. Liu, "Fabrication and characterization of SiO_2(f)/Si_3N_4 composites," *Journal of University of Science and Technology Beijing, Mineral, Metallurgy, Material,* vol. 14, pp. 454-459, 2007.

[112] X. Li, P. Wu, and D. Zhu, "Fabrication and properties of porous Si3N4–SiO2 ceramics with dense surface and gradient pore distribution," *Ceramics International,* vol. 40, pp. 5079-5084, 2014.

[113] G. J. Qi, "Interfacial reaction mechanisms of 3D SiO_2f/Si_3N_4 composites prepared by perhydropolysilazane," *Journal of Composite Materials,* vol. 45, pp. 1621-1626, 2011.

[114] Y. Huang, L. Zhou, Q. Tang, Z. Xie, and J. Yang, "Water-Based Gelcasting of Surface-Coated Silicon Nitride Powder," *Journal of the American Ceramic Society,* vol. 84, pp. 701-707, 2001.

[115] L. ShuQin, P. YuChen, Y. ChangQing, and L. JiaLu, "Mechanical and dielectric properties of porous Si_2N_2O–Si_3N_4 in situ composites," *Ceramics International,* vol. 35, pp. 1851-1854, 2009.

[116] P. Yuchen, L. Shuqin, Y. Changqing, H. zhengyu, M. jingtao, and L. Jialu, "Thermal shock resistance of in situ formed Si_2N_2O–Si_3N_4 composites by gelcasting," *Ceramics International,* vol. 35, pp. 3365-3369, 2009.

[117] G. You, J. Bi, Y. Chen, C. Yin, and C. a. Wang, "Effect of diatomite additive on the mechanical and dielectric properties of porous SiO_2-Si_3N_4 composite ceramics," *Journal of Wuhan University of Technology. Materials Science Edition,* vol. 31, p. 528, 2016.

[118] K. Liu, C. Zhang, B. Li, S. Wang, and F. Cao, "Effect of Pyrolysis Temperature on Properties of Porous Si_3N_4-BN Composites Fabricated Via PIP Route," *Journal of Materials Engineering and Performance,* vol. 22, pp. 3684-3688, 2013.

[119] Y. Feng, H. Gong, Y. Zhang, X. Wang, S. Che, Y. Zhao, *et al.*, "Effect of BN content on the mechanical and dielectric properties of porous BNp/Si_3N_4 ceramics," *Ceramics International,* vol. 42, pp. 661-665, 2016.

[120] M.-I. Kim and P. Zou, "Modeling of Drilling Forces Based on Twist Drill Point Angles Using Multigene Genetic Programming," *Mathematical Problems in Engineering,* vol. 2016, p. 9, 2016.

[121] J. Yu, H. Wang, and J. Zhang, "Neural network modeling and analysis of gel casting preparation of porous Si_3N_4 ceramics," *Ceramics International,* vol. 35, pp. 2943-2950, 2009.

[122] A. Garg, L. Rachmawati, and K. Tai, "Classification-driven model selection approach of genetic programming in modelling of turning process," *The International Journal of Advanced Manufacturing Technology,* vol. 69, pp. 1137-1151, 2013.

[123] J. Li, X. Yang, C. Ren, G. Chen, and Y. Wang, "Multiobjective optimization of cutting parameters in Ti-6Al-4V milling process using nondominated sorting genetic algorithm-II," *The International Journal of Advanced Manufacturing Technology,* vol. 76, pp. 941-953, 2015.

[124] M. Kök, E. Kanca, and Ö. Eyercioğlu, "Prediction of surface roughness in abrasive waterjet machining of particle reinforced MMCs using genetic expression programming," *The International Journal of Advanced Manufacturing Technology,* vol. 55, pp. 955-968, 2011.

[125] R. Jeyapaul, P. Shahabudeen, and K. Krishnaiah, "Simultaneous optimization of multi-response problems in the Taguchi method using genetic algorithm," *The International Journal of Advanced Manufacturing Technology,* vol. 30, pp. 870-878, 2006.

[126] K. K. Kandi, N. Thallapalli, and S. P. R. Chilakalapalli, "Development of Silicon Nitride-Based Ceramic Radomes — A Review," *International Journal of Applied Ceramic Technology,* vol. 12, pp. 909-920, 2015.

[127] D. Hanaor, M. Michelazzi, C. Leonelli, and C. C. Sorrell, "The effects of carboxylic acids on the aqueous dispersion and electrophoretic deposition of ZrO_2," *Journal of the European Ceramic Society,* vol. 32, pp. 235-244, 2012.

[128] T. Homma, "Properties of Fluorinated Silicon Oxide Films Formed Using Fluorotriethoxysilane for Interlayer Dielectrics in Multilevel Interconnections," *Journal of The Electrochemical Society,* vol. 143, pp. 1084-1087, 1996.

[129] T. Nagaveni, K. K. Kumar, and C. Rao, "Some Chemo-Rheological studies of aqueous Silicon Nitride suspensions in gelcasting process," in *5th International & 26th All India Manufacturing Technology Design and Research Conference (AIMTDR 2014), December 12th–14th 2014,* IIT Guwahati, Assam, India, 2014.

[130] T. Nagaveni, K. K. Kumar, and C. S. P. Rao, "Some Chemo-Rheological Studies of Aqueous Silicon Nitride Suspensions in Gelcasting process," presented at the Proceedings of the 5 th International & 26th All India Manufacturing Technology, Design and Research Conference (AIMTDR 2014) ,, IIT Guwahati, Assam, India, 2014.

[131] J.-Q. Dai, Y. Huang, Z.-P. Xie, X.-L. Xu, and J.-L. Yang, "Effect of acid cleaning and calcination on rheological properties of concentrated aqueous suspensions of silicon nitride powder," *J. Am. Ceram. Soc.,* vol. 85, pp. 293-298, 2002.

[132] D. Jia, Y. Shao, B. Liu, and Y. Zhou, "Characterization of porous silicon nitride/silicon oxynitride composite ceramics produced by sol infiltration," *Materials Chemistry and Physics,* vol. 124, pp. 97-101, 11/1/ 2010.

[133] S. Wang, D. Jia, Z. Yang, X. Duan, Z. Tian, and Y. Zhou, "Effect of BN content on microstructures, mechanical and dielectric properties of porous BN/Si_3N_4 composite

ceramics prepared by gel casting," *Ceramics International,* vol. 39, pp. 4231-4237, 2013.

[134] F. Bouville and S. Deville, "Dispersion of Boron Nitride Powders in Aqueous Suspensions with Cellulose," *Journal of the American Ceramic Society,* vol. 97, pp. 394-398, 2014.

[135] J. Yin, J. Chen, X. Liu, H. Zhang, Y. Yan, Z. Huang, *et al.*, "Co-Dispersion Behavior of ZrB_2–SiC–B_4C–C Powders with Polyethyleneimine," *Materials,* vol. 6, p. 4249, 2013.

[136] R. He, P. Hu, X. Zhang, W. Han, C. Wei, and Y. Hou, "Preparation of high solid loading, low viscosity ZrB_2–SiC aqueous suspensions using PEI as dispersant," *Ceramics International,* vol. 39, pp. 2267-2274, 4// 2013.

[137] Y. Zhang and J. Binner, "Effect of dispersants on the rheology of aqueous silicon carbide suspensions," *Ceramics International,* vol. 34, pp. 1381-1386, 2008.

[138] V. A. Hackley, "Colloidal processing of silicon nitride with poly (acrylic acid): II, rheological properties," *Journal of the American Ceramic Society,* vol. 81, pp. 2421-2428, 1998.

[139] M. Janney, S. Nunn, C. Walls, O. Omatete, R. Ogle, G. Kirby, *et al.*, "The handbook of ceramic engineering," *Am Ceram Soc,* vol. 74, pp. 612-618, 1998.

[140] Y. Liu, L. Gao, and J. Guo, "Comparative study on the stabilizing effect of 2-phosphonobutane-1, 2, 4-tricarboxylic acid and citric acid for alumina suspensions," *Colloids and Surfaces A: Physicochemical and Engineering Aspects,* vol. 193, pp. 187-195, 2001.

[141] P. Greil, "Processing of silicon nitride ceramics," *Materials Science and Engineering: A,* vol. 109, pp. 27-35,1989.

[142] D. C. Jia, Y. Zhou, and T. C. Lei, "Ambient and elevated temperature mechanical properties of hot-pressed fused silica matrix composite," *Journal of the European Ceramic Society,* vol. 23, pp. 801-808, 2003.

[143] G. You, J. Bi, Y. Chen, C. Yin, and C. a. Wang, "Effect of diatomite additive on the mechanical and dielectric properties of porous SiO_2-Si_3N_4 composite ceramics," *Journal of Wuhan University of Technology-Mater. Sci. Ed.,* vol. 31, pp. 528-532, 2016.

[144] F. Wagstaff, "Crystallization and melting kinetics of cristobalite," *Journal of the American Ceramic Society,* vol. 52, pp. 650-654, 1969.

[145] L. ShuQin, P. YuChen, Y. ChangQing, and L. JiaLu, "Mechanical and dielectric properties of porous Si_2N_2O–Si_3N_4 in situ composites," *Ceramics International,* vol. 35, pp. 1851-1854, 2009.

[146] L.-Y. Wang and M.-H. Hon, "The effect of cristobalite seed on the crystallization of fused silica based ceramic core—A kinetic study," *Ceramics International,* vol. 21, pp. 187-193, 1995.

[147] R.-G. Duan, G. Roebben, J. Vleugels, and O. Van der Biest, "In situ formation of Si_2N_2O and TiN in Si_3N_4-based ceramic composites," *Acta materialia,* vol. 53, pp. 2547-2554, 2005.

[148] X. Weiling, X. Peng, L. Heng, Z. Wei, and L. Yang, "Preparation and Dielectric Properties of Si_3N_4/BN (CB) Composite Ceramic," *High Temperature Materials and Processes,* vol. 35, pp. 523-529, 2016.

[149] Y. Liu, L. Gao, and J. Guo, "Comparative study on the stabilizing effect of 2-phosphonobutane-1,2,4-tricarboxylic acid and citric acid for alumina suspensions," *Colloids and Surfaces A: Physicochemical and Engineering Aspects,* vol. 193, pp. 187-195, 2001.

[150] N. Thallapalli and C. Rao, "Preparation and Characterization of Si_3N_4-BN Ceramic Composites by Gelcasting," *Material Science Research India,* vol. 13, pp. 28-33, 2016.

[151] A. Kovalčíková, J. Balko, C. Balázsi, P. Hvizdoš, and J. Dusza, "Influence of hBN content on mechanical and tribological properties of Si_3N_4/BN ceramic composites," *Journal of the European Ceramic Society,* vol. 34, pp. 3319-3328, 2014.

[152] W. Wan, J. Yang, J. Zeng, L. Yao, and T. Qiu, "Effect of solid loading on gelcasting of silica ceramics using DMAA," *Ceramics International,* vol. 40, pp. 1735-1740, 2014.

[153] M. H. Baziar, Y. Jafarian, H. Shahnazari, V. Movahed, and M. Amin Tutunchian, "Prediction of strain energy-based liquefaction resistance of sand–silt mixtures: An evolutionary approach," *Computers & Geosciences,* vol. 37, pp. 1883-1893, 2011.

[154] S. Luke and L. Panait, "Lexicographic parsimony pressure," presented at the Proceedings of the 4th Annual Conference on Genetic and Evolutionary Computation, New York City, New York, 2002.

[155] D. Searson, "GPTIPS Genetic Programming & Symbolic Regression for MATLAB User Guide," 2009.

[156] T. Graule, L. Gauckler, and F. Baader, "DIRECT COAGULATION CASTING- A NEW GREEN SHAPING TECHNIQUE. PT. 1. PROCESSING PRINCIPLES," *Industrial ceramics,* vol. 16, pp. 31-34, 1996.

[157] L. J. Gauckler, T. Graule, and F. Baader, "Ceramic forming using enzyme catalyzed reactions," *Materials Chemistry and Physics,* vol. 61, pp. 78-102,1999.

[158] R. Laucournet, C. Pagnoux, T. Chartier, and J.-F. Baumard, "Coagulation Method of Aqueous Concentrated Alumina Suspensions by Thermal Decomposition of Hydroxyaluminum Diacetate," *Journal of the American Ceramic Society,* vol. 83, pp. 2661-2667, 2000.

[159] R. Moreno, J. S. Moya, and J. Requena, "Slip casting of zircon by using an organic surfactant," *Ceramics International,* vol. 17, pp. 37-40, 1991.

[160] G. Tarì, J. M. F. Ferreira, A. T. Fonseca, and O. Lyckfeldt, "Influence of particle size distribution on colloidal processing of alumina," *Journal of the European Ceramic Society,* vol. 18, pp. 249-253, 1998.

[161] D. Hotza and P. Greil, "Review: aqueous tape casting of ceramic powders," *Materials Science and Engineering: A,* vol. 202, pp. 206-217, 1995.

[162] T. Kosmacˇ, S. Novak, M. Sajko, and D. Eterovicˇ, "A process for forming ceramic products from an aqueous suspension with a high solids content," *Patent EP 0-813-508 BI,* 1999.

[163] S. Novak and T. Kosmač, "Interactions in aqueous Al_2O_3–AlN suspensions during the HAS process," *Materials Science and Engineering: A,* vol. 256, pp. 237-242, 1998.

[164] T. Kosmač, S. Novak, and M. Sajko, "Hydrolysis-assisted solidification (HAS): A new setting concept for ceramic net-shaping," *Journal of the European Ceramic Society,* vol. 17, pp. 427-432, 1997.

[165] S. Novak, T. Kosmač, K. Krnel, and G. Dražič, "Principles of the hydrolysis assisted solidification (HAS) process for forming ceramic bodies from aqueous suspension," *Journal of the European Ceramic Society,* vol. 22, pp. 289-295, 2002.

[166] S. W. Sofie and F. Dogan, "Freeze Casting of Aqueous Alumina Slurries with Glycerol," *Journal of the American Ceramic Society,* vol. 84, pp. 1459-1464, 2001.

[167] T. Fukasawa, M. Ando, T. Ohji, and S. Kanzaki, "Synthesis of Porous Ceramics with Complex Pore Structure by Freeze-Dry Processing," *Journal of the American Ceramic Society,* vol. 84, pp. 230-232, 2001.

[168] T. Fukasawa, Z.-Y. Deng, M. Ando, T. Ohji, and Y. Goto, "Pore structure of porous ceramics synthesized from water-based slurry by freeze-dry process," *Journal of Materials Science,* vol. 36, pp. 2523-2527, 2001.

[169] H.-W. Kang, Y. Tabata, and Y. Ikada, "Fabrication of porous gelatin scaffolds for tissue engineering," *Biomaterials,* vol. 20, pp. 1339-1344, 1999.

[170] R. Mistler, D. Shanefield, and R. Runk, "Tape casting of ceramics," *Ceramic processing before firing,* pp. 411-448, 1978.

[171] P. Nahass, R. L. Pober, W. E. Rhine, W. L. Robbins, and H. K. Bowen, "Prediction and Explanation of Aging Shrinkage in Tape-Cast Ceramic Green Sheets," *Journal of the American Ceramic Society,* vol. 75, pp. 2373-2378, 1992.

[172] M. A. Janney and O. O. Omatete, "Method for molding ceramic powders using a water-based gel casting," ed: Google Patents, 1991.

[173] D. de Faoite, D. J. Browne, F. R. Chang-Díaz, and K. T. Stanton, "A review of the processing, composition, and temperature-dependent mechanical and thermal properties of dielectric technical ceramics," *Journal of Materials Science,* vol. 47, pp. 4211-4235, 2012.

[174] G. Y. Onoda, "Theoretical Strength of Dried Green Bodies with Organic Binders," *Journal of the American Ceramic Society,* vol. 59, pp. 236-239, 1976.

[175] S. A. Uhland, R. K. Holman, S. Morissette, M. J. Cima, and E. M. Sachs, "Strength of Green Ceramics with Low Binder Content," *Journal of the American Ceramic Society,* vol. 84, pp. 2809-2818, 2001.

[176] L. Zhou, Y. Huang, Z. Xie, and Y.-B. Cheng, "Gas-discharging reactions and their effect on the microstructures of green bodies in gelcasting of non-oxide materials," *Materials Letters,* vol. 45, pp. 51-57, 2000.

[177] R. Chen, C.-A. Wang, Y. Huang, L. Ma, and W. Lin, "Ceramics with Special Porous Structures Fabricated by Freeze-Gelcasting: Using tert-Butyl Alcohol as a Template," *Journal of the American Ceramic Society*, vol. 90, pp. 3478-3484, 2007.

[178] R. L. Coble and W. D. Kingery, "Effect of Porosity on Physical Properties of Sintered Alumina," *Journal of the American Ceramic Society*, vol. 39, pp. 377-385, 1956.

[179] K. Kirby, A. Jankiewicz, J. Lyon, and J. Barber, "Conformal firing of ceramic radomes," ed: Google Patents, 2002.

[180] B. Luo, M. Hu, F. Li, and G. Cao, "A novel material fabrication method for the PEM fuel cell bipolar plate," *International Journal of Hydrogen Energy*, vol. 35, pp. 2643-2647, 2010.

[181] B. C. H. Steele, "Appraisal of $Ce_{1-y}Gd_yO_{2-y/2}$ electrolytes for IT-SOFC operation at 500°C," *Solid State Ionics*, vol. 129, pp. 95-110, 2000.

[182] M. Molenda, K. Furczoń, A. Kochanowski, S. Zapotoczny, M. Szuwarzyński, B. Dudek, *et al.*, "Application of gelcasting process in ceria membranes formation," *Solid State Ionics*, vol. 188, pp. 135-139, 2011.

[183] S. P. Jiang, L. Zhang, H. Q. He, R. K. Yap, and Y. Xiang, "Synthesis and characterization of lanthanum silicate apatite by gel-casting route as electrolytes for solid oxide fuel cells," *Journal of Power Sources*, vol. 189, pp. 972-981, 2009.

[184] B. Lin, S. Zhang, L. Zhang, L. Bi, H. Ding, X. Liu, *et al.*, "Prontonic ceramic membrane fuel cells with layered $GdBaCo_2O_5^{+x}$ cathode prepared by gel-casting and suspension spray," *Journal of Power Sources*, vol. 177, pp. 330-333, 2008.

[185] X. Li, D. Li, B. Lu, and C. Wang, "Fabrication of bioceramic scaffolds with pre-designed internal architecture by gel casting and indirect stereolithography techniques," *Journal of Porous Materials*, vol. 15, pp. 667-671, 2008.

[186] X. Li, W. Bian, D. Li, Q. Lian, and Z. Jin, "Fabrication of Porous Beta-Tricalcium Phosphate with Microchannel and Customized Geometry Based on Gel-Casting and Rapid Prototyping," *Proceedings of the Institution of Mechanical Engineers, Part H: Journal of Engineering in Medicine*, vol. 225, pp. 315-323, 2011.

[187] K. Jono, M. Fuji, and M. Takahashi, "Porous Ceramics for Building Materials Fabricated by in situ Solidification Method Using Natural Polymer and Waste Resources," *Journal of the Ceramic Society of Japan, Supplement*, vol. 112, pp. S138-S143, 2004.

[188] M. Fuji, T. Kato, F.-Z. Zhang, and M. Takahashi, "Effects of surfactants on the microstructure and some intrinsic properties of porous building ceramics fabricated by gelcasting," *Ceramics International*, vol. 32, pp. 797-802,2006.

[189] M. Takahashi, R. L. Menchavez, M. Fuji, and H. Takegami, "Opportunities of porous ceramics fabricated by gelcasting in mitigating environmental issues," *Journal of the European Ceramic Society*, vol. 29, pp. 823-828, 2009.

[190] M. B. Dickerson, P. J. Wurm, J. R. Schorr, W. P. Hoffman, P. G. Wapner, and K. H. Sandhage, "Near net-shape, ultra-high melting, recession-resistant ZrC/W-based rocket nozzle liners via the displacive compensation of porosity (DCP) method," *Journal of Materials Science*, vol. 39, pp. 6005-6015, 2004.

[191] L. S. Gyger Jr, P. Kulkarni, H. A. Bruck, S. K. Gupta, and O. C. Wilson Jr, "Replamineform Inspired Bone Structures (RIBS) using multi-piece molds and advanced ceramic gelcasting technology," *Materials Science and Engineering: C*, vol. 27, pp. 646-653, 2007.

[192] L. García-Gancedo, S. M. Olhero, F. J. Alves, J. M. F. Ferreira, C. E. M. Demoré, S. Cochran, *et al.*, "Application of gel-casting to the fabrication of 1–3 piezoelectric ceramic–polymer composites for high-frequency ultrasound devices," *Journal of Micromechanics and Microengineering*, vol. 22, p. 125-129, 2012.

****